1979

Evaluation of Turbine Blade Root Damping

Curtis Beck

EVALUATION OF TURBINE BLADE ROOT DAMPING

by

Curtis M. Beck

A Thesis Submitted

in

Partial Fulfillment

of the

Requirements for the Degree of

MASTER OF SCIENCE

in

Mechanical Engineering

Approved by:

Prof. Neville F. Rieger

Prof. Alan H. Nye

Prof. Illegible Signature

Prof. _____
(Department Head)

DEPARTMENT OF MECHANICAL ENGINEERING
ROCHESTER INSTITUTE OF TECHNOLOGY
ROCHESTER, NEW YORK

November, 1979

ACKNOWLEDGEMENTS

The author would like to express his appreciation to those who have assisted him with this project.

To Professor Neville F. Rieger, his thesis advisor, for his interest and assistance during this test program.

To Kevin Cole, a co-worker in the early stages of the project, for his help in the finite element programming.

To Ken Hood, machine shop director, for his patience and assistance in the manufacture of the test apparatus.

To the Electric Power Research Institute, the sponsor, without whose funding this project could not have been undertaken.

ABSTRACT

A test program has been conducted to measure the vibration damping of three designs of steam turbine blades. These blades were tested in their root attachments, sectioned from retired rotors. Blade loading was accomplished in a new type of blade damping test rig and damping was evaluated in the lowest tangential and axial blade modes. The test environment was room temperature air.

The damping rig concept and development is presented in detail as well as results of an intensive test program. The blade designs are designated as Types A,B,and C, where Types A and B were of a fir tree root design and Type C was a ball and shank design. A total of 86 blades were tested and the influence of vibration amplitude, applied axial (simulated centrifugal) load, and vibration mode on damping logarithmic decrement was studied. For the designs studied, the most important findings were:

a) Logarithmic decrement was inversely related to blade centrifugal load. High centrifugal loads resulted in low damping ratios.

b) Logarithmic decrements varied in an almost linear manner with vibration amplitude for most tests. Constant logarithmic decrement conditions were not observed.

c) The damping test rig worked well in this test series. Long LP blades may cause problems without some design changes.

d) Results were highly reproducable per each blade group tested. Typical scatter was observed when comparing the results of one blade group to another.

e) Changing the initial excitation amplitude did not cause any changes in the vibration decay. There is one characteristic decay trace for each centrifugal load.

Test data was reduced by hand, which caused some difficulty as the damping ratio approached 1.0. An error in the third decimal place could greatly effect the logarithmic decrement value. It is recommended that a microprocessor be used in future tests.

TABLE OF CONTENTS

LIST OF FIGURES

LIST OF TABLES

AUTHORS FORWARD

The work described in this report has been done according to the job objectives as agreed upon by the Electric Power Research Institute (EPRI), who sponsored the research. The intention of EPRI was not to fund development of new damping theory, but rather to develop a test apparatus and procedure for determining actual blade root damping values.

A less detailed account of the project results has been sent to EPRI under the title, Damping Tests on Steam Turbine Blades, and, according to contract stipulations, the following disclaimer must be enclosed.

"LEGAL NOTICE"

" This work was prepared by Rochester Institute of Technology as an account of work sponsored by the Electric Power Research Institute, Inc. ("EPRI"). Neither EPRI, members of EPRI, nor Rochester Institute of Technology, nor any person acting on behalf of either:

" a. Makes any warranty or representation, express or implied, with respect to the accuracy, completeness, or usefulness of the information contained in this report, or that the use of any information, apparatus, method, or process disclosed in this report may not infringe privately owned rights; or

" b. Assumes any liabilities with respect to the use of, or for damages resulting from the use of, any information, apparatus, method or process disclosed in this report."

DESCRIPTION OF COMMONLY USED TERMINOLOGY

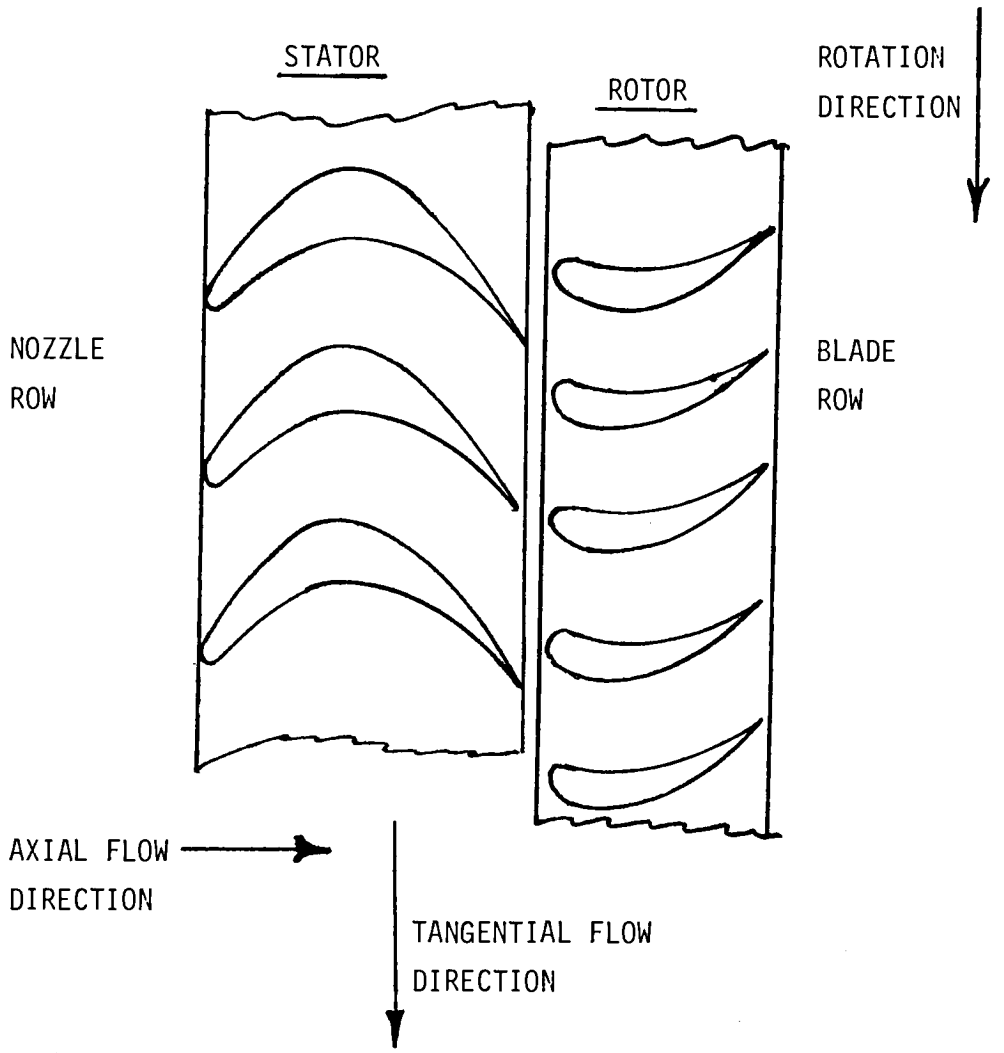

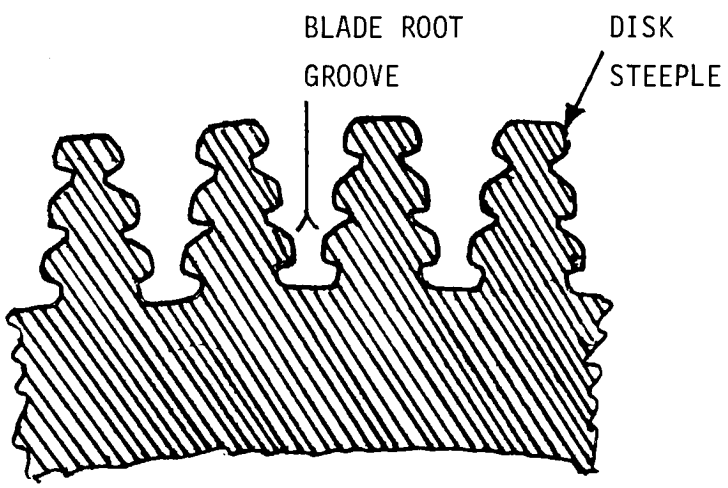

'FIR TREE' DISK SECTION

1. INTRODUCTION

1.1 Nature of Studies

It is estimated that 15 percent[1] of all forced outages of steam power plants are due to turbine blade failure. These blade failures generally occur due to fatigue as a result of excessive vibration. Excitation may arise from flow irregularities at nozzle passing frequency, irregular steam flow due to construction of a nozzle row, or transient excitation from the generator. For example, a diaphragm joint will cause a two-per-rev excitation due to the nature of its construction. Blade fatigue becomes possible when resonant forcing is strong and blade group damping is low in the resonating mode. At resonance, the limiting factors are therefore the strength of the excitation and the modal damping present. A major factor affecting blade group fatigue design is the lack of damping values with respect to various types of blades and their operating conditions (including sensitivity to structural tolerances).

The objective of this investigation was to develop an inexpensive, easy to use damping test rig and investigate the damping characteristics of several types of steam turbine blades in a laboratory environment. This report describes certain studies of the mechanical damping properties of steam turbine blades in their disk attachment structures, as shown in figure 1.1, with the major interest in how damping is influenced by centrifugal load, vibration amplitude, and root type. No attempt was made to determine what percentage of the overall damping was attributable to a specific damping phenomena (e.g. stick-slip, material, gas dynamic, etc.). The function of the rig was to support the blades and disk sections and to apply a simulated centrifugal load such that the load on the blade root was equivilent to the load seen under actual operating conditions. The rig also had to be designed such that it did not contribute any damping to the blade/root system.

This report covers; a) a review of blade damping literature, b) the development of the test rig, c) testing of three types of blade/root configurations, and d) a description in chart form of logarithmic decrement behavior under the test conditions previously described.

---

1 From Rieger [10]

Since each of the three blade types was of different root design and blade length, three damping rigs needed to be built. Each rig was designed by finite element analysis to avoid any rig natural frequencies occuring within the range of blade test frequency. The finite element predictions were corroborated with the use of accelerometers on the rigs before testing began.

The program of damping tests was as follows. Each blade pair was inserted in the test rig. The blade pair was vibrated, and the decay trace which followed removal of the blade excitation was plotted. The envelope of the decay trace was drawn with a french curve and logarithmic decrement was calculated at several amplitude locations along each curve. In particular, the influence of the following factors was investigated:

a. Blade bending vibrations in the steam flow tangential direction.
b. Blade bending vibrations in the steam flow axial direction.
c. Influence of simulated blade centrifugal load.
d. Root attachment type.
e. Blade structure and vane length.

Blade damping test results were then reduced,and are presented as charts of logarithmic decrement vs. blade tip displacement as a function of centrifugal load for each blade type and for each of the two vibration directions. Trends which appear in these charts are discussed in Section 7. Conclusions are discussed in Section 8.

1.2 Objectives of Project

The objectives of the project were:

1. To build and verify a blade damping rig such that an alternate method for obtaining damping test data would be available for use under controlled laboratory conditions. This is needed because of the difficulties involved with *in situ* and wheelbox damping tests.

2. To demonstrate the effectiveness of this rig for obtaining vibration decay traces for steam turbine blades in their actual disk attachments.

3. To measure the damping characteristics for a number of blade/root geometries in sufficient quantities,in order to obtain some indication of the amount of statistical varience involved. To see how damping changes as centrifugal load and/or excitation force changes.

4. To reduce the damping test data and plot the results in the form of charts of logarithmic decrement vs. vibration amplitude. To do this for each blade/root type, simulated centrifugal load, and vibration frequency tested.

Objective 1 was met by designing and building the test rigs shown in figures 1.3 to 1.5. Separate test rigs were required because the three blade types obtained for testing had different blade lengths; as shown in figure 1.2. A single, expandable rig design was considered but rejected because of the additional friction likely at the joint of any expandable rig. Construction details for the test rigs are described in Section 5 of this report.

Objective 2 was met by demonstrating that each of the three types of blade pairs gave clean, single-mode vibration decay traces when tested in their respective rigs. Decay traces were obtained for a total of 86 blade pairs. Each blade pair was tested in its lowest tangential and axial mode.

Objective 3 was met by reducing the decay traces to tables of logarithmic decrement vs. decay trace amplitude. The decay trace amplitude was then calibrated against a known blade tip displacement. Between six and twelve data points per decay curve were obtained. This resulted in between three and six logarithmic decrement values respectively.

Objective 4 was met by plotting logarithmic decrement vs. blade tip displacement as a function of centrifugal load for each of the blade types tested. The plots obtained are given in Section 6 of this report.

In general, the results show that a reasonably simple relationship exists between logarithmic decrement and vibration amplitude for the blade types tested. The only uncontrolled variable was the blade root tolerances. The results show a degree of scatter which is believed to be primarily due to the varience in blade root dimensions.

1.3 Work Scope

The following breakdown of tasks is a list in chronological order of the project objectives as was indicated in the original work proposal.

Task 1. Design Damping Rig

a. Obtain blades and root disk attachments
b. Develop detailed design for test rig A.
c. Prepare manufacture drawings.
d. Design flexure link and blade pair arrangement.
e. Design welding jig.
f. Specify test equipment.
g. Design necessary electronic equipment.

Task 2. Finite Element Calculations

a. Develop finite element model of damping rig.
b. Develop finite element model for single blade and blade pair.
c. Calculate all natural frequencies and mode shapes.
d. Experimentally determine natural frequencies and mode shapes to verify finite element predictions.
e. Perform design analysis to achieve dynamic isolation of blade pair modes from coupled rig/blade structural modes.

Task 3. Manufacture Test Rig and Blade Pairs

a. Manufacture rig loading frame and welding jig from drawings.
b. Manufacture prototype flexure link.
c. Obtain test stand. Attach rig to test stand. Experimentally determine finite element correlation for rig without blades.
d. Weld prototype blade pair. Install blade pair and test for natural frequency. Make any flexure link design modifications necessary.
e. Once proper flexure link is obtained, have machine shop fabricate necessary number of links and machine remaining blades to proper length. Experimentally determine finite element correlation for rig with blade pair installed.

Task 4. Prototype Tests

a. Obtain suitable exciter.
b. Obtain strain gage amplifier.
c. Obtain strain calibration equipment.
d. Mount strain gages on blade pairs.
e. Test to calibrate strain gages in tensile test machine and make sure gages are located properly with blade principal axes.
f. Install blades in rig and demonstrate experimental procedure.
g. Debug the design if any problems occur. Once program is operational proceed with construction of rigs for type B and C blades.

Task 5. Test Program

a. Conduct damping tests for three types of blade/root configurations.
b. Determine the effect of:
   (i) Three different types of blade attachment geometries.
   (ii) Different blade lengths (between blade groups).
   (iii) Axial force simulating centrifugal load (three or more axial loads for each blade pair tested).
   (iv) Amplitude of vibration.
   (v) Mode of vibration effect (two modes in detail).
   (vi) Scatter of results.

Task 6. Data Reduction

a. Obtain logarithmic decrement values corresponding to several vibration amplitudes for each test.
b. Plot results for;
   (i) Each blade attachment design.
   (ii) Each simulated centrifugal load.
   (iii) Each separate mode.
   (iv) Several vibration amplitudes per test.
   (v) Each level of excitation used.
c. Present damping results in a manner suitable for use in dynamic stress calculations.

Task 8. Final Report and Presentation of Results

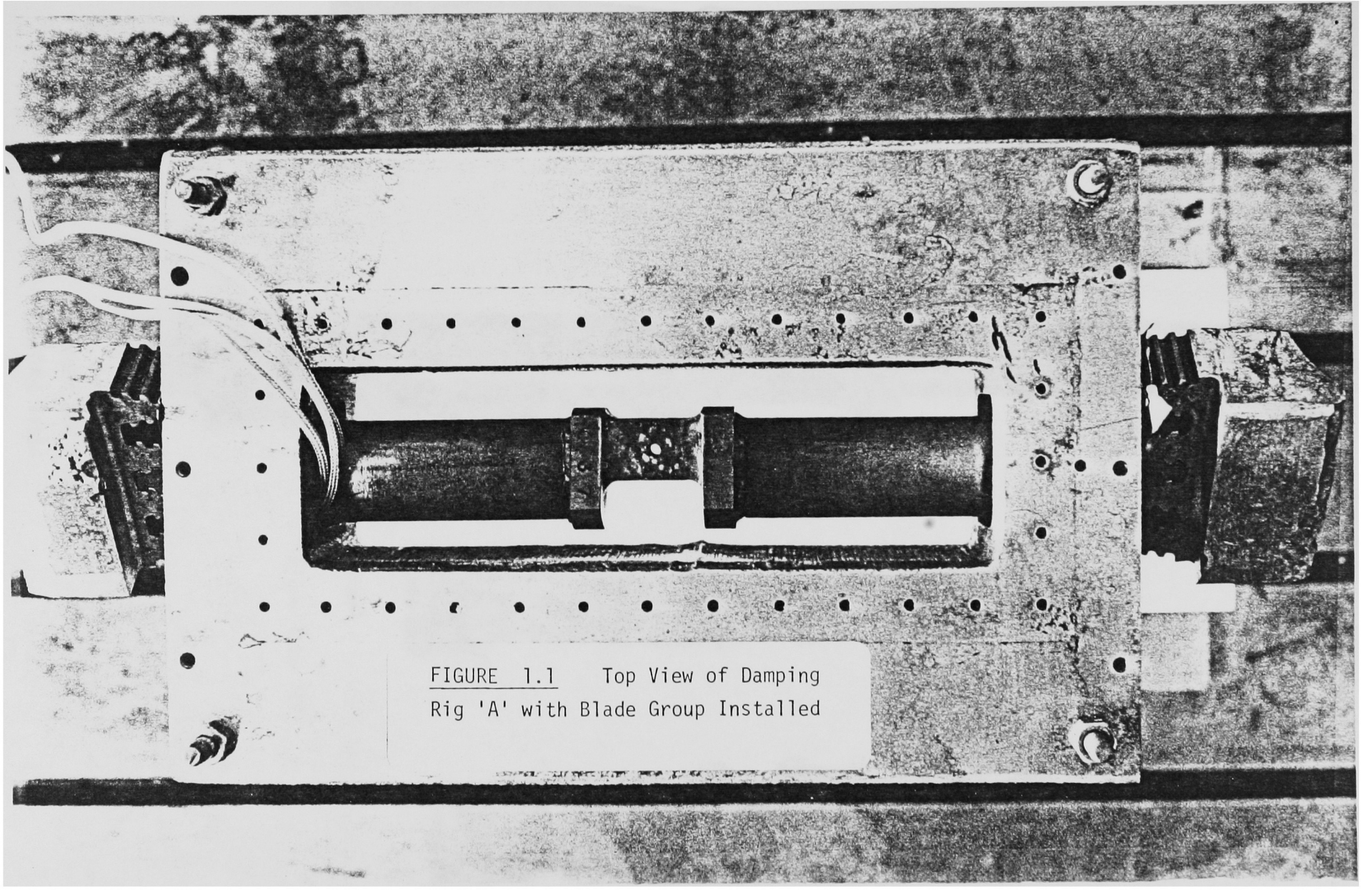

FIGURE 1.1 Top View of Damping Rig 'A' with Blade Group Installed

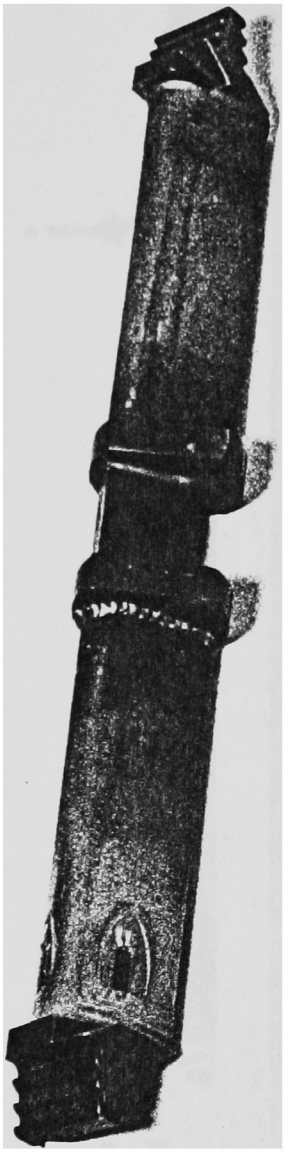

Blade Type 'A'

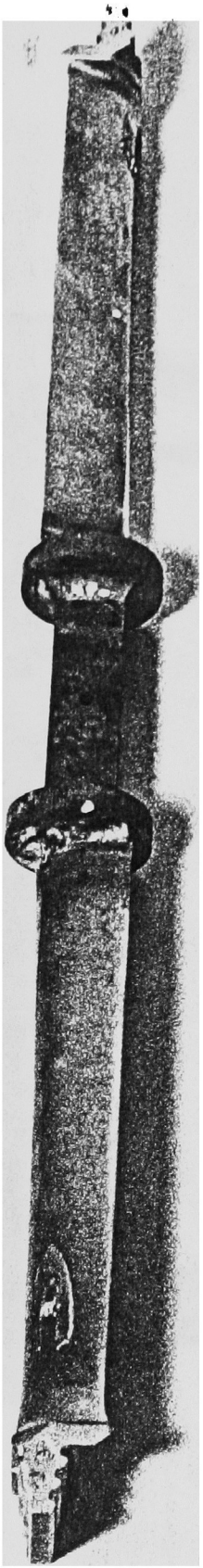

Blade Type 'B'

Long Shank

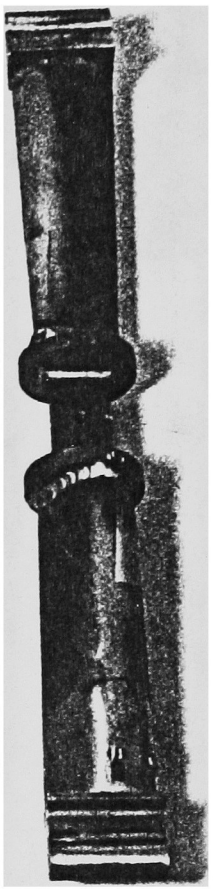

Short Shank

Blade Type 'C'

FIGURE 1.2 Blades and Flexure Links Used in Damping Tests

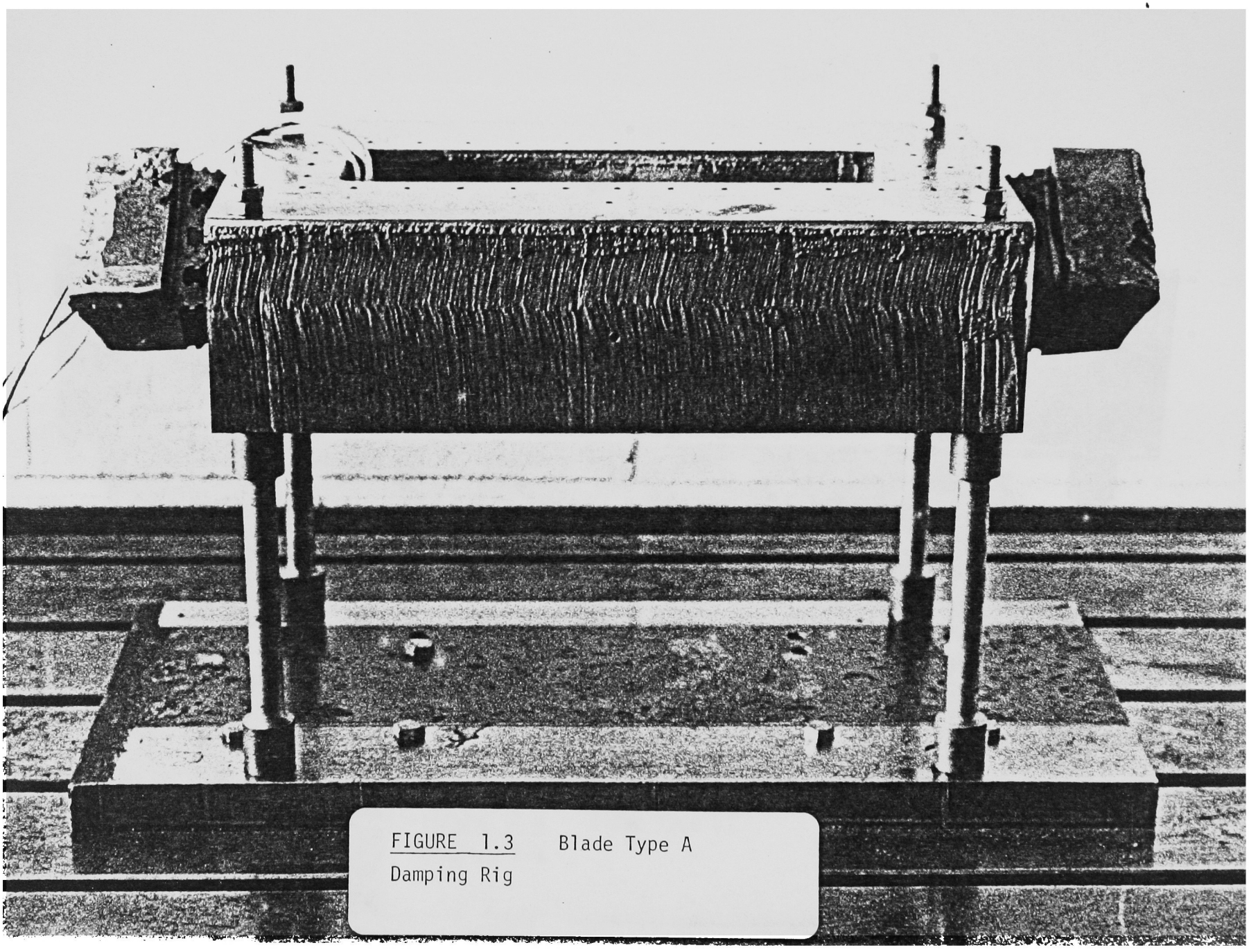

FIGURE 1.3 Blade Type A
Damping Rig

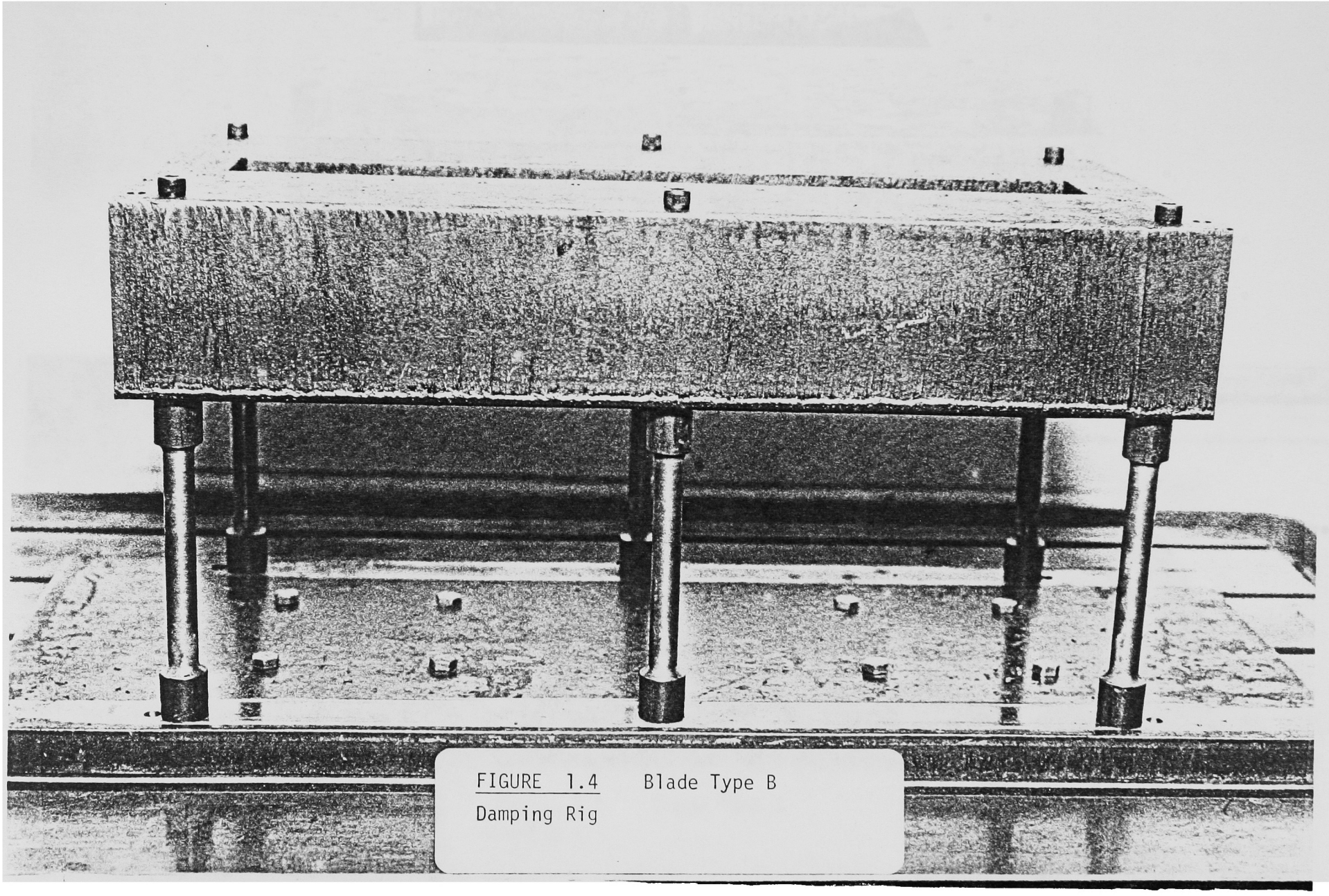

FIGURE 1.4 Blade Type B
Damping Rig

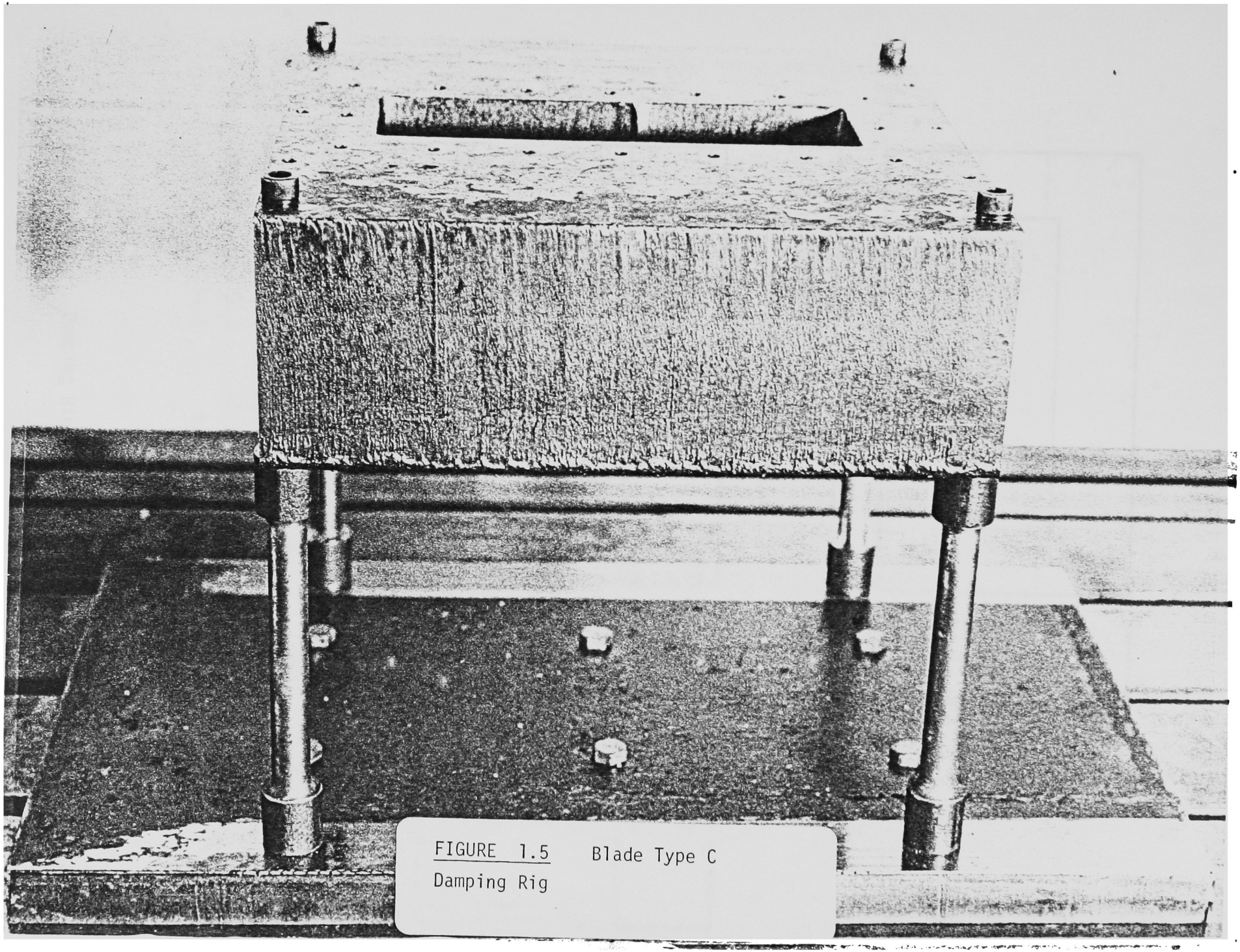

FIGURE 1.5 Blade Type C
Damping Rig

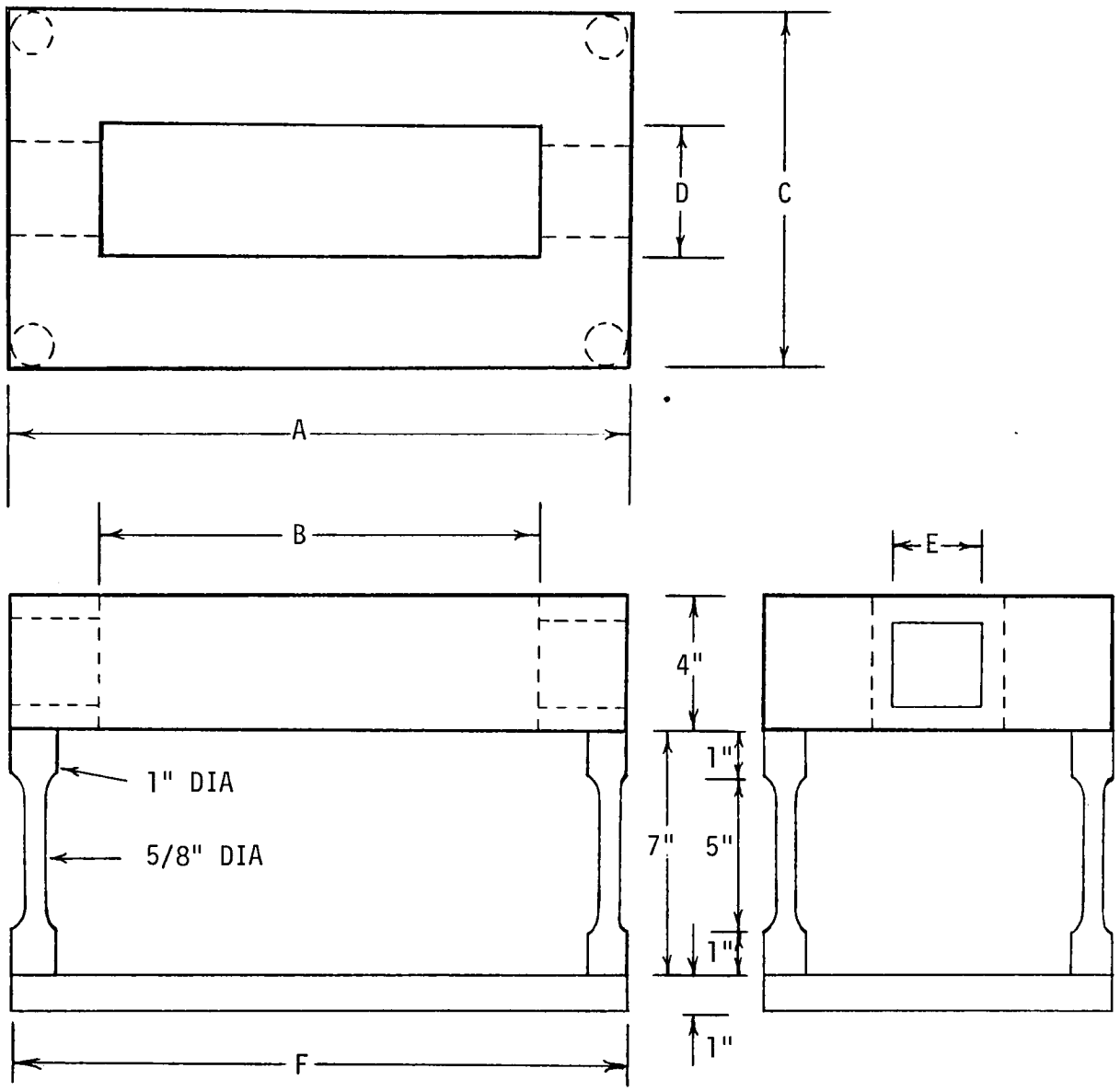

DAMPING RIG	DIMENSION (INCHES)					
	A	B	C	D	E	F
Type A	15.0	10.5	10.0	3.0	2.0 sq	21.0
Type B	22.5	19.0	12.0	2.5	2.625 sq	30.0
Type C	11.5	8.0	12.0	2.5	2.0 sq	20.0

Figure 1.6 Damping Rig Dimensions

2. LITERATURE REVIEW

2.1 General

A background literature search for information on blade damping under the catagories Blades; Blading; Vibration; Damping; and Turbomachinery was conducted for the years 1960 through 1979.

A review of titles and abstracts in the Engineering Index revealed very few applicable papers. Fully 30% of the pertinent papers were written in Russian. Another 10% were in Polish, with the remainder being primarily of Indian origin. The majority of papers in the Index were concerned with noise suppression or the theory of vibrating beams.

By and large, the Shock and Vibration Digest has the largest selection of abstracts in the above catagories. The Digest features several authors each month who have relatively short papers published. The references of these papers are invaluable in locating relevant work. Most of the work has been done in the United States and published in the Transactions of the ASME. Much of the work done has been in testing and developing friction damping theory for simple beams. Some previous blade damping tests have been published, but there is definitely a shortage of such reports in the open literature. Many tests are known to have been conducted on blade damping by gas and steam turbine manufacturers. However, their findings are seldom reported in the open literature.

A considerable amount of work has been done similar to that done by Jarrett and Warner [5] to determine mathematical expressions for analytically determining natural frequencies and mode shapes for blade vibrations. No consideration is given to damping. Unfortunately, much of the work presented is in the form of theory or computer programs with little or no supportive experimental work.

2.2 Previous Blade Damping Tests

In 1958, DiTaranto [1] investigated blade damping with the use of hollow blades in which 0.005 inch diameter wires were inserted. When the blade

vibrated, the wires rubbed together, thus dissipating energy via friction damping. For stationary and low speed (1125 RPM) tests copper wires were used. High speed tests used stainless steel wires.

DiTaranto's findings were that the damping of a stationary wire-filled blade with wires stressed to 7,000 psi was an order of magnitude higher than that of the stationary hollow blade for equal excitations. The damping in a high speed (8000 RPM) rotating blade was double that of a blade with wires stressed to 7,000 psi. He recognized methods of damping as being in four catagories:

1. Insertion of particles and/or wires of different sizes into hollow blades.
2. Use of two flat cantilevered plates under normal force, rubbing together as they vibrated.
3. Root damping of the vibrating blade, with normal force being the critical factor again. Too great a force prevents relative blade-root motion.
4. Tuned dampers, which are relatively effective only in narrow frequency bands.

Two years previous to Di Taranto's investigating catagory one, Goodman and Klumpp [3] were investigating the second catagory: flat cantilevered plates under a normal force. They analyzed a uniform pressure joint made up of two cantilevered bars with a common interface. Although damping was satisfactorily increased over a single bar, it was hardly applicable to turbine blading.

Blade damping tests have been conducted by Grady [13] and Wagner [15]. Grady headed an investigation into the dovetail damping of steam turbine blades. His report details the effect of tolerance mismatch between the blade root and disk. Blade tolerance was altered, and each test consisted of measuring the dynamic root stress and frequency after the blade was impulsed with 50 lb_f. The tests were zero RPM and one of his conclusions was that the optimum root flexibility for maximum damping occurs at 50 - 60% that of rigid welded joint. It is not known if this conclusion would be true if centrifugal effects were included.

According to Rieger [12], Wagner [15] has conducted tests to measure blade group damping in a single test turbine stage. Blade groups instrumented with strain gages were caused to vibrate by rotating them through a stationary water jet. Dynamic strain decay rates of the instrumented blade groups were recorded to measure the damping present. The influence of wheel speed and of turbine back pressure on damping was investigated. It was found that for the conditions studied, the damping logarithmic decrement value was generally less than, but in the order of, two percent damping. Spin tests are desirable for the centrifugal effects but the stage setup is very costly. If centrifugal effects can be generated, then cheaper, impulse bench tests can be performed. Halvorsen and Brown [4] discuss impulse testing techniques and give response functions and signal processing requirements. For natural frequency investigation impulse techniques are the cheapest and simplest to use, no matter whether a water jet or hammer is doing the forcing.

2.3 Friction Damping

Beards [2] [6] is a principal investigator of friction damping in structures. He says, "Frictional damping occuring in joints is the major contributor to the total inherent damping in structures. Although difficulties of analysis and fears of fretting corrosion have stifled enthusiasm for this form of damping, we cannot continue to ignore it." Beards [2] gives curves of decay time vs. frictional force to demonstrate advantages of friction damping. He is concerned with surface preparation to avoid fretting corrosion and fretting fatigue through development of better epoxies or grease-like substances.

Previous work by Goodman and Klumpp [3] has already been mentioned.

2.4 Material Damping

Of all damping investigations, material damping seems to have a disproportionately large share. Grady [11], and Schabtach and Fehr [14] used almost identical test specimen design in their investigations of material damping. However, Schabtach and Fehr carried their tests a few steps further and investigated high temperature effects. Jones [16]

has also done an extraordinarily large amount of high temperature testing. The high temperature effects concern themselves primarily with gas turbines and relatively few applications to the lower temperatures seen in steam turbines.

Cochardt [8] explains the damping in high-strength ferromagnetic alloys in terms of the magneto-strictive effect,using energy expressions similar to Lazan's method of attacking the problem.

Lazan [7] [9] has done much of the experimental work that is indexed and available today. He has investigated damping constants and stress distribution and has compiled a list of material damping properties for several hundred metals and alloys in terms of frequency, stress amplitude, type of loading, amount of cold working, etc. He also lists phenolics, wood, and other engineering materials. Almost 2,000 materials are indexed.

Conclusion

Rieger [17] discusses his findings on previous steam turbine blade damping tests and concludes that: a) no meaningful technical development has occured in the area of steam turbine blade damping for at least the past 20 years, and b) that most of the damping technology effort in this time period has been directed toward gas turbine blading.

At this point it is difficult to argue with any of the theories presented, because most have no supportive experimentation. However, it is clear that no inexpensive bench test rig for turbine blade testing has been previously reported in the open literature.

3. DESIGN AND CONSTRUCTION OF TEST RIG

3.1 Design Principles

The primary design requirements for each test rig were:

a. To transmit longitudinal blade root loads to simulate full blade centrifugal load during operation.

b. To avoid coupling between the blade pair and any rig natural frequency.

The above requirements were accomplished by preparing a finite element model for each rig. Since the natural frequencies for blade Types A,B, and C were known from vibration tests on the blades provided, it was simple to change component sizes to shift the natural frequencies of the test rigs to create rig "dead" zones in the regions of the blade pair natural frequencies.

Once the basic design of a rig was completed, a finite element model was made for the corresponding blade pair component, and the flexure link design was undertaken. The cross section of the link was changed until the blade pair natural frequency matched the natural frequency previously obtained by experiment for a single, free-standing blade of the same design. Another criteria in the flexure link design was that the cross section should be sufficient to carry the applied axial tension without yielding, and also have flanges whose diameters were greater than the blade airfoil chord so the blade could be fully heliarc-welded to the flexure link around the perimeter of the airfoil. It was also required to orient the flexure link so that the blade would vibrate in its plane of least stiffness when excited tangentially, and in its plane of maximum stiffness when excited axially. This condition could only be achieved for the Type A blades, for which both right and left-handed blades were available, and since the blade centroids are required to be in line with each other. Other blade combinations (right-hand blade welded to right-hand blade) gave frequencies and modal directions which were somewhat, but not greatly, different from the true vibration conditions.

The original test rig design called for a shrink fit to be achieved by passing a gas coolant through hollow-side columns. Once cooled down, the blade pair would be inserted with its disk attachments, and then shims would be added to take up the initial axial dimensional difference, i.e. slack. When the rig then warmed up to ambient temperature the blade pair would be axially loaded by the axial growth of the rig. A schematic for this design is shown in figure 3.1. It was estimated that the ΔT to shrink this rig and insert the shimming necessary to obtain 2.5 tons of simulated centrifugal load was 40°F below ambient. This temperature differential is evidently small, so tests were conducted to determine whether the same axial strain could be achieved by locally heating the flexure link to a temperature of approximately 300°F. This procedure offered the possibility for saving the expense of boring the cooling ports in the rig side columns, and that of acquiring, developing, and operating the cooling apparatus during testing. It was found that a flexure link temperature of approximately 375 °F would produce the equivalent local elongation necessary to add the shims and obtain the 2.5 ton load. At no time did the link or blade approach red heat, which could have altered their material properties.

The assembled rig was bolted to a T-slotted table surface. This table provided a massive, i.e., dynamically inert, foundation for the test rig. This table is shown in figure 3.2. Foil type strain gage transducers were attached to the blade pairs tested to obtain the dynamic strain (vibration) as well as the static strain (simulated centrifugal load). Gage location and function is talked about in the following subsection. Strain gage signals were passed through strain amplifiers and to a spectrum analyzer for fast Fourier Transform anslysis. Data from the analyzer was transferred to a digital plotter and subsequently reduced, see Figure 3.3 .

3.2 Rig Construction and Blade Loading Details

Each of the three test rigs was made from a 4.0 inch thick steel plate, supported on cylindrical legs, 0.625 inch in diameter and 7.0 inches long. These legs were bolted down to a 1.0 inch thich plate which was, in turn, bolted to the aforementioned T-slot table. All steel used in rig construction was AISI 1020 hot rolled (or drawn) steel. Details of these rigs are shown in figures 1.3 through 1.6, for blade Types A,B,and C respectively.

The first finite element model and rig construction had legs 6.0 inches long. Correlation between the finite element predictions and experimentally determined rig frequencies and modes is presented in Section 4 of this report. During the testing of blade Type A, it was found that the six-inch legs did not allow easy installation of the vibration exciter. Although there was sufficient space to connect the exciter to the blade pair being tested, seven-inch legs were installed to permit greater accessibility. Test rig natural frequencies were found by performing accelerometer tests on the rigs in conjunction with a spectrum analyzer. The finite element element calculations were redone for the seven inch legs and are given in Section 4.

The original design called for the legs to be welded in place to form a rigid connection, thereby eliminating any damping which may have resulted from a bolted type construction. However, it was also apparent that the leg dimensions, either diameter or length, might have to be altered at some point to accomodate changes in the instrumentation or natural frequency. Bolting was therefore selected as being more suitable if any such changes were to be made. Bolted construction was used for certain introductory tests for blade Type A, and it was determined by accelerometer tests that the vibration which could be transmitted into the rig was 36 db lower than that generated by the blade group excitation.

The overall length of each blade group between loading platforms at each end was a few thousandths of an inch longer than each respective rig. Blade pairs were inserted via holes bored in each end of the four inch plate, as shown in figure 3.4. The large center opening in each rig was flame-cut by the material supplier. After flame-cutting, each rig was stress relieved.

Once the blade group was inserted into the rig, the disk attachments were slid on. The flexure link of the blade pair was heated with an acetylene torch, and as the blade group expanded, thin metal shims of suitable thickness were placed between the disk steeples and the test rig body. The blade groups were placed such that the wide portion of the central flexure link was either parallel or normal to the table surface, depending on the direction in which the vibration was being generated. When the required number of shims to obtain a desired load had been inserted, the flexure link was cooled with ice water. As the link cooled, the blade group was strained by the

Initially, some concern was expressed regarding overheating of the blades and altering the material properties. Fortunately, the flexure link absorbed most of the heat and the blade tip temperature was approximately 325°F. Since the blade tips were relatively thin, the temperature a distance of 1.25 inches from the blade tip was below 212°F, as the cooling water did not boil away.

The magnitude of the steady lengthwise or axial load along the blade pairs, i.e., the simulated centrifugal load, was measured using a foil-type strain gage mounted along the blade leading edge. The strain gage was wired into a quarter strain-bridge configuration. Bending, as a result of misalignment during loading, was monitored and eliminated using the output of two foil gages in the flow tangential direction. One gage was mounted on the pressure surface and the other was mounted an equal distance from the centroid on the suction surface. As the blades cooled down, they were continually adjusted such that the bending gages registered a zero output voltage. Axial and tangential vibration signals were obtained from these axial and bending gages respectively.

When data was available on the service conditions of the blades, care was taken to ensure that each blade pair was strained to a similar load condition as was seen during turbine operation. Centrifugal loads generated during testing ranged from 1000 lbs. to 6000 lbs.

3.3 Blade, Root, and Blade Pair Details

Three different types of blade root and disk attachment combinations were tested. These geometries are shown in their pretest condition in figure 1.2. The corresponding root sections are shown in figure 3.5.

The Type A blades were of straight cross section, without taper or twist. These were mounted on a fir-tree root, and they were typical blades from an I.P. stage. The blade length was about six inches from the top of the platform to the tenon. Each fir-tree had three hooks per side. The fir tree depth was about 1.0 inches by 1.25 inches axial length. Both left-hand and right-hand blades were supplied as well as corresponding left and right-hand disk sections.

The rotor was sectioned such that a piece of disk holding thirty blades was received for both flow directions. Several loose blades were also supplied. The rotor was stored outdoors and was either deliberately or accidently covered with a coat of tar. The large disk sections were flame cut into five pieces (since there were six blades per group), the tenons and covers were removed with a bandsaw, and the blades were driven out of their root grooves. The blades were then soaked in kerosene to remove the tar, and were later wire brushed. The blades were machined to an overall length of 7.100 inches. The distance from the base of the platform to the blade tip was therefore 6.200 inches. The flexure link was 2.600 inches with a tolerance of -0.000 inch; +0.020 inch. This formed a blade pair of approximately 15.010 inches. The overall length of damping rig A was 15.000 inches as given in figure 1.6.

Type B blades also had a fir-tree root construction, but they had a longer tapered and twisted vand section than the Type A blades. The vane length was approximately 9.5 inches from platform to the tip of the tenon, with the tenon being about 0.400 inch long. The fir-tree was approximately the same size as the Type A blade, again with three hooks per side. No disk root sections were obtained with these blades. However, the blade supplier sent a blueprint of the disk root groove. The minimum root groove tolerance envelope was used to program a traveling wire EDM machine. The machine was capable of holding a tolerance of $\pm$ 0.0002 inch. Two blocks of hardened AISI 4150 steel were used for the disk material since large blocks of stainless steel of the type used in the original turbine could not be obtained. The end result was fabricated disk sections as similar to the originals as could be made locally. Upon receipt, the Type B blade roots were each coated with a heavy duty epoxy resin which was difficult to remove. In order to remove the epoxy from the inner hook radius, compressed air in conjunction with a fine, crushed glass was used in an operation similar to sandblasting. This left a smooth, clean surface comparable to the surface on the EDM'ed root sections.

The Type B flexure link was 4.500 inches long with a tolerance of -0.000 in.; +0.020 in. The length from the base of the platform to the blade tip was machined to 9.0 inches. The overall length of the damping rig was therefore 22.5 inches.

Type C blades were short, tapered, twisted blades with a shell-type vane section. The vane length was approximately 4.75 inches from platform to cover. The root sections of these blades were of a ball and shank construction, which came in two sizes (long and short shank), as shown in figure 1.2. The long and short shanks alternated around the disk sections as shown in figure 3.5. Both long and short shank blades were tested in this program. The Type C blades and disk sections were supplied as sectioned from a turbine which had been in use for some time, with considerable oxide film on the blades and roots. The blades were shipped in their disk attachments with five blades per group. The covers and tenons were cut off and the blades were driven out of their disk sections. Before reassembly and testing, the blades were soaked in kerosene and wire brushed.

The Type C flexure link was 2.000 inches long, also with a tolerance of -0.000 in.; +0.020 in. The blades were ground to a length of 4.700 inches since very little material needed to be removed. The overall length of the damping rig was 11.5 inches.

The length of each flexure link was decided upon during the initial sizing of each rig. The correct blade group natural frequency was obtained by changing the size of the flexure link flange and cross section as described in Section 4. Suitable welding jigs for each blade group were designed and built such that the blades would be properly aligned with each other. The blade clamps on these jigs were positioned such that warping due to the high welding temperature would be kept to a minimum.

Dimensions of all three rigs are given in figure 1.6. The tolerances on both the rigs and the blades was $\pm$0.002 inch. This allowed the assembled blade groups to protrude a few thousandths of an inch beyond the ends of each respective rig. Therefore, the disk attachments could be slipped on prior to heating.

3.4 Instrumentation and Electronics

The mode shapes of the test rigs with and without blades were experimentally determined using piezoelectric accelerometers in conjunction with an electromagnetic shaker. The PCB accelerometers have a sensitivity of 100 MV/g at 100 Hz. With amplifiers, the output sensitivity could be increased to a maximum of 10 v/g. A flat frequency response curve was obtained for the accelerometers from 20 Hz to 2500 Hz. The transverse sensitivity was less than one percent. The accelerometer output was analyzed for frequency spectrum and amplitude by using a real-time analyzer. The rigs were vibrated with a PM Vibration Exciter Type 4809 manufactured by Brüel & Kjaer. The type 4809 is a compact, permanent magnet, electro-dynamic exciter with a 10 lb_f force rating. It is capable of vibrating small test specimens over a frequency range from 10 Hz to 20 Khz. Its moving coil has a nominal impedance of 2 ohms with a maximum current rating of 5 amps RMS.

The power amplifier for the exciter was a Type 2706, also manufactured by B & K. The type 2706 is transistorized and rated at 75 VA. It has protective, switchable current limits to safeguard against overloading the system, and is made for use with Type 4809 and 4810 vibration exciters.

The frequency input to the power amplifier was from an Audio Oscillator model 200 DR manufacutred by Hewlett-Packard. The oscillator was equipped with a variable gain control and had a frequency range from 7 Hz to 70 KHz.

The performance of the oscillator, power amplifier, shaker system was checked with the accelerometer, analyzer, plotter setup. A wiring schematic is shown in figure 3.6. The response obtained is given in figure 3.7, 3.8, and 3.9. The results were almost identical to the manufacturer's specifications, shown in figure 3.10(a).

Measurement of (a) a blade steady axial load, (b) natural frequency, and (c) amplitude decay were each accomplished using foil-type strain

gages. The axial load on the blades was measured using a two-arm Wheatstone bridge arrangement of the gages and a single-arm bridge arrangement, figure 3.3. The gages in the two-arm bridge were aligned and set at equal distances from the bending neutral axis, in opposing strain fields. This arrangement allows the sensing of pure bending strains, and therefore can be used to insure that the blades are aligned properly in the rig. The single-arm gage is then used to measure the axial load on the blades. The gages were mounted slightly above the blade platform, since this region of the airfoil sees the largest strain when a bending load is applied at the blade tip. The relationship between impulse direction and strain gage location is shown in figure 3.11. Note that the blade vibratory response was measured using the same strain gages. Vibration amplitude and frequency data from a given load impulse was obtained in this manner.

The strain gages used were of WK and WA series, manufactured by Micro Measurements, Inc. These gages provide high accuracy at elevated temperatures. The WA series gages were specified with an 06 temperature expansion coefficient, 0.250" gage length, and a nominal resistance of 350 ohms. The gage factor was 2.08 $\pm$ 0.5 percent, and the transverse sensitivity was -0.20 percent. The WK series gages also had an 06 temperature expansion coefficient (6.33×10^{-6} in/in°F). The gage length was 0.062 inches and the nominal resistance was 350 ohms. The gage factor is 2.06 $\pm$ 1.0 percent and the transverse sensitivity is -0.80 percent.

The strain gages used for Type A and B blades were the WA series. These gages were bonded to the blades with M-Bond 100 (Eastman 910). Strain gages used for the type C blades were of the WK series. The WK gages were adhered to the blades with M-Bond 600 epoxy. After mounting, all gages were coated with M-Coat A, an air-drying polyruethane which provides moisture protection, and ensures a better chance for survival if the gage is bumped or scraped. The strain gage amplifiers were Accudata 118 amplifiers, manufactured by Honeywell, Inc. The amplifiers were equipped with variable bridge power supplies and with variable gains. The constant voltage bridge supply was set between 8 and 10 volts, and the gain was adjusted to provide a calibrated output. Calibration of the strain gage

output was achieved by using both the static load technique and the shunt resistor technique. The shunt calibration of the strain amplifiers is discussed in Section 5.1. A picture of the amplifiers used during the tests is shown in figure 3.12. After shunt calibration, the amplifiers readout was checked with a Tinius Olsen Universal Tester. Each blade type was, (in turn), wired to the amplifiers and pulled in the tension test machine. This served as a static load calibration check, and as a test to make sure the welds to withstand relatively high loads.

The strain gage response was analyzed on a 444A Nicolet real-time spectrum analyzer. The input signal is digitized and stored in the memory of the analyzer. The available output from this analyzer was either frequency vs. amplitude or amplitude vs. time, ie. decay trace. Output copies were plotted on a Tektronics Interactive 4662 digital plotter. A picture of the analyzer and plotter is shown in figure 3.13. The axial frequencies of the Type A and Type C blades required filtering of the strain gage signal due to other* natural frequencies adjacent to the natural frequency of the mode being studied. Special 9th order Butterworth band pass filters were built to remove the unwanted modes. A typical filter response is shown in figure 3.14. The filter response was designed to insure appropriate band width and roll-off characteristics in each instance. A typical filter circuit for this is shown in figure 3.15. Typical response with and without filters is shown in figures 3.16 and 3.17. A schematic of impulse test instrumentation is shown in figure 3.3.

* These 'other natural frequencies' were the predominant tangential modes which showed up in the axial spectra.

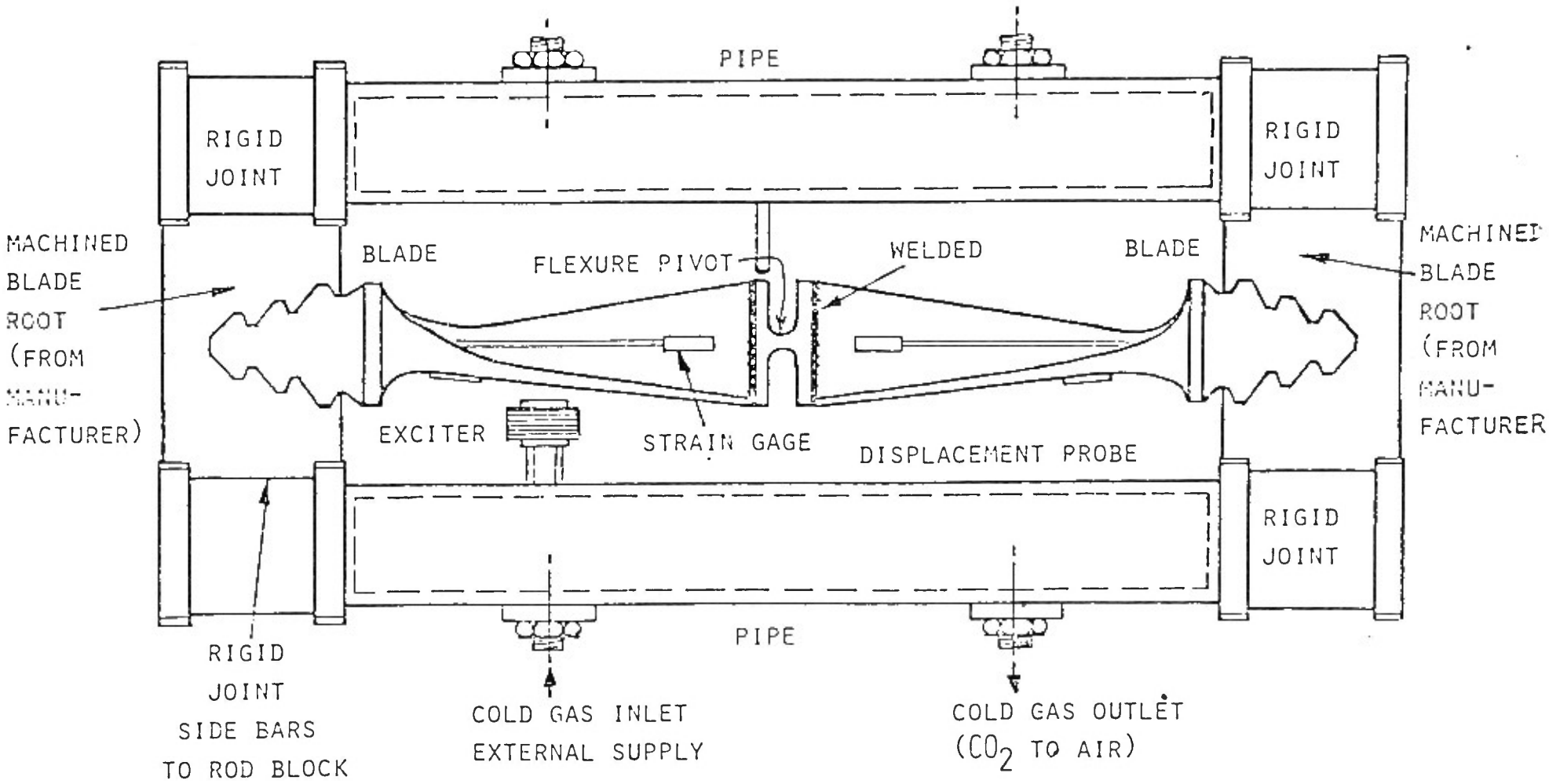

FIGURE 3.1 Original Design Concept Incorporating Shrinkage Method

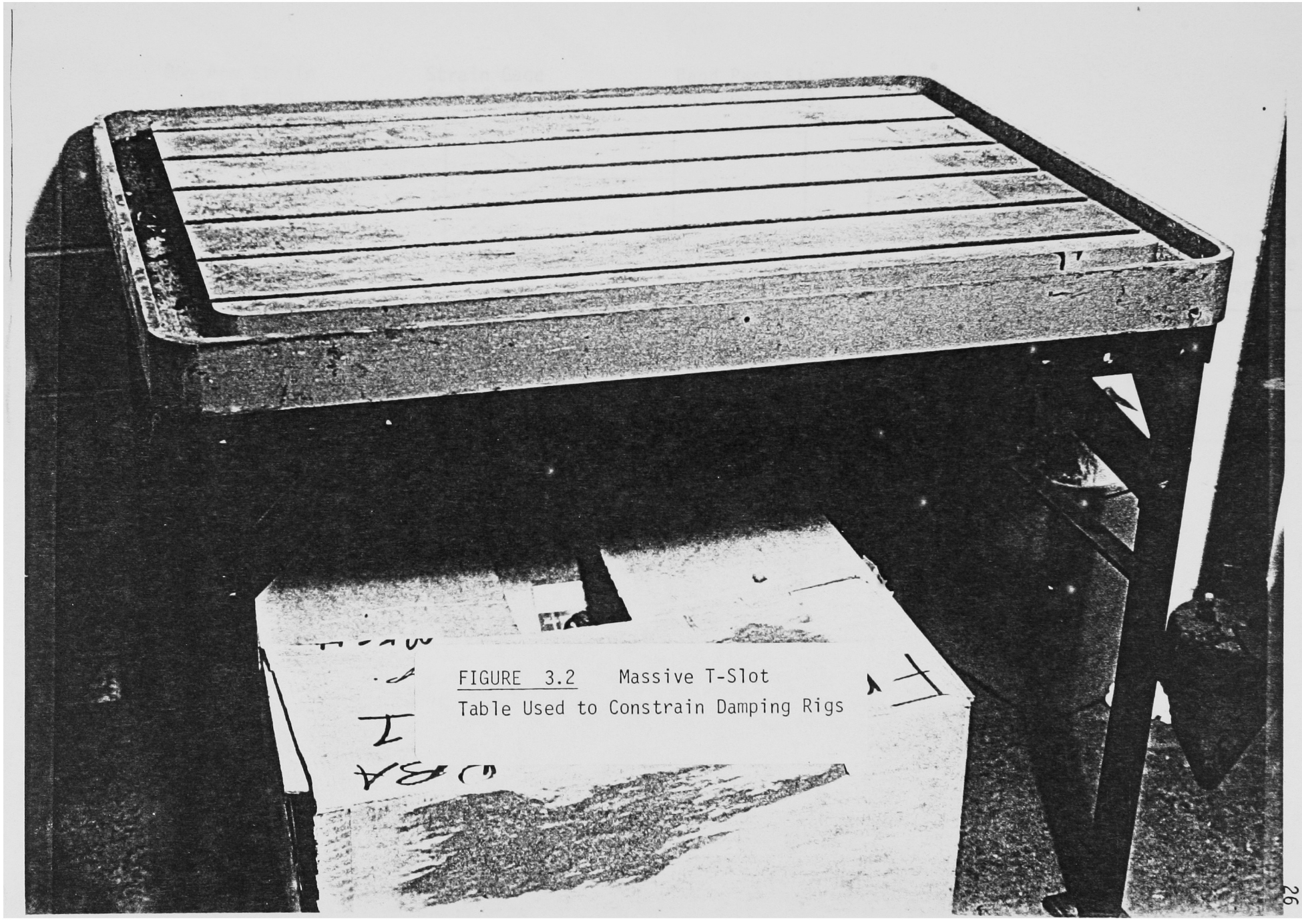

FIGURE 3.2 Massive T-Slot
Table Used to Constrain Damping Rigs

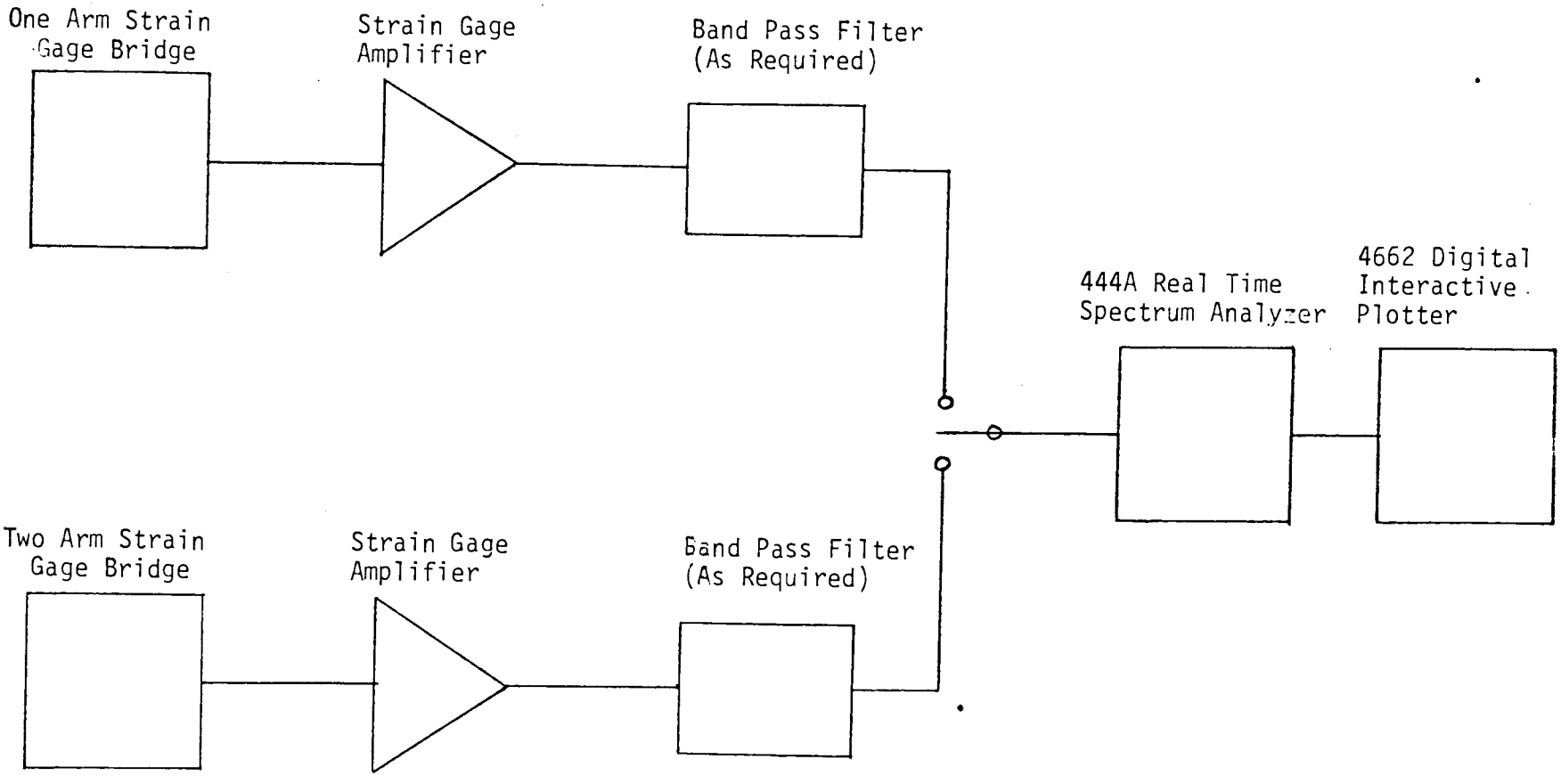

FIGURE 3.3 Schematic of Test Instrumentation

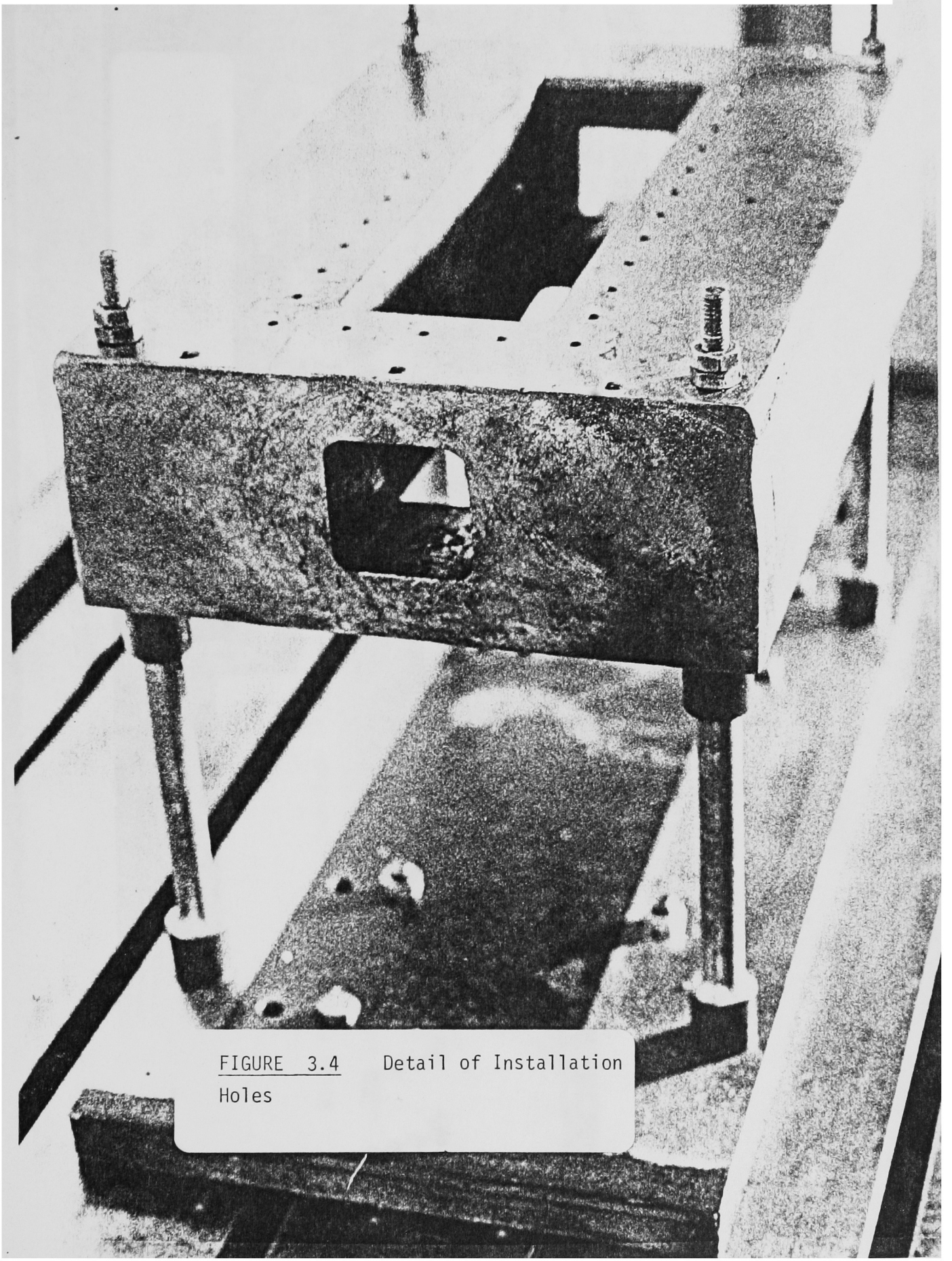

FIGURE 3.4 Detail of Installation Holes

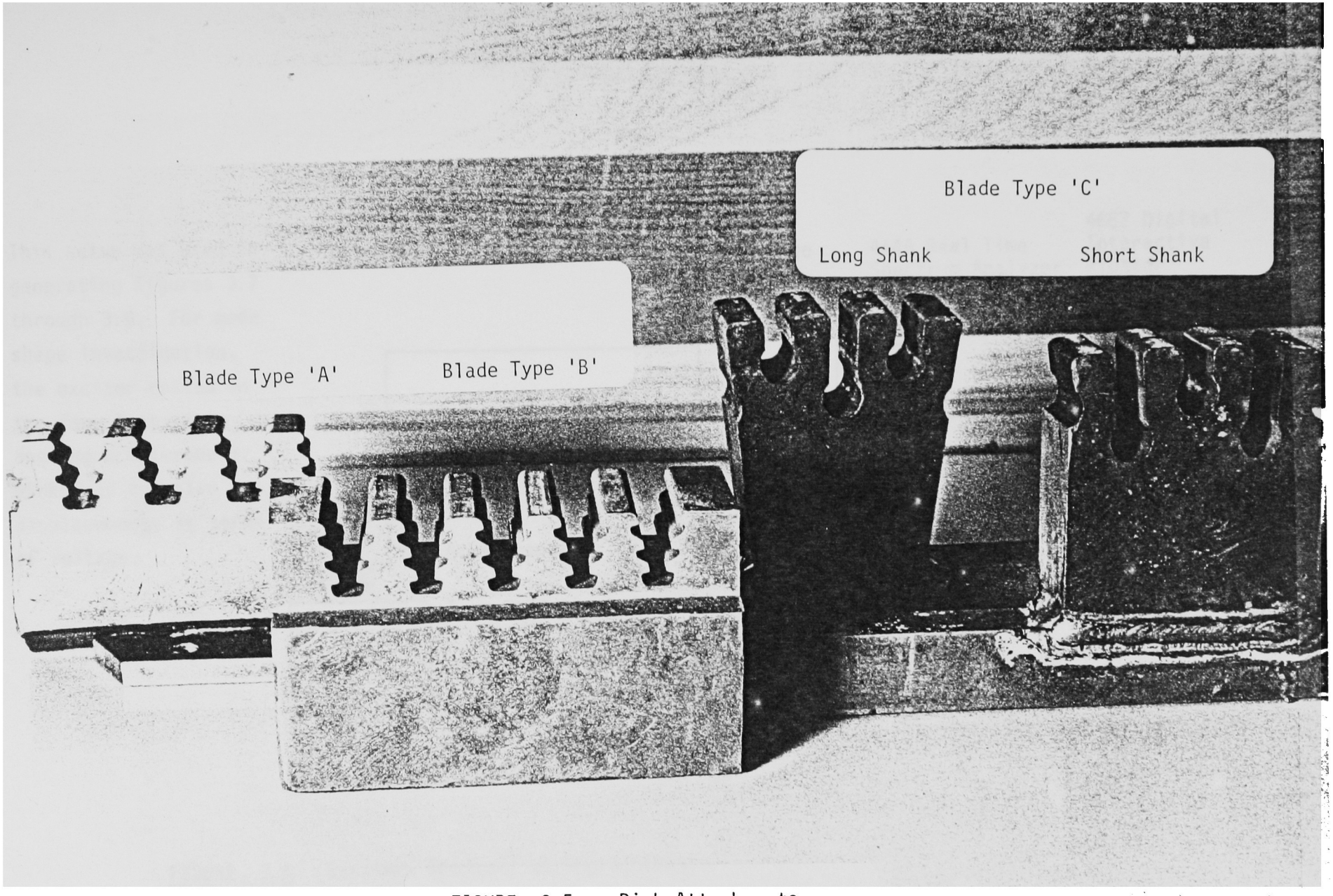

FIGURE 3.5 Disk Attachments

This setup was used in generating Figures 3.7 through 3.9. For mode shape investigation, the exciter rested on the four inch plate and the accelerometer picked up relative displacements in terms of voltage.

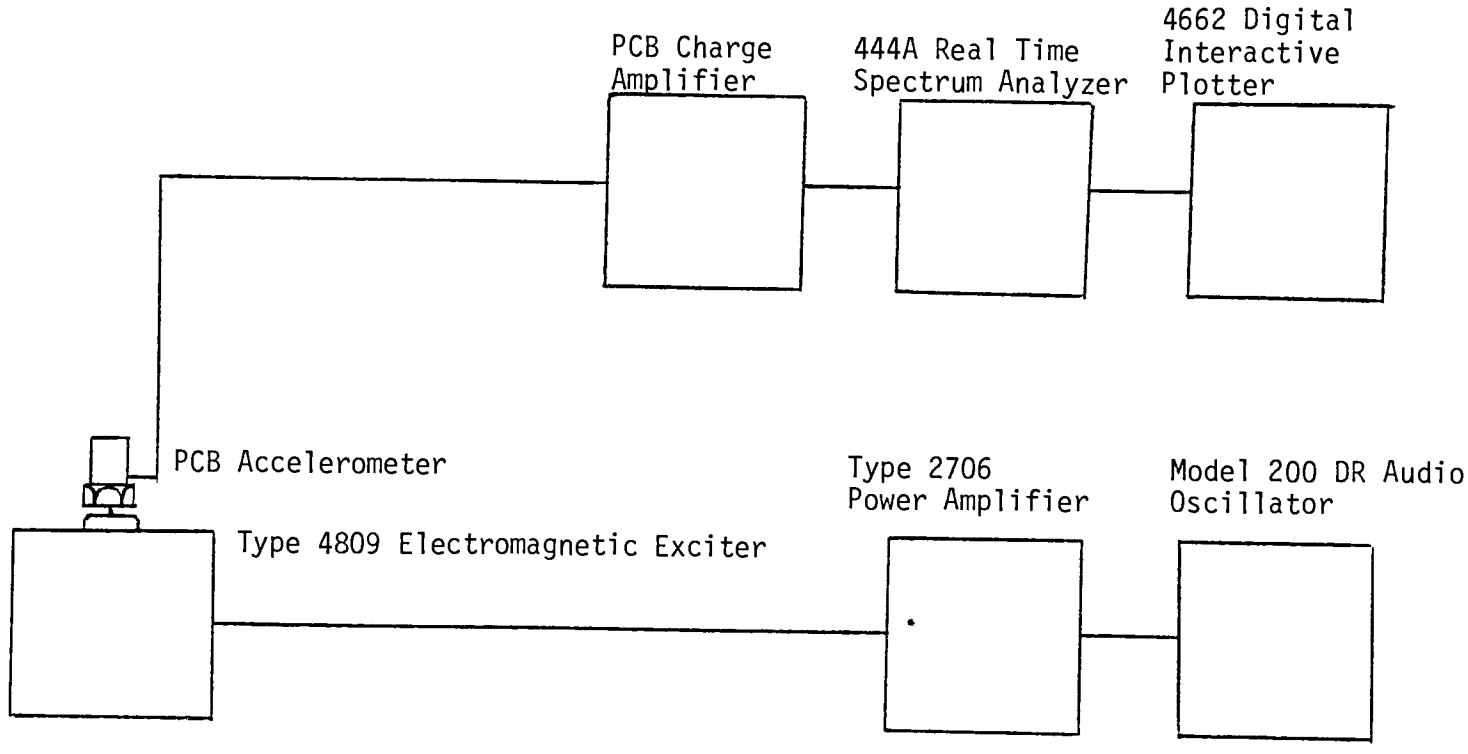

FIGURE 3.6 Exciter, Analyzer Wiring Schematic

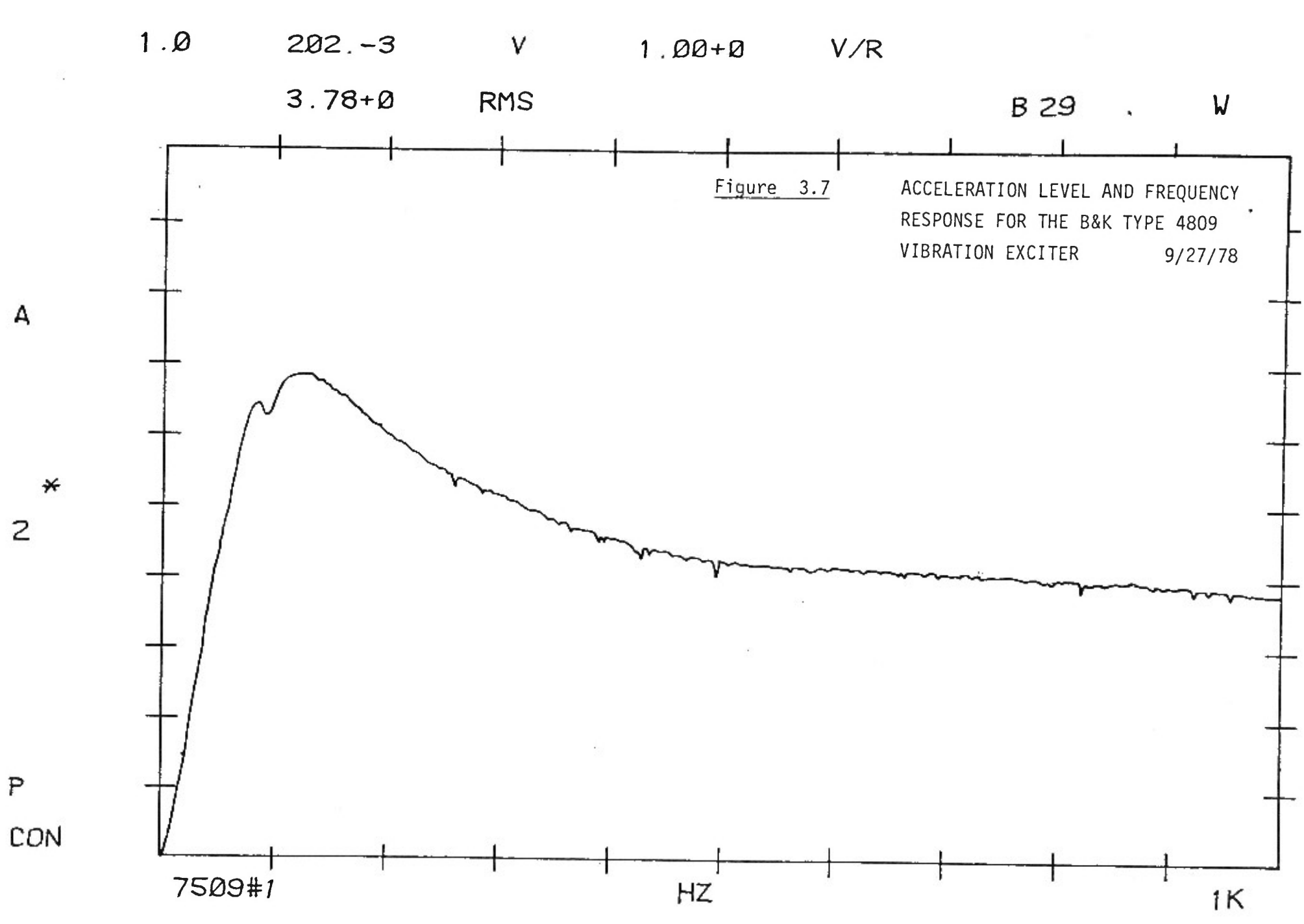

Figure 3.7 ACCELERATION LEVEL AND FREQUENCY RESPONSE FOR THE B&K TYPE 4809 VIBRATION EXCITER 9/27/78

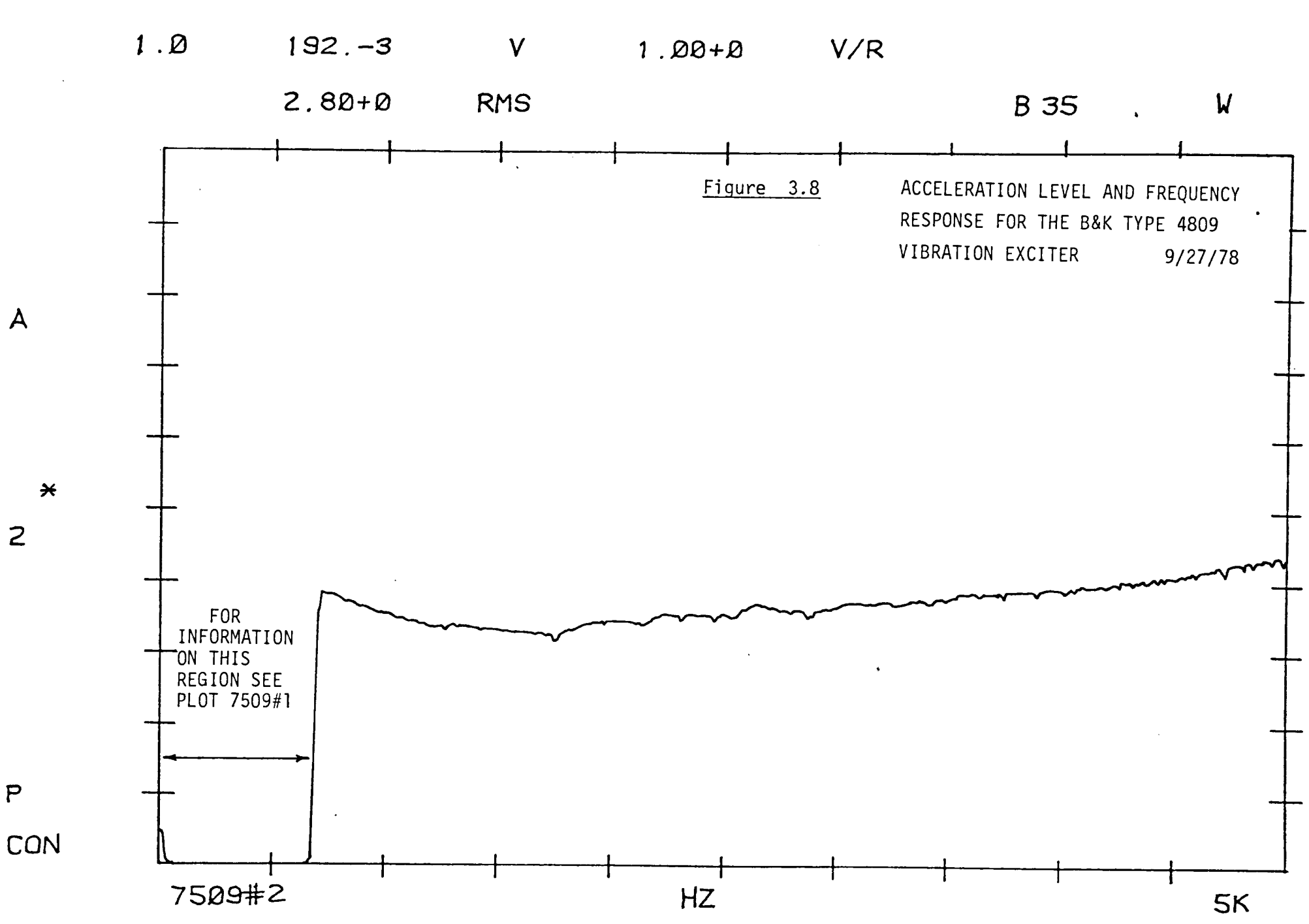
1.Ø 192.-3 V 1.ØØ+Ø V/R
2.8Ø+Ø RMS B 35 W
Figure 3.8
ACCELERATION LEVEL AND FREQUENCY
RESPONSE FOR THE B&K TYPE 4809
VIBRATION EXCITER 9/27/78
A
*
2
P
CON
FOR
INFORMATION
ON THIS
REGION SEE
PLOT 7509#1
7509#2
HZ
5K

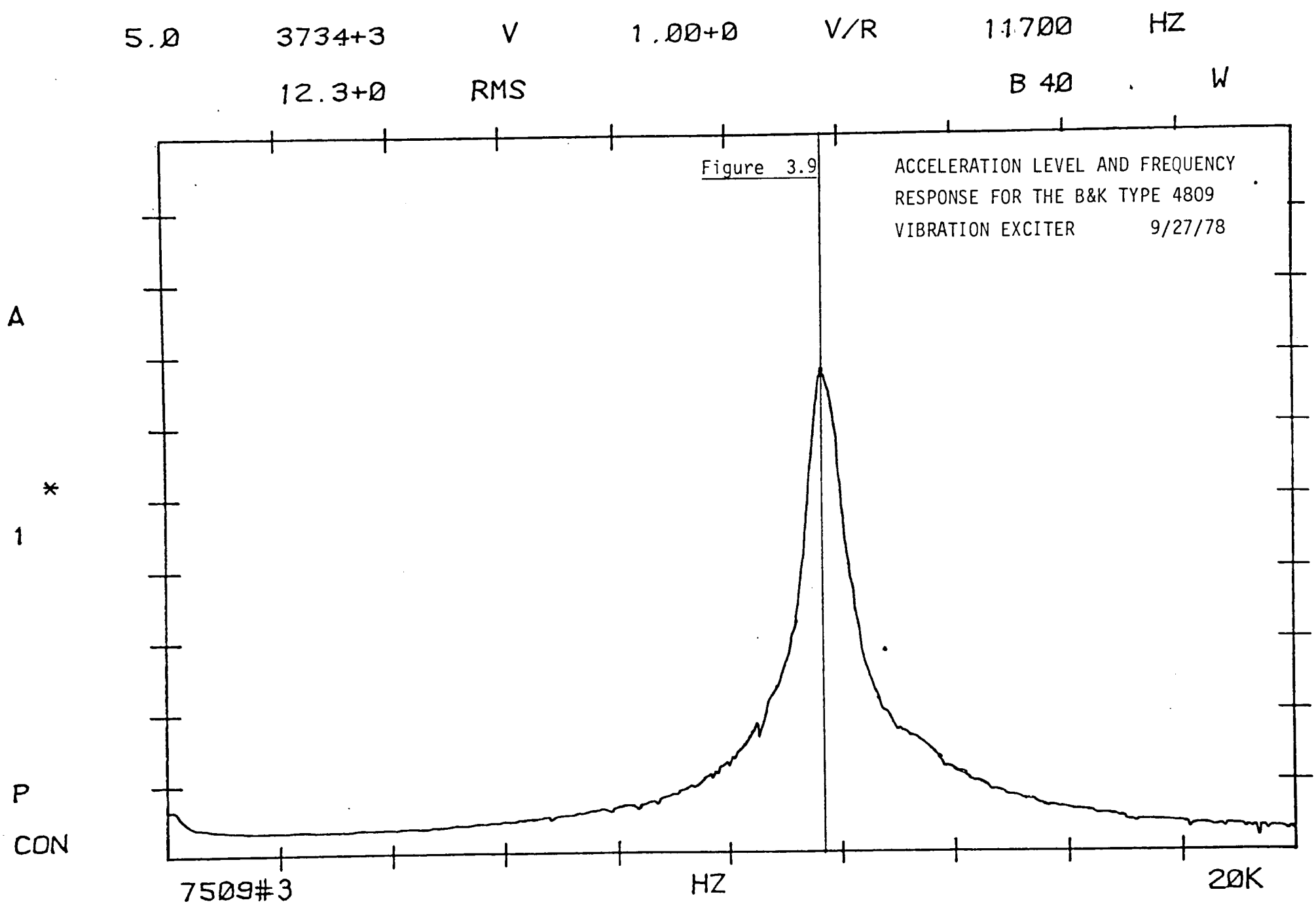
5.Ø
3734+3
V
1.ØØ+Ø
V/R
11.7ØØ
HZ
12.3+Ø
RMS
B 4Ø
W
Figure 3.9
ACCELERATION LEVEL AND FREQUENCY
RESPONSE FOR THE B&K TYPE 4809
VIBRATION EXCITER 9/27/78
A
*
1
P
CON
7509#3
HZ
2ØK

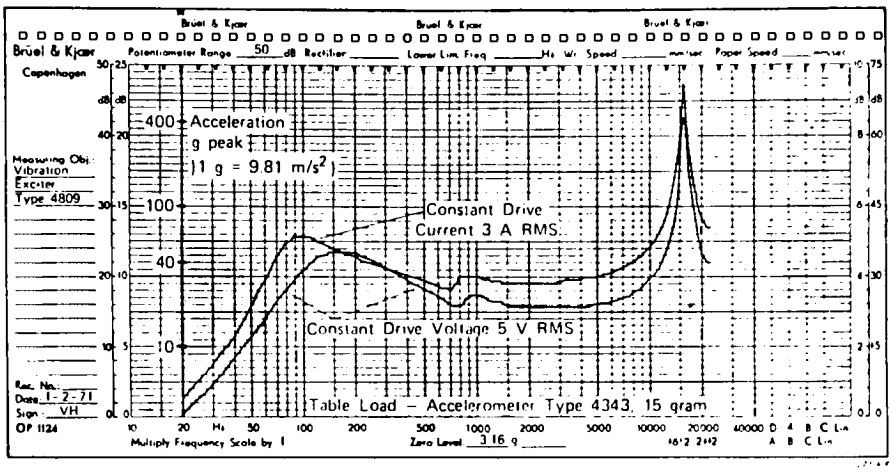

(a) Constant voltage and constant current frequency response of Vibration Exciter Type 4809

Specifications 4809

Rated Force:
44,5 Newton, 10 lbf Sine Peak
(60 Newton, 13,5 lbf with air cooling)

Frequency Range:
10 Hz to 20 kHz Bare table

Axial Resonent Frequency:
20 kHz Bare table

Maximum Bare Table Acceleration:
736 m/s² (75 g)
(1000 m/s², 100 g, with air cooling)

Maximum Displacement:
8 mm (0,315 in) peak-to-peak

Maximum Velocity:
1,65 m/s (65 in/s) peak

Dynamic Weight of Moving Element:
60 gram (0,132 lb)

Dynemic Flexure Stiffness:
12 Newton/mm (69 lb/in)

Maximum Input Current:
5 A RMS
(7 A RMS with air cooling)

Coil Impedance:
2 Ω at 500 Hz

Strey Magnetic Field:
20×10^{-3} tesla at table face
8×10^{-3} tesla at 12,7 mm (0,5 in) above table face

Teble Size:
29 mm (1,14 in) diameter

Fastening Threed:
10—32 UNF

Totel Weight:
8,3 kg (18,3 lb)

Dimensions:
Diameter: 149 mm (5,87 in)
Height: 143 mm (5,63 in)

(b) Numerical Specifications

Figure 3.10 Manufacturers Specifications for B&K Type 4809 Vibration Exciter

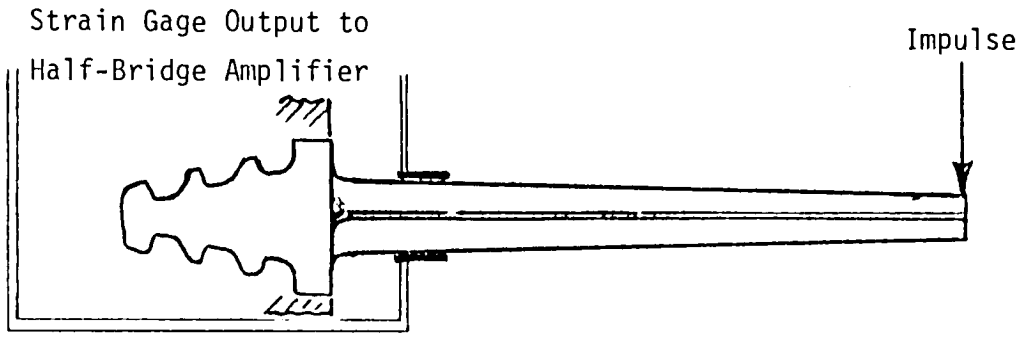

a) Excitation in Blade Tangential Direction

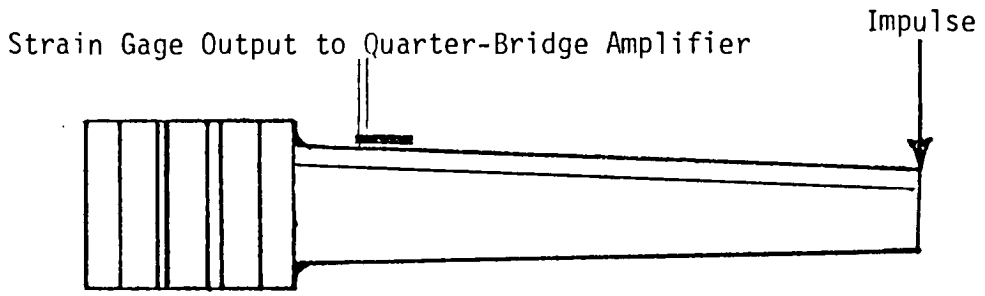

b) Excitation in Blade Axial Direction

FIGURE 3.11 Relationship Between Impulse Direction and Strain Gage Connections For All Blade Tests

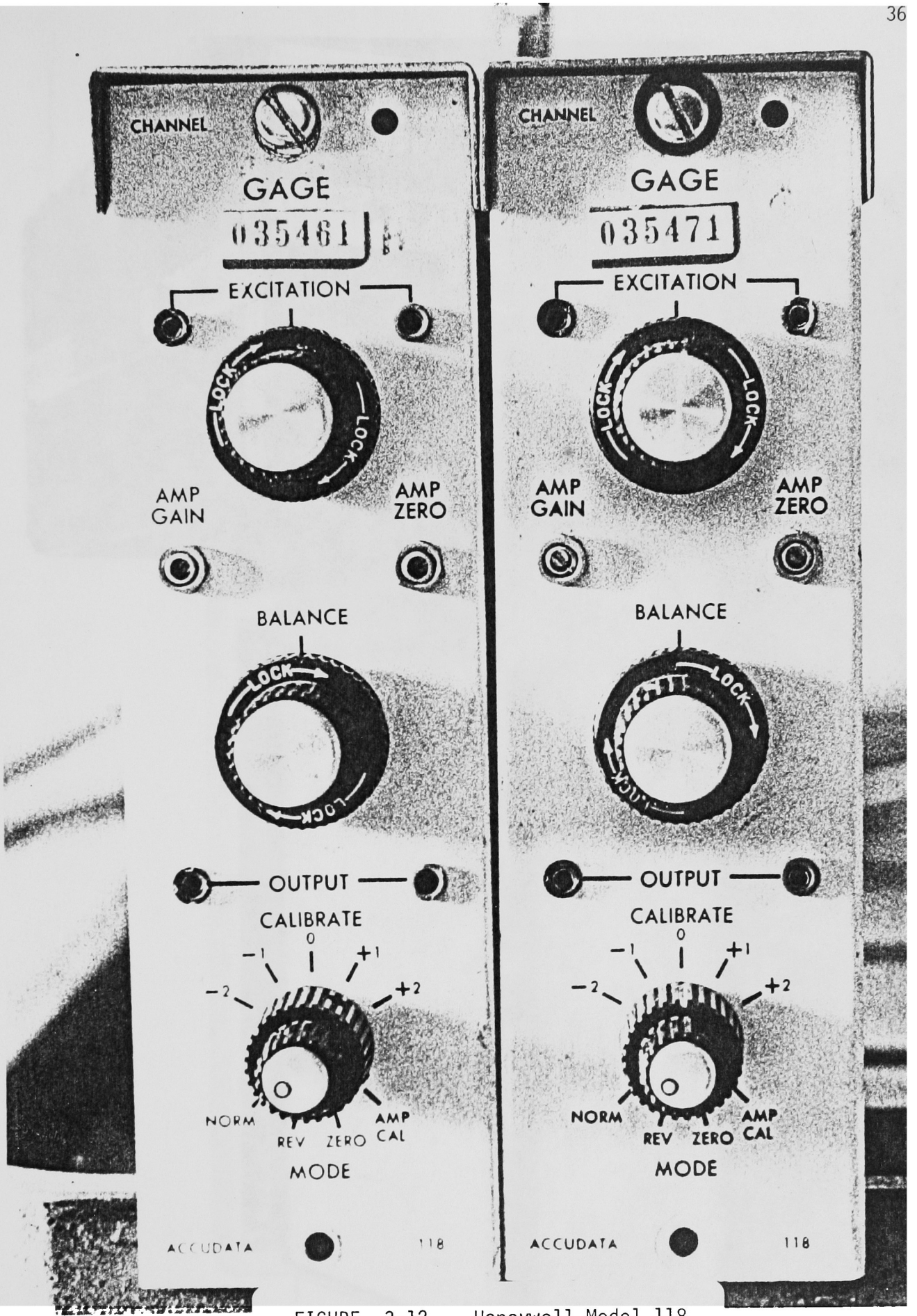

FIGURE 3.12 Honeywell Model 118 Strain Amplifiers

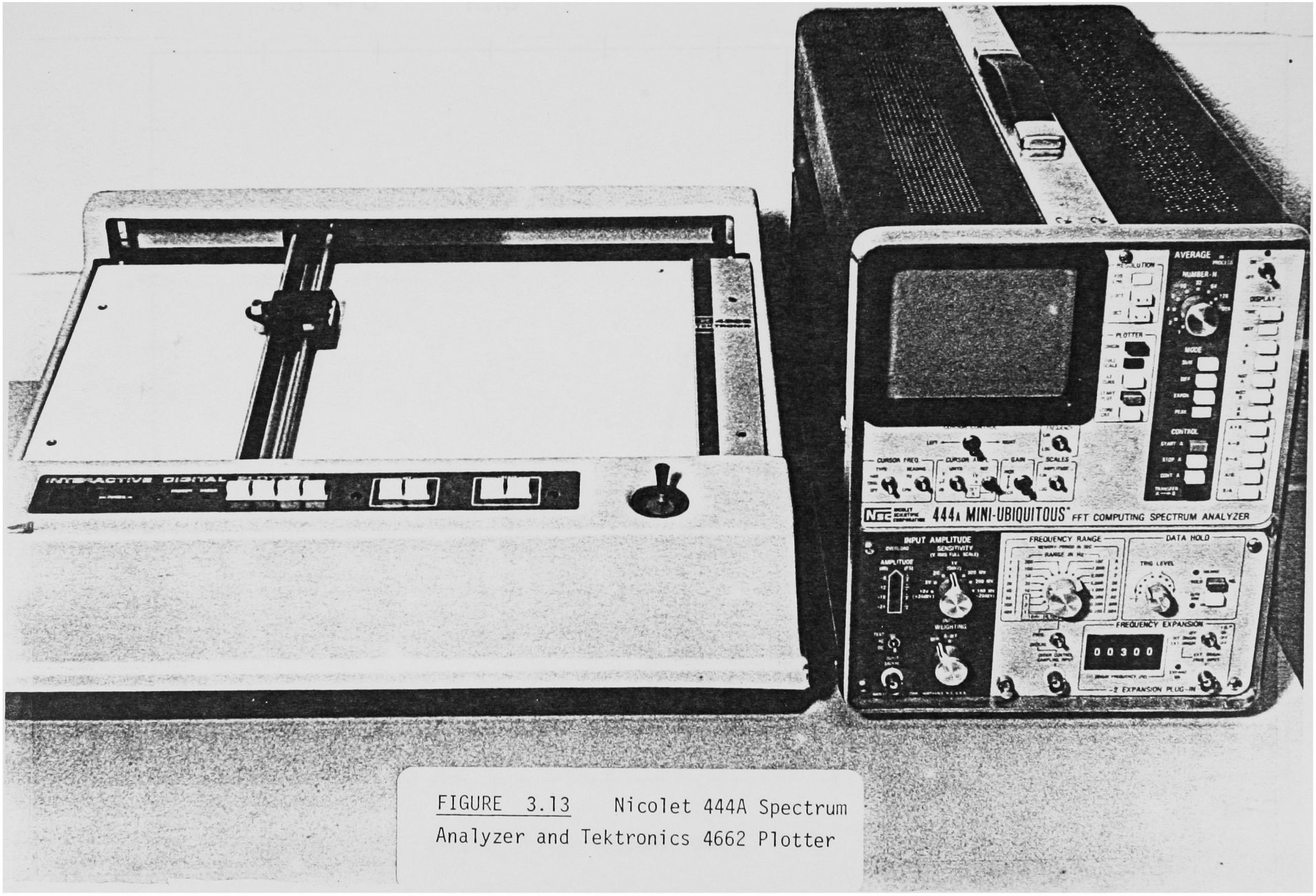

FIGURE 3.13 Nicolet 444A Spectrum Analyzer and Tektronics 4662 Plotter

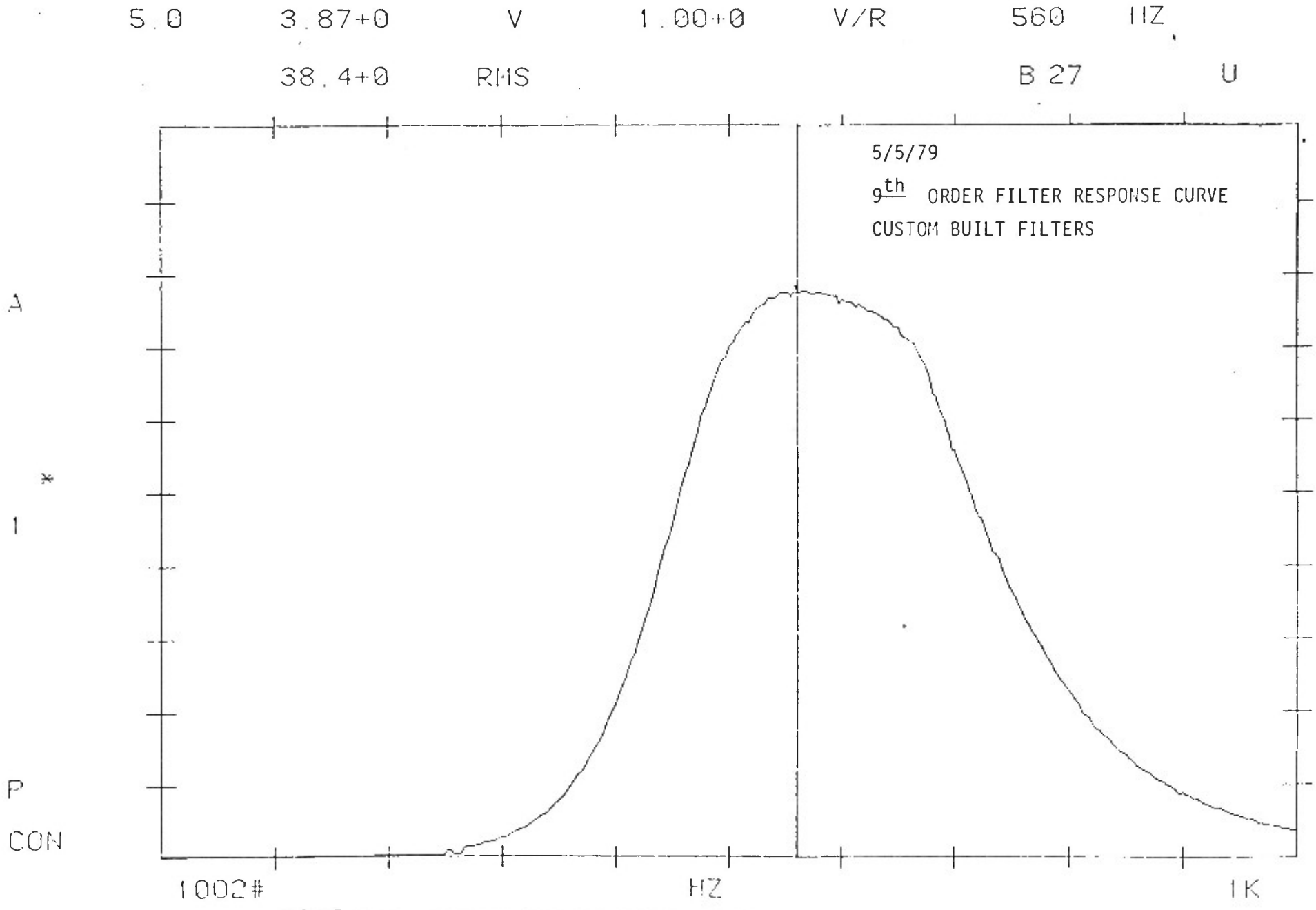

FIGURE 3.14 Typical Filter Response Curve

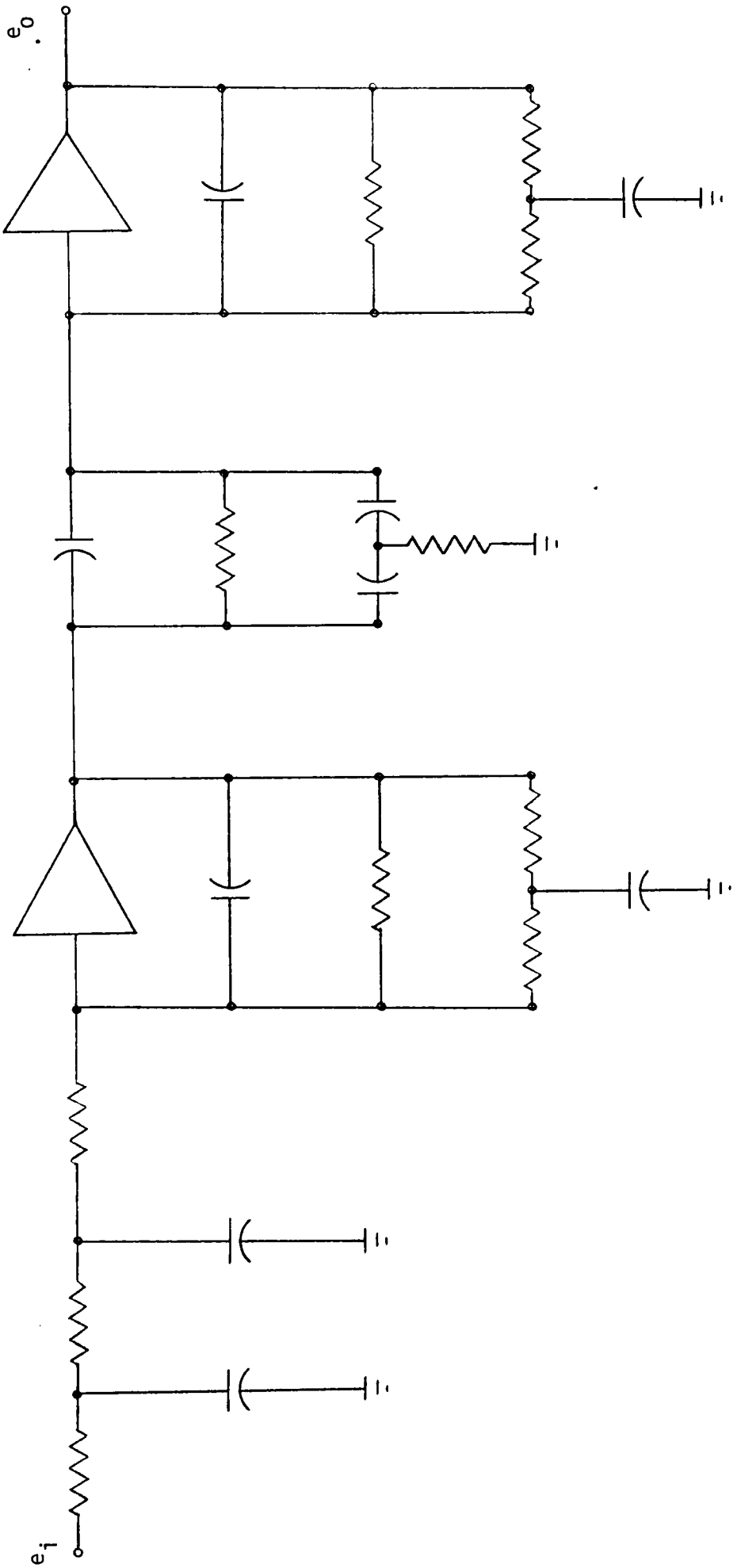

FIGURE 3.15 Schematic of Typical Butterworth Filter

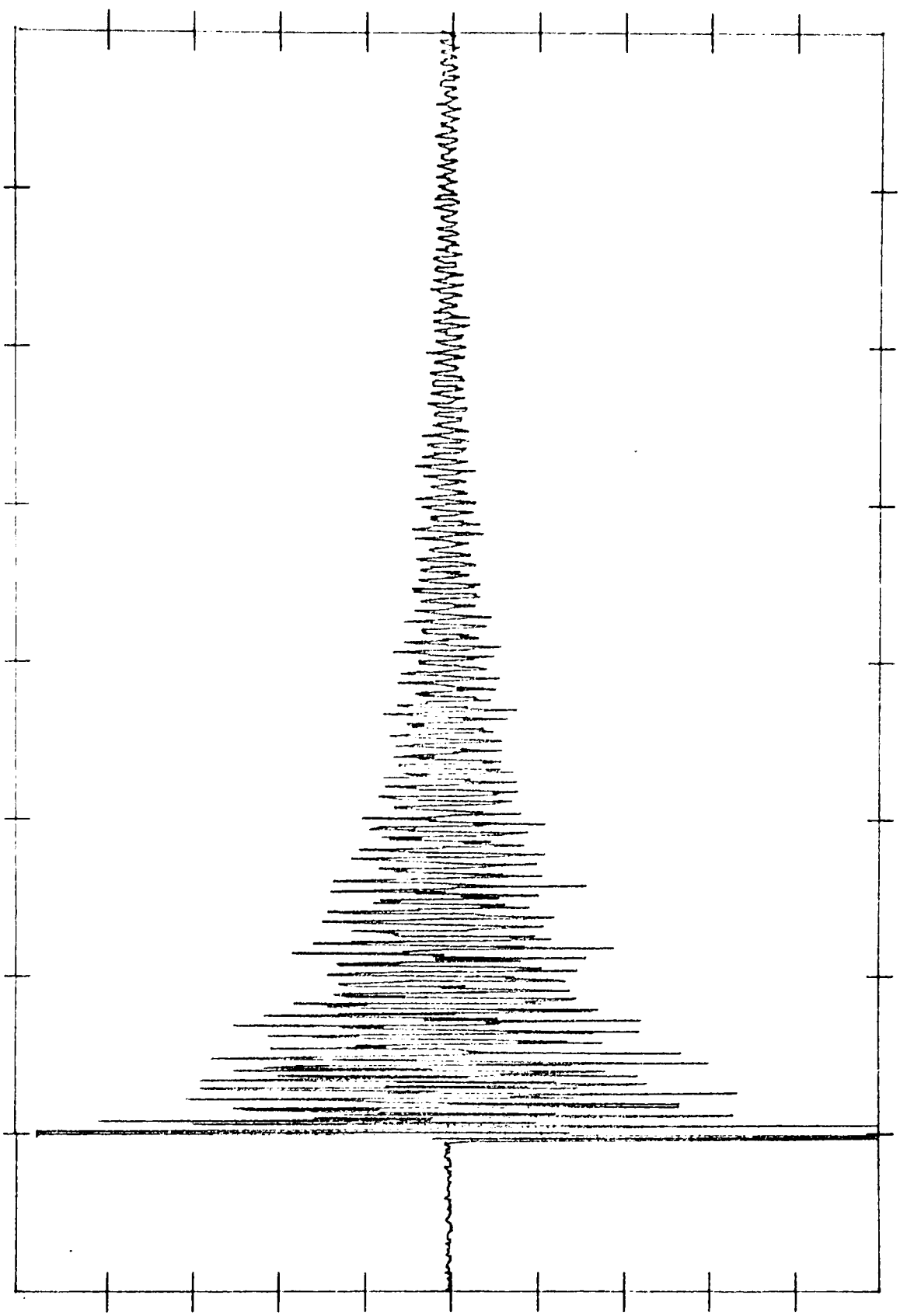

FIGURE 3.16 Typical Vibration Decay Trace Before Filtering

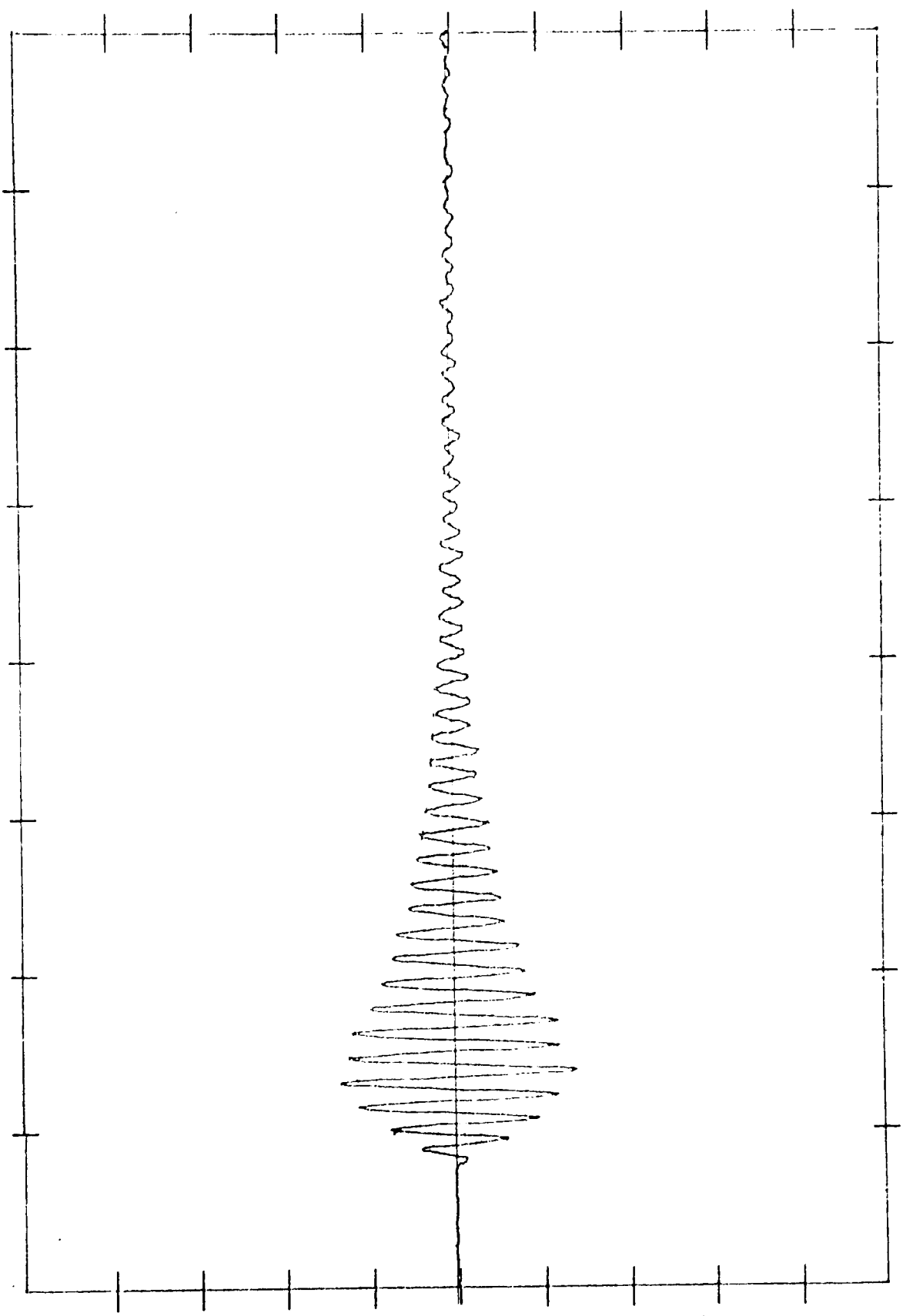

FIGURE 3.17 Typical Vibration Decay Trace After Filtering

4. NATURAL FREQUENCY DETERMINATIONS AND FINITE ELEMENT ANALYSIS OF TEST RIG DYNAMICS

4.1 General

Natural frequencies of each of the three blade types were determined in a zero-RPM bench test on a single, free-standing blade. The resultant frequencies were then used for a computer design of each respective blade group flexure link and blade damping rig. Computer analyses were performed to find the location of test rig natural frequencies and the mode shapes. Some preliminary calculations were made with the ANSYS Program, using 3D solid elements and beam elements for the blade Type A rig. The calculations described in this section cover all three test rigs. These calculations were all made using the SAP IV Program. Experimental measurements of natural frequencies and mode shapes were obtained for the Type A and Type B test rigs, both with and without the test blade pair included. These experimental results were successfully correlated with the computer results. This correlation showed that:

a) Blade group natural frequencies were very close to those experimentally determined through the use of computer design of the flexure links.
b) Calculated damping rig natural frequencies correlate well with experimentally determined frequencies.
c) For the frequency range in which the blade damping rig operates, no significant coupling occurs between the rig modes and the blade pair modes.
d) In the range of blade damping rig operation, no mounting table modes coupled with the blade pair modes.
e) The performance described in (b) and (c) was observed both for six-inch legs and seven-inch legs in the test rig.

4.2 Single Blade Tests

In the cases of blade Types A, B, and C, the blades were held in the vise of a massive Bridgeport vertical mill. The methods of clamping the blades are shown in figure 4.1 (a) and (b). The blades were not mounted in their respective disk segments at this time because the high damping in the root

at zero-RPM due to the lack of hook loading would have significantly lowered the blade natural frequency. The findings are concurrent with reference [15]. The manner of clamping the blades gave the root stiffness similar to that which it would see somewhere in its operating speed range. Strain gages were mounted to measure vibration in the tangential direction, as this is the direction of the lowest N.F. Each blade was impulsed in its tangential direction at the blade tip to ensure mode 1 vibration.

Figure 4.2 is the plot of the spectral analysis of the vibration of blade, Type A. The location of the spike indicates that the tangential mode 1 frequency is 360.0 Hz. Previous work with this blade Type by Rieger [12] has shown the mode 1 natural frequency of a six blade group to be 345.3 Hz at operating speed. Accounting for the increase in stiffness obtained by removing the cover/tenon mass from the blade tip, the blade natural frequency would increase slightly. It is therefore felt that this clamping method is suitable for this type of natural frequency determination.

Figure 4.3 is the plot of the spectral analysis of the vibration of blade Type B. In this instance the tangential mode 1 frequency is 196.25 Hz. This is a reasonable number since Type B blades are longer, tapered, and in general more flexible than Type A blades.

Figure 4.4 is the plot of the spectral analysis of the vibration of a long shank, Type C blade, Note the width of the base of the natural frequency spike around 585.0 Hz. This indicates that there is a larger degree of damping than in the previous two blade types, as can be seen by comparison. This fact is explicable by referring to figure 4.1 and noticing the larger clamping surface area used in holding blade Type C as opposed to the relatively small clamping areas used to hold blade Types A and B.

Since the clamping techniques used approximates the stiffness each blade sees at operating speeds, it was expected that blade Type C would show the highest logarithmic decrement of the three blade types tested. This observation was borne out when damping test data was analyzed. The obvious

problem at this point is that blade Type C has two different shank lengths. This means that at any condition other than a total blade root lock-up at high speed, or a welded condition for bench testing, there will be a different natural frequency for each shank type due to different stiffnesses. Since only one rig and flexure link design were to be used, it was assumed that the 585 Hz was a representative frequency value.

4.3 Finite Element Analysis of Rig Type A

Three finite element models were developed. Model A.1 consisted of 18 three-dimensional beam elements, each of which elements had tension, torsion, and bending analysis capabilities. Twelve additonal beam elements were used to model the four, six-inch legs which support the rig frame, figure 4.5. Model A.1 represents the rig without the blade pair. Model A.2 incorporates the blade pair under test. The blade pair is represented by twelve additional beam elements. These twelve elements incorporate refinements made to the blade pair model used in initial calculations. Model A.3 is similar to A.2 except that the legs were lengthened from six inches to seven inches. All three models for blade Type A thus excluded any effects arising from the mounting table.

4.3.1 Results for Model A.1

Table 4.1 is a summary of the natural frequencies of the rig without the blade pair. Modes 1, 2, 6, 7, and 8 have experimental results but no computer results. This is because these modes represent mounting table modes which are not included in the computer model. Mode 3 has the rig vibrating as a rigid body against its legs in the y-y direction, for which there was no experimental value because no accelerometer readings were taken in the y-y direction. This was not necessary since extensive readings were taken in the x-x and z-z directions. From examination of the table, it is seen that no rig or mounting table natural frequencies are found in the region of 360 Hz. Figures 4.6 through 4.11 show the computer results for the damping rig on its supports without the blade pair.

4.3.2 Results for Model A.2

Table 4.2 is a summary of the natural frequency results of the rig mounted on six-inch legs with the blade pair included. Again, there are some modes (1, 5, 7, 8) which have experimental results but no computer results, for the same reason as explained above. Mode 2 consists of the rig vibrating as a rigid body against its legs in the y-y direction, and has no experimentally determined value, as explained in Model A.1. Modes 11 and 13 are uncoupled blade modes which were not found experimentally because they were out of the frequency range of interest. In the region of interest around 360 Hz, no rig or mounting table natural frequencies were found. Only the first z-z blade mode exists. Figures 4.12 through 4.21 show the calculated rig modes for this case.

4.3.3 Results for Model A.3

Table 4.3 gives the computer results for this case. It can again be observed that in the region around 360 Hz, no rig natural frequencies are present. The mounting table natural frequencies remain nearly constant as given in Table 4.2. It can therefore be concluded that either six-inch or seven-inch legs would be suitable for the rig. Figures 4.22 through 4.31 show the computer results for this case.

4.4 Accelerometer Correlation of Test Rig A Dynamics

As mentioned in the previous sections, and as listed in Tables 4.1, 4.2, and 4.3, experimental frequency analysis of test rig A was conducted. These results were compared to computer predictions to satisfy one of the original project objections: rig design by finite elements.

Rig natural frequencies were located by impulsing the rig with a hammer and monitoring the vibration with an accelerometer and a spectrum analyzer. Figure 4.32 shows the respective locations of the accelerometer and applied force as well as the I.D. numbers of the corresponding spectral analysis plots, figures 4.33 to 4.37 for model A.1.

Once the natural frequencies were found, the associated mode shapes had to be identified. An electromagnetic shaker was placed on the rig and controlled via an oscillator and power supply. The shaker was set for a

given natural frequency, as determined in the above procedure and monitored by the spectrum analyzer through the accelerometer. By noting the output voltage of the accelerometer as it was moved from one location on the rig to another, respective displacements could be established. Plotting the magnitudes of these displacements gave the mode shape associated with the exciting frequency. It should be noted that if the accelerometer was placed on a node there was a 1000X decrease in output voltage. For test rig A as many of the natural frequencies were investigated as reasonably possible. In further tests (Types B and C), only the modes near the test frequencies were investigated.

Figure 4.38 is the portion of the data log generated when correlation of model A.1 was undertaken. No blades are installed and the legs are six inches long. Data was obtained for correlation of models A.2 and A.3 but is not presented here as it is an additional 18 pages of figures.

4.5 Type A Flexure Link Design

After the correlation was completed for model A.1, model A.2 was built to determine flexure link dimensions. It was known that no rig natural frequencies existed around 360 Hz, and the addition of the blade pair was not expected to change this. The flexure link had to be designed such that; (a) blade natural frequency would be near 360 Hz, (b) the blades would vibrate in their plane of least stiffness, (c) the link cross-section could carry the applied load, and (d) the link flanges were large enough to overlap the airfoil periphery for welding purposes.

The required dimensions of the flexure link for the Type A blades were determined using the finite element program, SAP IV. From previous experimental work, the first natural frequency of the blade group was known to be approximately 360 cycles/sec. The flexure link dimensions were varied until the blade pair and flexure link combinations gave the required 360 cycles/sec in its first vibration mode. The blade pair/flexure link combination was modeled without the damping rig for these calculations, since the computer studies reported earlier have shown that no interaction occurred between the first blade-pair mode and

and the rig rigid body modes. Each end of the blade pair was considered to be built-in (clamped) at the level of the first hooks. The model was constructed using a total of ten beam elements (four for each blade and two for the flexure link), using specified material and geometry properties for the blades and flexure link. The orientation of the flexure link was such that its plane of least stiffness was parallel to the plane of least stiffness of the blades. This orientation agreed with calculations and test data on the Type A blade group. A sketch of the flexure link is shown in figure 4.39.

The accuracy of the model was felt to be quite good, based on comparable results obtained with a simple beam model with a rectangular cross-section. Ten beam elements were used in this case, and comparison to theory indicated less than one percent error existed with classical analysis results for the first three modes. The enclosed sketch shows the final dimensions for the Type A flexure link. When these blades were subsequently tested in the rig, an average first natural frequency of approximately 360 cycles/sec. for the blade pairs was found, as desired.

Computer and experimental analyses have been performed on the Type A blade damping apparatus. From these analyses it has been shown that no coupling exists between the test rig and the mounting table natural frequencies, nor between the rig and the first bending mode of the blade pair in the z-z direction. It has also been shown that both six-inch and seven-inch legs will achieve this desired decoupling.

4.6 Finite Element Analysis of Rig Type B

Three finite element models were developed. Model B.1 consisted of 18 three-dimensional beam elements, each of which had torsion, tension, and bending analysis capabilities. Twelve additional beam elements were used to model four, seven inch legs which support the frame. The second model incorporated two additional legs located midspan along each side column. A copy of the computer printout for the second model's mode shapes and natural frequencies is given in figure 4.40. A third model incorporated a blade group composed of 19 additional beam elements. A schematic is shown in figure 4.41. The third model was used to determine flexure link dimensions.

4.7 Accelerometer Correlation of Test Rig B Dynamics

In depth accelerometer tests such as those done for Test Rig A were not done for Test Rig B, since the original computer design objective had already been achieved. Figures 4.42 through 4.49 are copies of data log entries correlating computer predictions and experimental tests. Once again, the correlation is quite good.

4.8 Type B Flexure Link Design

Since the Type A flexure link design was successful using the tangential mode 1 natural frequency, it was decided to achieve similar success using the axial mode 1 natural frequency for Type B flexure link design. First, the blade natural frequencies were measured experimentally. This test gave the required natural frequencies which the flexure link was required to achieve. Second, a finite element beam model of a single Type B blade was constructed and calculated, using the finite element program, SAP IV. This model was then refined to correlate its natural frequencies with experimental results for a single blade. Lastly, a blade pair with flexure link was modeled with finite elements, and the cross-sectional properties of the flexure link were changed until the desired natural frequency of the blade pair was obtained.

For design purposes, information was required on Type B blade natural frequencies and, more importantly, on the blade group natural frequencies in the turbine during operation. Unlike the Type A design, information on these parameters was not available. The following procedure was used.

First, the root section of a single blade (without tenon or cover, Section A-A, figure 4.50), was removed at the first hook level and a steel block was welded in place of the removed root, as shown. This enabled the block to be clamped tightly in a vise, leaving the platform free to move. This was an effective means of modeling the case of a free blade in a turbine. The blade was then struck, and the first axial natural frequency was found to be 215 cycles/sec., using the Nicolet Spectrum Analyzer (see Table 4.4). This frequency is lower than that of the blade group because in practice, the

net effect of the cover at the blade tip causes an overall increase in structural stiffness. The blade group natural frequency was, therefore, assumed to be 105 percent of the single blade natural frequency, and was calculated to be 225 cycles/sec. Also, the natural frequencies calculated by the finite element method are estimated to be about 10 cycles/sec. low when the effect of centrifugal stiffening is taken into account. Therefore, the value to be attained by the blade pair in combination with the flexure is 255 cycles/sec.

The final experiment was to obtain a value for the first natural frequency of a 9-inch long blade (measured from the bottom of the platform to a point approximately 1/2 inch from the tip of the blade, Section B-B, figure 4.50). This was required because the blades in the damping rig were designed for this length after tip machining, and correlation with the finite element model was required (see Table 4.4). The frequency obtained for this case was 262.5 cycles/sec.

4.8.1 Blade Models

Model 1. A single 9-inch blade was modeled using seven beam elements whose section properties were specified individually. The properties found for each section included the location of the centroid, the orientation of the plane of least stiffness, the principal moments of inertia, torsional stiffness, and the cross-sectional area. The platform was not taken into account, but instead, the last section was extended to the top of the root where it was considered to be rigidly clamped. Figure 4.51 shows the location of each section axially, while figure 4.52 shows each corresponding cross-section. Results from this model yielded a first natural frequency of 199.7 cycles/sec. and the mode shape shown in figure 4.53. This result was low compared to that predicted experimentally, so the model was revised.

Model 2. A separate section was used for the blade platform to make the model more accurate. The cross-sectional properties were determined for the rectangular section and included in the model. Results, figure 4.54, showed a first natural frequency of 239.8 cycles/sec., which indicated that further revision of the model was needed.

Model 3. The cross-sectional areas were recalculated and were found to be slightly lower than those originally calculated. The effect of this was to increase the first natural frequency to 264.5 cycles/sec. This agrees to within 0.8 percent of the experimental value. The mode shape (not shown) is very similar to figure 4.54. As a further check of the model, the amount of mass removed from the blade in proceeding from Section A-A to Section B-B in figure 4.50, was determined and added to the blade model at the extreme end node point. Results from this calculation showed a first natural frequency at 220.7 cycles/sec., which compares to within three percent of the experimental results and the correlation with the finite element model developed for this case.

The blade pair flexure link construction and orientation is shown in figure 4.55. The overall length from platform bottom to platform bottom is 22.5 inches. Each blade is nine inches from the bottom of the platform to the flexure link face. The blades were modeled using the Type B blade model Number 3 from Section 4.8.1. The flexure link is composed of three beam elements and has the dimensions as shown in figure 4.55. Computer results for this case indicate a first natural frequency of 207 cycles/sec. The flexure link dimensions shown in figure 4.55 were used for the test of this case. Figure 4.56 is the shape of the first mode. Note that blade tip displacement is not purely in the 'y' direction, but occurs in the 'z' direction also. This is due to the extreme twist of the airfoil.

4.9 Blade Type C Calculations

No finite element calculations were made for either of the Type C blades, long shank or short shank. No test data was available on the blade group natural frequencies to guide these calculations. Although zero rpm bench testing of a blade was performed, the relation between the zero rpm frequencies and running-speed range frequencies was uncertain because of the type of the blade root design involved, figure 3.5. The flexure link was, therefore, proportioned from the two previous flexure link designs. The resulting natural frequencies were expected to correspond to the middle-speed range frequency values in the turbine. This also corresponds to the maximum axial load values used to design the flexure link cross-section.

However, finite element calculations were done for the rig without a blade pair installed. The model used is shown in figure 4.57. Computer results are listed in figure 4.58. The tangential natural frequency from the bench test (fig. 4.4) is 410. Hz. Comparing this frequency to the tangential frequency obtained during testing [data sheet 5.3.3] shows the flexure link design worked well. Similar correlation is also true in the axial direction. Comparison of figures 4.4 and 4.58 show a large 'dead' zone between blade testing frequencies and rig natural frequencies. A sketch of the flexure link is shown in figure 4.59.

4.10 Comments

a. The Type A, B, and C test rigs were designed so that no rig natural frequencies occurred within the frequency ranges of the blade pairs during testing. This ensured that the blade modes would be decoupled from the rig modes when the damping tests were performed.

b. Adequate correlation between test natural frequencies and calculated natural frequencies of the blade pairs was achieved for design requirements in all cases.

TABLE 4.1 Rig Type A Natural Frequencies Without Blades

Number	Natural Frequency ----Results (Hz)-------- Experimental	Computer	Percent Difference	Description
1	35	-	-	Mounting Table vibrating against its supports in z-z direction.
2	75	-	-	Mounting Table vibrating against its legs in x-x direction.
3	-	88.43	-	Rig rigid body mode vibrating against its legs in y-y direction.
4	90	88.86	1.3	Rig rigid body mode vibrating against its legs in x-x direction.
5	110	115.80	5.0	Rig rigid body mode rotation against its legs in the z rotational direction.
6	270	-	-	Mounting Table vibrating against its legs in the z-z direction.
7	465	-	-	Mounting Table in plane mode.
8	670	-	-	Mounting Table rocking against its legs in the z-z direction about the x rotational axis.
9	715	722.1	1.0	Rig rigid body mode vibrating against its legs in z-z direction with some mounting table interaction.
10	785	771.6	1.7	Rig rigid mode rocking against its legs in the z-z direction about the x rotational axis.
11	1035	1018.0	1.6	Rig rigid mode rocking against its legs in the z-z direction about the y rotational axis.

TABLE 4.2 Rig Type A Natural Frequencies With Blades (6 Inch Legs)

Number	Natural Frequency ----Results (CPS)------- Experimental	Computer	Percent Difference	Description
1	70	-	-	Mounting table vibrating against its legs in x-x direction.
2	-	84.55	-	Rig rigid body mode vibrating against its legs in y-y direction.
3	85	84.96	0.0	Rig rigid body mode vibrating against its legs in x-x direction.
4	100	108.9	8.2	Rig rigid body mode rotation against its legs in z direction.
5	270	-	-	Mounting table vibrating against its legs in z-z direction
6	347.5	344.3	0.9	Blade pair vibrating in the z-z direction.
7	465	-	-	Mounting table in plane mode
8	675	-	-	Mounting table rocking against its legs in the z-z direction about the x rotational axis.
9	710	700.4	1.4	Rig rigid body mode vibrating against its legs in z-z direction with some mounting table interaction.
10	780	771.6	1.1	Rig rigid mode rocking against its legs in z-z direction about the x rotational axis.

TABLE 4.3 Rig Type A Natural Frequencies With Blades (7 Inch Legs)

Number	Computer Results (CPS)	
1	73.49	Rig rigid body mode vibrating against its legs in y-y direction.
2	73.88	Rig rigid body mode vibrating against its legs in x-x direction.
3	95.01	Rig rigid body mode rotation against its legs in the z rotational direction.
4	344.2	Blade pair vibrating against its legs in the z-z direction.
5	668.7	Rig rigid body mode vibrating against its legs in z-z direction with some mounting table interaction.
6	737.5	Rig rigid mode rocking against its legs in the z-z direction about the x rotational axis.
7	886.3	Rig rigid mode vibrating against its legs in the z-z direction about the y rotational axis.
8	902.7	Blade pair vibrating in the y-y direction.
9	1150	Blade pair second harmonic in z-z direction with no coupling with damping rig.
10	1729	First in plane rig flexural mode.

TABLE 4.4 Blade Type B Experimental Results

Test Number	Blade Description	Support Conditions	Natural Frequency (cycles/sec)
1	Full blade without tenon. Section A-A,Figure 1A	Side by side, platform free	215
2	Full blade without tenon. Section A-A,Figure 1A	Side by side, platform free	214
3	Full blade without tenon. Section A-A,Figure 1A	Side by side, platform free	215
		Average	215
4	9 inch blade Section B-B,Figure 1A	Side by side, platform free	260
5	9 inch blade Section B-B,Figure 1A	Side by side, platform free	265
		Average	262.5

TABLE 4.5 Correlation Between Experimental and Finite Element Results.

Blade Description	Experimental Results	Finite Element Results		
		Model 1 (cycles/sec)	Model 2 (cycles/sec)	Model 3 (cycles/sec)
9 inch blade Section B-B,Figure 1A	262.5	199.7	239.8	264.5
	Percent Error	23.9	8.7	0.8
Full blade without tenon Section A-A,Figure 1A	215			220.7
	Percent Error			2.6

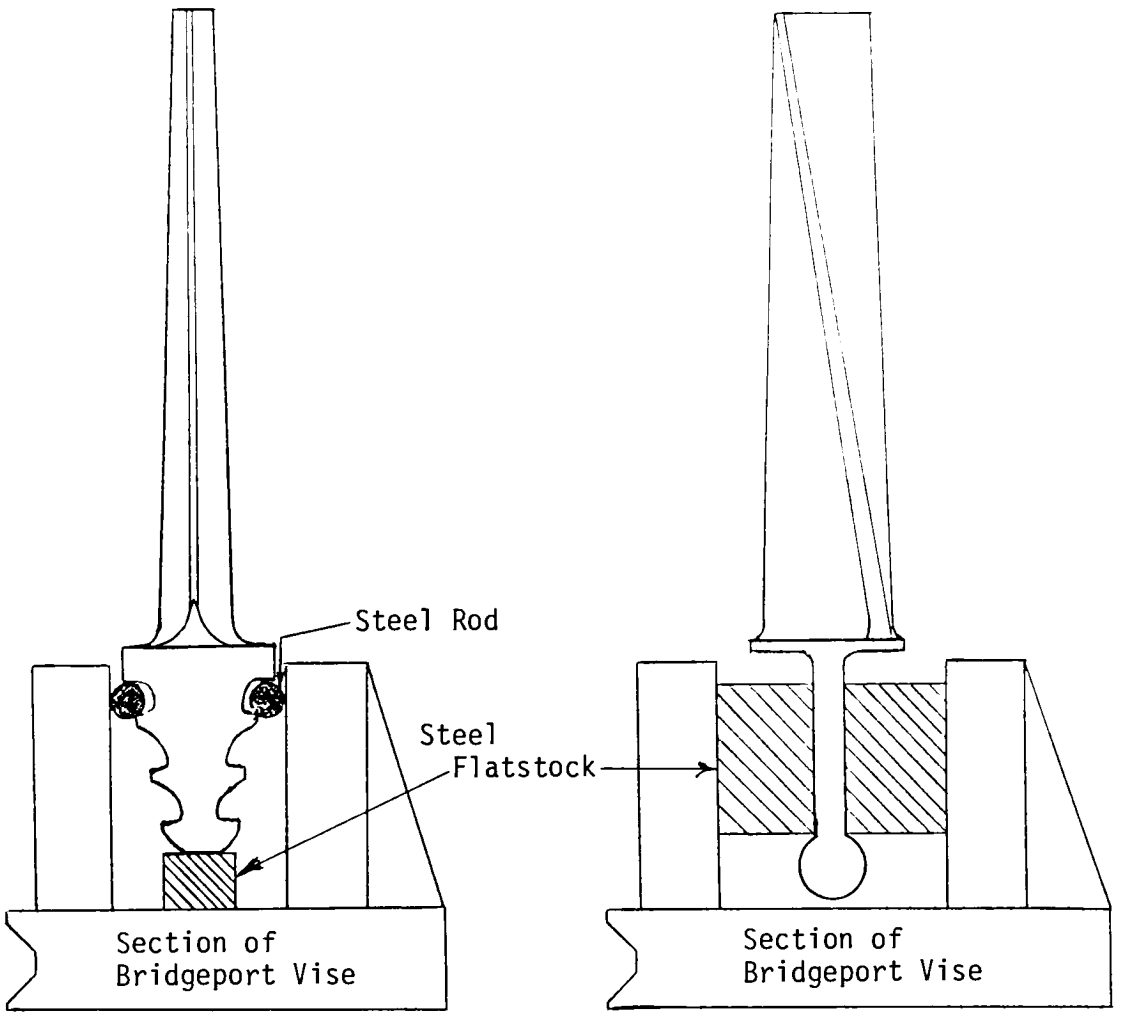

a) Blade Types A and B

b) Blade Type C, Long Shank

FIGURE 4.1 Clamping Methods for Single Blade Tests

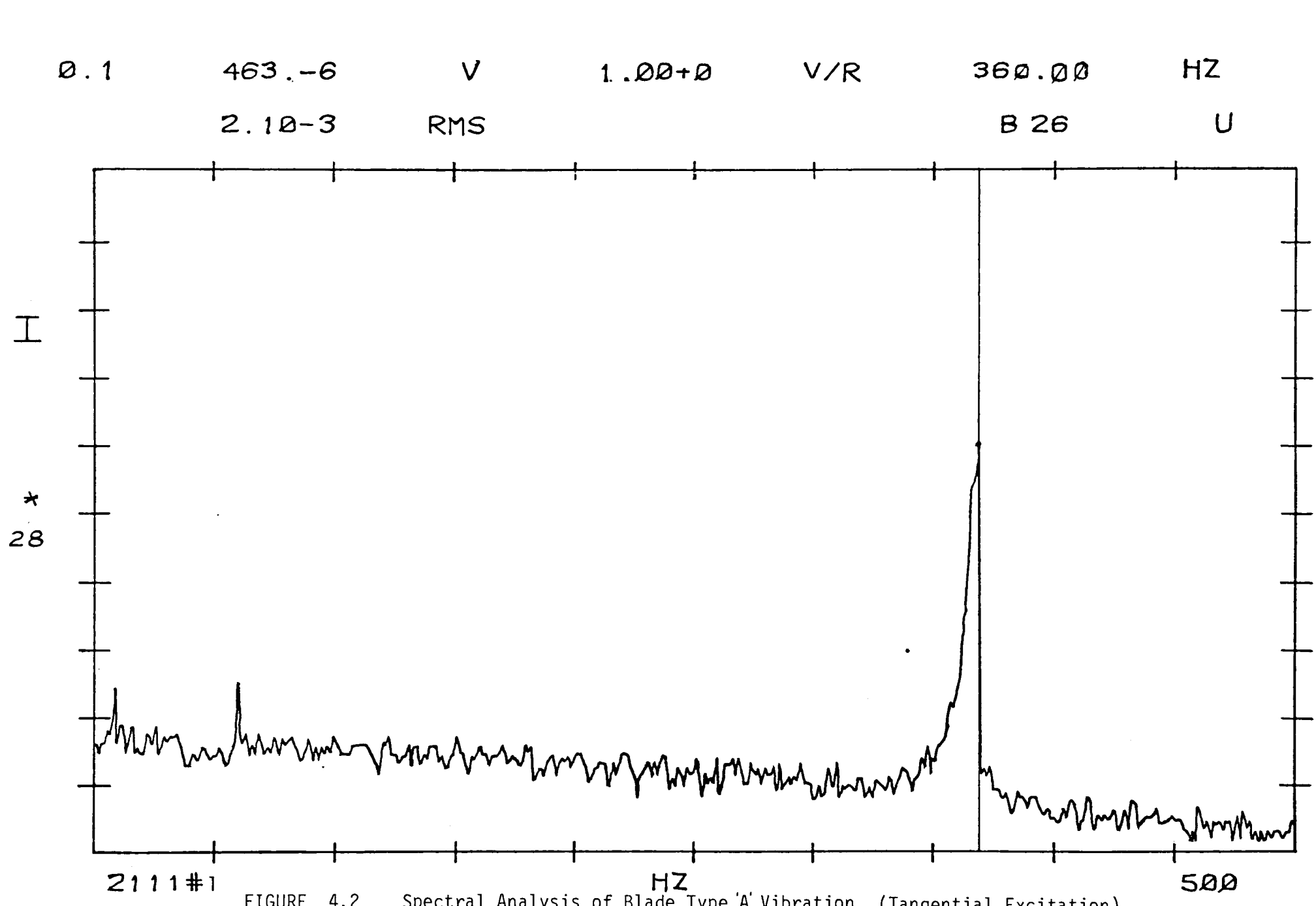

FIGURE 4.2 Spectral Analysis of Blade Type 'A' Vibration (Tangential Excitation)

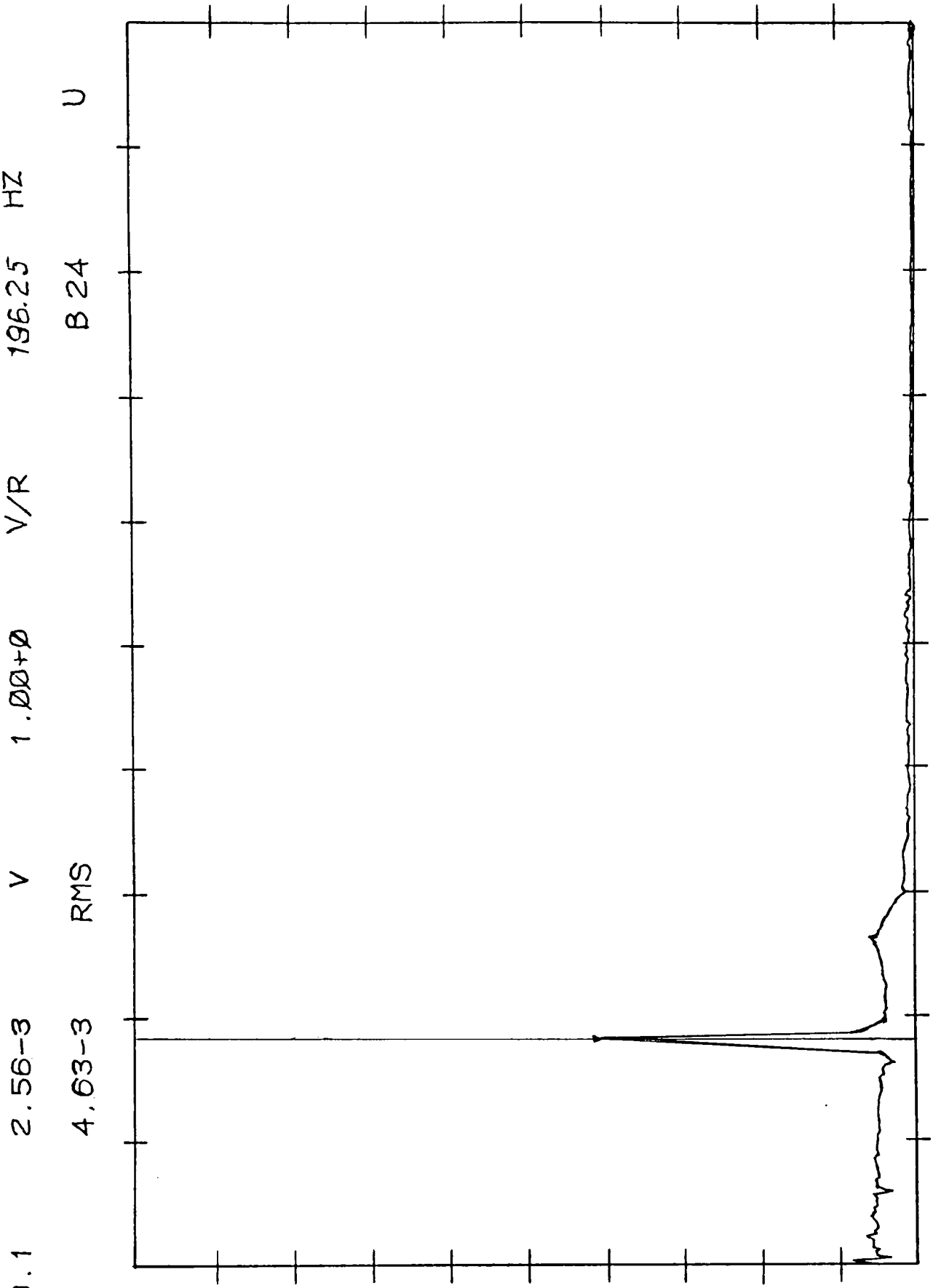

FIGURE 4.3 Spectral Analysis of Blade Type 'B' Vibration (Axial Excitation)

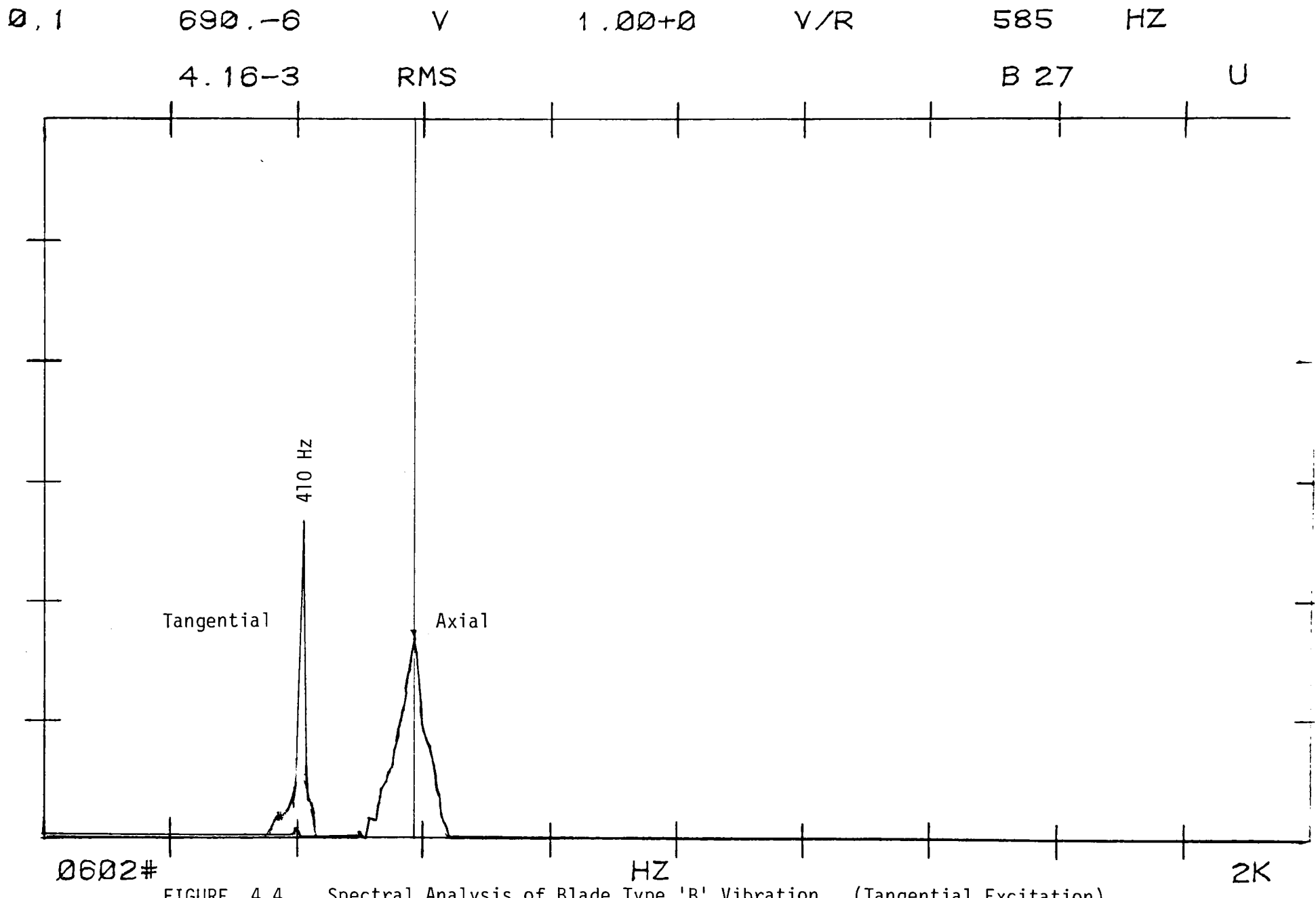

FIGURE 4.4 Spectral Analysis of Blade Type 'B' Vibration (Tangential Excitation)

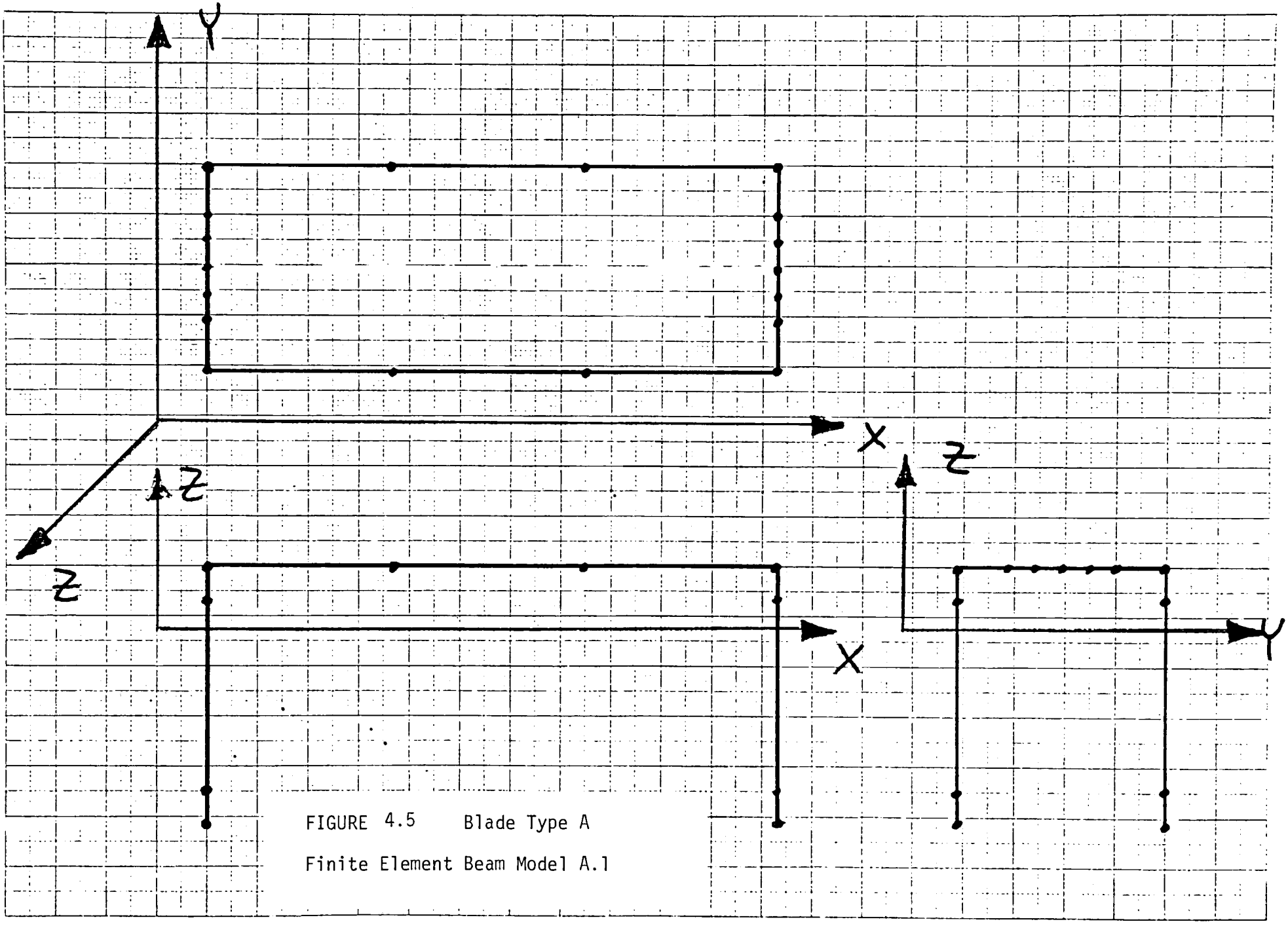

FIGURE 4.5 Blade Type A

Finite Element Beam Model A.1

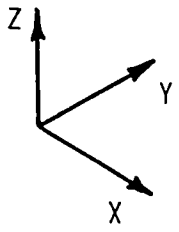

FIGURE 4.6
TEST RIG A BEAM MODEL, 6 INCH LEGS
WITHOUT BLADES MODE #3
F = 88.43 CYCLES/SEC

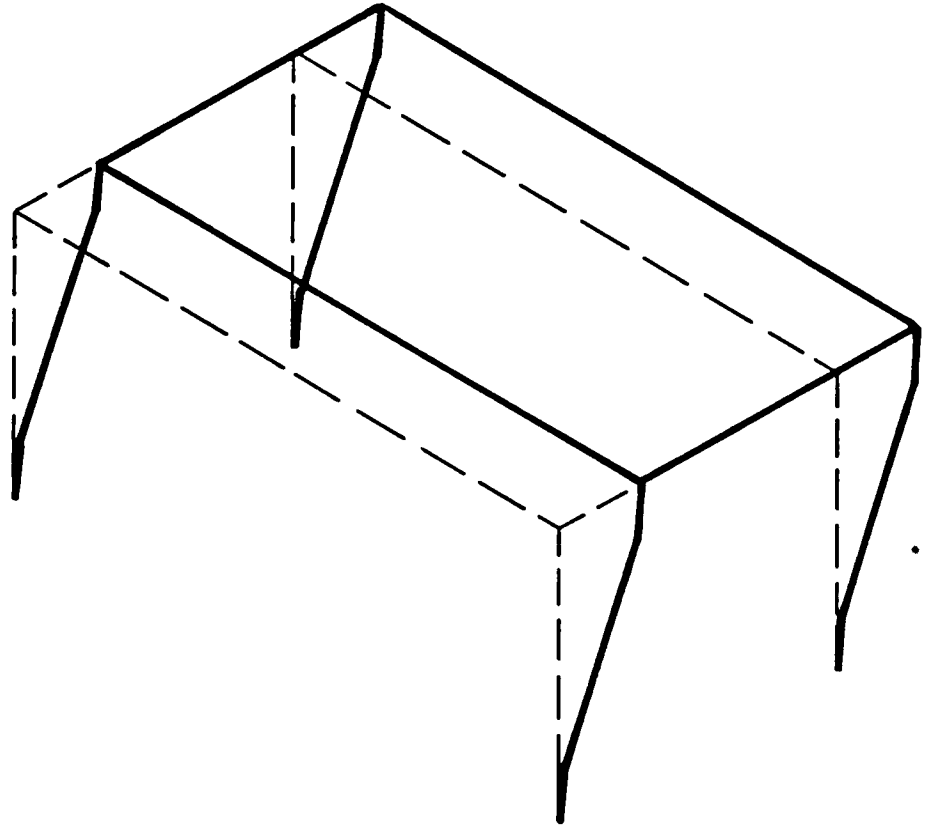

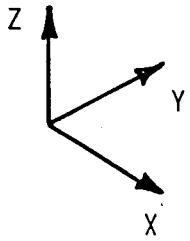

FIGURE 4.7
TEST RIG A BEAM MODEL, 6 INCH LEGS
WITHOUT BLADES MODE #4
F = 88.86 CYCLES/SEC

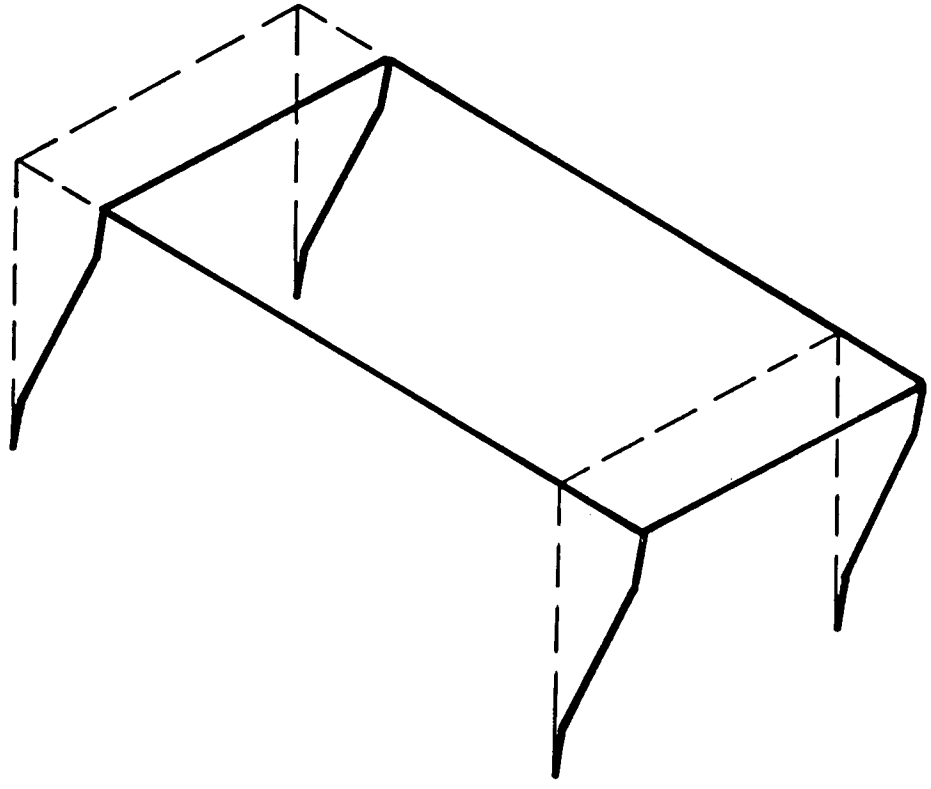

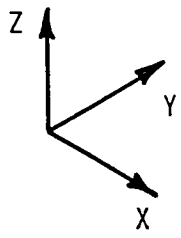

FIGURE 4.8
TEST RIG A BEAM MODEL, 6 INCH LEGS
WITHOUT BLADES MODE #5
F = 115.8 CYCLES/SEC

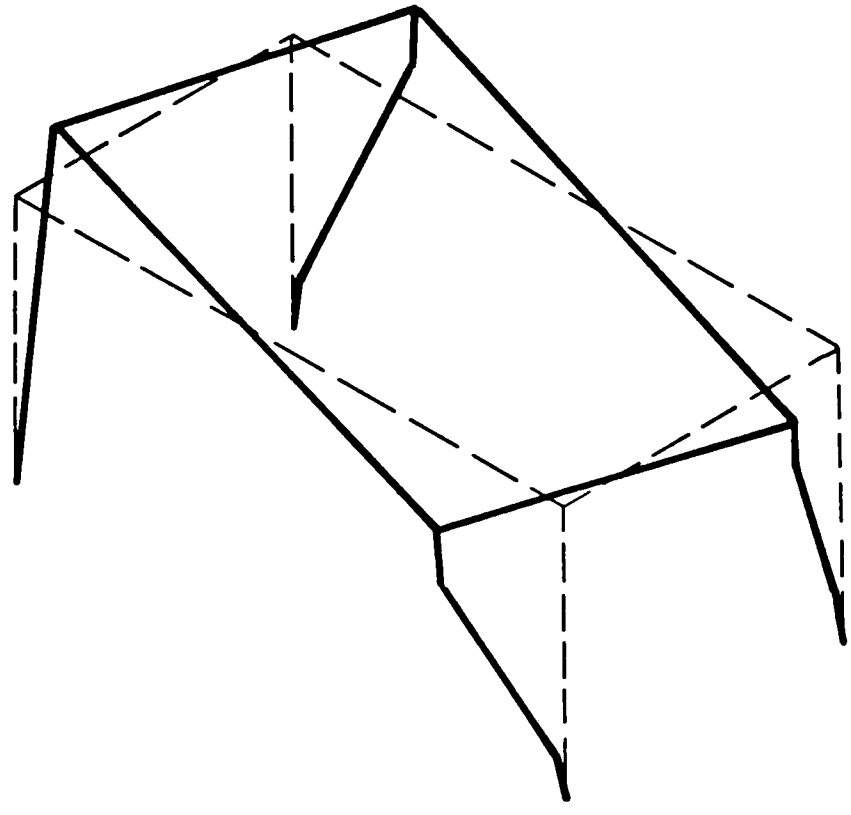

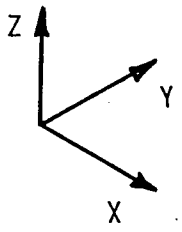

FIGURE 4.9
TEST RIG A BEAM MODEL, 6 INCH LEGS
WITHOUT BLADES MODE #9
F = 722.1 CYCLES/SEC

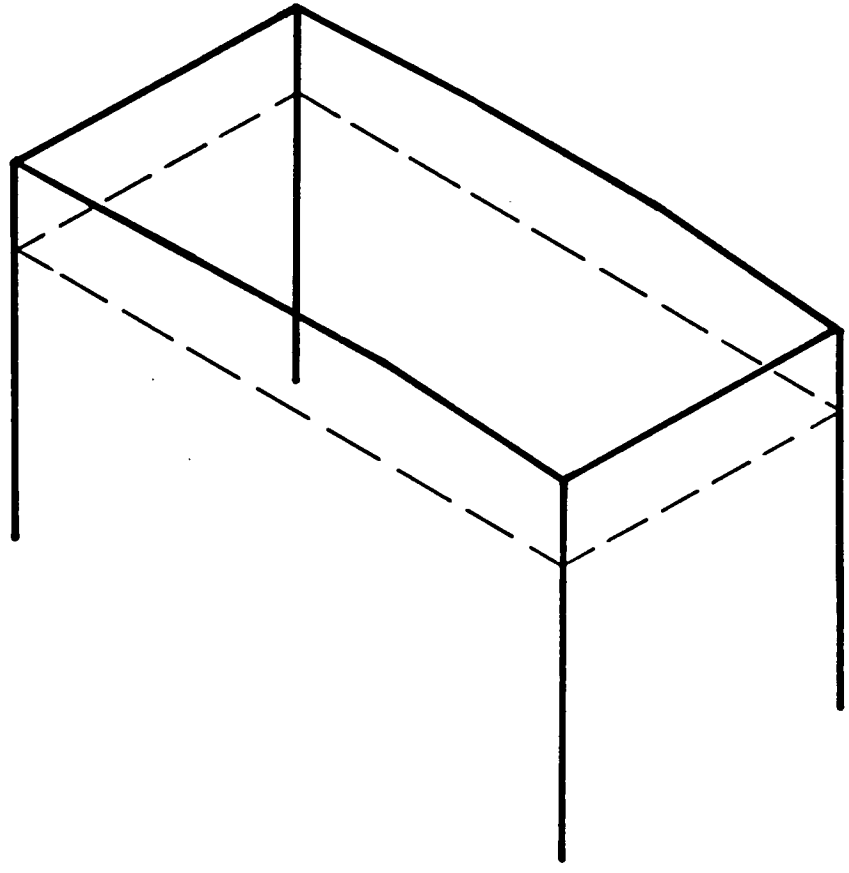

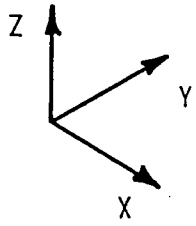

FIGURE 4.10
TEST RIG A BEAM MODEL, 6 INCH LEGS
WITHOUT BLADES MODE #10
F = 771.6 CYCLES/SEC

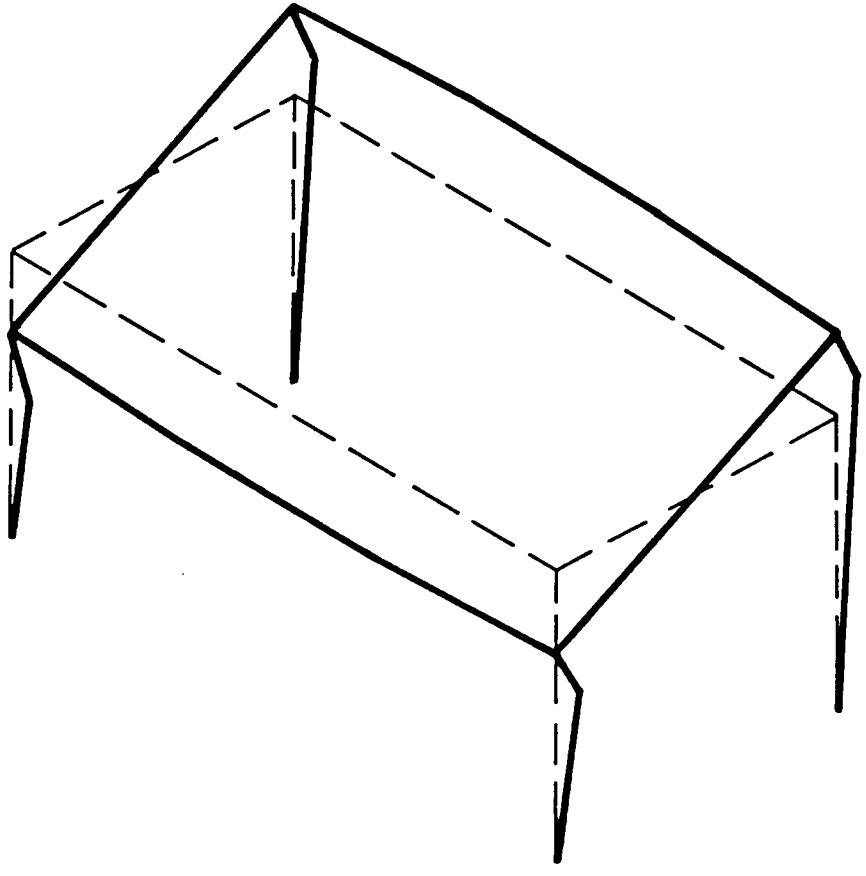

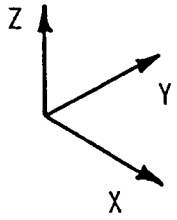

FIGURE 4.11
TEST RIG A BEAM MODEL, 6 INCH LEGS
WITHOUT BLADES MODE #11
F = 1018 CYCLES/SEC

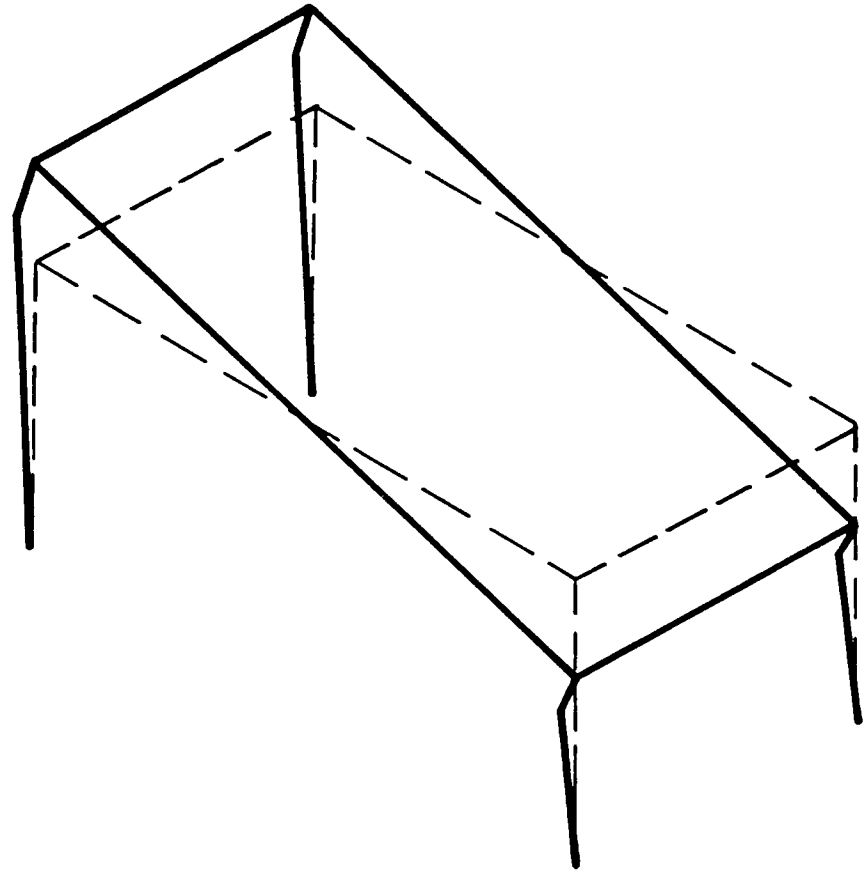

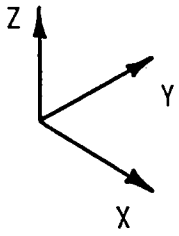

FIGURE 4.12
TEST RIG A BEAM MODEL, 6 INCH LEGS
WITH BLADES MODE # 2
F = 84.55 CYCLES/SEC

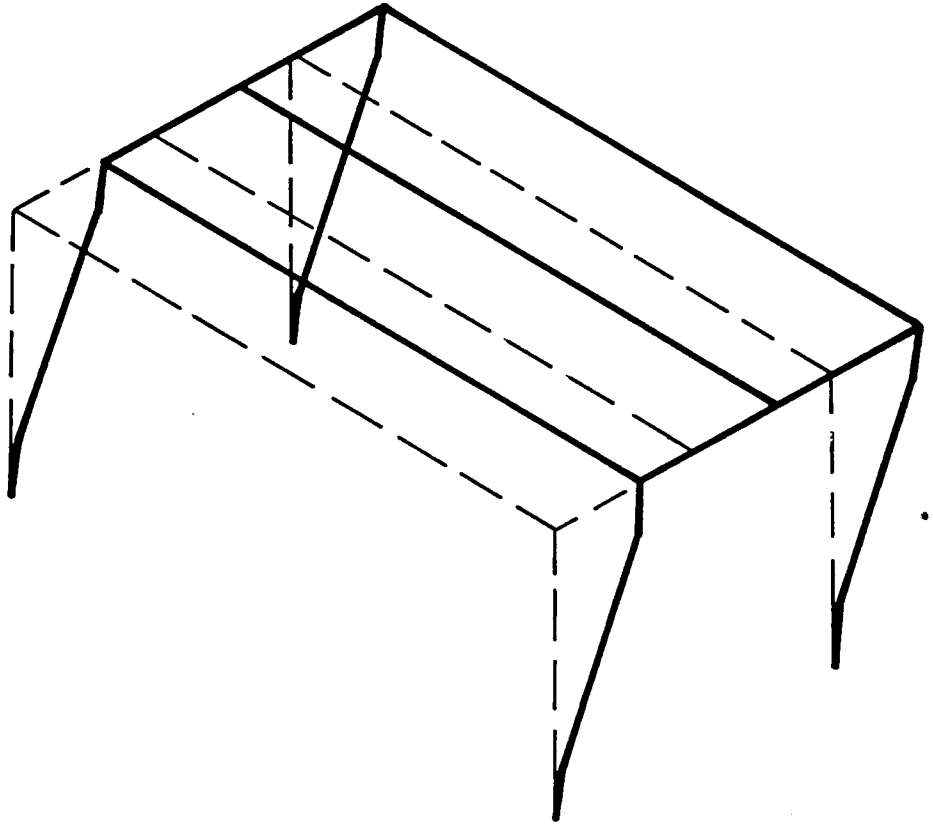

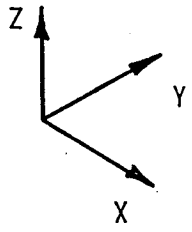

FIGURE 4.13
TEST RIG A BEAM MODEL, 6 INCH LEGS
WITH BLADES MODE #3
F = 84.96 CYCLES/SEC

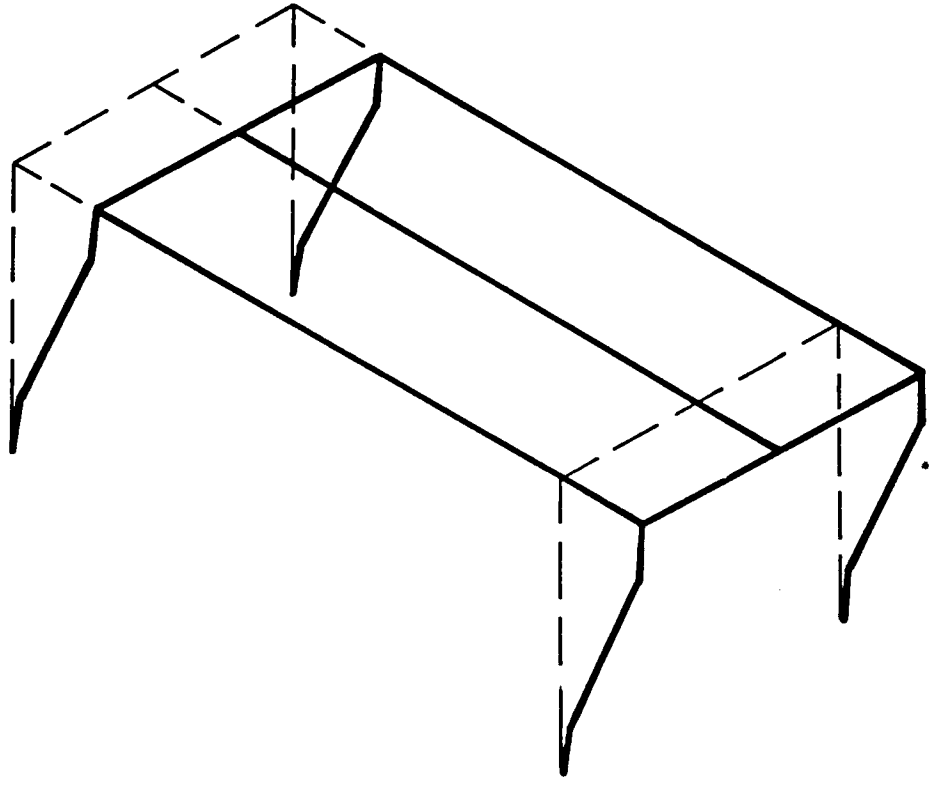

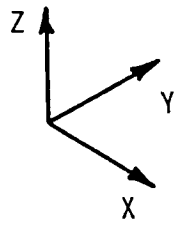

FIGURE 4.14
TEST RIG A BEAM MODEL, 6 INCH LEGS
WITH BLADES MODE #4
F = 108.9 CYCLES/SEC

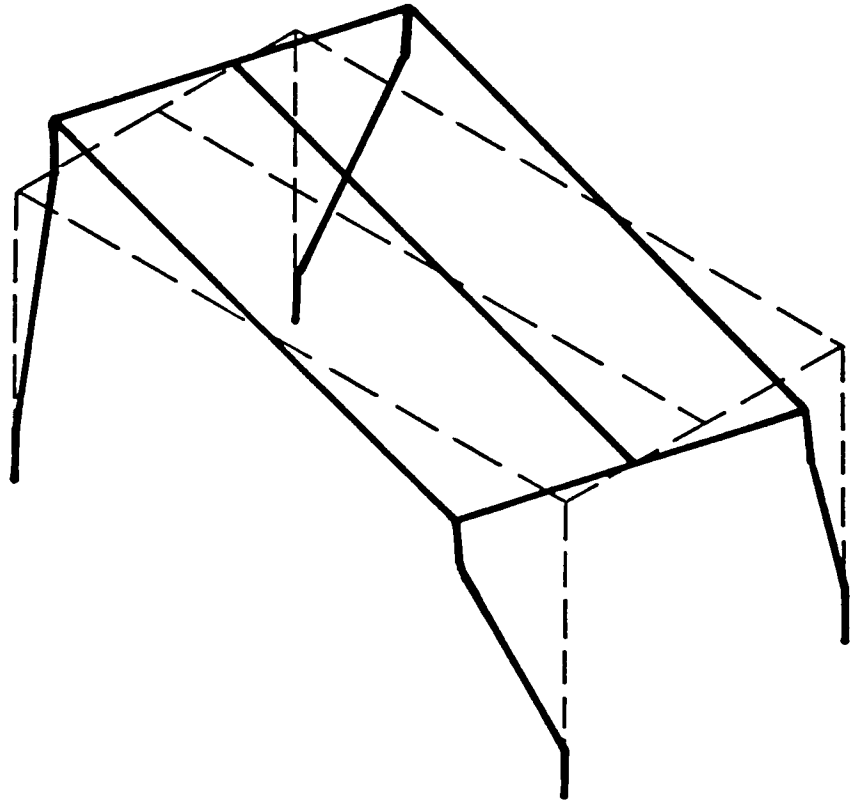

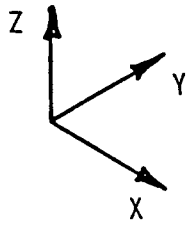

FIGURE 4.15
TEST RIG A BEAM MODEL, 6 INCH LEGS
WITH BLADES MODE #6
F = 344.3 CYCLES/SEC

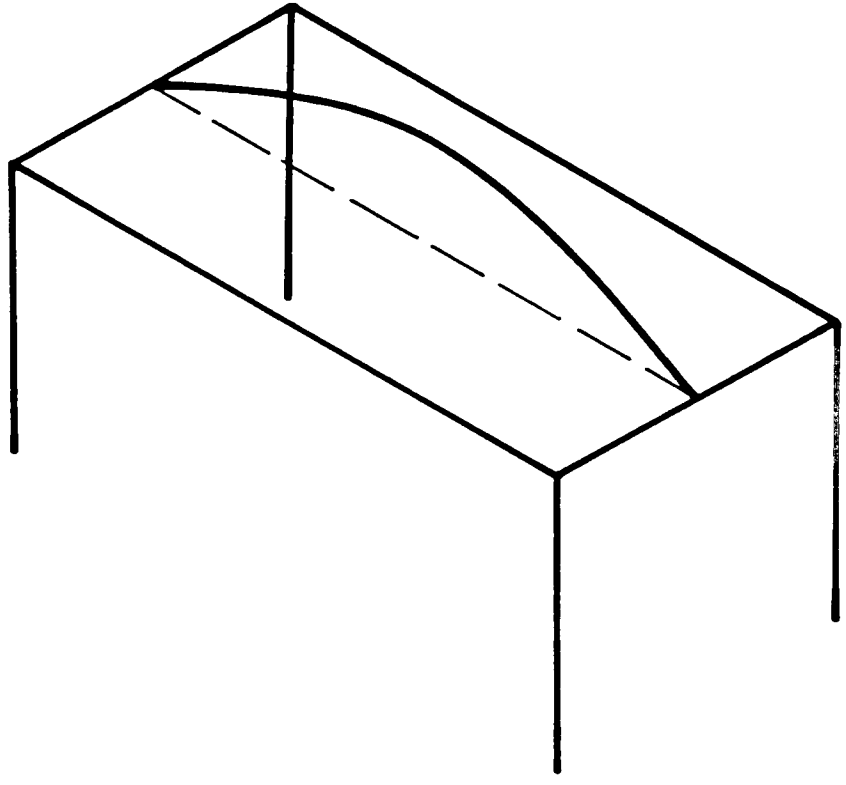

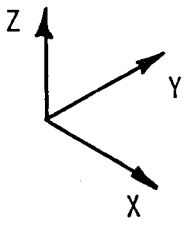

FIGURE 4.16
TEST RIG A BEAM MODEL, 6 INCH LEGS
WITH BLADES MODE #9
F = 700.4 CYCLES/SEC

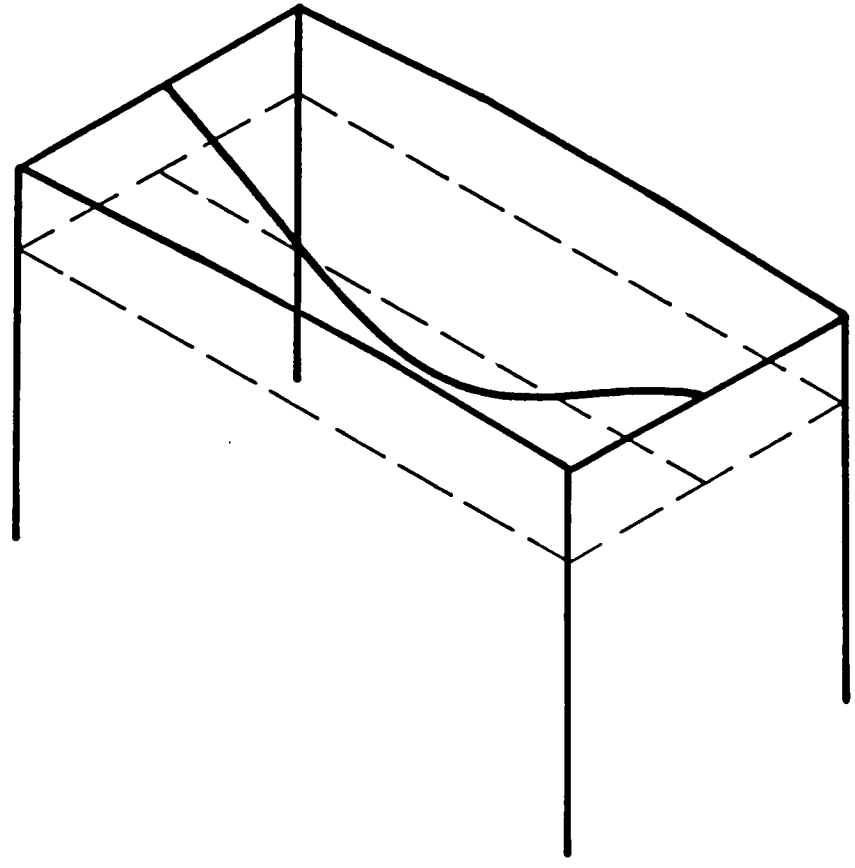

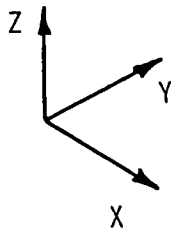

FIGURE 4.17
TEST RIG A BEAM MODEL, 6 INCH LEGS
WITH BLADES MODE #10
F = 771.6 CYCLES/SEC

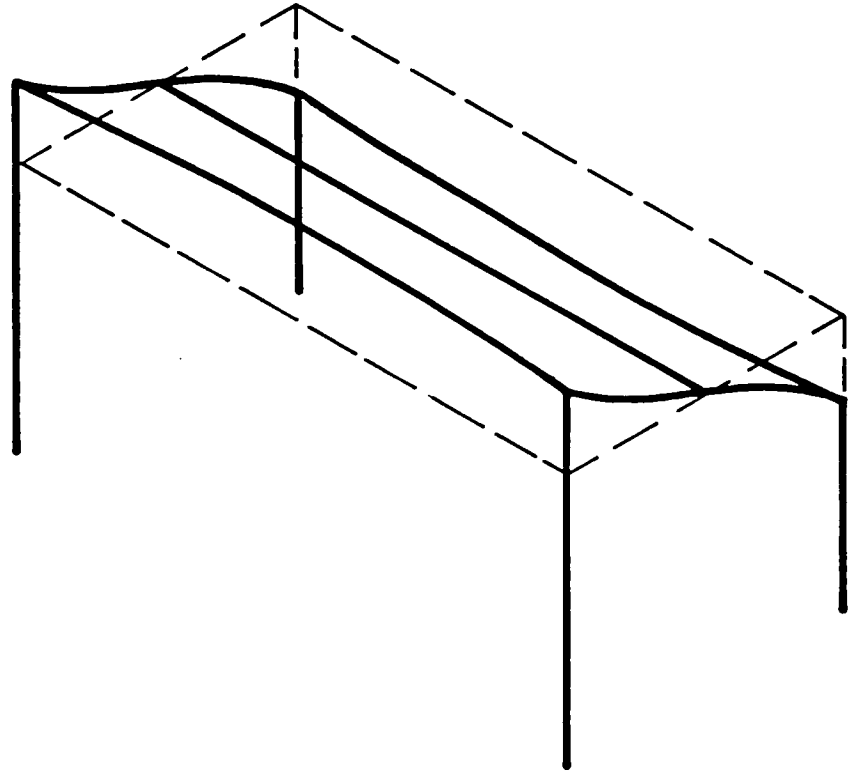

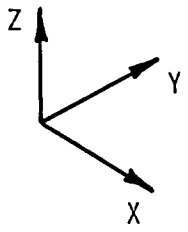

FIGURE 4.18
TEST RIG A BEAM MODEL, 6 INCH LEGS
WITH BLADES MODE #11
F = 902.7 CYCLES/SEC

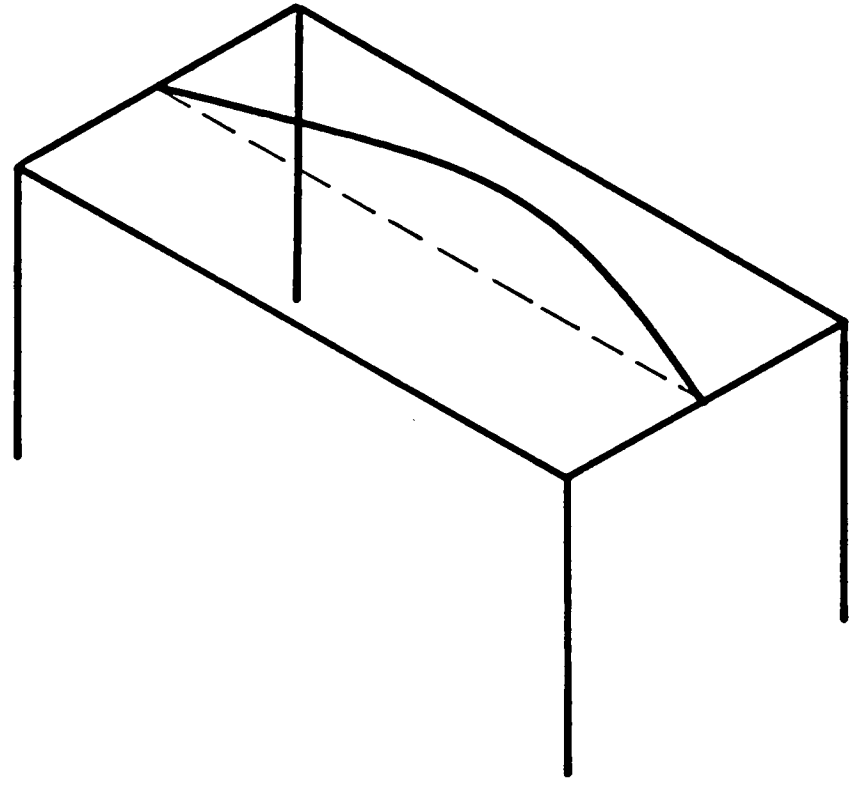

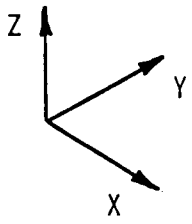

FIGURE 4.19
TEST RIG A BEAM MODEL, 6 INCH LEGS
WITH BLADES MODE #12
F = 930.5 CYCLES/SEC

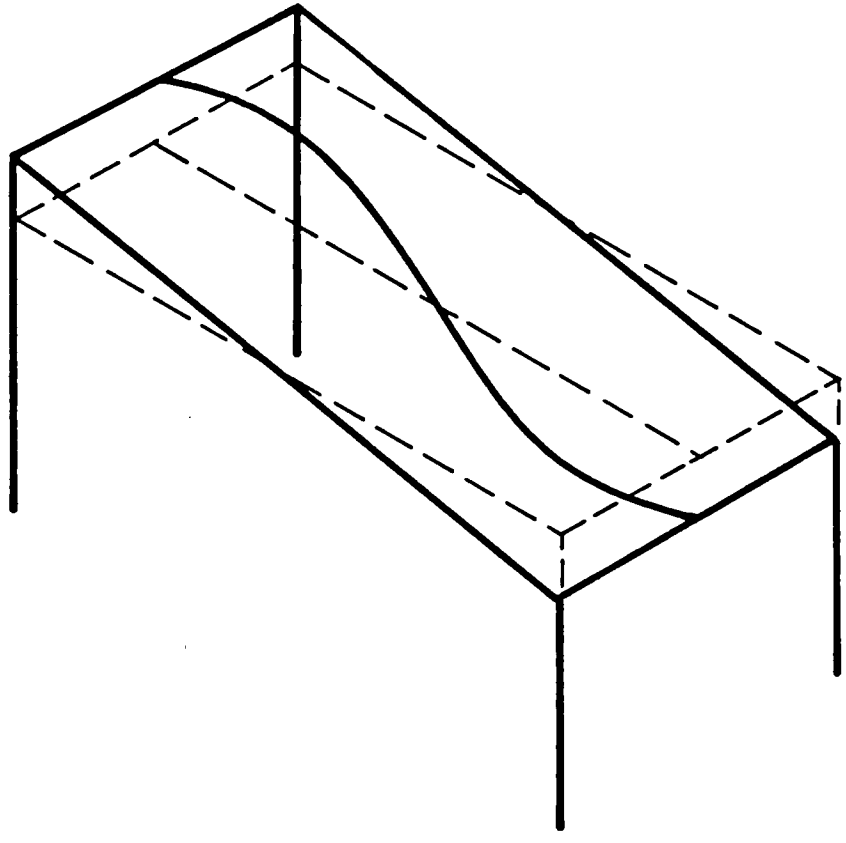

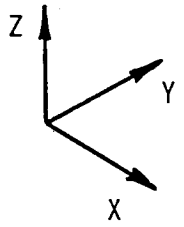

FIGURE 4.20
TEST RIG A BEAM MODEL, 6 INCH LEGS
WITH BLADES MODE #13
F = 1151 CYCLES/SEC

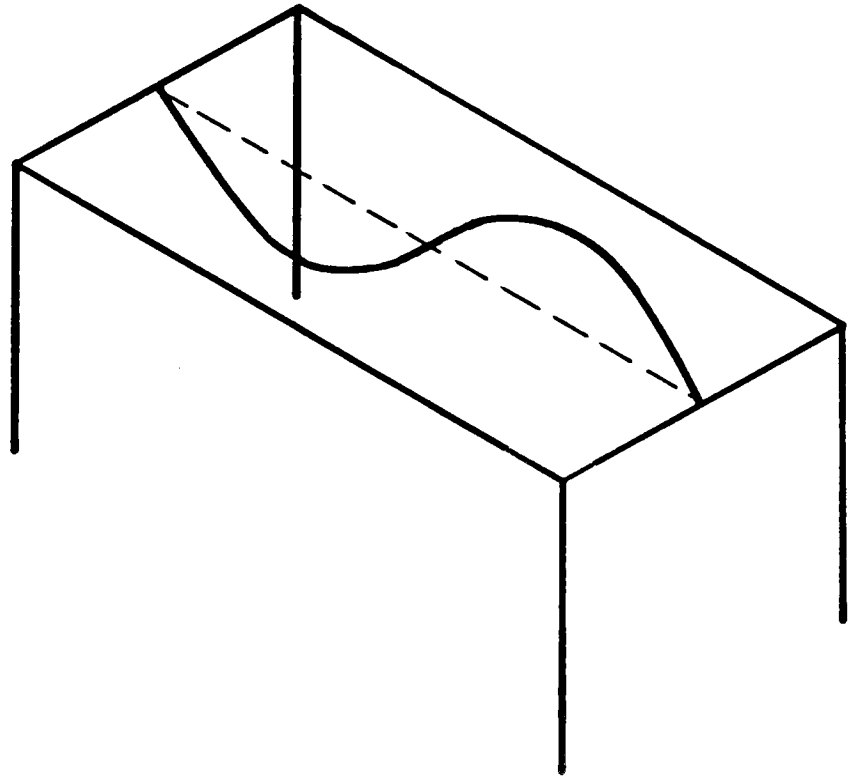

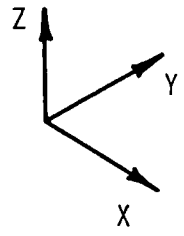

FIGURE 4.21
TEST RIG A BEAM MODEL, 6 INCH LEGS
WITH BLADES MODE # 14
F = 1729 CYCLES/SEC

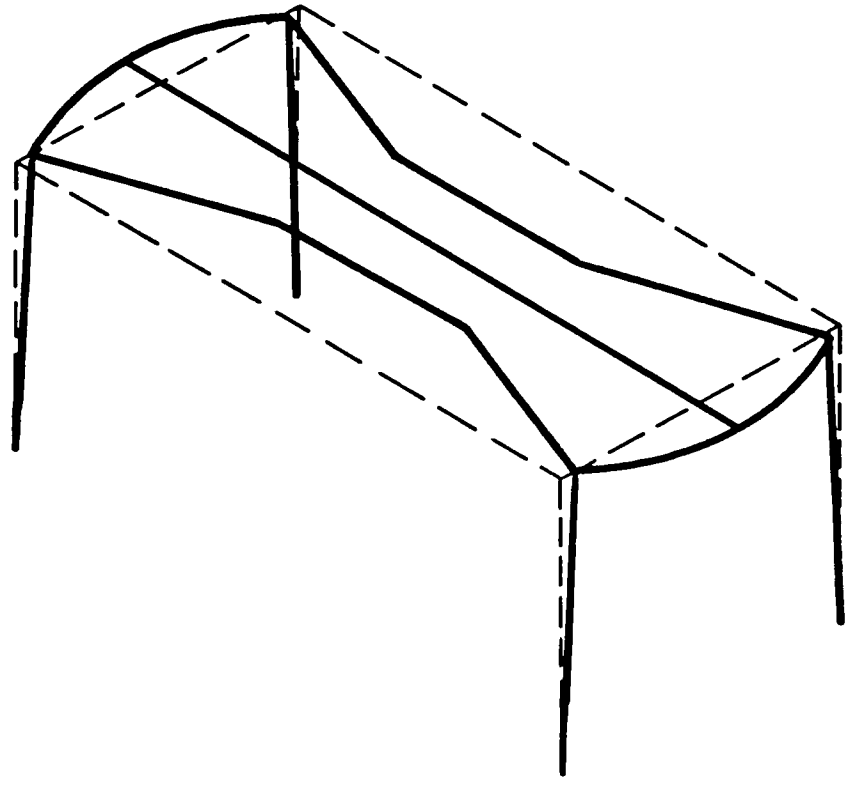

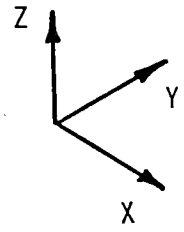

FIGURE 4.22
TEST RIG A BEAM MODEL, 7 INCH LEGS
WITH BLADES MODE #1
F = 73.49 CYCLES/SEC

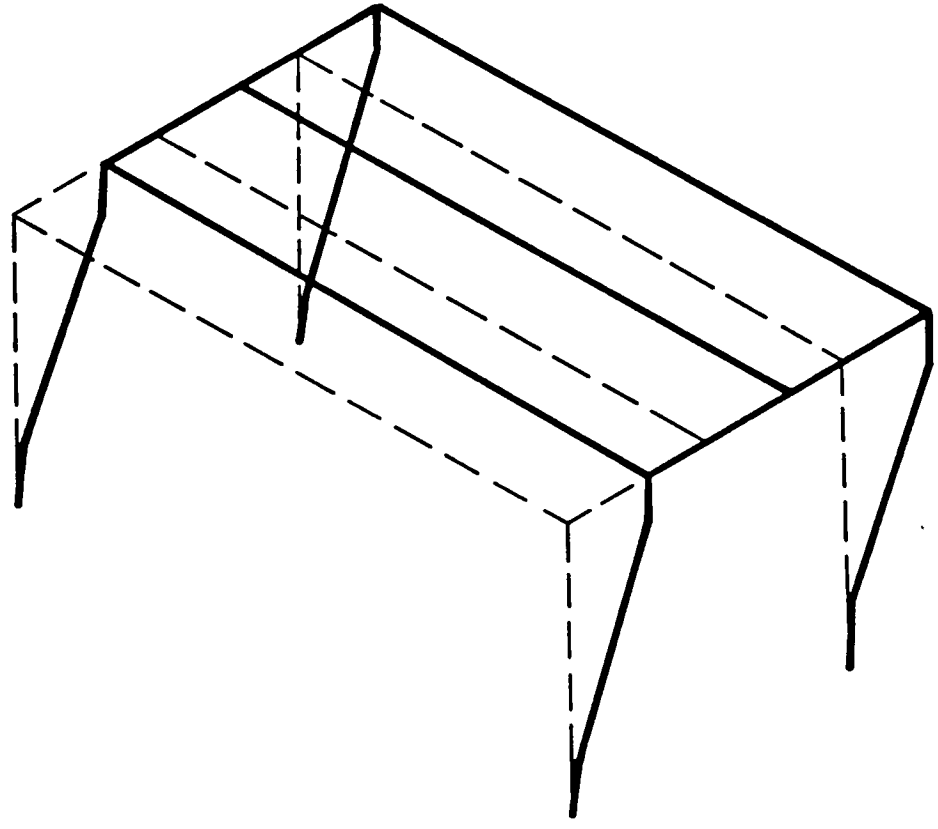

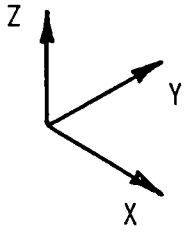

FIGURE 4.23
TEST RIG A BEAM MODEL, 7 INCH LEGS
WITH BLADES MODE #2
F = 73.88 CYCLES/SEC

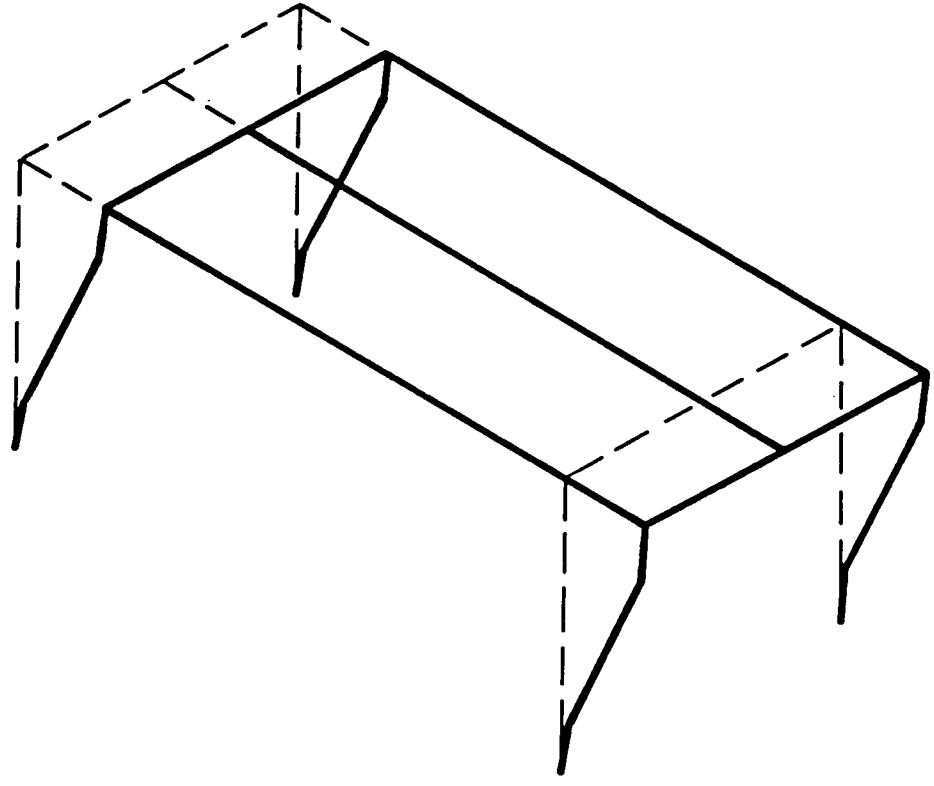

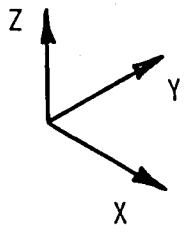

FIGURE 4.24
TEST RIG A BEAM MODEL, 7 INCH LEGS
WITH BLADES MODE #3
F = 95.01 CYCLES/SEC

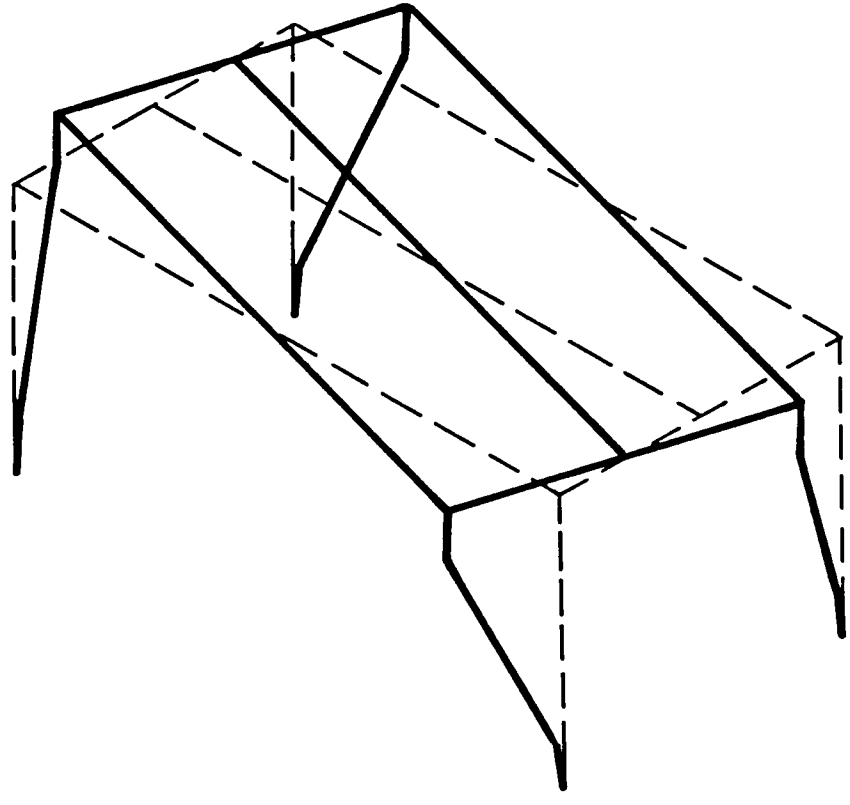

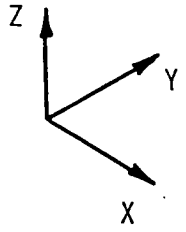

FIGURE 4.25
TEST RIG A BEAM MODEL, 7 INCH LEGS
WITH BLADES MODE # 4
F = 344.2 CYCLES/SEC

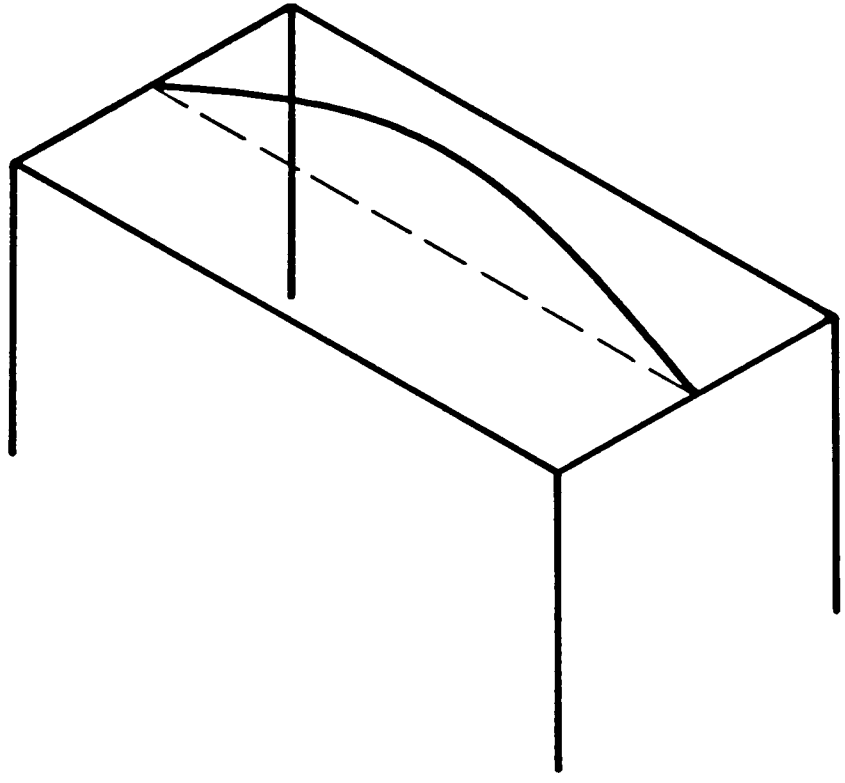

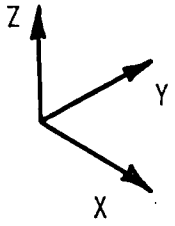

FIGURE 4.26
TEST RIG A BEAM MODEL, 7 INCH LEGS
WITH BLADES MODE #5
F = 668.7 CYCLES/SEC

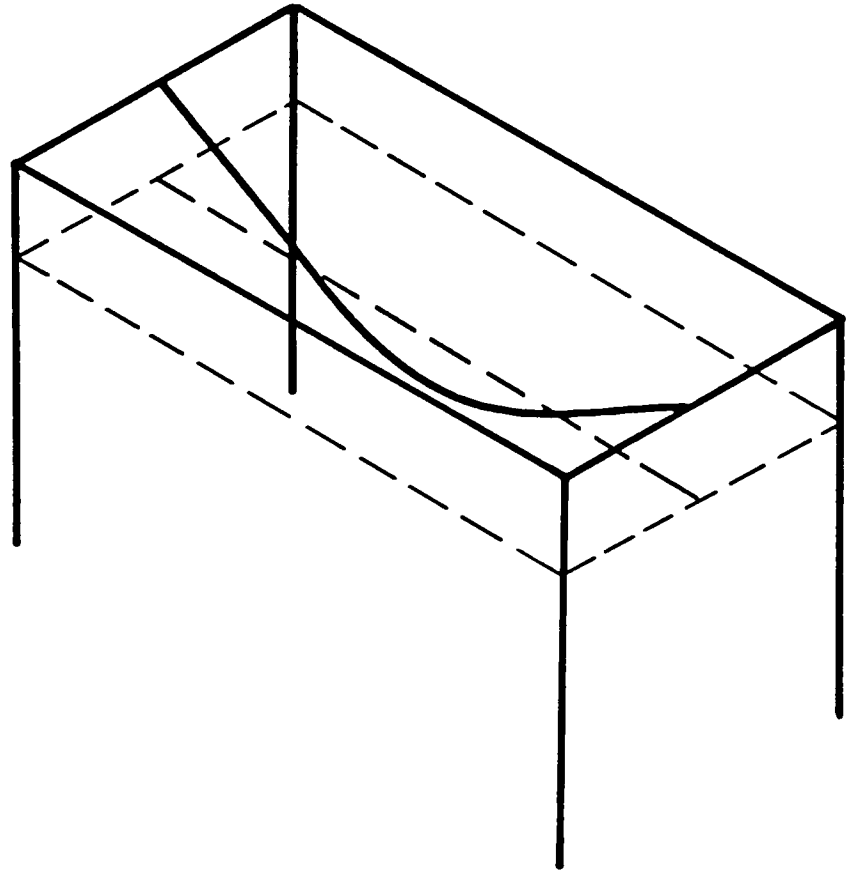

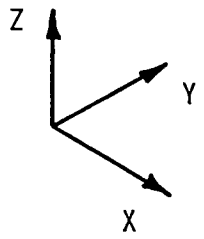

FIGURE 4.27
TEST RIG A BEAM MODEL, 7 INCH LEGS
WITH BLADES MODE #6
F = 737.5 CYCLES/SEC

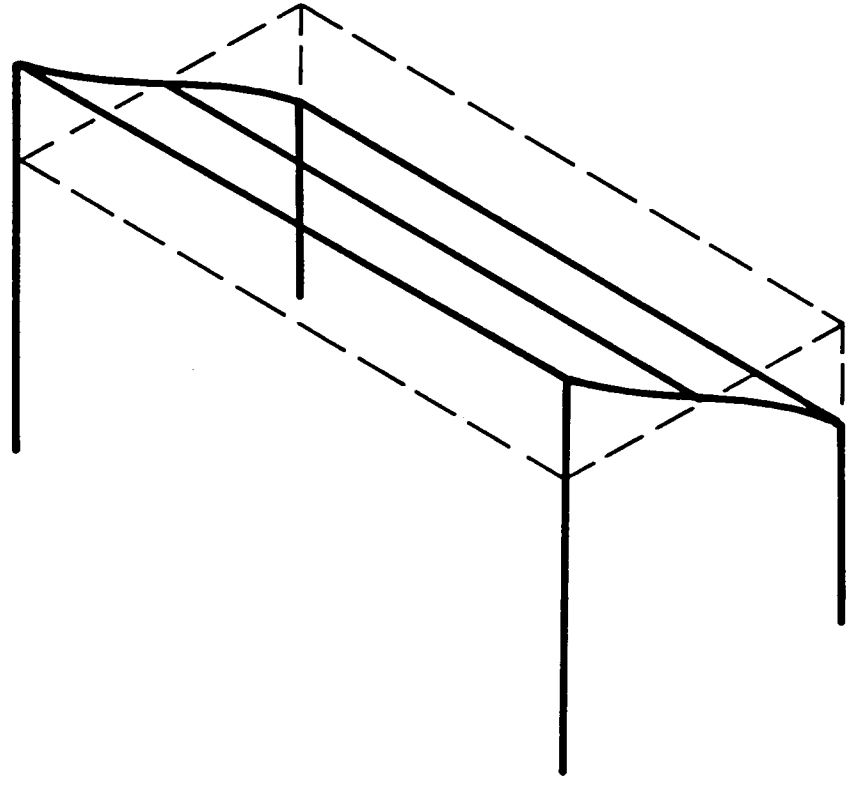

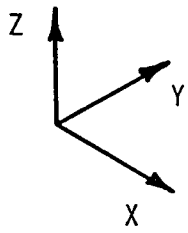

FIGURE 4.28
TEST RIG A BEAM MODEL, 7 INCH LEGS
WITH BLADES MODE #7
F = 886.3 CYCLES/SEC

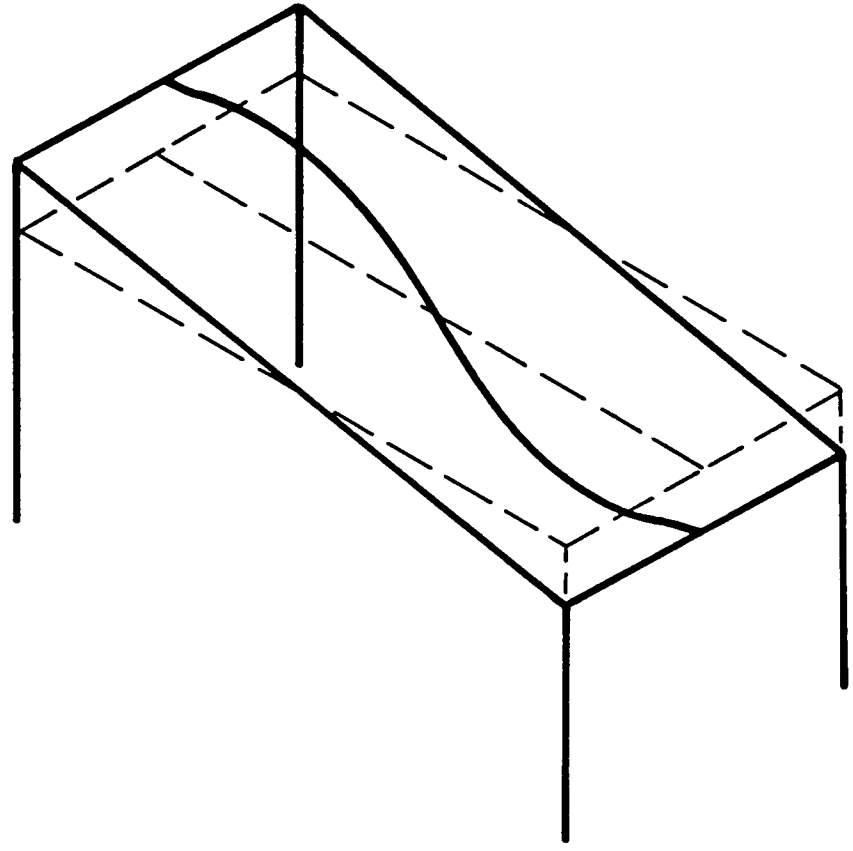

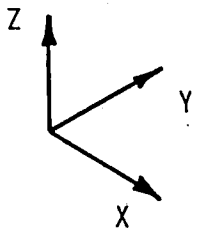

FIGURE 4.29
TEST RIG A BEAM MODEL, 7 INCH LEGS
WITH BLADES MODE #8
F = 902.7 CYCLES/SEC

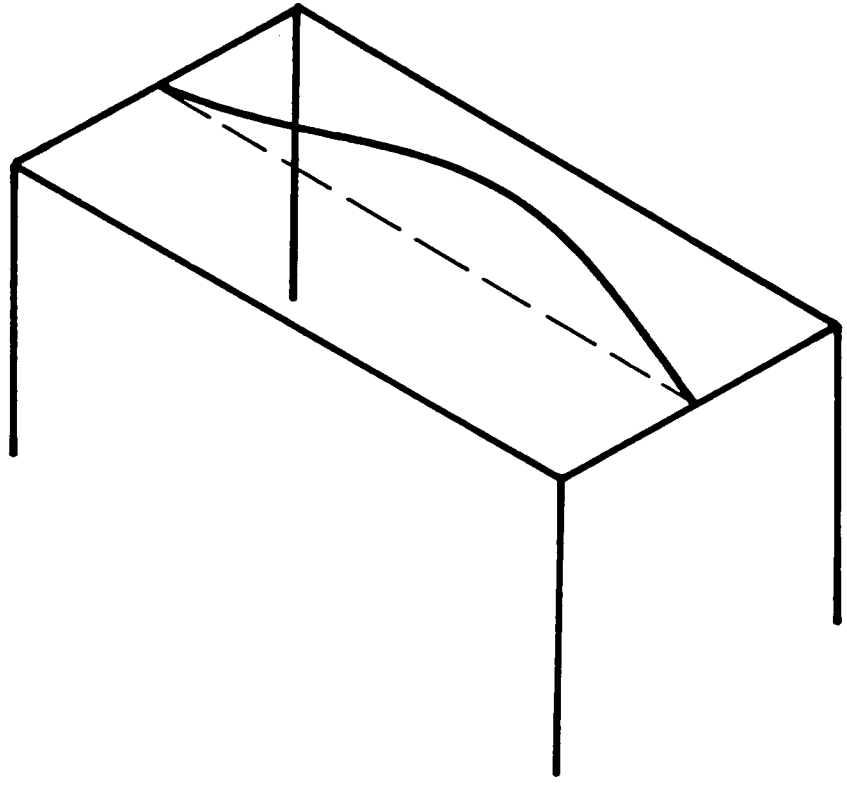

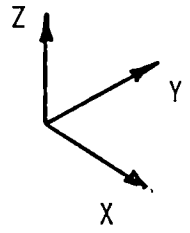

FIGURE 4.30
TEST RIG A BEAM MODEL, 7 INCH LEGS
WITH BLADES MODE #9
F = 1150 CYCLES/SEC

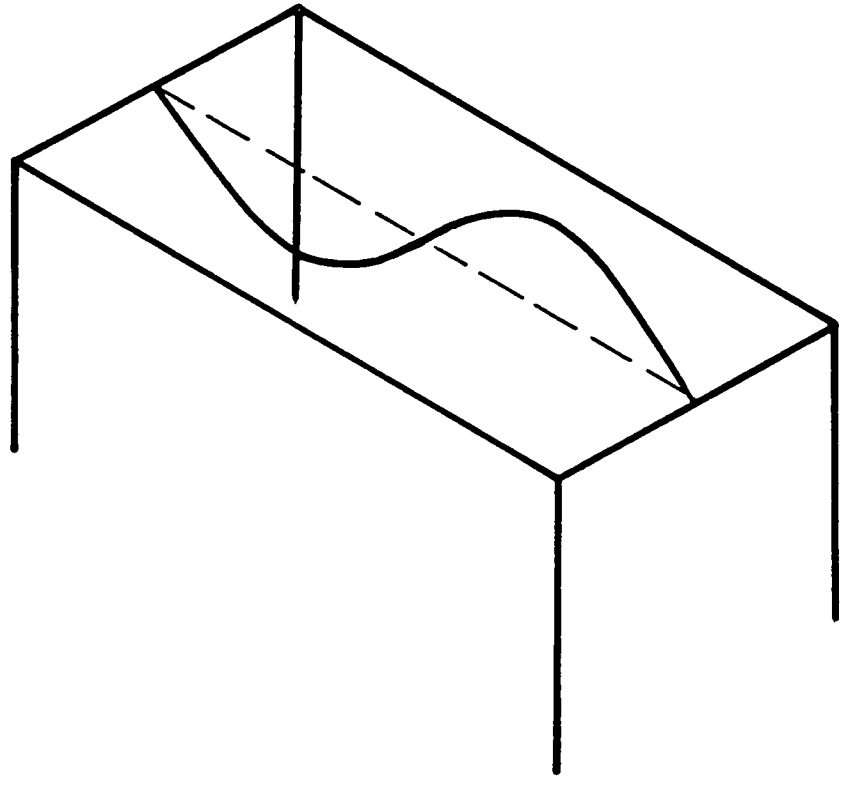

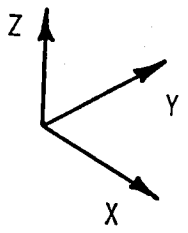

FIGURE 4.31
TEST RIG A BEAM MODEL, 7 INCH LEGS
WITH BLADES MODE #10
F = 1729 CYCLES/SEC

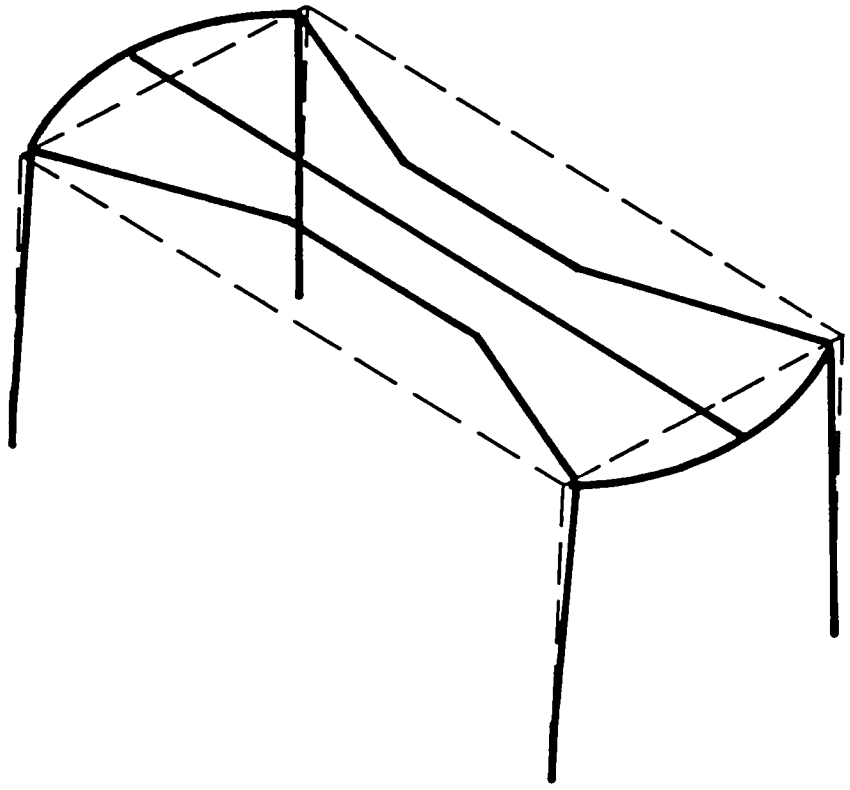

1/8/79

No Blades

6" legs

#35 Table + Rig ; struck up + down accelerometer in center of bedplate

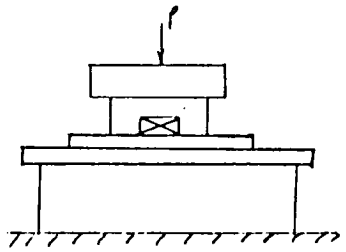

#36 Table + Rig ; struck up + down accelerometer on 4" plate

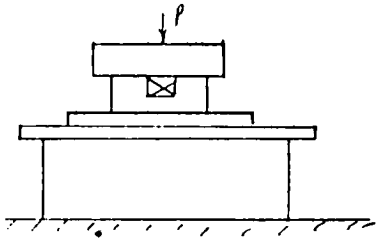

#37 Table + Rig ; struck up + down accelerometer on table in front of rig

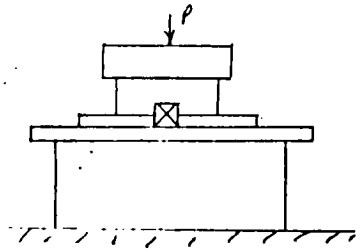

#38 Table + Rig ; struck end for end accelerometer on 4" plate

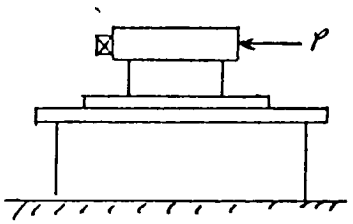

#39 Table + Rig ; struck end for end accelerometer on table (side)

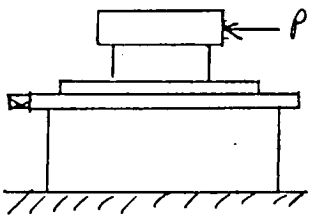

FIGURE 4.32 Accelerometer Locations for Rig 'A' Correlation Tests

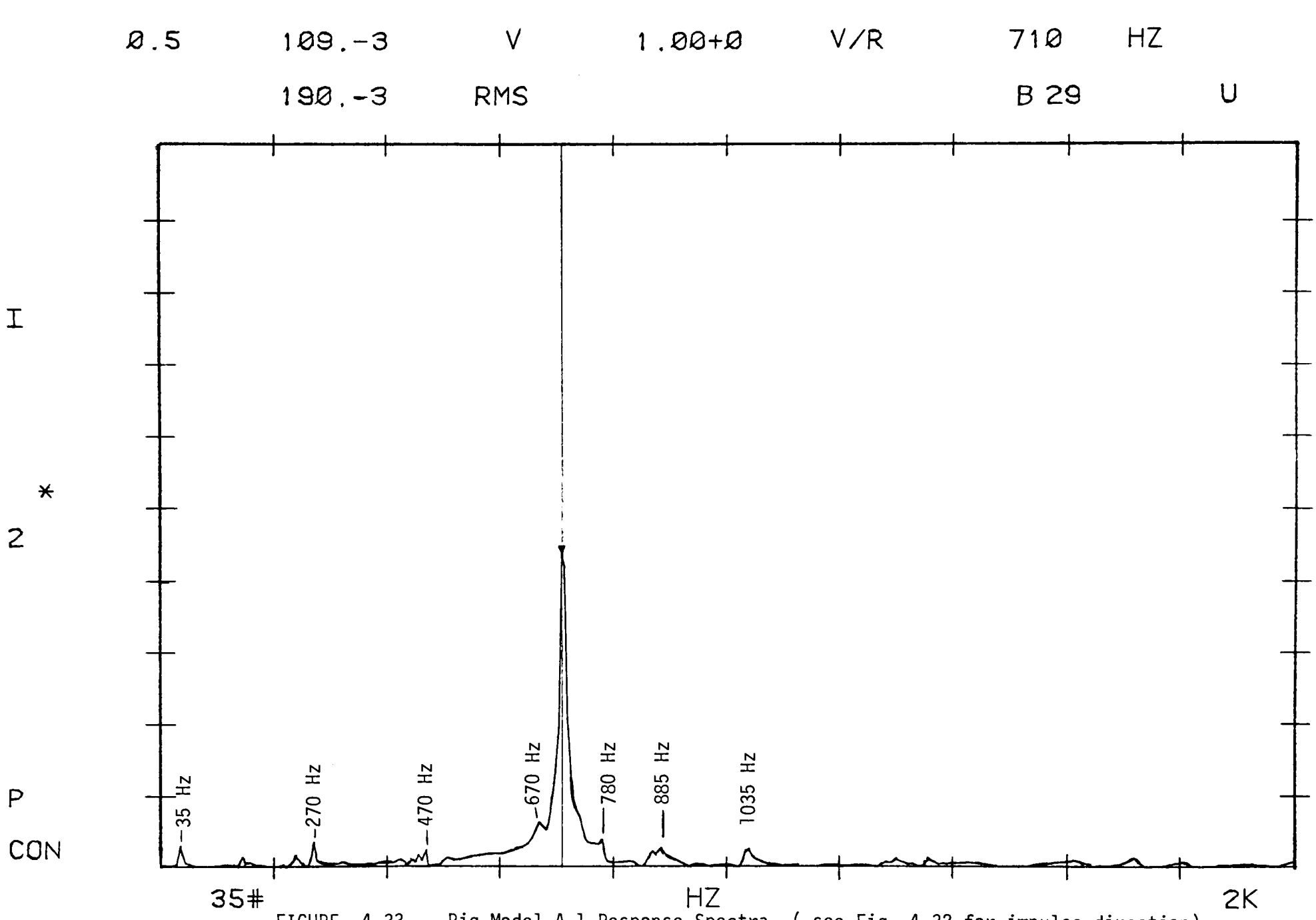

FIGURE 4.33 Rig Model A.1 Response Spectra (see Fig. 4.32 for impulse direction)

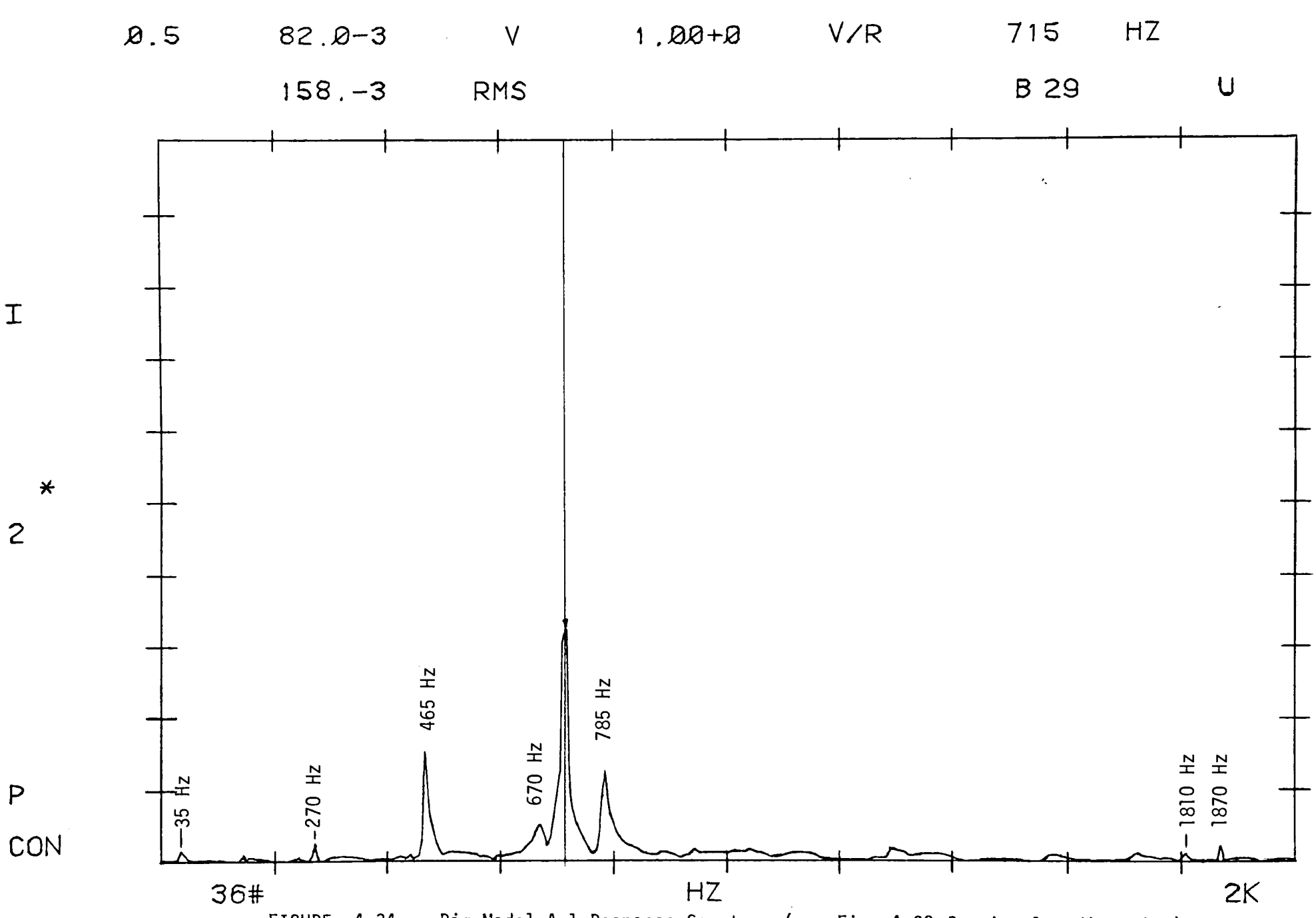

FIGURE 4.34 Rig Model A.1 Response Spectra (see Fig. 4.32 for impulse direction)

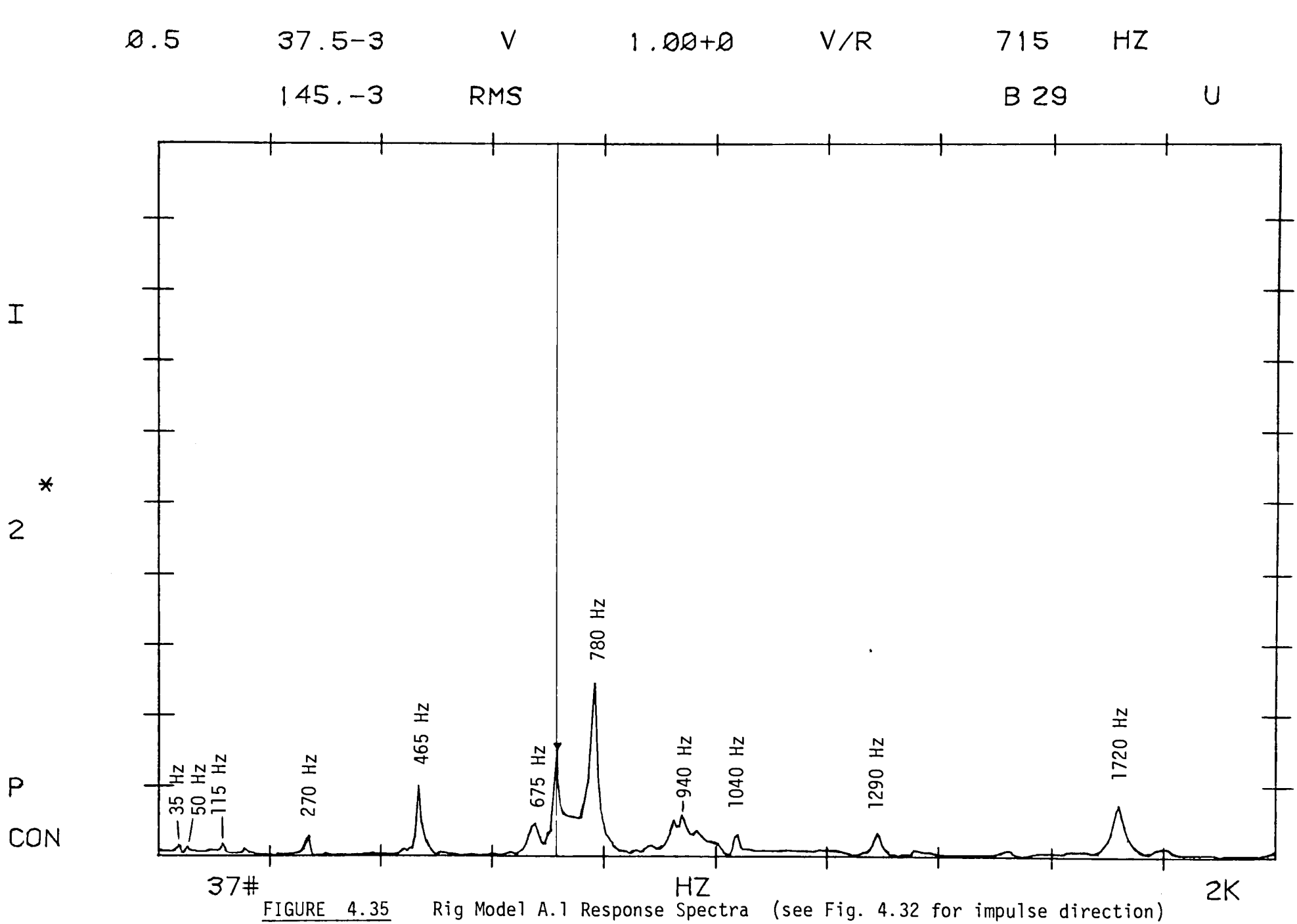

FIGURE 4.35 Rig Model A.1 Response Spectra (see Fig. 4.32 for impulse direction)

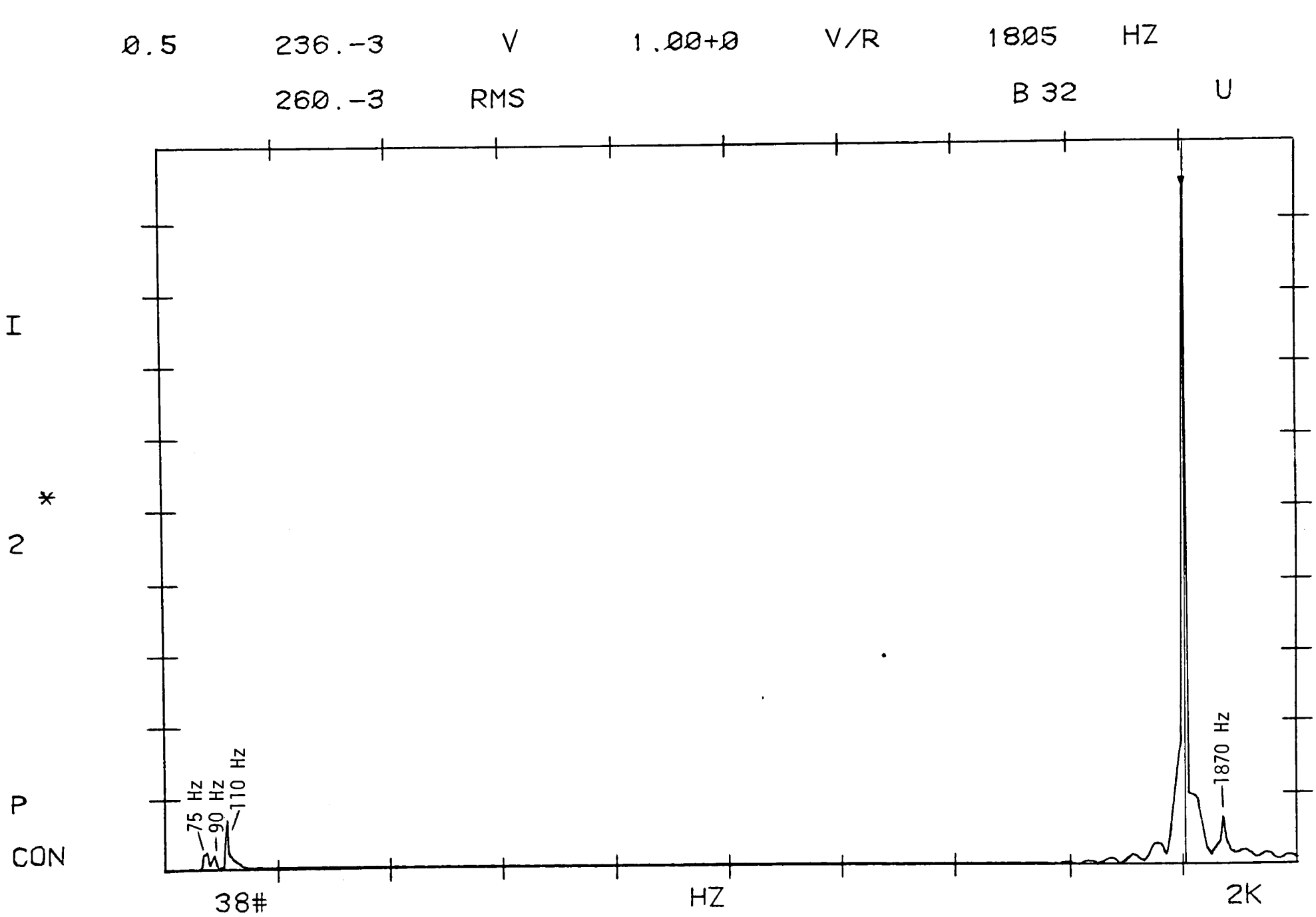

FIGURE 4.36 Rig Model A.1 Response Spectra (see Fig. 4.32 for impulse direction)

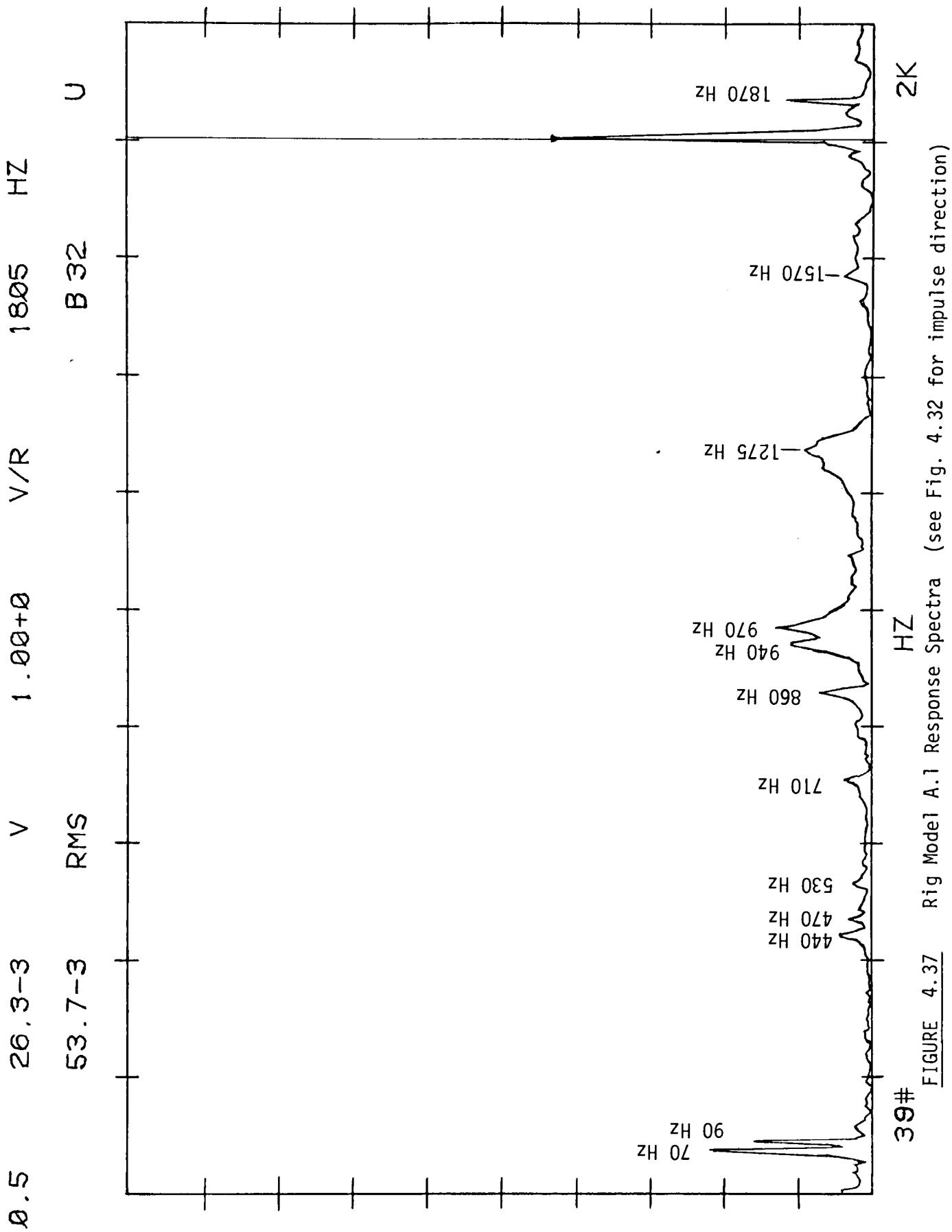

FIGURE 4.37 Rig Model A.1 Response Spectra (see Fig. 4.32 for impulse direction)

MODE DATA FOR RIG BOLTED TO TABLE

NO BLADES

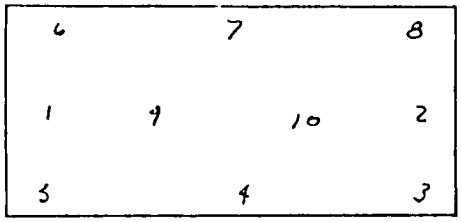

Table

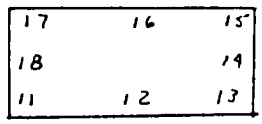

Rig

ACCELEROMETER POSITIONS (*3)

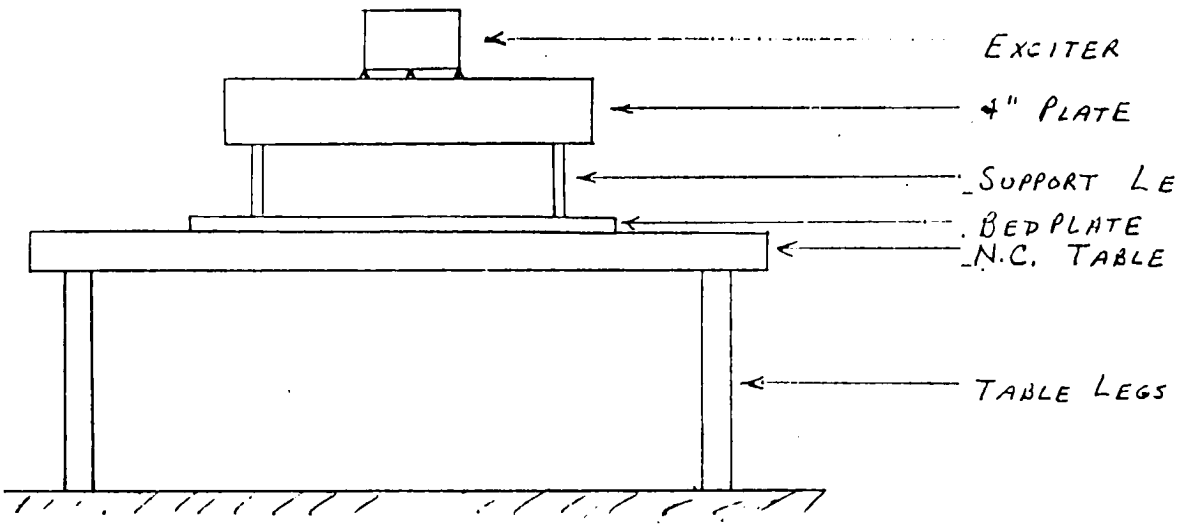

Frequencies investigated correspond to plot 36

f = 715 Hz APS - X100 NSA - 500MV

Units - V x 10^{-3} Two Runs

1.	60.5	59.0	10.	128.	122.
2.	55.5	51.2	11.	158.	156.
3.	15.6	13.7	12.	195.	185.
4.	28.8	23.2	13.	184.	173.
5.	77.8	74.2	14.	198.	184.
6.	14.7	13.9	15.	208.	189.
7.	21.3	25.2	16.	233.	215.
8.	77.8	75.7	17.	208.	197.
9	132.0	126.0	18.	186.	179.

f = 670 Hz APS - X100 NSA - 500 MV

Units $V \times 10^{-3}$ Two Runs

1.	27.5	28.5	10.	38.3	37.2
2.	11.4	12.7	11.	57.9	55.4
3.	24.2	26.8	12.	57.5	55.3
4.	34.3	34.1	13.	42.5	42.8
5.	66.4	71.0	14.	44.6	43.0
6.	21.0	23.9	15.	50.0	47.1
7.	37.2	34.0	16.	71.5	67.2
8.	54.9	58.0	17.	76.6	74.8
9.	32.7	31.2	18.	69.4	67.1

f = 465 Hz APS - X100 NSA - 500 MV

Units $V \times 10^{-3}$ Two Runs

1.	94.5	92.5	10.	31.4	42.8
2.	4.2	5.8	11.	217.	203.
3.	15.5	13.9	12.	246.	234.
4.	74.9	85.1	13.	260.	250.
5.	11.2	9.5	14.	13.5	12.5
6.	9.5	10.5	15.	251.	243.
7.	190.0	187.0	16.	318.	285.
8.	9.3	7.5	17.	318.	273.
9.	55.0	15.4	18.	62.5	54.2

f = 270 Hz APS - X100 NSA - 500MV

Units - V x 10^{-3} Two Runs

1.	105.0	103.0	10.	42.7	42.0
2.	74.7	73.7	11.	68.3	67.3
3.	36.8	34.3	12.	62.7	60.0
4.	82.2	76.3	13.	55.4	54.5
5.	89.3	88.3	14.	39.3	39.0
6.	24.0	24.0	15.	27.3	27.0
7.	133.0	129.0	16.	27.1	26.7
8.	24.2	26.4	17.	35.6	37.1
9.	54.7	52.5	18.	53.7	53.4

f = 350 Hz HPS - X100 NSH - 500MV

Units - V x 10^{-3} Two Runs

1.	16.8	16.4	10.	11.7	11.9
2.	7.5	7.0	11.	11.8	11.8
3.	4.5	4.2	12.	8.6	8.7
4.	3.9	4.6	13.	6.5	6.5
5.	3.0	3.0	14.	3.2	3.2
6.	25.0	24.7	15.	1.0	1.0
7.	10.1	10.0	16.	1.0	1.0
8.	1.9	1.7	17.	2.8	3.5
9.	16.7	16.1	18.	8.3	8.1

WEHLE RESEARCH LABORATORY
ROCHESTER INSTITUTE OF TECHNOLOGY
PHONE 475-6104
CURT BECK

"A" FLEXURE LINK
TOLERANCE: +0.020 -0.000 (LENGTH)
MATERIAL: AISI 1020 STEEL
MILLED FROM 2 INCH DIAMETER BARSTOCK
ALL DIMENSIONS IN INCHES

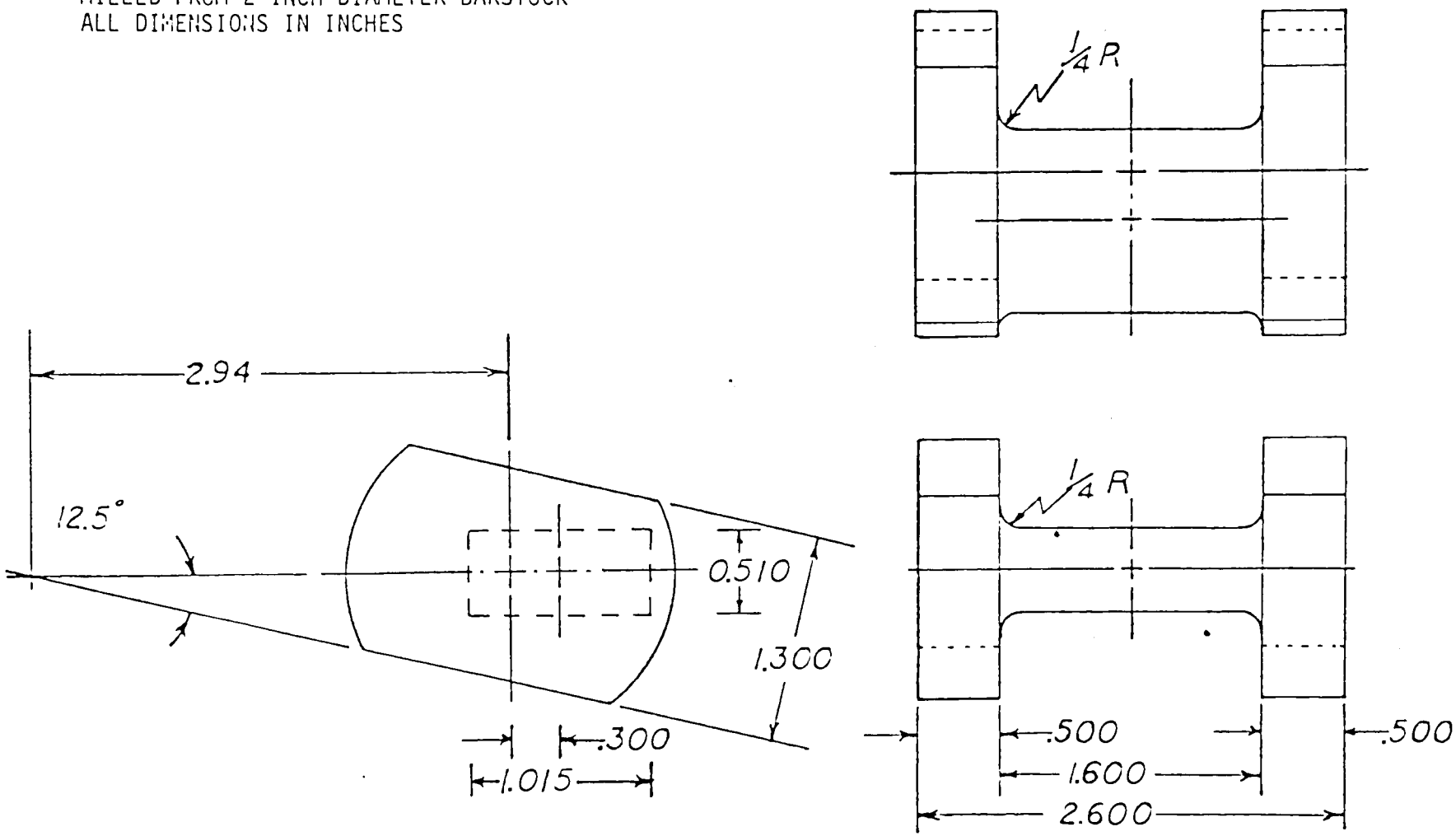

FIGURE 4.39 BLADE TYPE "A" FLEXURE LINK

PRINT OF FREQUENCIES

MODE NUMBER	CIRCULAR FREQUENCY (RAD/SEC)	FREQUENCY (CYCLES/SEC)	PERIOD (SEC)	TOLERANCE
1	.3510E 03	.5586E 02	.1790E-01	.2363E-15
2	.3530E 03	.5618E 02	.1780E-01	.0000E 00
3	.4941E 03	.7864E 02	.1272E-01	.2384E-15
4	.2860E 04	.4551E 03	.2197E-02	.1818E-10
5	.2936E 04	.4673E 03	.2140E-02	.1116E-11
6	.3859E 04	.6142E 03	.1628E-02	.9470E-11
7	.4735E 04	.7536E 03	.1327E-02	.4166E-08
8	.5288E 04	.8416E 03	.1188E-02	.2479E-06

PRINT OF EIGENVECTORS

FIGURE 4.40 Computer Printout of Rig B.2 Natural Frequencies

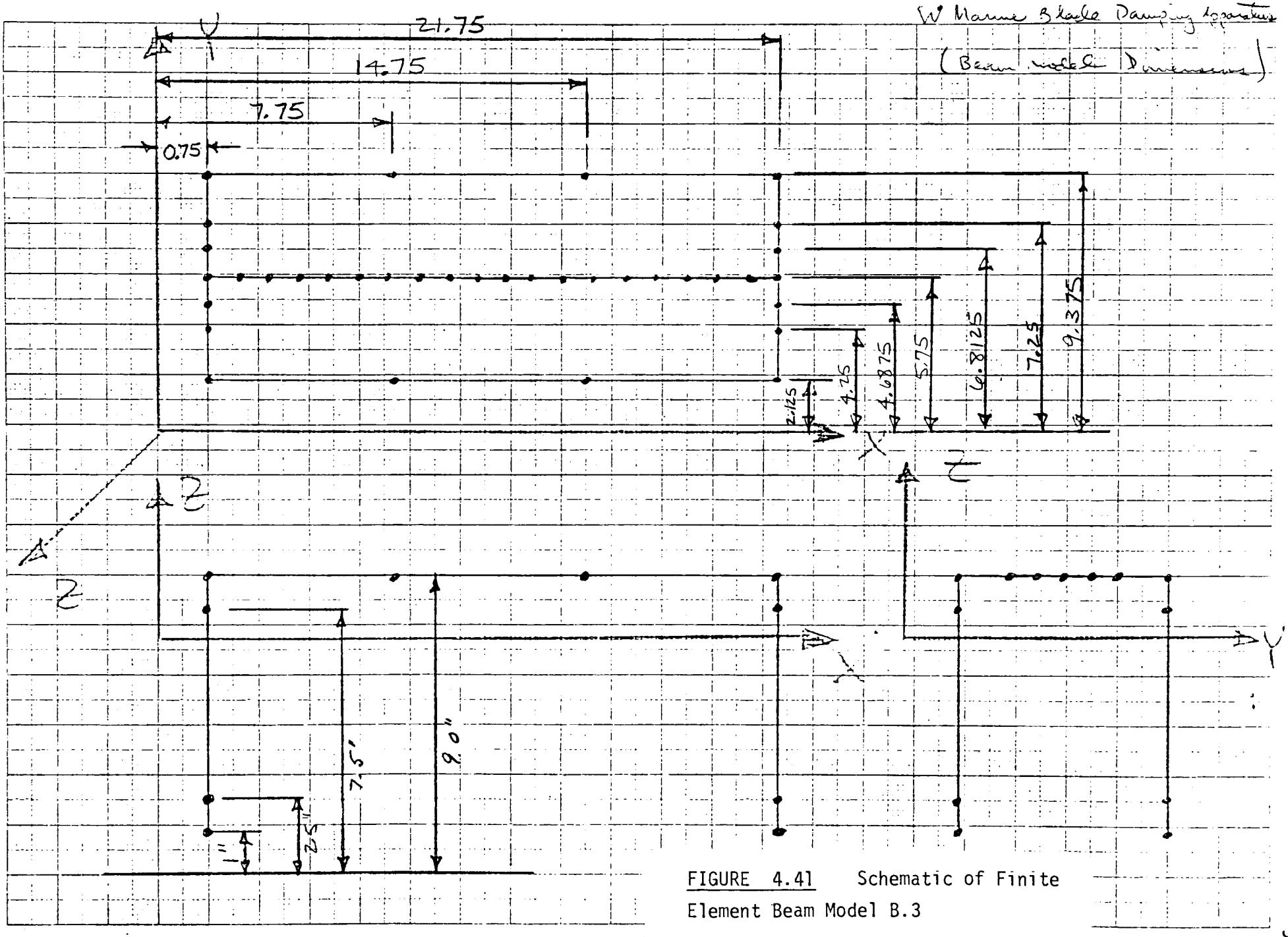

FIGURE 4.41 Schematic of Finite Element Beam Model B.3

4/30/79 RIG TYPE B : NO BLADES 7" legs

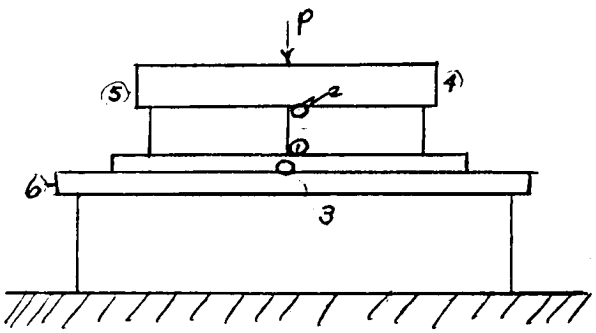

Plot

#1055 Table & Rig struck up & down accelerometer in center of bedplate (1)

#1056 Table & Rig struck up & down accelerometer on 4" plate (2) two plots: 2 frequency ranges

#1057 Table & Rig; struck up & down accelerometer on table in front of rig. (3)

#1058 Rig struck on end (4) accelerometer on 4" plate (5)

#1059 Table & Rig struck on end (4) accelerometer on table (6)

FIGURE 4.42 Accelerometer Locations for Rig 'B' Correlation Tests

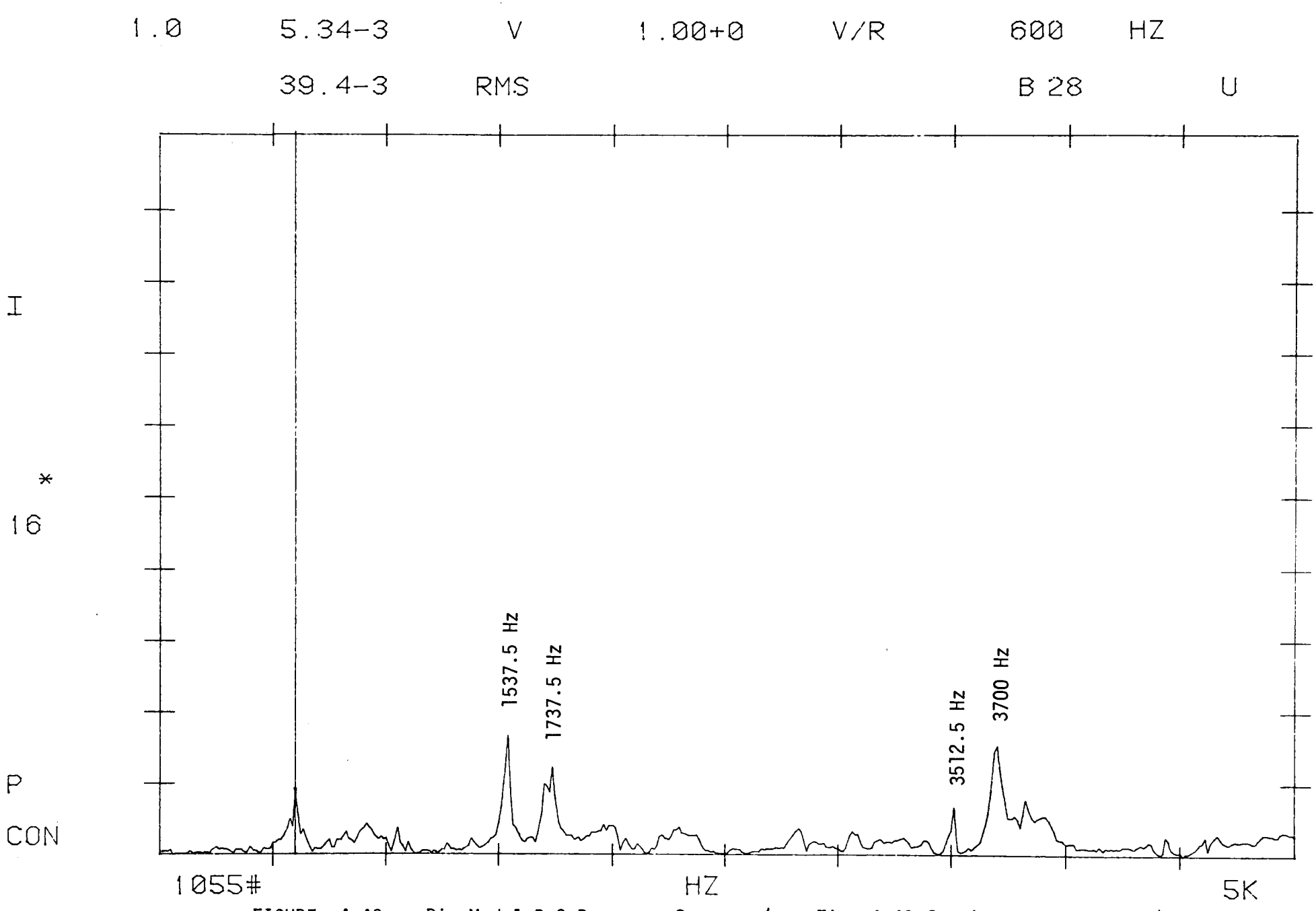

FIGURE 4.43 Rig Model B.2 Response Spectra (see Fig. 4.42 for impulse direction)

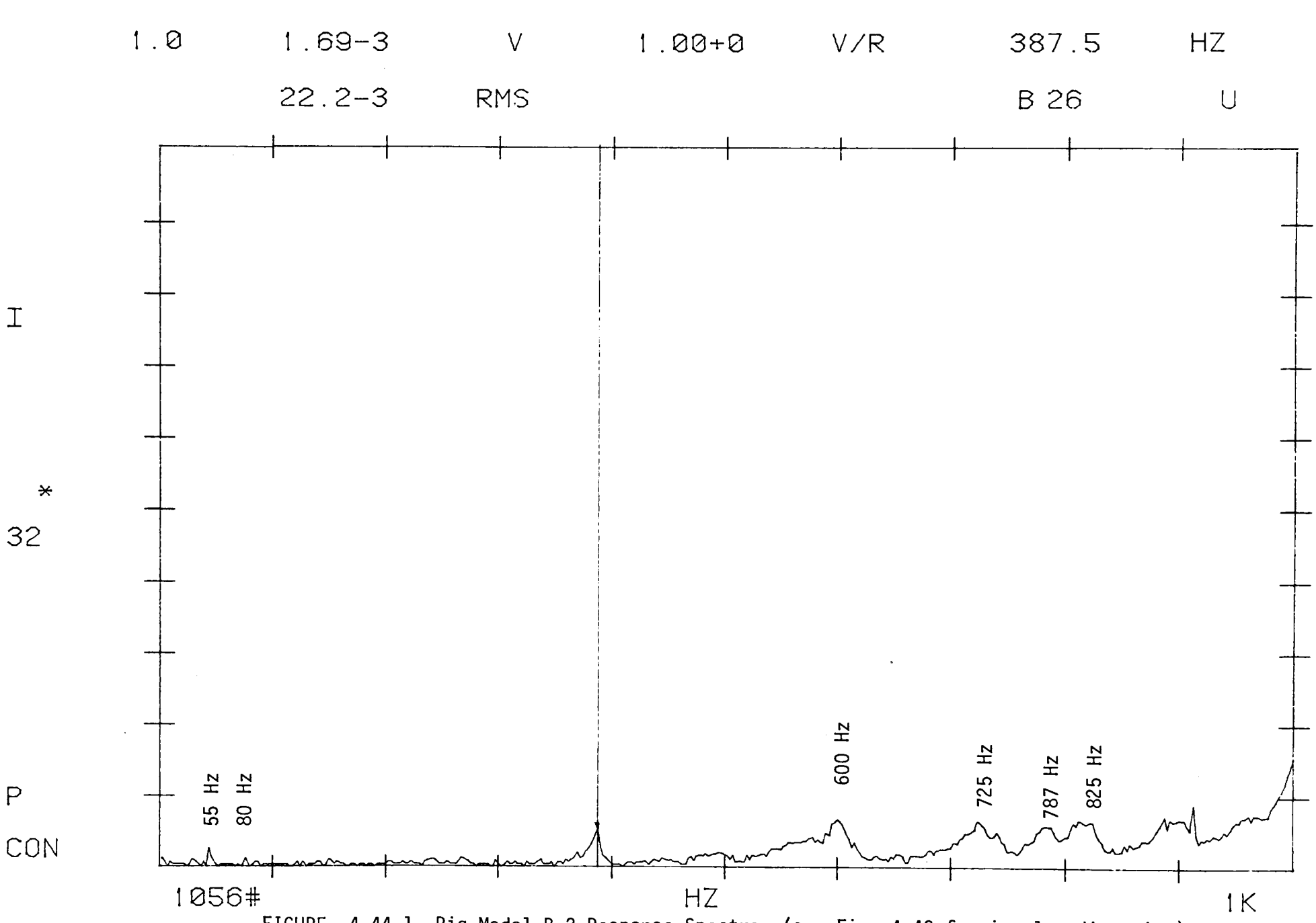

FIGURE 4.44.1 Rig Model B.2 Response Spectra (see Fig. 4.42 for impulse direction)
Zero to One Kilohertz Range

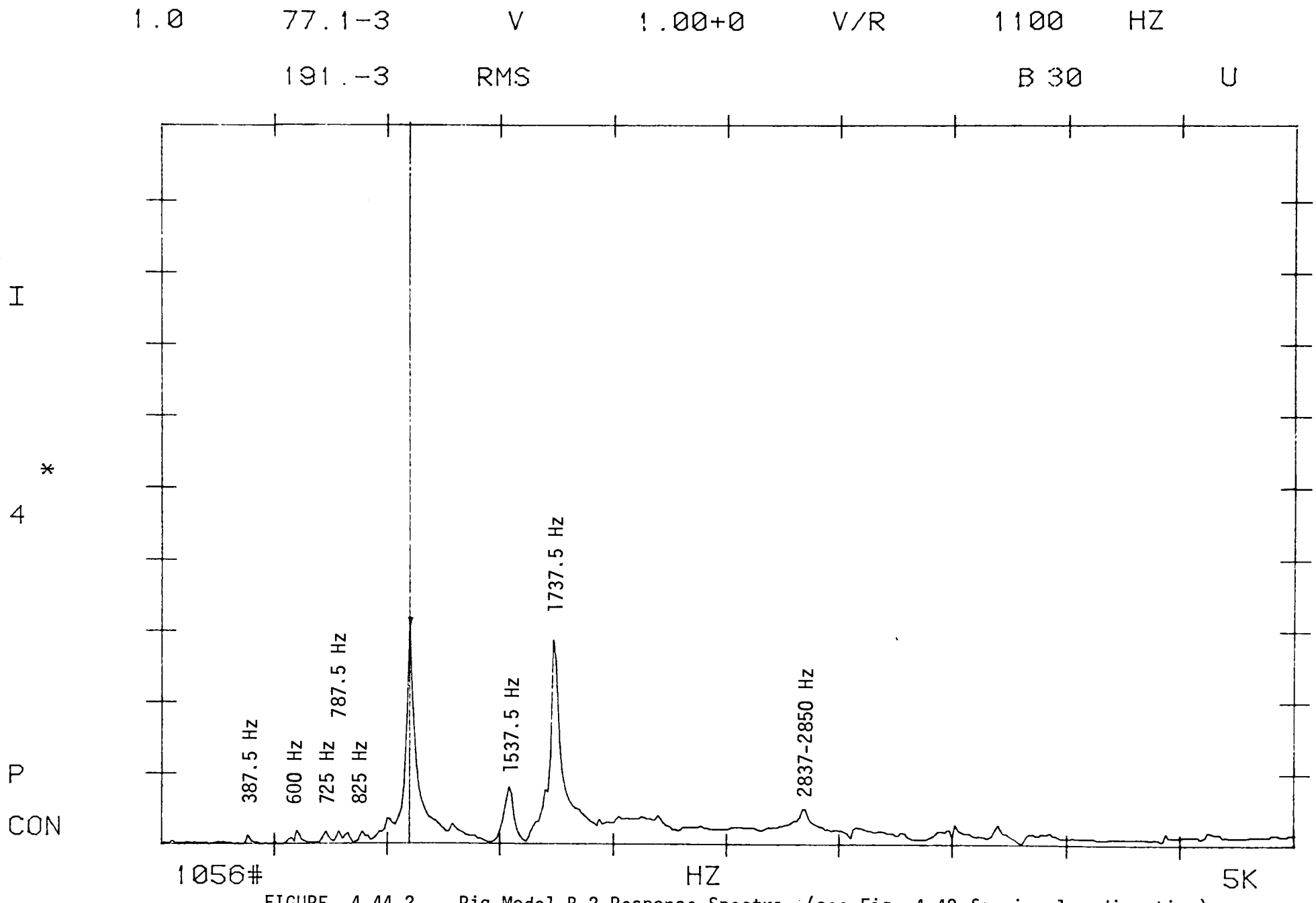

FIGURE 4.44.2 Rig Model B.2 Response Spectra (see Fig. 4.42 for impulse direction)
Zero to Five Kilohertz Range

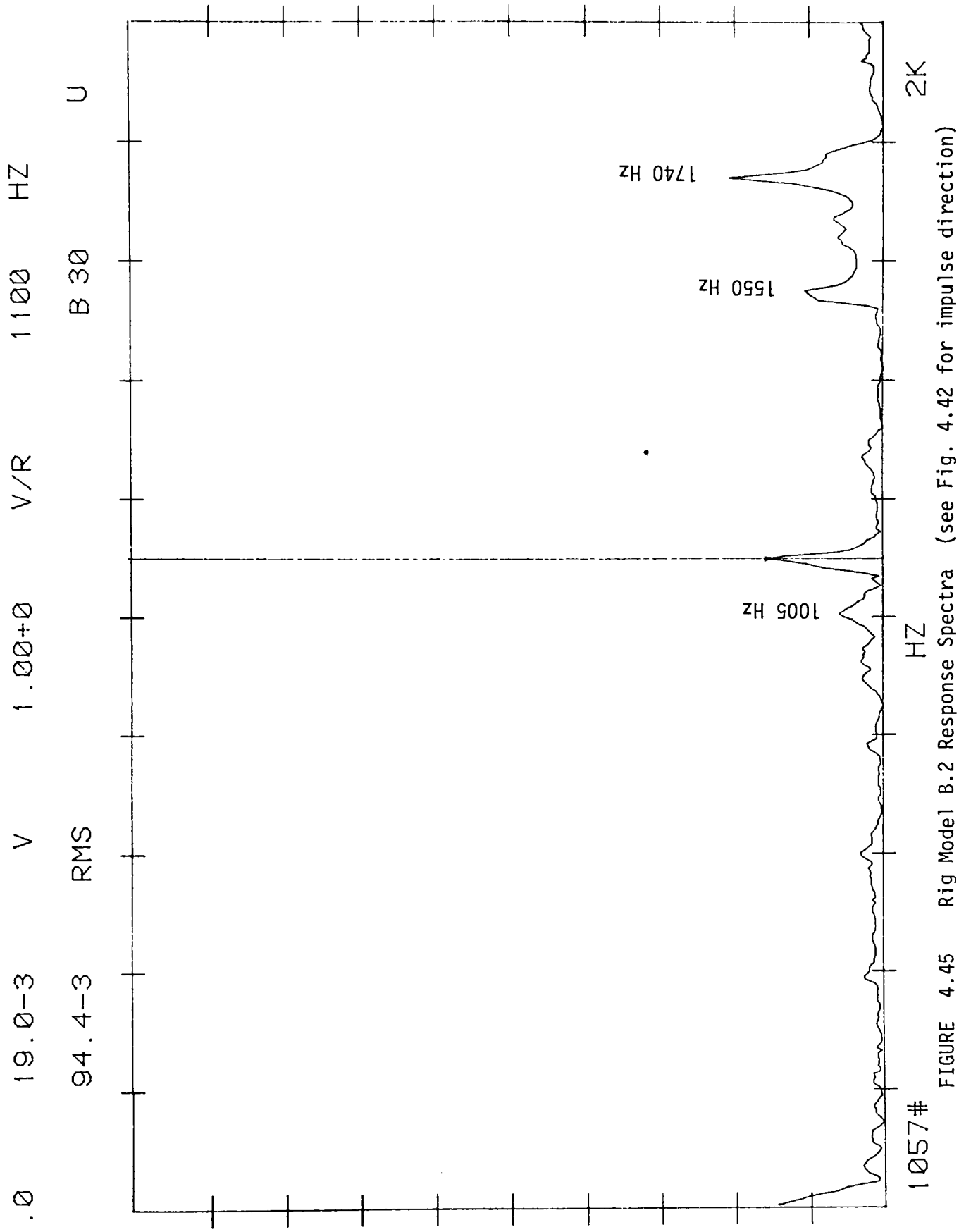

FIGURE 4.45 Rig Model B.2 Response Spectra (see Fig. 4.42 for impulse direction)

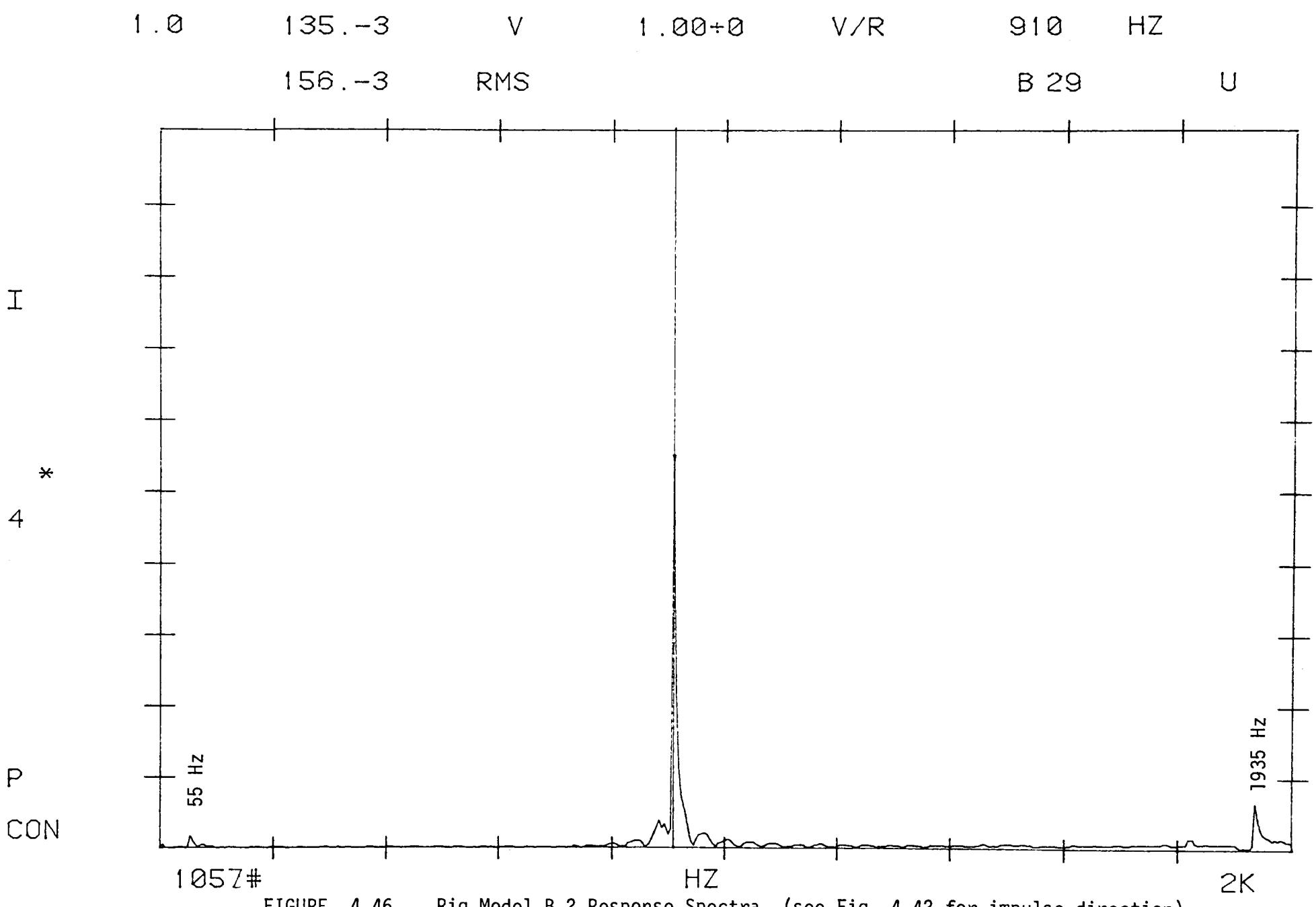

FIGURE 4.46 Rig Model B.2 Response Spectra (see Fig. 4.42 for impulse direction)

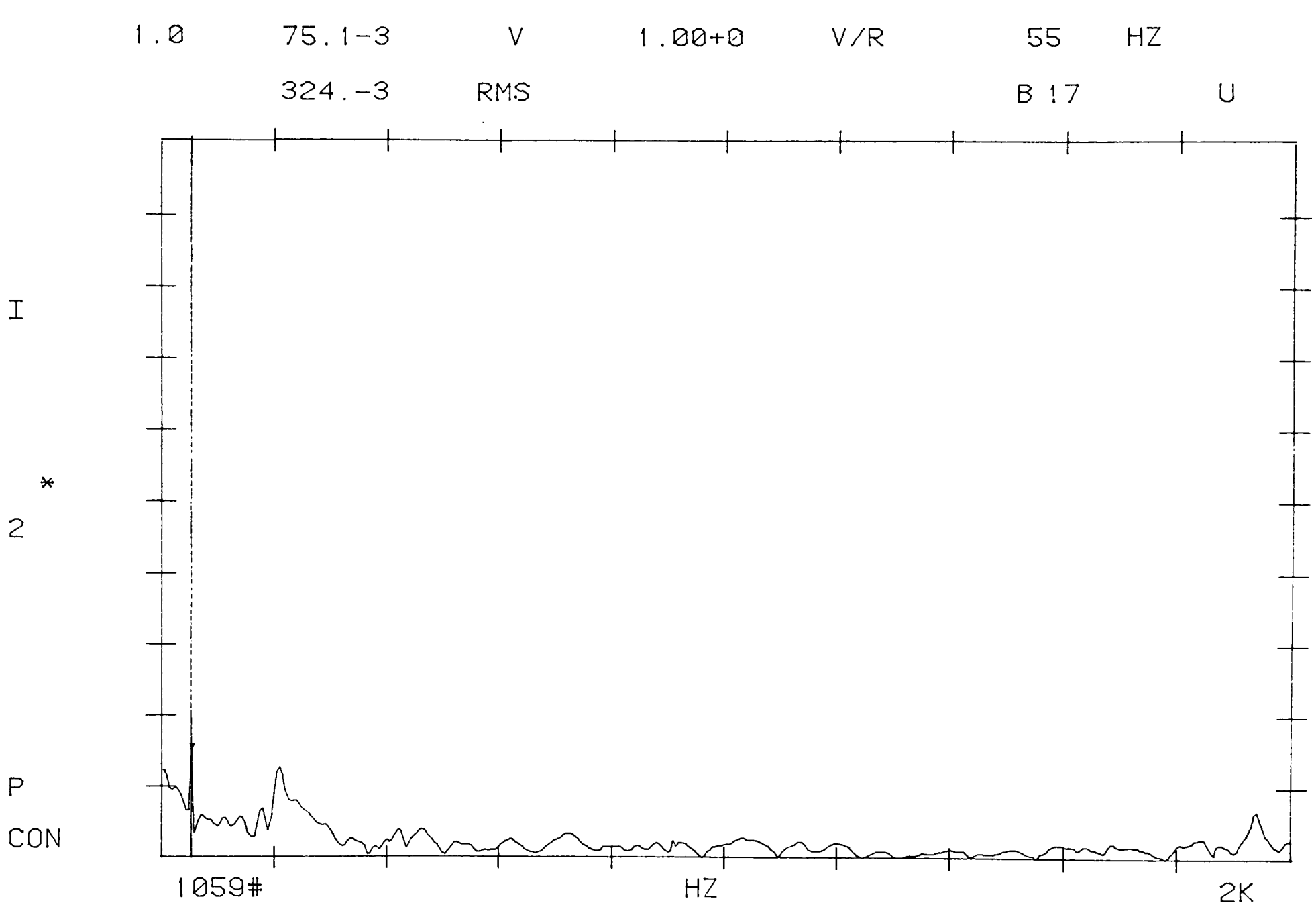

FIGURE 4.47 Rig Model B.2 Response Spectra (see Fig. 4.42 for impulse direction)

Accelerometer tests @ 1110 Hz
same setup as for rig A except 4" plate location

Position	Accel · V $\times 10^{-3}$
1	2.47
2.	5.37
3.	9.46
4.	4.45
5.	1.67
6	6.89
7.	11.2
8.	12.8
9	6.87
10.	2.67
11	12.1
12	1.73
13.	3.99
14	10.8
15	9.03
16.	7.93
17	8.85
18	16.6
19	26.2
20	5.73

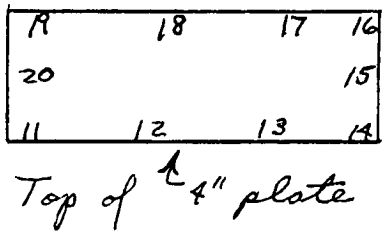

No significant freqaencies around 260 Hz.
No further tests will be conducted.

FIGURE 4.48 Frequency Investigation for Modal Analysis Correlation

Natural Frequency Comparisons

Mode	Finite Element Prediction (Hz)	Experimental Determination (Hz)
1	55.9	55.0
2	56.2	
3	78.6	80.0
4	455.1	388.0
5	467.3	
6	614.2	600.0
7	753.6	725.0
8	841.6	825.0

NOTE: 190 to 270 Hz; Testing Range - No Rig Activity

FIGURE 4.49 Comparison of Computer Predictions and Experimental Results for Model B.2

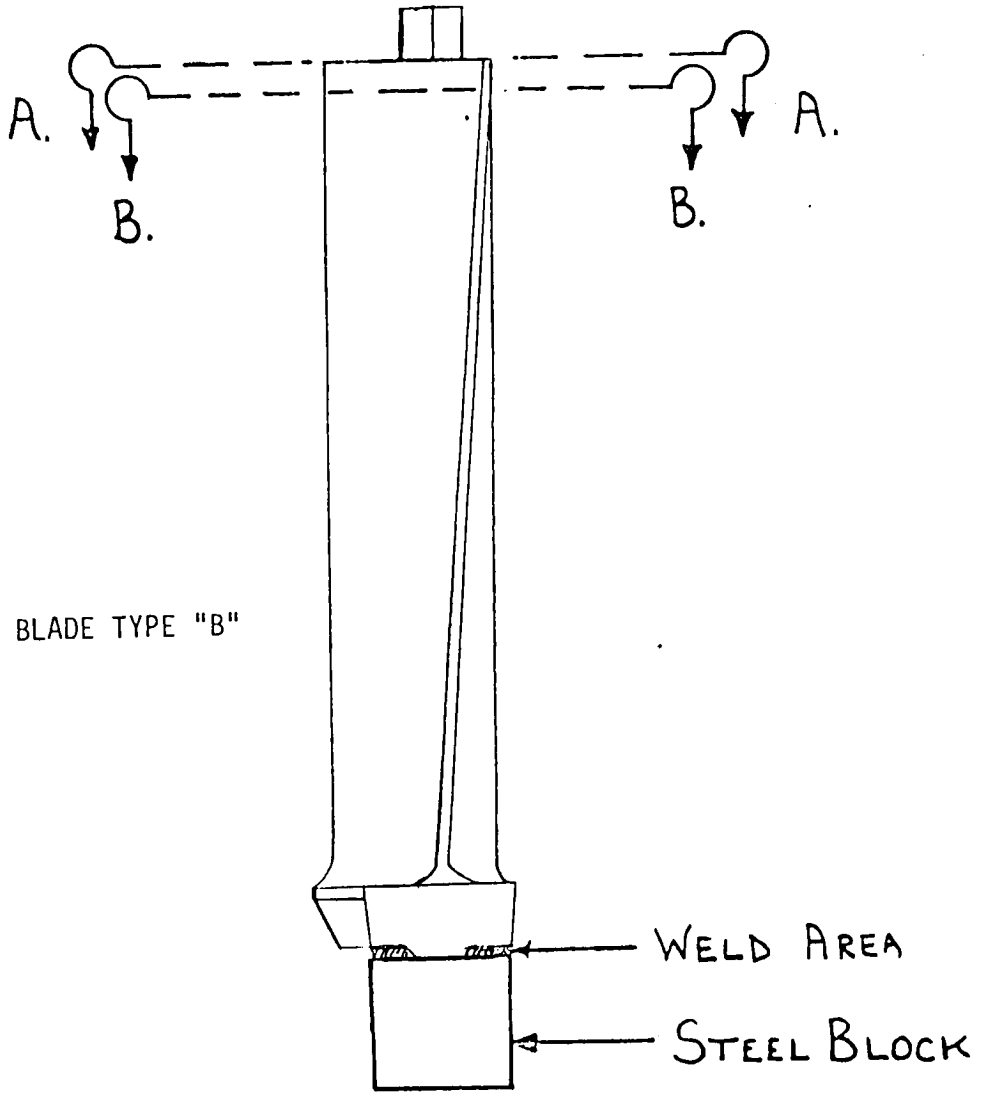

FIGURE 4.50 Experimental Configuration of Single Blade

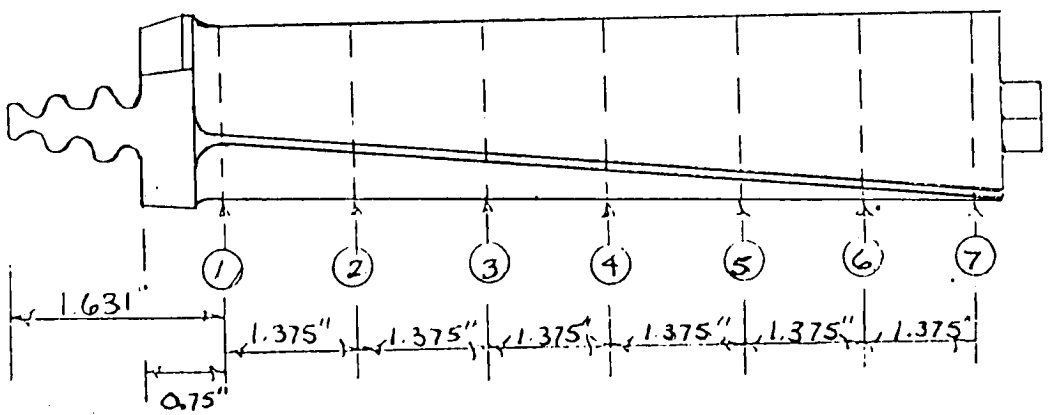

FIGURE 4.51 Axial Locations of Blade Cross Sections

Section 2

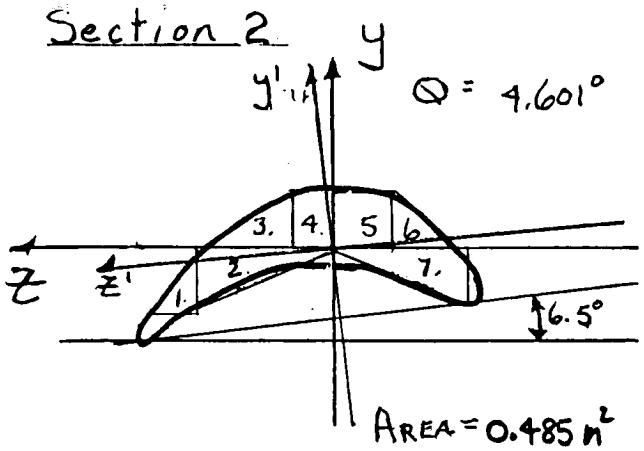

AREA = 0.485 in²

Section 3

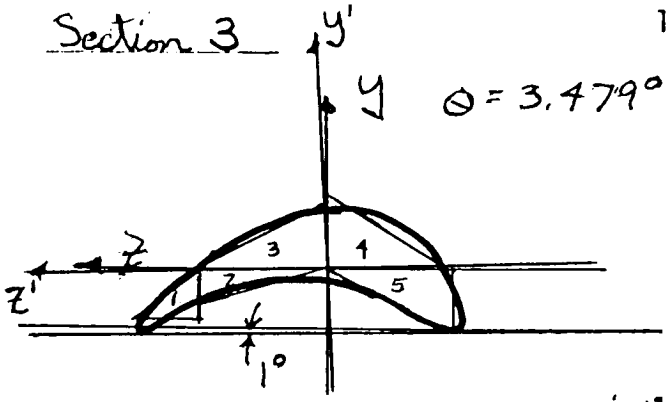

AREA = 0.410 in²

Section 4

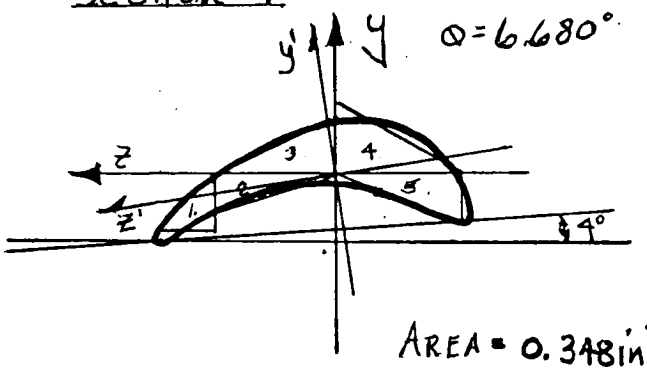

AREA = 0.348 in²

Section 5

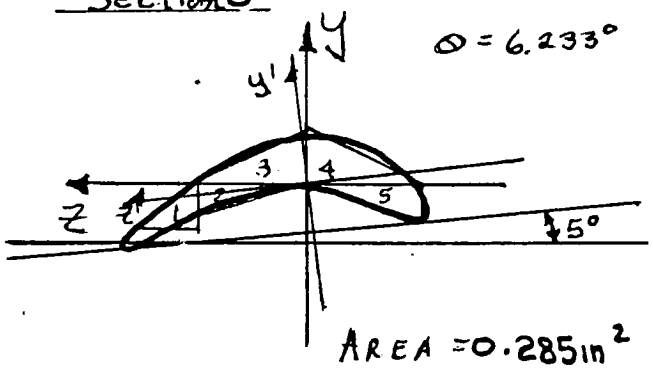

AREA = 0.285 in²

Section 6

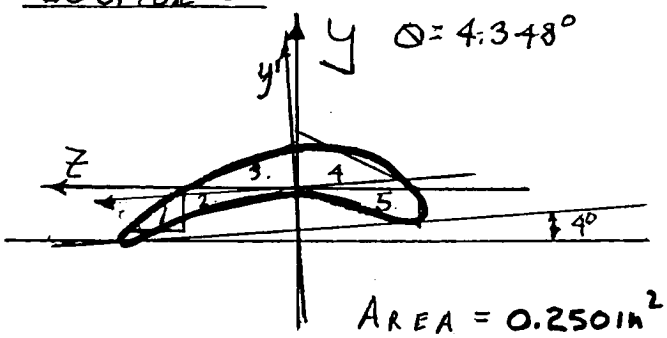

AREA = 0.250 in²

Section 7

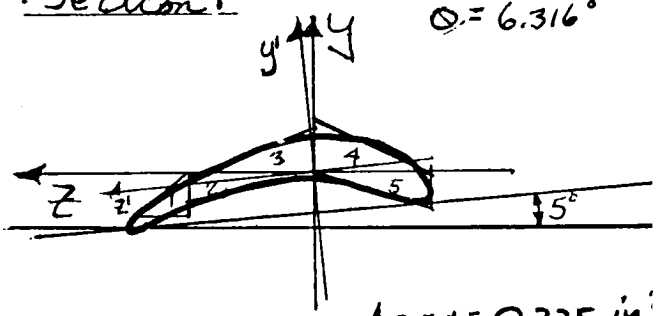

AREA = 0.225 in²

Section 8

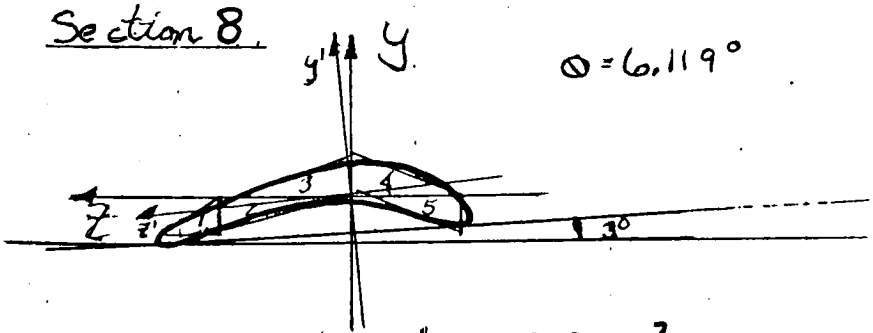

AREA = 0.200 in²

FIGURE 4.52 Blade Type "B"

Cross Section Dimensions

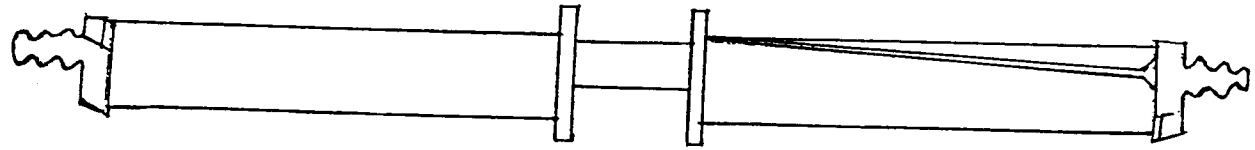

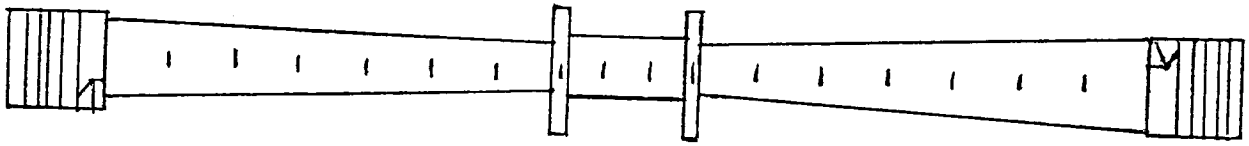

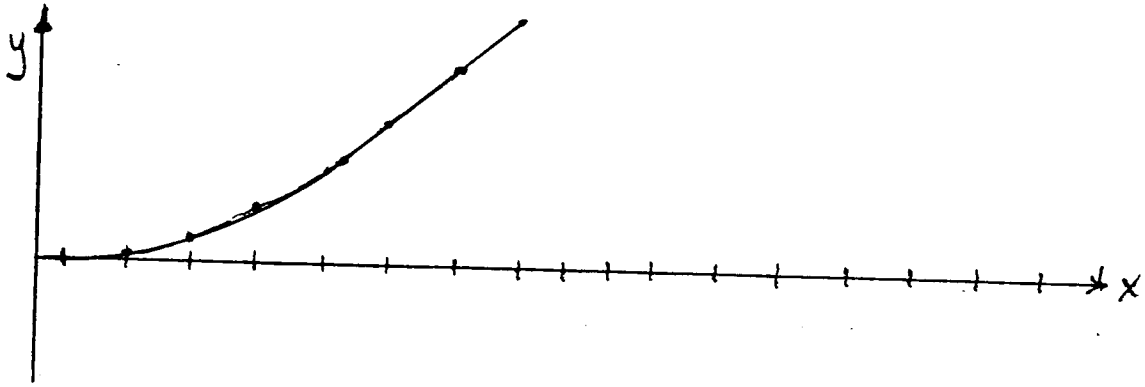

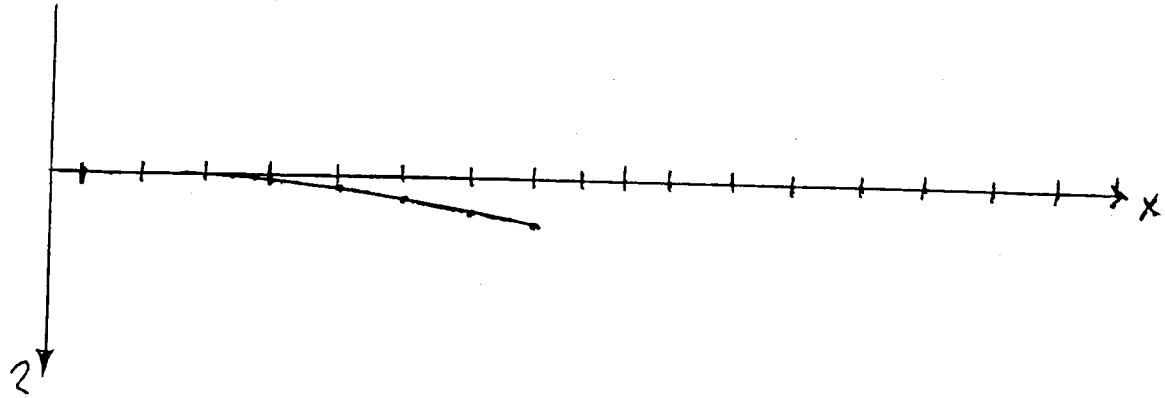

FIGURE 4.53 Model 1: Mode Shape of

Left Blade Rigidly Mounted. f= 199.7 H

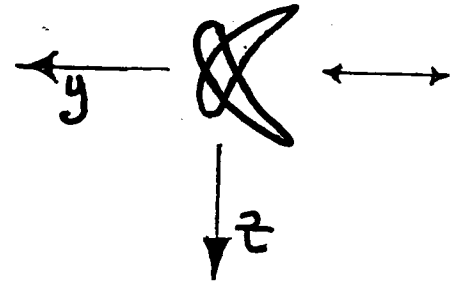

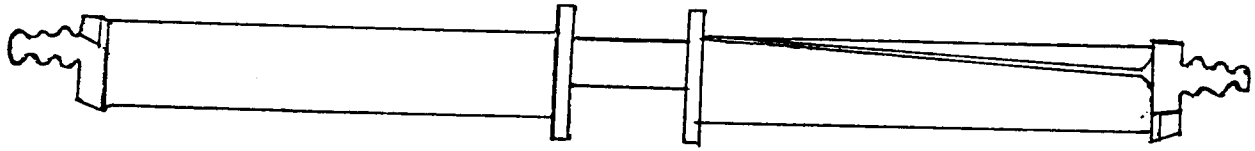

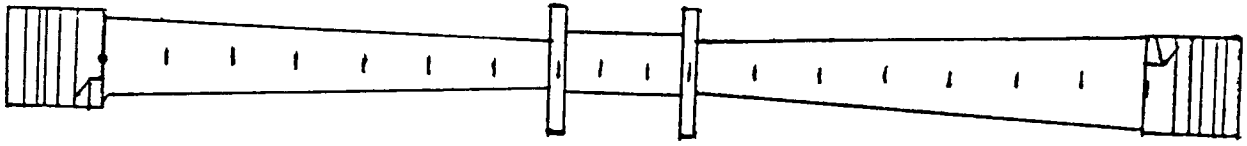

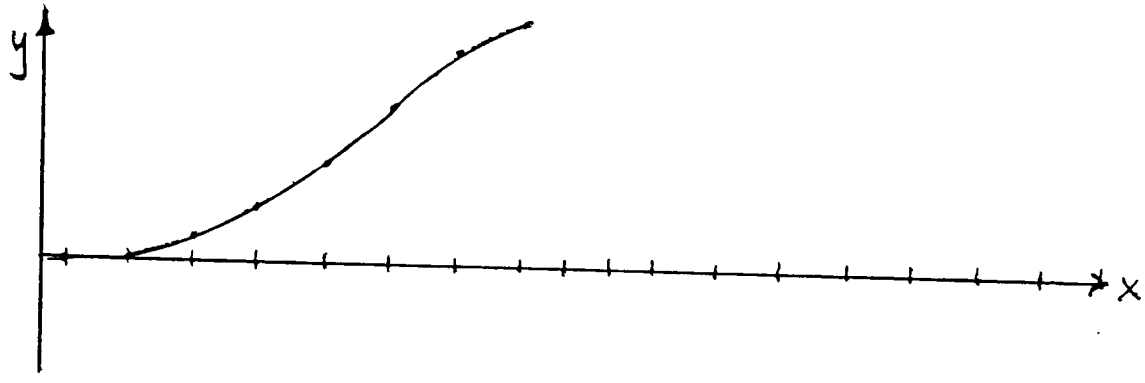

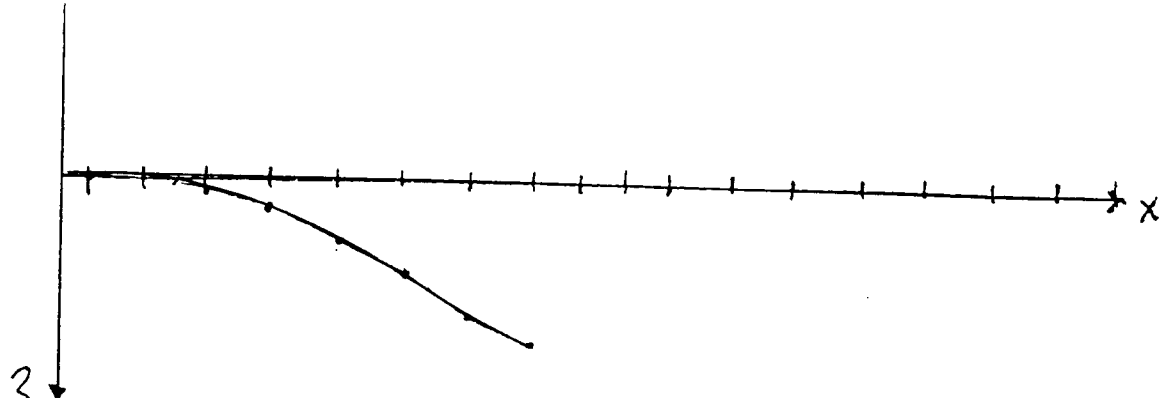

FIGURE 4.54 Model 2: Mode Shape of

Left Blade Rigidly Mounted. f= 239.8 H

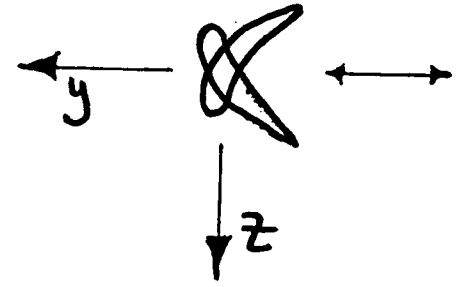

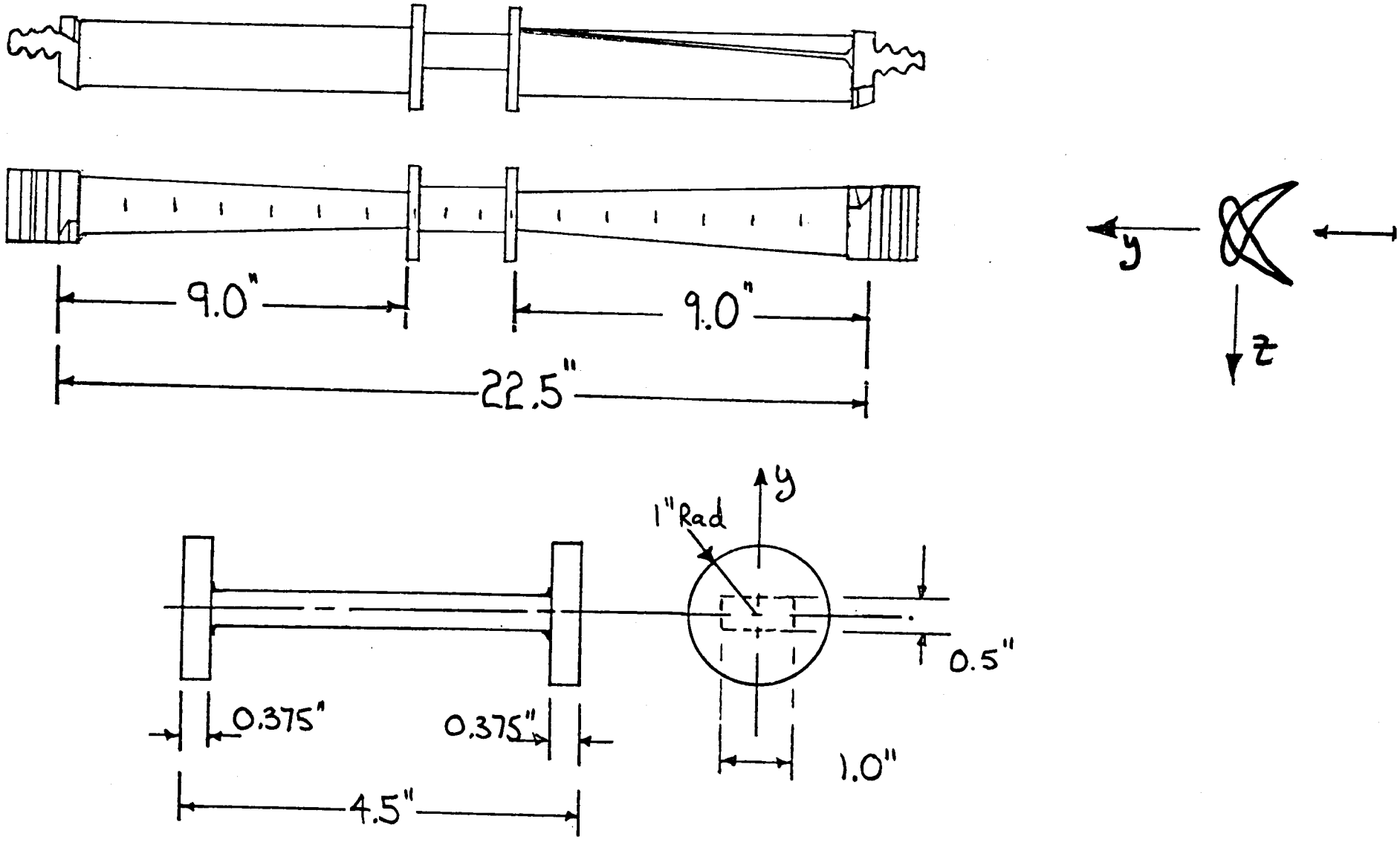

FIGURE 4.55 Blade Pair in Combination w/ Flexure Link. Flexure Link Dimen.

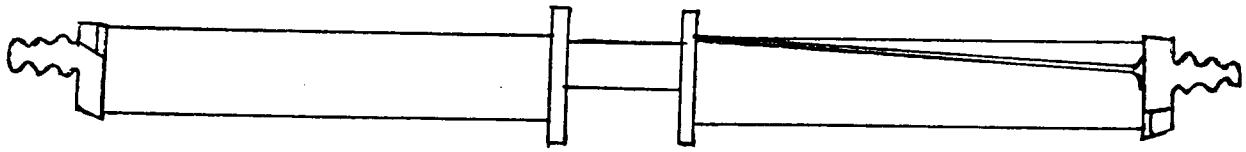

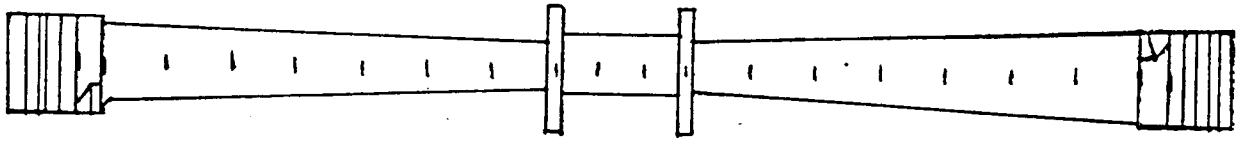

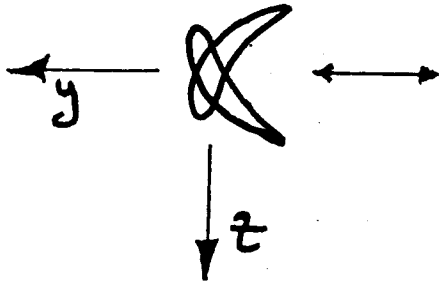

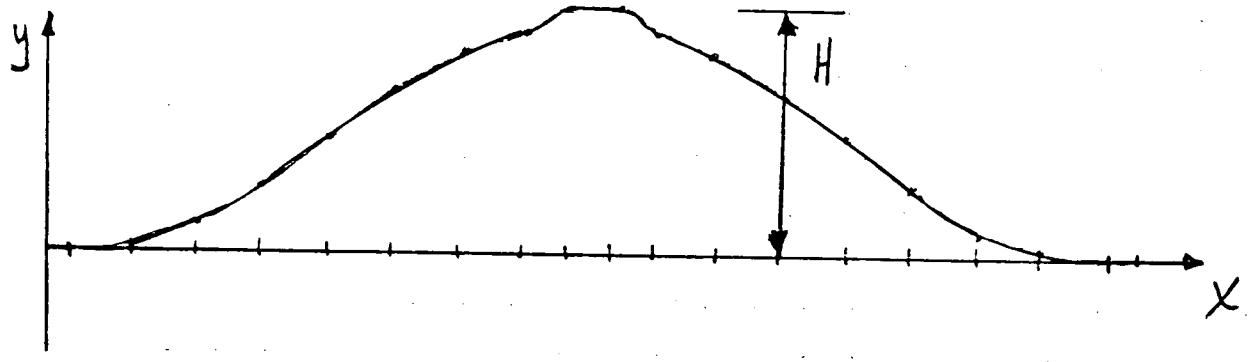

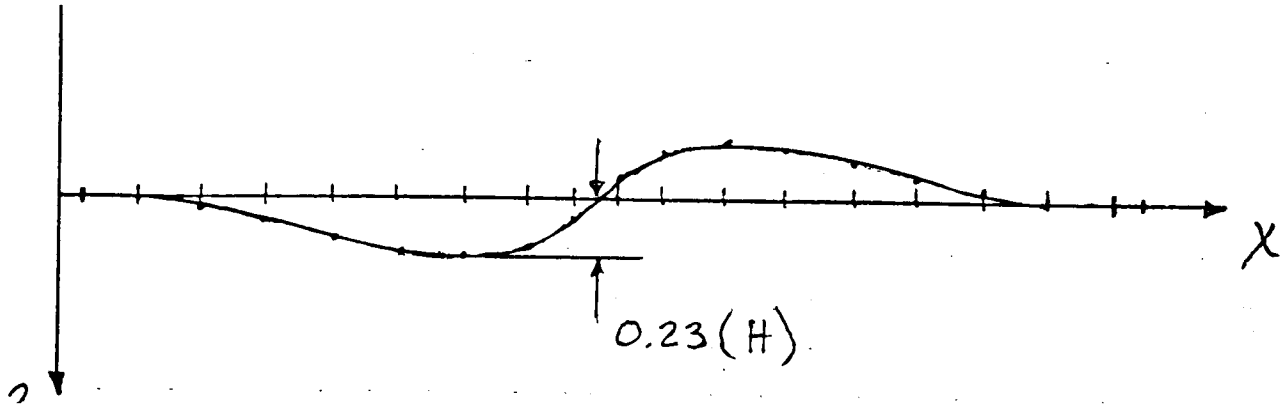

FIGURE 4.56 Mode Shape #1 For Blade Pair w/ Flex. Link. f= 207. Hz

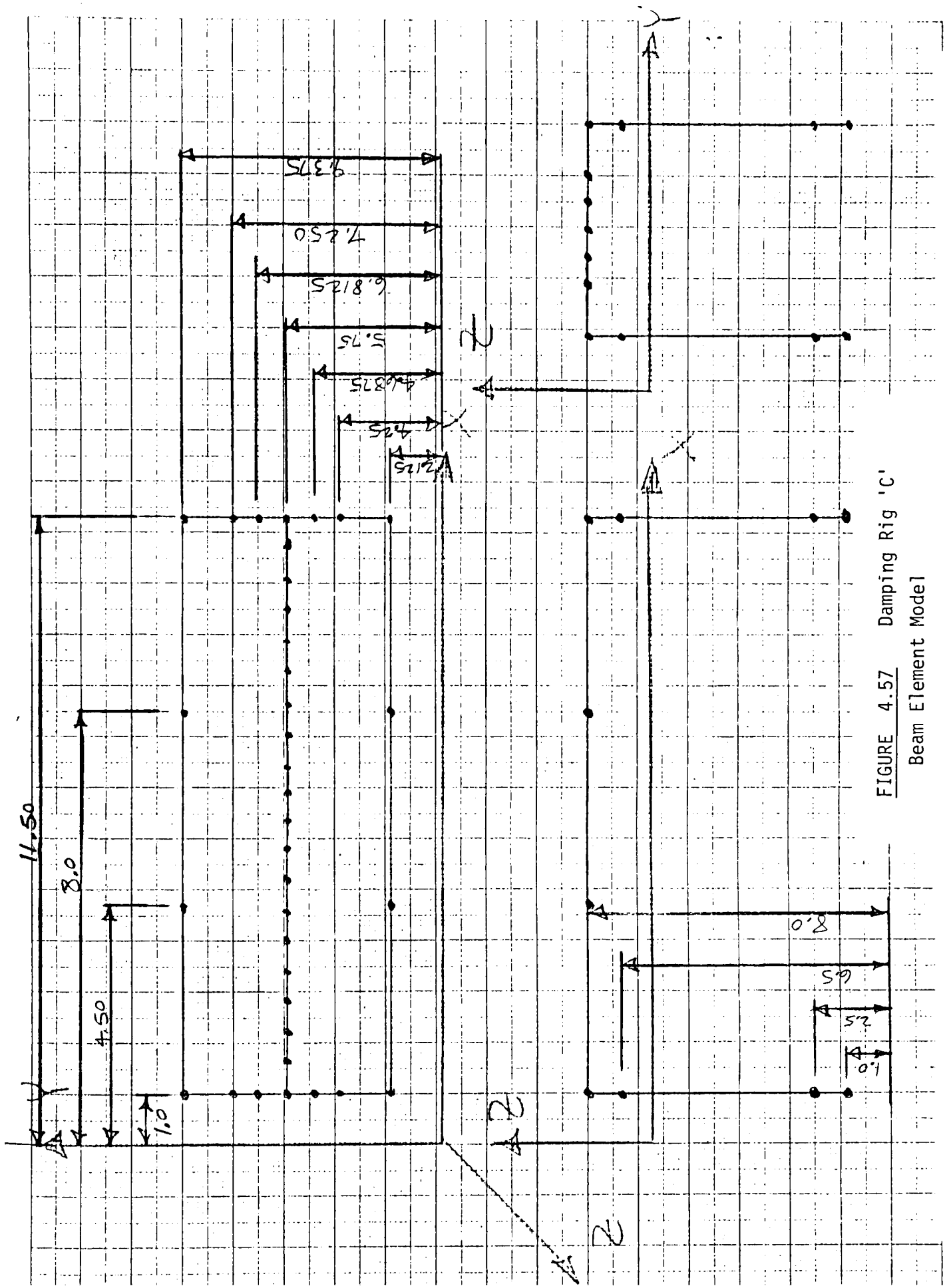

FIGURE 4.57 Damping Rig 'C'
Beam Element Model

PRINT OF FREQUENCIES

MODE NUMBER	CIRCULAR FREQUENCY (RAD/SEC)	FREQUENCY (CYCLES/SEC)	PERIOD (SEC)	TOLERANCE
1	.4611E 03	.7339E 02	.1363E-01	.3422E-15
2	.4625E 03	.7361E 02	.1358E-01	.6802E-16
3	.5881E 03	.9359E 02	.1068E-01	.5470E-15
4	.4209E 04	.6700E 03	.1493E-02	.2102E-15
5	.4506E 04	.7171E 03	.1394E-02	.3670E-15
6	.5906E 04	.9240E 03	.1082E-02	.7504E-13
7	.9492E 04	.1511E 04	.6619E-03	.5168E-10
8	.1338E 05	.2130E 04	.4694E-03	.1843E-05

PRINT OF EIGENVECTORS

FIGURE 5.58 Computer Printout of Rig 'C' Natural Frequencies

Wehle Research Lab
Rochester Institute Of Technology
Ph. 475-6104
Curt Beck

'C' Flexure Link
Tolerance: -0.000, +0.020 in.
Material: AISI 1020 Steel
Milled From 1.5 Inch Diameter Barstock
All Dimensions in Inches

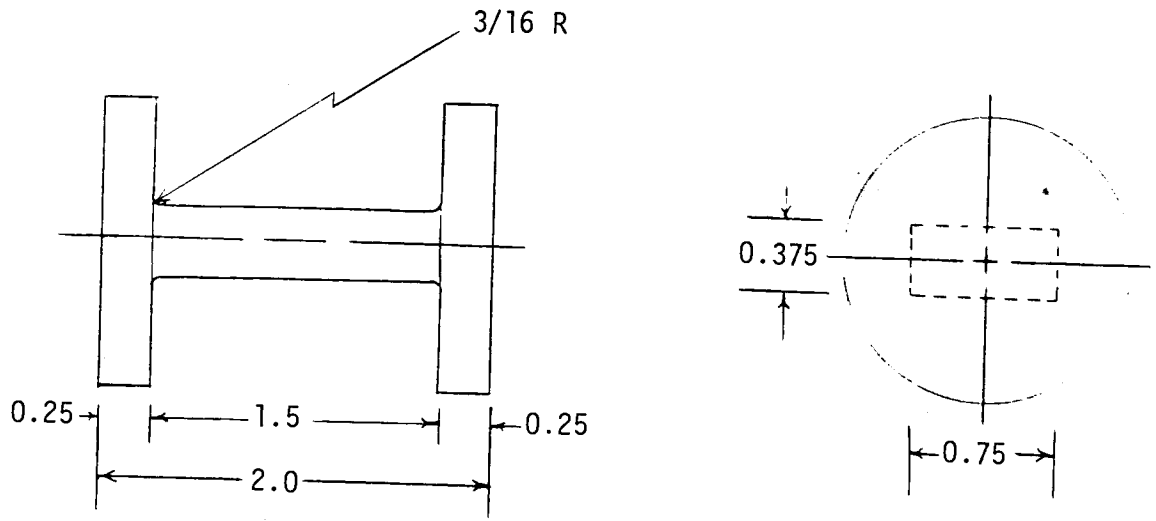

FIGURE 4.59 Flexure Link 'C' Dimensions

5.0 TEST PROCEDURES

5.1 General

Testing was undertaken in the following sequence. Steps 1 through 6, and 8 through 10 apply for all testing. Step 7 for Phase I testing is discussed in Section 5.2. Step 7 for Phase II testing covers procedures used for most of the data obtained in this study.

Step 1. The strain gages and instrumentation circuit shown in figure 3.3 were wired in place.

Step 2. The strain amplifier excitation voltage was adjusted to +9.65 volts and +10.10 volts for the half and quarter bridges, respectively. The particular blade group was then installed with its two root sections projecting through the end holes in the frame.

Step 3. Strain amplifier knob locations are shown in figure 3.12. The strain amplifier MODE and CALIBRATE knobs were set to 'Normal' and '0' respectively, and the BALANCE control was adjusted to give a zero volt output. With the CALIBRATE knob remaining at '0', the MODE was moved to 'Zero' and the 'Amp Zero' control screw was adjusted to give a zero volt output. Next, the MODE and CALIBRATE knobs were set to 'Normal' and '-2', respectively. The 'Amp Gain' control screw was adjusted such that the output voltage was +4.71 volts. The CALIBRATE knob was returned to '0' and the BALANCE control was again adjusted to give a zero volt output and locked in place. The steps mentioned in Item 2 were repeated to check output voltage. Several iterations were often necessary to obtain all desired voltages simultaneously. This procedure balanced and calibrated the bridge circuit. For the given combination of strain gages and resistors, a gain of +4.71 resulted in an output voltage directly calibrated in microstrain. For example, an output voltage of +2.34 volts corresponded to a tensile strain of 234 με. The gain calculations are shown below.

Representing a Given Strain (Quarter Bridge)

$$R_{CAL} = \frac{S\ R_a}{N_a\ F \frac{\Delta L}{L}}$$

where

R_{CAL} = Calibration Resistor = 357,000 ohms

S = Type of calibration: 1, if single shunt, 2, if double shunt = 1

N_a = Number of active arms in the strain gage bridge or transducer = 1

F = Gage Factor of the transducer or strain gage = 2.08 (from manufacturer)

$\frac{\Delta L}{L}$ = Strain, or length change/unit length of bridge gage arm = ?

Using the internal calibration resistor to simulate a loaded strain gage, the resulting $\Delta L/L$ for direct strain readout is 4.713×10^{-4} in/in. or 471.3 μ in/in. Therefore, by setting the calibration voltage to +4.71 volts, an output reading of +2.34 volts only has to have the decimal point moved two places to the right to get a micro strain value. The (+) or (-) sign represents tension or compression, respectively.

Step 4. Disk attachment sections were slid on to the blade pair roots. The flexure link was then heated in a localized area with a acetylene torch. The expanded blade pair then had shims inserted between the disk rim shoulder and the adjacent rig frame. The rig was the cooled by gently sprinkling with water as described in Section 3.2.

Step 5. As the blade pair cooled, the bending gage output was monitored and blade pair position was adjusted so that the bending gage output voltage was zero.

Step 6. Once the system had cooled to a steady-state condition, the micro-strain output of the axial gage was noted and the strain amplifier output of the channel of interest was input to the spectrum analyzer. Figure 3.11 shows the channel-directions vs. gage correlation.

Step 7. The 'Auto Arm' button of the analyzer was set and the blade group was gently rapped with an impulse blow using a peen end of a ball hammer, on the flexure link. The resulting vibration decay trace obtained from the strain gage signal was then stored, or 'captured' using the transient capture capability of the analyzer. The stored decay trace was then plotted as shown in figure 5.1. Two more decay plots were obtained for this particular blade pair orientation, at impulse load values different from the first impulse. These vibrations were then calibrated against blade tip displacement.

Step 8. Using the D.C. voltage offset capability of the analyzer, a load-displacement plot could be generated and measured. First, a plot was made of the gage output in the direction of interest with no blade tip displacement. Next, a weight of known magnitude was suspended from the center of the flexure link and the blade tip deflection was measured with a dial indicator. This blade tip movement caused a displacement in the D.C. voltage, which was then plotted on the same plot mentioned above. An example of such a plot is given in figure 5.2. This procedure was used to convert amplitude values on the vibration decay trace to known blade tip displacement values. Plot numbers, frequency range, micro strain, and calibration information was recorded for each load and each vibration direction. A typical data sheet is shown in figure 5.3.1-(.3) for blade Types A, B, and C.

Step 9. On completion of testing at one load level, the flexure link of the blade pair in use was then reheated and the number of load-generating shims was changed to obtain another blade pre-load value. Steps 5 through 7 were then repeated. In this manner, data was obtained for

three centrifugal loads, for both directions in which each blade pair was tested.

Step 10. The decay traces were then processed to obtain logarithmic decrement values by drawing the envelope of the decay curve, figure 5.4 , and calculating the logarithmic decrement at several locations along that curve. Decay amplitude values were converted to blade tip displacements using Step 8 information. The logarithmic decrement values were then calculated using the expression:

$$\text{Logarithmic decrement } \delta = \frac{1}{r} \log_e \frac{x_n}{x_{n+r}}$$

where

x_n is the vibration half-amplitude for the nth cycle

x_{n+r} is the vibration half-amplitude for the n+r cycle

r is the number of cylces between n and n+r cycles

Logarithmic decrement was then plotted vs. blade tip displacement for values of simulated centrifugal load. A typical reduced decay trace is shown in figure 5.4. Charts of damping logarithmic decrement vs. blade tip displacement are shown in figures 6.25 through 6.111.

5.2 Frequency and Amplitude Tests

Two requirements of the project were to investigate the effects of varying the excitation frequency and the excitation amplitude.

It was decided to test the blade groups at: (a) their natural frequency (b) one-third of nozzle passing frequency, and (c) at nozzle passing frequency. This was accomplished by fastening the electromagnetic shaker to the flexure

link. A clearance hole was drilled through the flexure link in the flow tangential direction for a #10 screw. The exciter was then hooked up with a soft spring decoupler to isolate the mass of the exciter coil from the blade pair so as not to induce any damping. A 10-32 tapped hole was made in the flexure link in the axial direction for similar purposes. A diagram of the exciter setup is shown in figure 5.5. These holes were also used to support the calibration weights.

The effect of amplitude variation on damping was determined by impulsing the blade and following steps 1-10 of the General Procedures. Three different force levels were used. The response was plotted, and determination of damping variations was made by overlaying the plots on a light box. The interest was in determining a qualitative change, if any, and not a quantitative one. The general scatter of data would make determining a characteristic damping value hard enough without trying to determine the variation for one blade group within a scatter band.

The results of frequency and amplitude investigation are given in Section 6.

5.3 Tests on Blade Type A

The effect of vibration frequency and amplitude were investigated during the Type A blade studies. The tests were conducted as described in Section 5.2. It was determined that excitation via the electromagnetic exciter was unacceptable (see Section 6.1) even for natural frequency forcing. It was also determined that amplitude variation had no effect on damping logarithmic decrement. Therefore, amplitude and frequency tests were not conducted on B and C type blades.

An obvious alternative to the electromagnetic exciter was impulse-excitation of the decay through a blow from a hammer onto the flexure link. It was found that a smart, well-placed rap on the flexure link would usually initiate a clean decay trace, free from any rig or blade harmonics. After full consideration of both excitation procedures, the impulse method was adopted as part of the test sequence. The decay traces achieved by rapping were far superior to those obtained by forced excitation. This was due to the rig detuning mentioned earlier, and also because the blade pairs themselves had widely separated modes. Where coupling occurred between blade pair modes, (Type A and Type C twisted blades), electrical signal filtering was also used

to exclude unwanted effects: see Section 3.4.

There were no problems in testing in the blade turbine tangential direction. However, when the blade was excited in its turbine axial direction, the tangential fundamental frequency also entered the response spectrum, figure 5.8. The spectrum for axial excitation shown then showed two frequency components; one at 560 Hz representing axial vibration and the other at 360 Hz representing the tangential vibration component. Since present interest was only with the axial mode damping, the tangential component was filtered out electronically, using a specially designed circuit. This was done using the Butterworth filter system described in Section 3.4. Other testing and data reduction otherwise proceeded as outlined in Section 5.1. The response curve for this filter is shown in figure 5.6.

5.4 Tests on Blade Type B

Only left-hand, Type B blades were available for testing. Because of the orientation of the airfoil cross-section, the blade tips were out-of-plane from each other as shown in figure 1.2. During testing, this orientation together with the airfoil twist caused certain displacements to occur in directions other than that of specific test interest. This problem was minimized by monitoring the appropriate strain gages in each instance.

No actual disk segments were available for testing with the Type B blades, so two disk segments were manufactured. The proportions of the fir-tree root were obtained from a blueprint submitted by the turbine blade supplier. A pair of blade roots were manufactured from AISI 4150 material by the EDM process. The minimum root groove tolerance envelope was used to program a travelling wire EDM machine which could hold a +0.0002 inch tolerance. AISI 4150 steel was used because it was the only readily-obtainable steel with strength characteristics comparable to those of the AISI 403 steel disk material. A photo of a disk segment manufactured in this manner appears in figure 3.5.

All welding of the blades to the flexure links was done by heliarcing with a 316 stainless steel rod. The final strength obtained was stated to be about 96 percent of the unwelded material. The extreme temperatures

involved are highly localized. This avoids annealing the blade material which the alternative of gas welding would require. Certain problems arose during the welding process from the stellite erosion shield inserts which exist in the Type B blade tips. The stellite was held in place by a considerable amount of brazing material which had a vaporization temperature lower than the heliarcing temperature. When the heliarc tip approached the stellite, the brass would boil out into the 316 stainless steel weld material and form a local, poor-quality, slag-type weld. Several of the initial Type B blade pairs which were tested broke at the weld due to this condition, as the blade pair axial load was applied. Those pairs which survived were tested using the same procedure in Section 5.1.

Because of the 45 degree twist and the taper of the Type B blades, there were two distinct natural frequencies associated with axial and tangential directions. This clear separation of modes made additional signal filtering unnecessary.

5.5 Tests on Blade Type C

The Type C blades were of ball and shank construction, figure 2.5. An alternating pattern of long-shank and short-shank blades was used, as shown. Six Type C blade pairs of each shank length were tested.

The Type C blades also had stellite leading edge inserts, but the amount of brazing used to hold them in place was not enough to cause problems of the type encountered when welding the Type B blades. However, since the twist and taper was not as great in this case as with the Type B blades, there was some coupling between vibrations in the tangential direction and the axial direction. The axial frequency did not appear in tangential tests, but the tangential frequency appeared in axial tests. The unwanted mode was filtered out in the manner described for Type A tests. The response curve for the Type C filter is shown in figure 5.7. No other problems were encountered with the Type C tests. Testing proceeded as described in Section 5.1.

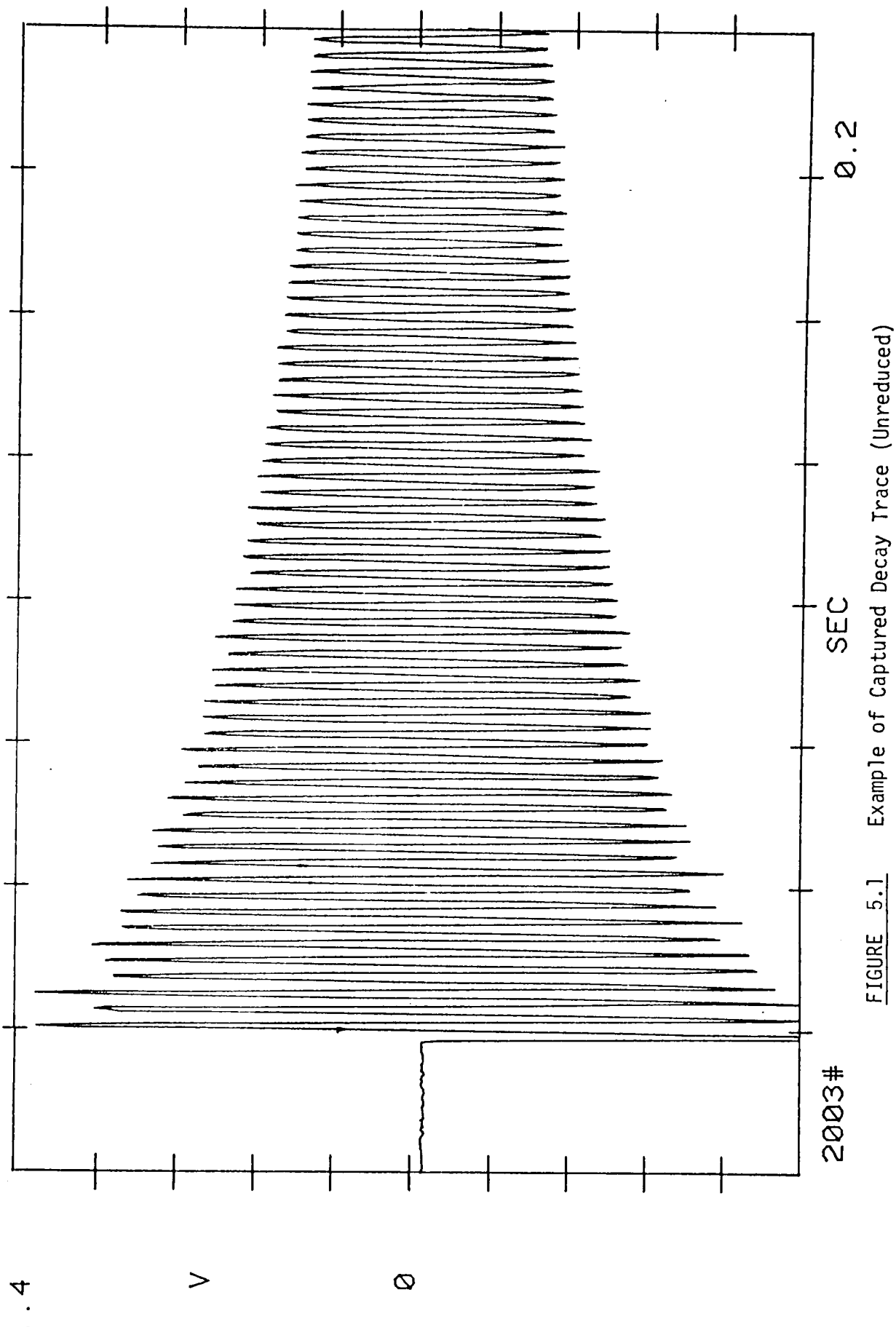

FIGURE 5.1 Example of Captured Decay Trace (Unreduced)

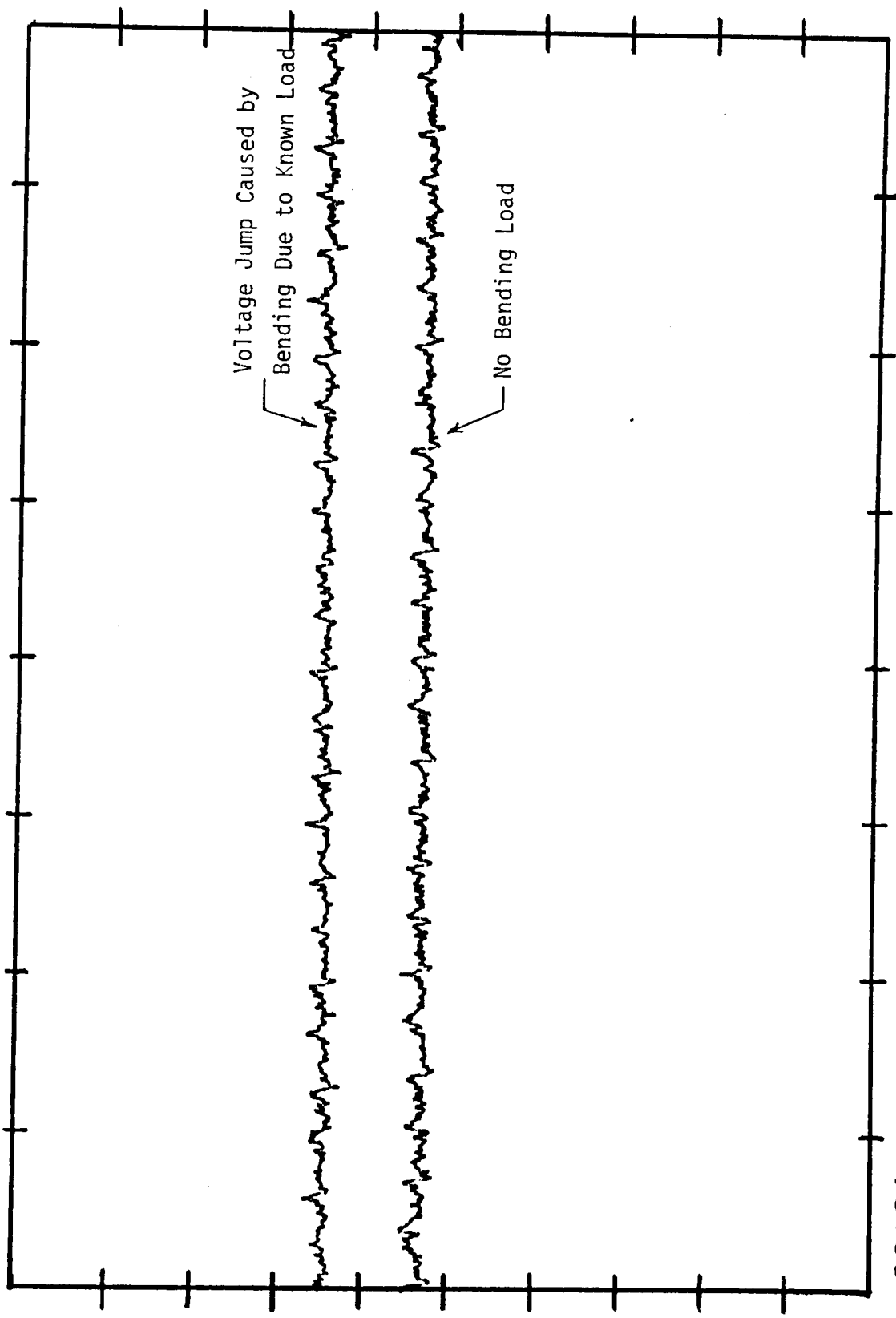

FIGURE 5.2 Example of D.C. Voltage Offset Calibration

A = 0.41 in² AIR TESTS

PLOT NUMBERS	MICRO STRAIN	FREQUENCY (Hz)	MODE	DISP. (IN) 11.45 LBS	LOAD (LBS)
6/19			TAN		
4421-4424	239-236	188.75-190	T	0.0019	2921
4425-4428	367-354	195-197.5	T	0.0018	4434
4429-4432	447-442	201.25-201.25	T	0.0016	5467
4321-4324	247-241	186.25-187.5	T	0.002	3001
4325-4328	366-359	195-195	T	0.0018	4459
4329-4332	450-447	201.25-201.25	T	0.0016	5517
5221- FLEXURE DATA NOT COMPONENT. SEE PLOTS	LINK BENT OUT ACCEPTABLE. STRONG	OF TANGENTIAL PLANE. AXIAL FREQUENCY			
5521-5524	241-230	185-186.25	T	0.0019	2897
5525-5528	369-363	195-195	T	0.0018	4502
5529-5532	451-447	198.75-198.75	T	0.0017	5523
5121-5124	244-236	195-192.5	T	0.0019	2952
5125-5128	366-361	200-200	T	0.0018	4471
5129-5132	449-445	203.75-203.75	T	0.0016	5498
4021-4024	244-241	186.25-186.25	T	0.0020	2983
4025-4028	366-358	196.25-196.25	T	0.0018	4453
4029-4032	452-440	201.25-201.25	T	0.0016	5486
4521-4524	245-239	185-185	T	0.0020	2977
4525-4528	366-~~402~~ 361	195-193.75	T	0.0017	4471
6/20					
4529-4532	452-448	200-200	T	0.0016	5535
4821-4824	243-240	183.75-183.75	T	0.0019	2970
4825-4828	370-364	195-195	T	0.0018	4514
4829-4832	451-~~365~~ 406	201.25-201.25	T	0.0017	5271
5421-5424	244-239	190-190	T	0.0021	2970
5425-5428	371-365	200-200	T	0.0017	4526
5429-5432	452-442	206.25-205	T	0.0015	5498
4721-4724	244-240	185-186.25	T	0.0020	2977
4725-4728	371-367	197.5-196.25	T	0.0018	4539
4729-4732	454-451	203.75-203.75	T	0.0016	5566
5321-5324	245-239	187.5-187.5	T	0.0018	2977
5325-5328	371-366	197.5-197.5	T	0.0017	4533
5329-5332	448-445	203.75-203.75	T	0.0016	5492
5021-5024	244-238	186.25-187.5	T	0.0020	2964

FIGURE 5.3.1 Typical Data Sheet

Rig 'A'

PLOT NUMBERS	MICRO STRAIN	FREQUENCY (Hz)	MODE	DISP. (IN) 11.9560	LOAD (LB
3/28					
3301 ⇒ 3305	275 → 272	345 - 350	1	.0006	3366
3306 → 3310	487 → 482	370 - 370	1	.00055	5164
3311 → 3314	496 → 490	370 - 370	1	.0006	6068
3201 → 3205	390 → 389	360 - 360	1	.00055	4794
3206 → 3209	350 → 340	350 - 350	1	.0006	4247
3210 - 3213	228 → 228	345 - 345	1	.0006	2806
3/29					
3401-3405	169 - 167	340 - 345	1	.0006	2068
3407-3411	453 - 453	355 - 355	1	.0006	5576
3412-3416	367 - 363	350 - 350	1	.0006	4493
2901 - 2906	387 - 381	350 - 350	1	.0006	4727
3/30					
2907 - 2911	366 - 360	335 - 335	1	.0009	4468
2912 - 2916	224 - 243	320 - 320	1	.0010	2874
2301 - 2305	310 - 311	345 - 345	1	.0006	3822
→ REPLACED LEAD WIRES - BENDING					
2306 - 2310	318 - 316	355 - 355	1	.0006	3902
3/31					
2311 - 2315	219 - 217	340 - 340	1	.0007	2683
2601 - 2606	474 - 475	365 - 365	1	.0006	5841
2607 - 2611	338 - 335	350 - 350	1	.0006	4142
2612 - 2616	273 - 273	340 - 340	1	.0006	3360
1901 - 1906	317 - 297	340 - 340	1	.0006	3779
1907 - 1911	341 - 338	350 - 350	1	.0006	4179
4/1					
1912 - 1916	138 - 134	325 - 325	1	.0007	1674
4/2					
2701 - 2705	378 - 377	350 - 350	1	.0006	4647
2706 - 2710	295 - 293	335 - 340	1	.0007	3619
2711 - 2715	466 - 467	355 - 355	1	.00055	5742
2401 - 2405	253 - 249	335 - 335	1	.0006	3090
2406 - 2410	419 - 418	355 - 355	1	.0006	5151
2411 - 2415	321 - 315	345 - 345	1	.0006	3914
3001 - 3005	254 - 252	335 - 335	1	.0006	3114
3006 - 3010	418 - 418	350 - 355	1	.0006	5145

FIGURE 5.3.3 Typical Data Sheet

Rig 'C'

$A = 0.318\ IN^2$

PLOT NUMBERS	MICRO STRAIN	FREQUENCY (Hz)	MODE	DISP. (IN) 11.45 Lbs.	LOAD (LBS
7/19 TAN. - SHORT					
6901-6904	105 - 94	400-400	TAN	0.0015	950
6905-6908	183 - 173	405-405	"	0.0014	1700
6909-6912	262 - 258	420-420	"	0.0013	2482
6801-6804	105 - 104	430-430	"	0.0015	995
6805-6808	183 - 180 RUBBING?	435-440	"	0.0013	1735
6809-6812	262 - 260	440-440	"	0.0013	2490
6701-6704	107 - 105	390-390	"	0.0015	1010
6705-6708	183 - 182	400-400	"	0.0014	1745
6709-6712	262 - 254	415-420	"	0.0012	2460
7/20					
7101-7104	105 - 101	410-415	"	0.0014	988
7105-7108	183 - 176	420-425	"	0.0012	1715
7109-7112	262 - 256	435-430	"	0.0012	2470
6601-6604	105 - 103	395-395	"	0.0014	993
6605-6608	186 - 182	405-410	"	0.0013	1755
6609-6612	263 - 255	420-420	"	0.0012	2473
7001-7004	105 - 99 (1 BENDING GAGE RUN ON QUARTER BRIDGE)	405-405	"	0.0015	972
7005-7008	183 - 178	415-415	"	0.0014	1727
7009-7012	263 - 254	425-425	"	0.0012	2462
LONG SHANKS	AMPS REWIRED				
6001-6004	105 - 105	405-405	"	0.0013	1000
6005-6008	189 - 186	400-395	"	0.0012	1788
6009-6012	265 - 260	395-400	"	0.0012	2503
6101-6104	108 - 107 (BADLY BENT)	410-410	"	0.0013	1028
6105-6108	192 - 191	410-415	"	0.0012	1828
6109 6112	261 - 260	410-400	"	0.0012	2480
6201-6204	107 - 105	415-415	"	0.0013	1013
6205-6208	186 - 185	415-420	"	0.0012	1775
6209-6212	263 - 260	420-420	"	0.0011	2493
6301-6304	105 - 102 (STRAIGHTEST)	360-360	"	0.002	985
6305-6308	183 - 181	380-385	"	0.0017	1738
6309-6312	262 - 261	395-400	"	0.0015	2495
6401-6404	106 - 104	390-390	"	0.0014	1003
6405-6408	183 - 183	400-400	"	0.0013	1750
6409-6412	261 - 260	410-410	"	0.0012	2480

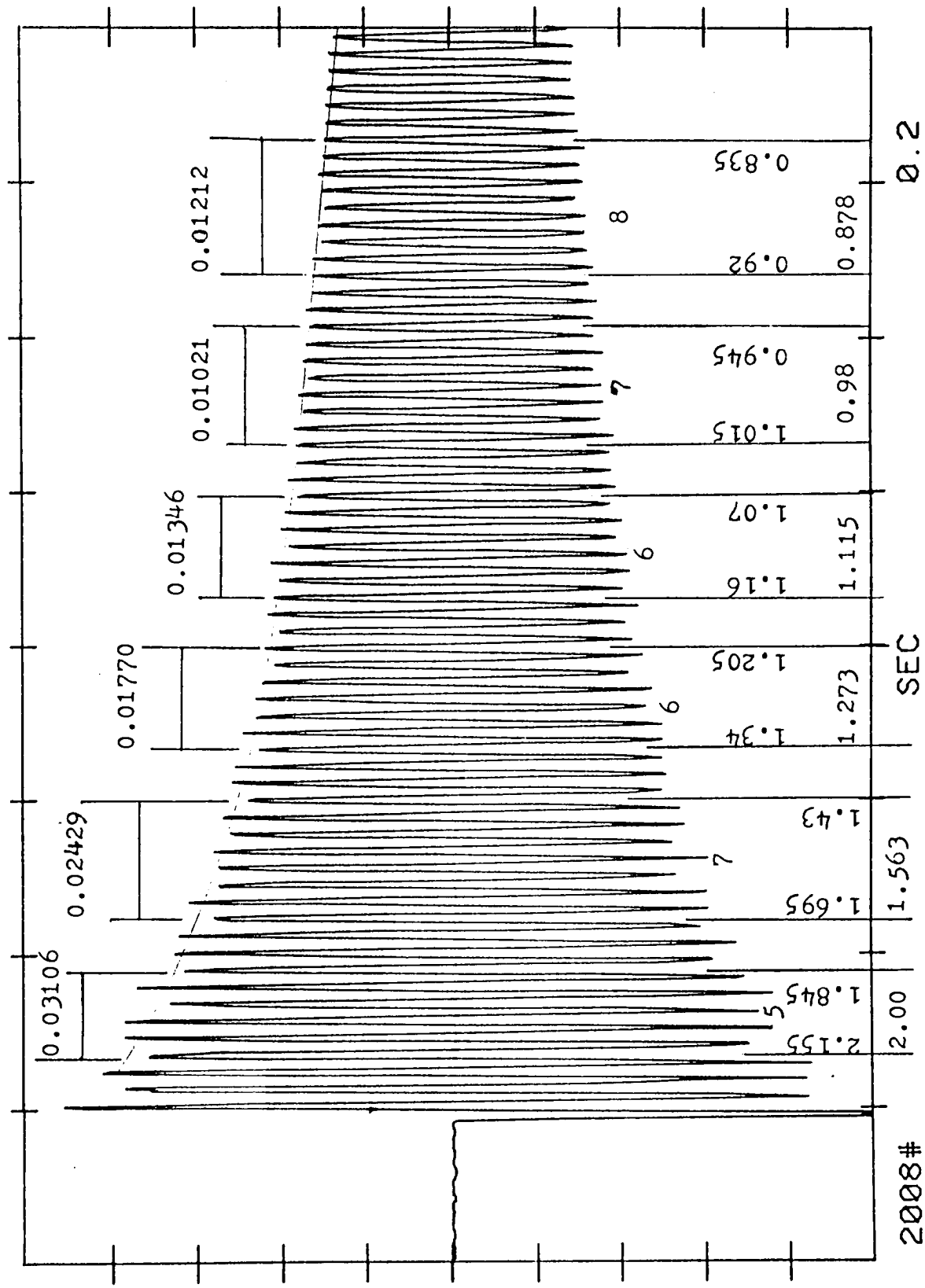

FIGURE 5.4 Example of Captured Decay Trace (Reduced)

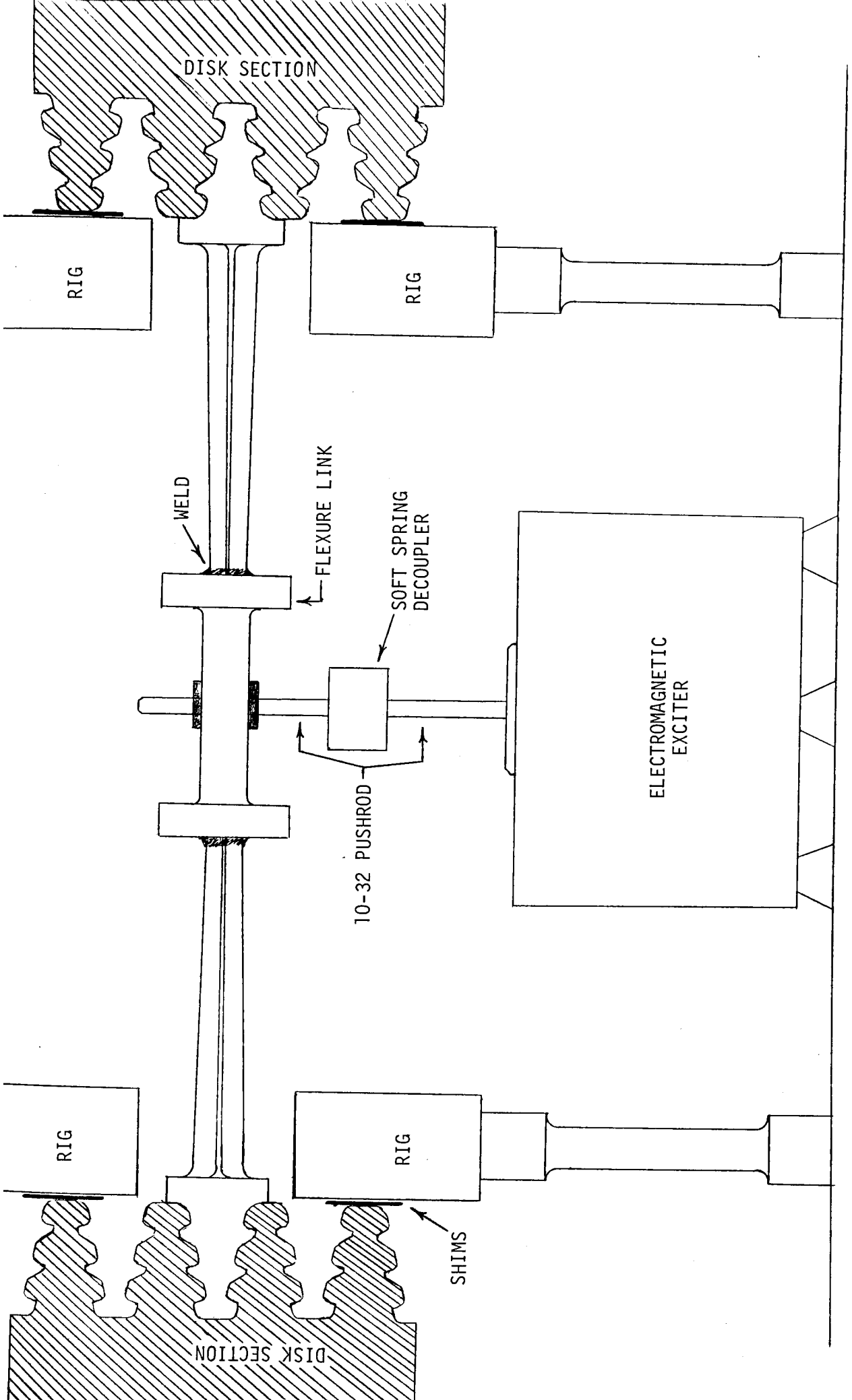

FIGURE 5.5 Schematic of Vibration Exciter Setup

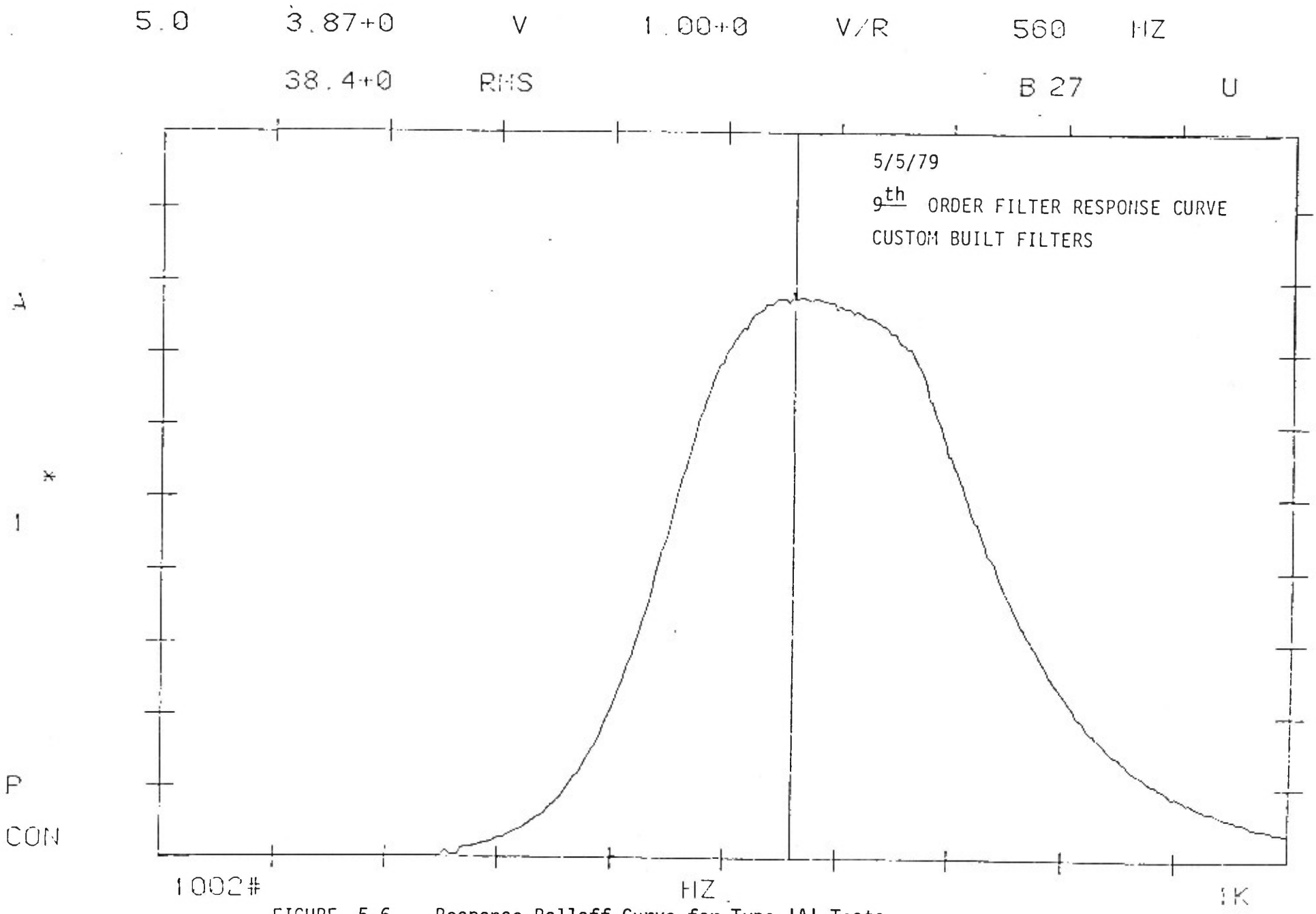

FIGURE 5.6 Response-Rolloff Curve for Type 'A' Tests

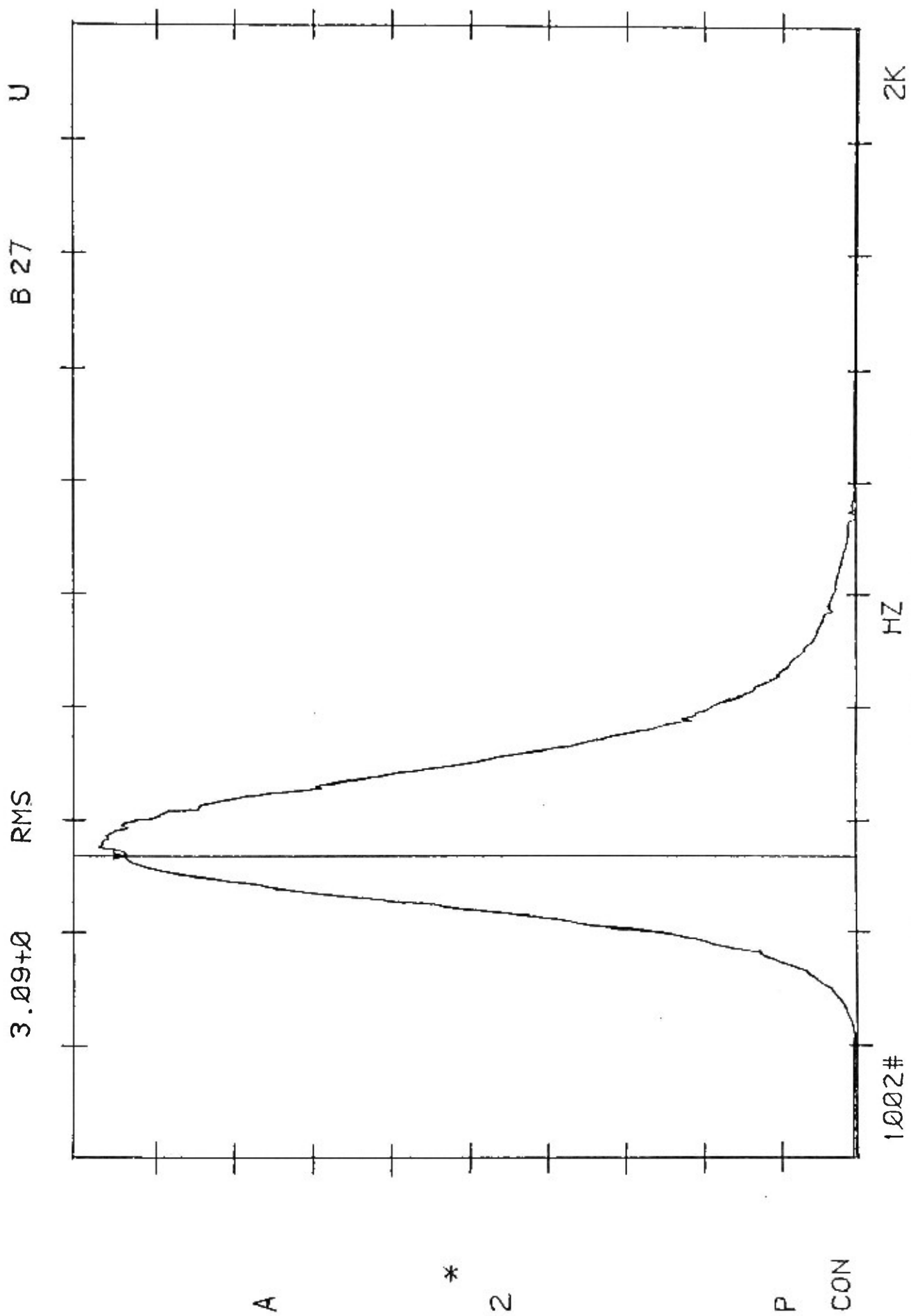

FIGURE 5.7 Response-Rolloff Curve for Type 'C' Tests

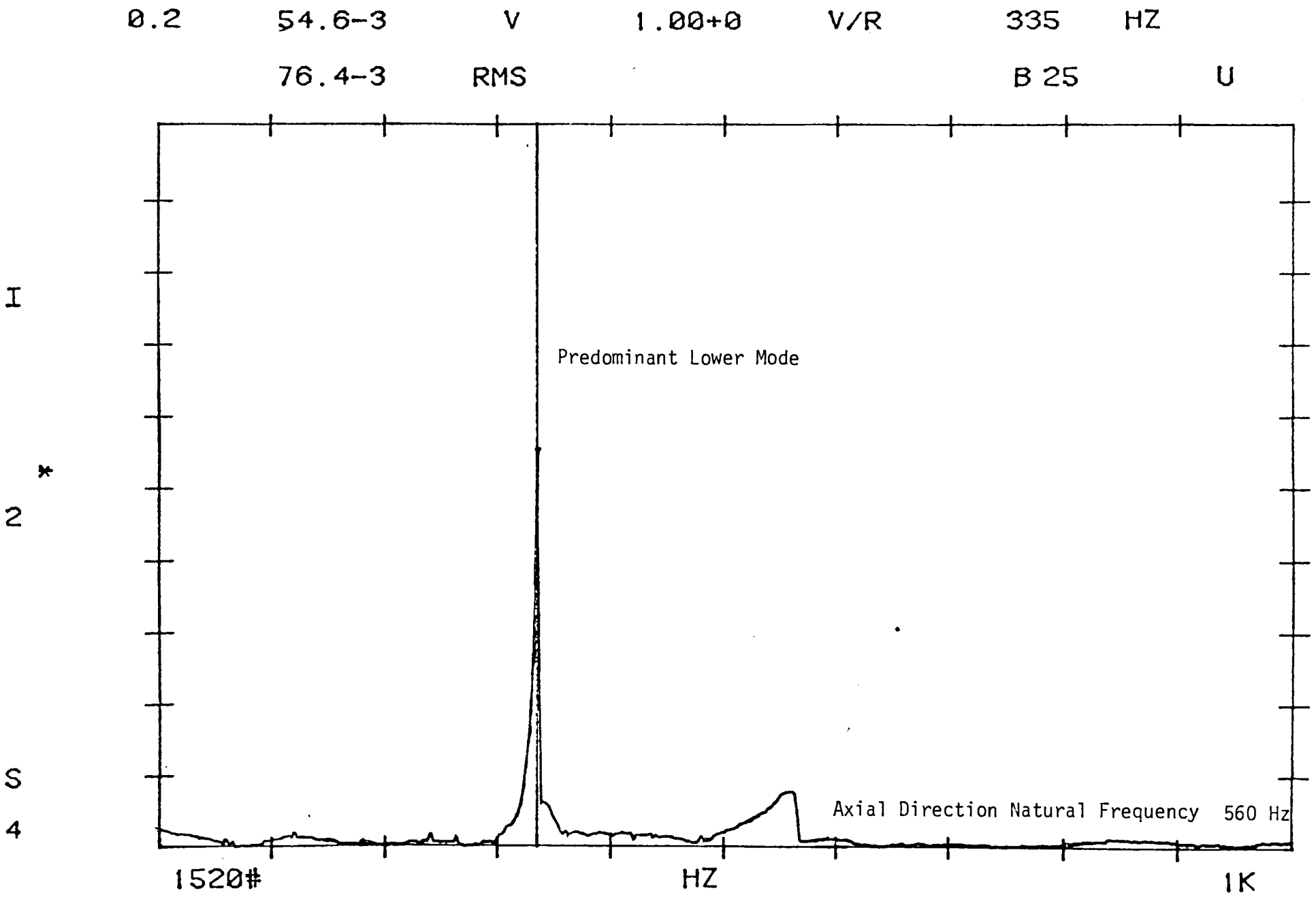

FIGURE 5.8 Unfiltered Type "A" Response Spectrum (Axial Vibration)

6 TEST RESULTS

6.1 Excitation Frequency and Amplitude Variation Test Results

First, an electromagnetic vibration exciter was used to excite the blade groups, both at Nozzle Passing Frequency (NPF) and at one-third NPF. In both cases, the blades were excited at the selected frequency. The forced excitation was then shut off abruptly and the decay trace was captured. It was found with both frequencies that the blade vibration immediately translated into the lowest natural mode for the test direction, irrespective of the former excitation frequency. Therefore, excitation at NPF and one-third NPF could not be evaluated with this rig. A rotating rig with flow induced vibrations is one of the possible alternatives (if not the only one).

It was also found that the mass of the exciter coil, even with the decoupler, lowered the natural frequency of the blade group during natural frequency excitation, as compared to impulse results. For example, if the impulsed natural frequency was found to be 360 Hz, the exciter was hooked up and the oscillator set for 360 Hz. By monitoring frequency with the spectrum analyzer, the natural frequency could be seen to drop from 360 Hz to 350 Hz when the power was shut off. This indicates some mass effect due to the exciter. Preliminary tests revealed the following problems with this excitation approach:

a. The parasitic mass of the exciter moving coil was undesirably large and this exerted an influence on the natural frequency of the blade being tested.

b. The exciter possessed sufficient internal damping to clearly influence the initial decay cycles of the blade pair. This suggests that the decay traces would probably contain exciter damping of unknown proportions. As this damping could not be readily 'calibrated-out', it was considered an unacceptable source of error in the blade damping results.

c. The electromagnetic field of the exciter was relatively slow to collapse (in two or three cycles at 60 Hz, compared with blade N.F. 360 Hz for Type A blades). This slow field collapse rate influenced the initial portion of the blade pair decay curve. See figure 6.1.

The above items made forced-excitation of the blade decay unacceptable. Since only the natural frequency could be excited, it was decided to use the impulse technique.

It was found that all vibration decays were associated with a single characteristic decay curve for a given blade pair and excitation direction, irrespective of the amplitude at which the forcing excitation had been applied. Curves were obtained for the same mode initiated at different amplitudes. The overall decay curve for the blade consistently reproduced the same rate of amplitude decay in all details for each test. Data plots for blade group A-31 are shown in figures 6.2 to 6.19. The resulting curves of Logarithmic Decrement vs. Blade Tip Displacement as a Function of Vibration amplitude are given as figures 6.20 through 6.22. Data from figures 6.2 to 6.7 is for figure 6.20. Data from figures 6.8 to 6.13 is for figure 6.21, and data from figures 6.14 to 6.19 is for figure 6.22.

It is clear to see that initiation amplitude has little of no effect on the characteristic damping curves for the three simulated centrifugal loads tested. An indication of this trend was witnessed before figures 6.20 through 6.22 were plotted by overlapping respective decay traces on a light box.

It is also clear to see how much data is necessary to generate a few logarithmic decrement curves. In subsequent impulse testing, three loads were obtained for each blade pair; and 87 blade pairs were tested, resulting in approximately 4.5 reams of plotted data. This data was reduced by hand and then input in a n'th order linear regression routine to determine the best curve fit for the logarithmic decrement plots. An example of

regression input and output data is given in figures 6.23 and 6.24.

6.2 Air Tests on Blade Type A. Figures 6.25 through 6.62

Tangential Mode. Damping data obtained from amplitude decay tests conducted in air for 23 different pairs of Type A blades in the tangential mode is given in figures 6.25 through 6.47. Logarithmic decrement is plotted as a function of blade tip displacement for different axial loads ranging from 2700 ± 250 lbs. to 5200 ± 250 lbs. The following significant trends can be observed:

1. Blade damping decreases with increase of axial load.
2. Blade damping increases in a linear manner with blade tip displacement for low axial loads.
3. For higher axial loads, damping decreases initially with blade displacement and then increases again; see figures 6.25, 6.27, 6.29, 6.32 and 6.41. In some cases the logarithmic decrement drops suddenly and then increases again; see figures 6.29, 6.41, and 6.45.

Axial Model. Damping data for Type A blades in the axial mode is given in figures 6.48 through 6.62. The following trends can be seen from these plots:

1. While blade damping decreases with axial load as observed in the case of tangential mode, some exceptions appear to exist eg. figures 6.54 and 6.55.
2. Blade damping increased with blade displacement but the fit was not linear for lower loads as had been observed in the case of the tangential mode.
3. The tendency for damping to decrease initially and then to increase with blade tip displacement does not seem to occur in the axial mode damping data. Instead, axial damping increases with amplitude or may remain constant with amplitude.

6.3 Air Tests on Blade Type B. Figures 6.63 through 6.87

Tangential Mode. Damping data obtained from tests conducted in air for

eleven (11) different groups of Type B blades when vibrated in the tangential mode, is given in figures 6.63 through 6.73. Logarithmic decrement is plotted as a function of blade tip displacement for three different axial loads: 3000 ± 200, 4500 ± 200, and 5500 ± 200 lbs. Since blade Type B has a similar type of blade root as blade Type A, (although the blade section itself if different), fewer data points were used to make these plots. Similar significant trends to those observed in Section 6.2 were found for blade Type B, as follows:

1. Blade damping decreases with an increase in axial load.
2. Blade damping increases in a linear manner with blade tip displacement for low axial loads.
3. For higher axial loads, there is a small initial damping decrease with blade displacement, and then an increase; see figures 6.63, 6.70, 6.72 and 6.73. The tendency for the logarithmic decrement to drop off suddenly and then to increase again is also found in some cases; see figures 6.63, 6.67, 6.68 and 6.70 for medium loads.

Axial Mode. Damping data for Type B blades in the axial decay mode is given in the figures 6.74 through 6.87.

1. As in the case of blade Type A given in 6.2, the blade damping decreases with axial load in most cases, with the exception of that shown in figures 6.76, 6.78 and 6.82.
2. Blade damping increases with blade displacement, but the linear curve observed in the tangential mode for lower loads was not found in this case, with the exception of figure 6.74. This may be due to the smaller number of points plotted in this case.
3. As in the tangential mode, the damping showed some tendency to decrease initially and then to increase with the increase of blade tip displacement; see figures 6.75 and 6.79. A distinct peak can be observed in the cases of figures 6.83 and 6.86. A possible explanation for this peak is given in the following section.

6.4 Air Tests on Blade Type C. Figures 6.88 through 6.111.

Tangential Mode. Figures 6.88 through 6.98 show the damping data obtained from tests conducted in air for eleven (11) different groups of Type C blades in the tangential mode. Figures 6.88 thorugh 6.92 were obtained from tests on long-shank blades, while figures 6.93 thorugh 6.98 were obtained from tests on short-shank blades. Logarithmic decrement is plotted as a function of blade tip displacement for three different axial loads, ie. 1000 +50 lbs., 1750 +50 lbs, and 2500 +50 lbs. These blades were of a ball and shank type construction. It was found that:

i) For Long-Shank Blades

   a) Blade damping increases with an increase of blade tip displacement in a linear manner for all but the lowest blade tip displacements. At lower blade tip displacements, data scatter increases and the damping-displacement relation is no longer linear.

ii) For Short-Shank Blades

   a) Damping data again increases with blade tip displacement, generally in a linear manner. Increased axial load does not have as pronounced an effect as was observed with the long shanks.

   b) Low and high centrifugal loads seem to give linear variations with logarithmic decrement while the medium centrifugal loads give a curved relation at lower blade tip displacements. This changes to a linear relationship at larger tip displacements.

   c) No decrease in damping occurred on the low amplitude regions as had been seen with the Type B blades. However, in some cases, the damping was fairly constant and grew slowly over an initial range of blade tip displacements, primarily with the 1750 lbs test load; see figures 6.93, 6.97 and 6.98.

Axial Mode. Vibration tests were conducted at the same three axial loads as the tangential tests. Damping results are given in figures 6.99 through 6.104 for long shanks, and in figures 6.105 through 6.110 for short shanks. It was found that:

i) For Long-Shank Blades

a) Increase in blade axial loading caused little increase in the damping. The data points for the three axial loads fall in scatterbands which overlap each other. There appears to be one general curve for the load range 1000 lbs through 2500 lbs. The previously observed pattern of logarithmic decrement decreasing with increased axial load does not appear to apply in this case. This suggests that the roots may be locked up at the loads used.

ii) For Short-Shank Blades

a) Axial damping appears to be an order of magnitude higher for short-shank blades than for the long-shank blades. No obvious reason for this increase was found. The test data was thoroughly checked. Again the logarthmic decrement values are generally linearly related to blade tip displacements.

b) No relationship between logarithmic decrement and axial load was found. The scatterbands again overlap, as was found for the long-shank tests.

Figure 6.111 is for damping tests run on blade group C-60 with the steel blade roots filling the adjacent disk slots. It was felt that this condition should be investigated and compared to tests without adjacent blades since the long shank blade root appeared reasonably flexible. It was found that damping did not drop at the high centrifugal load as in figure 6.88. This is because the ball was not able to spread the disk groove apart at high load when blades were adjacent to the test blade. Therefore, the sides of the disk groove remained in contact with the blade shank causing more rubbing, and thereby damping, during excitation. This is not felt to be a problem with Types A, B,or C short shank blades due to the relatively higher stiffnesses of the disk steeples.

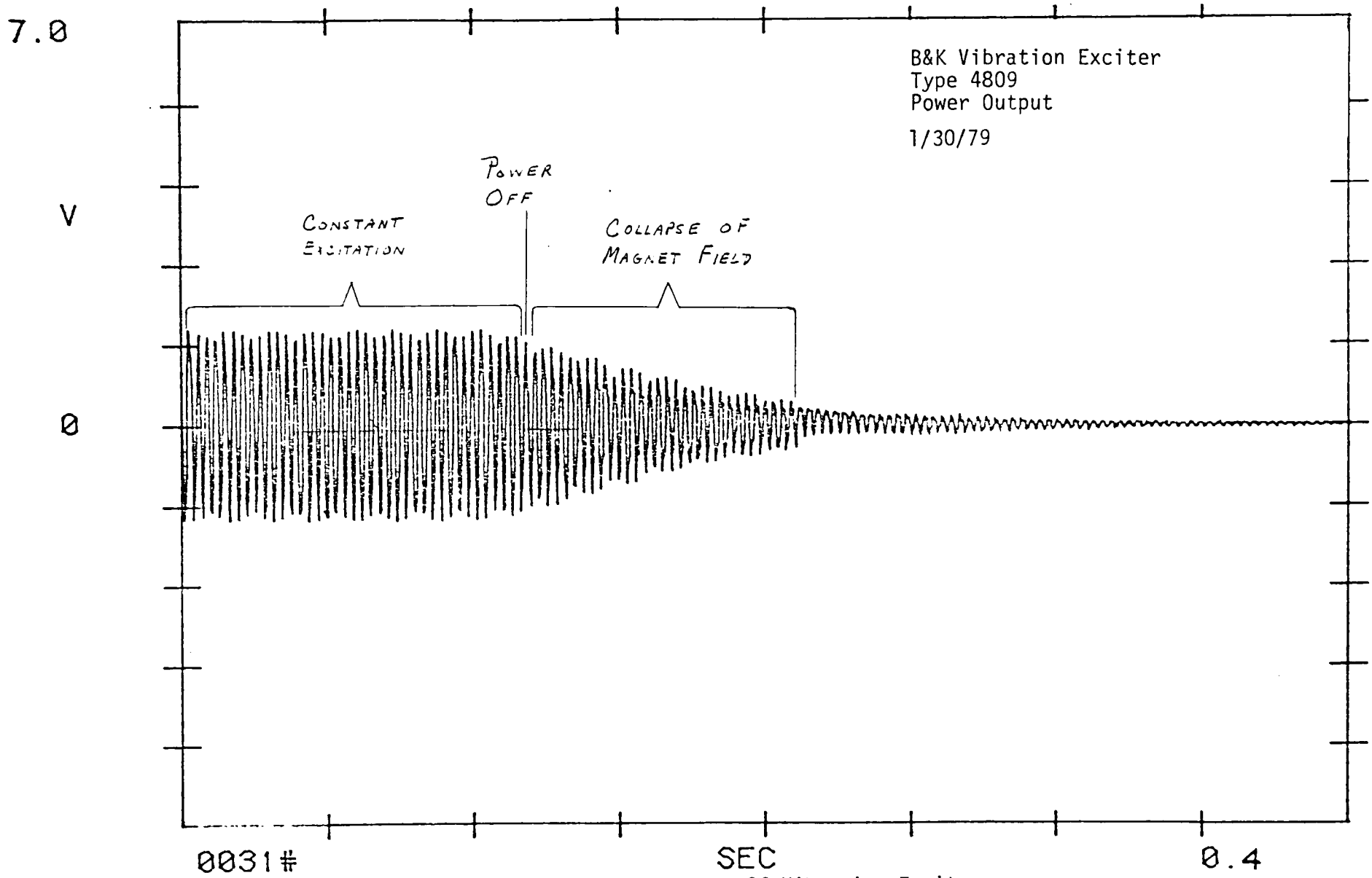

FIGURE 6.1 Plot Of Field Collapse Of Vibration Exciter

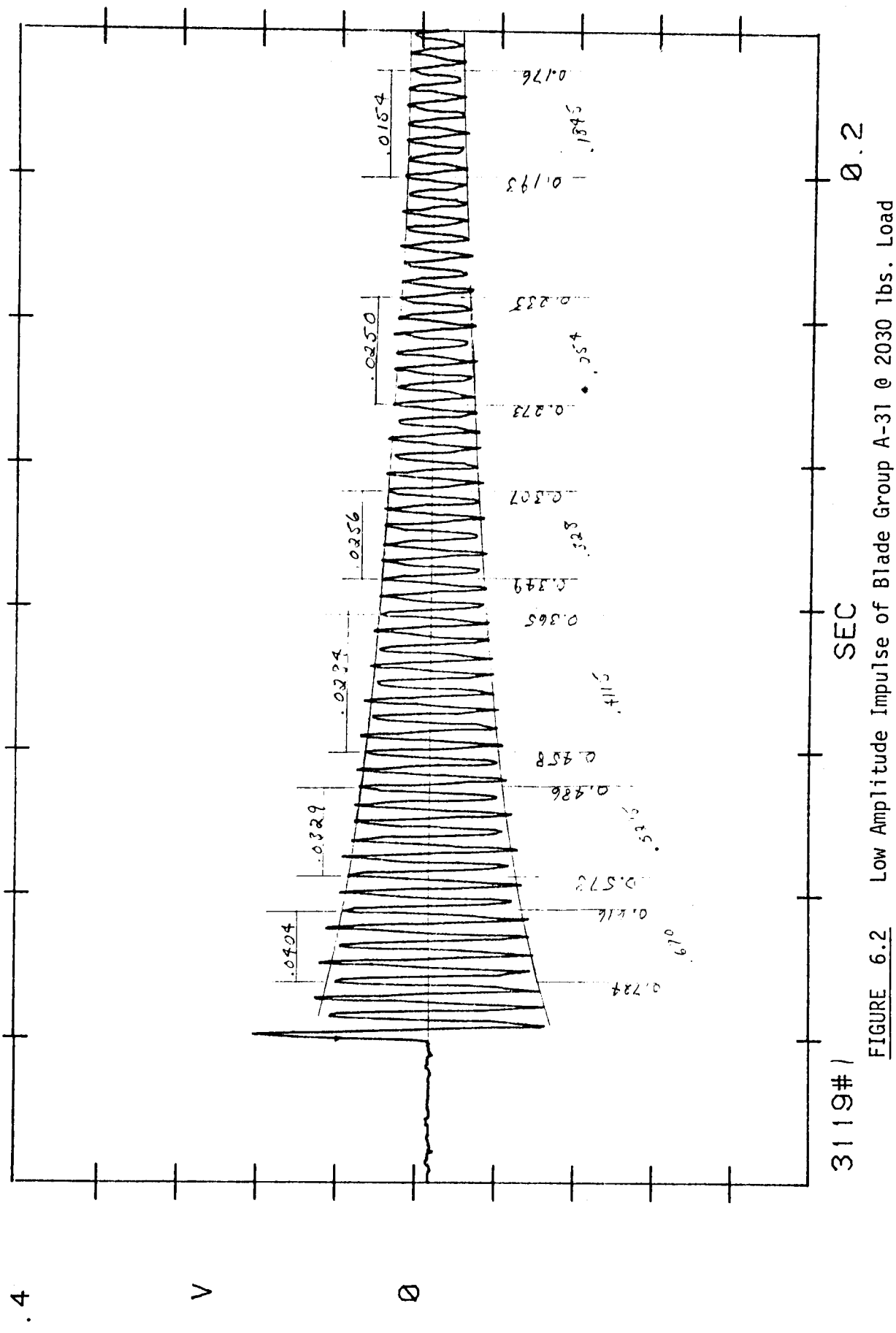

FIGURE 6.2 Low Amplitude Impulse of Blade Group A-31 @ 2030 lbs. Load

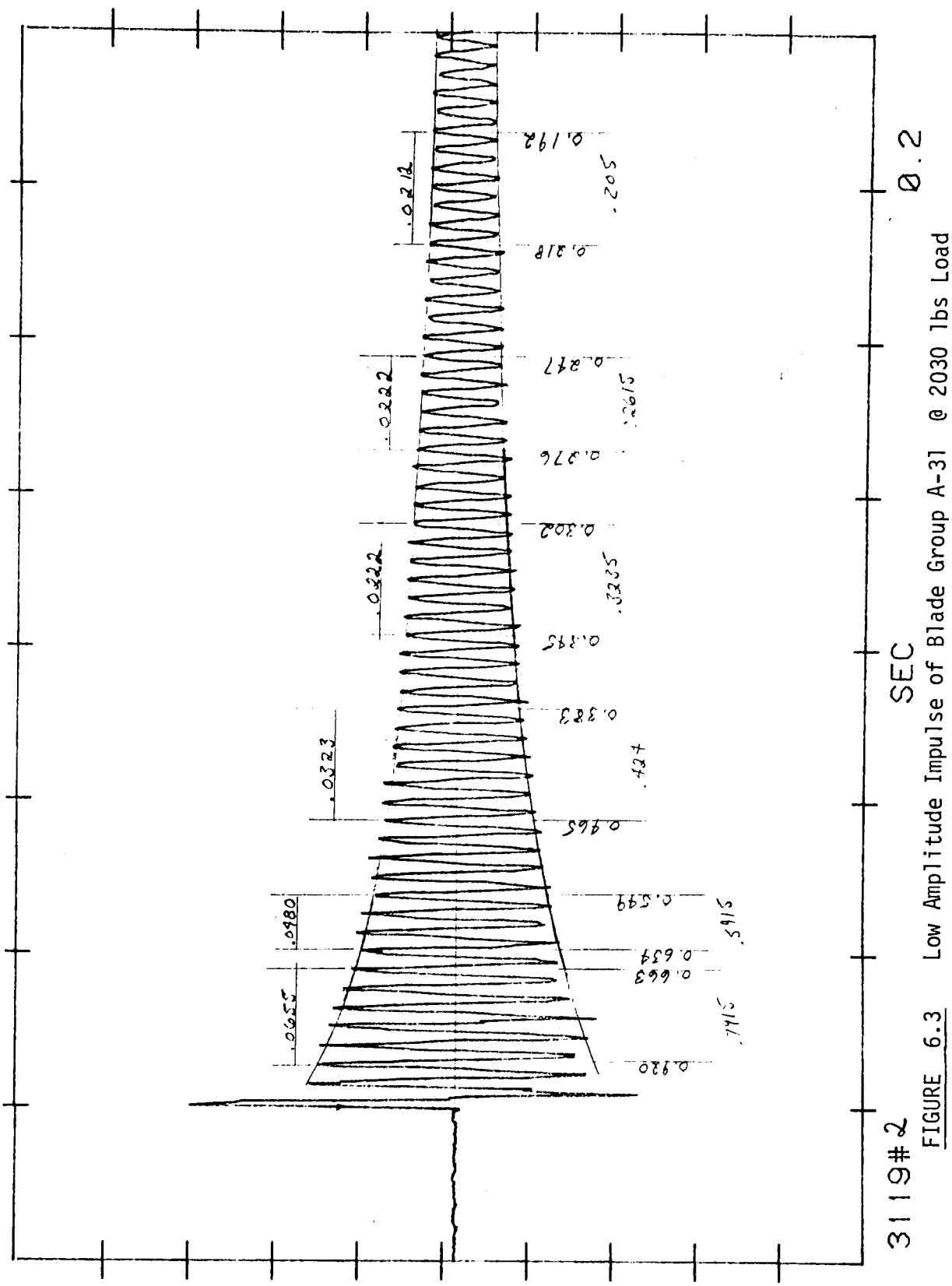

FIGURE 6.3 Low Amplitude Impulse of Blade Group A-31 @ 2030 lbs Load

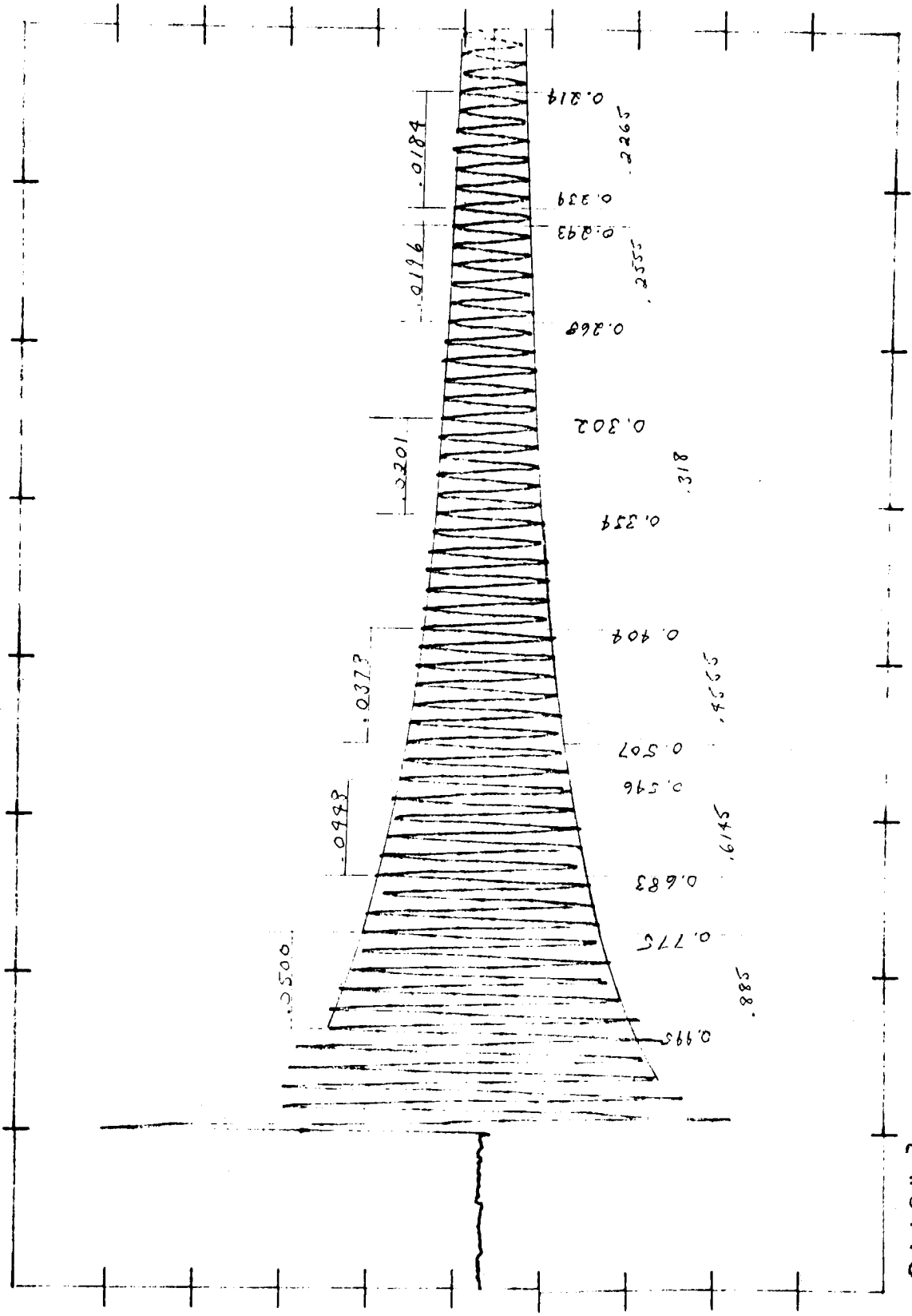

FIGURE 6.4 Medium Amplitude Impulse of Blade Group A-31 @ 2030 lbs Load

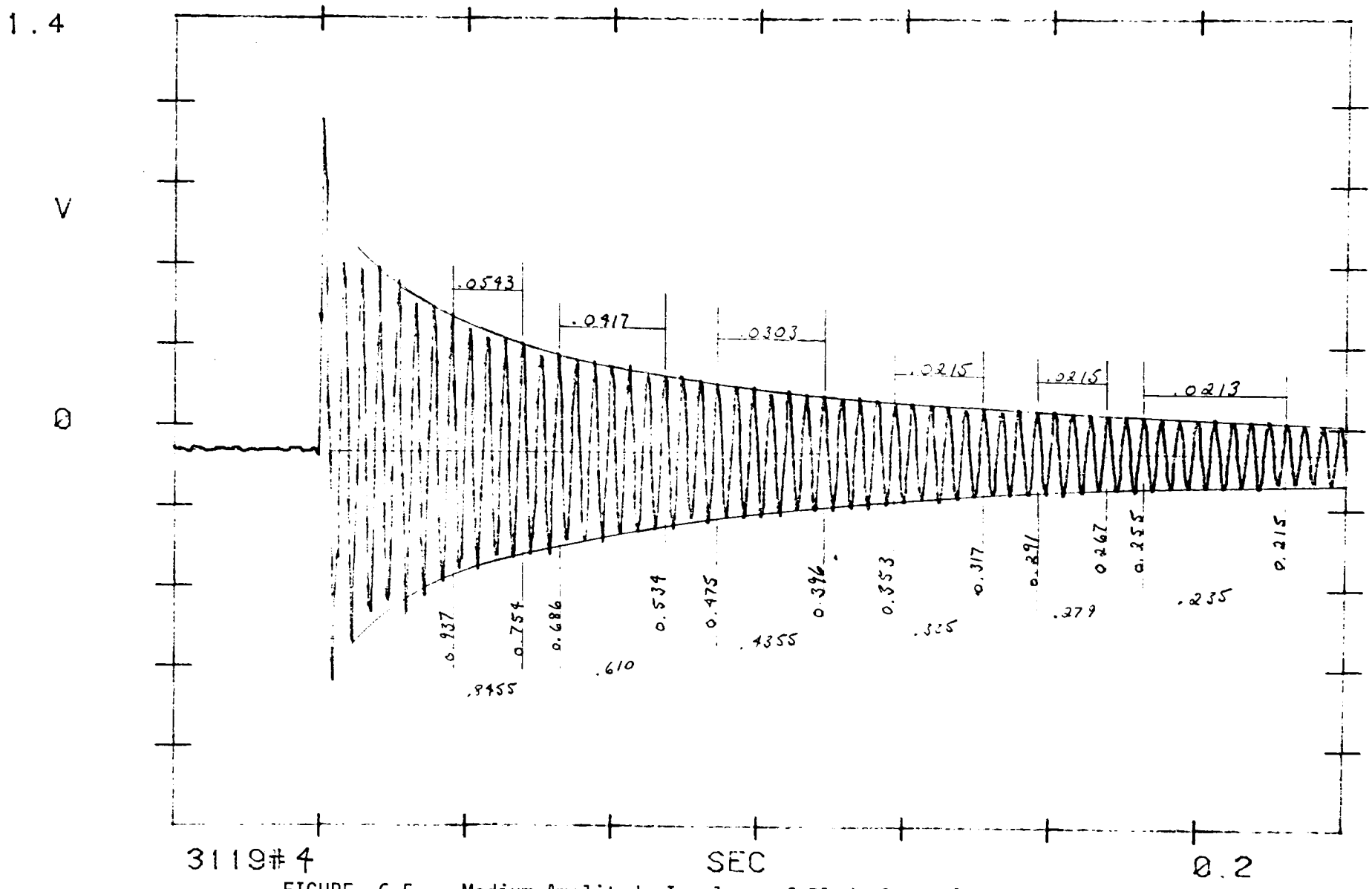

FIGURE 6.5 Medium Amplitude Impulse of Blade Group A-31 @ 2030 lbs Load

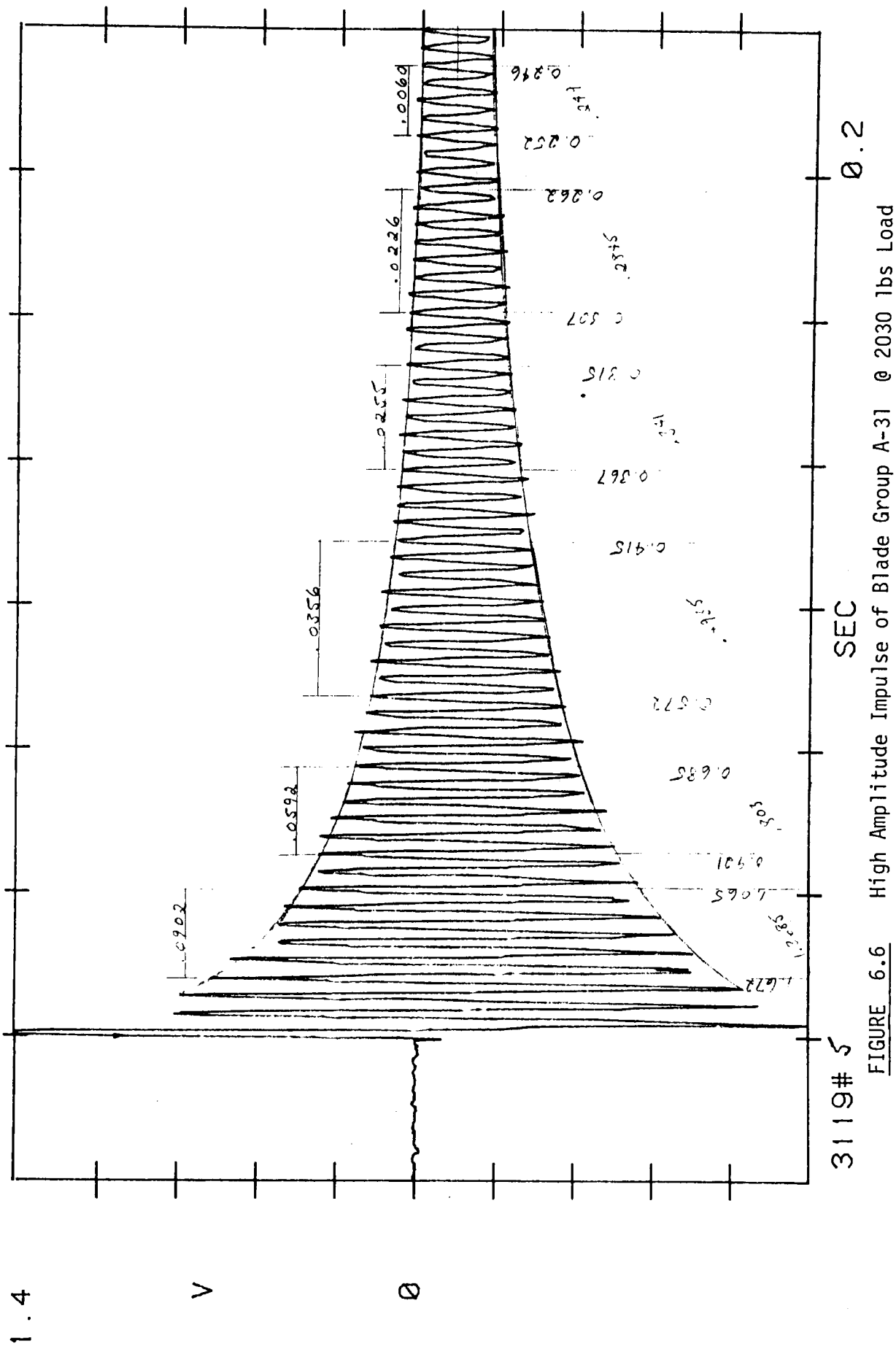

FIGURE 6.6 High Amplitude Impulse of Blade Group A-31 @ 2030 lbs Load

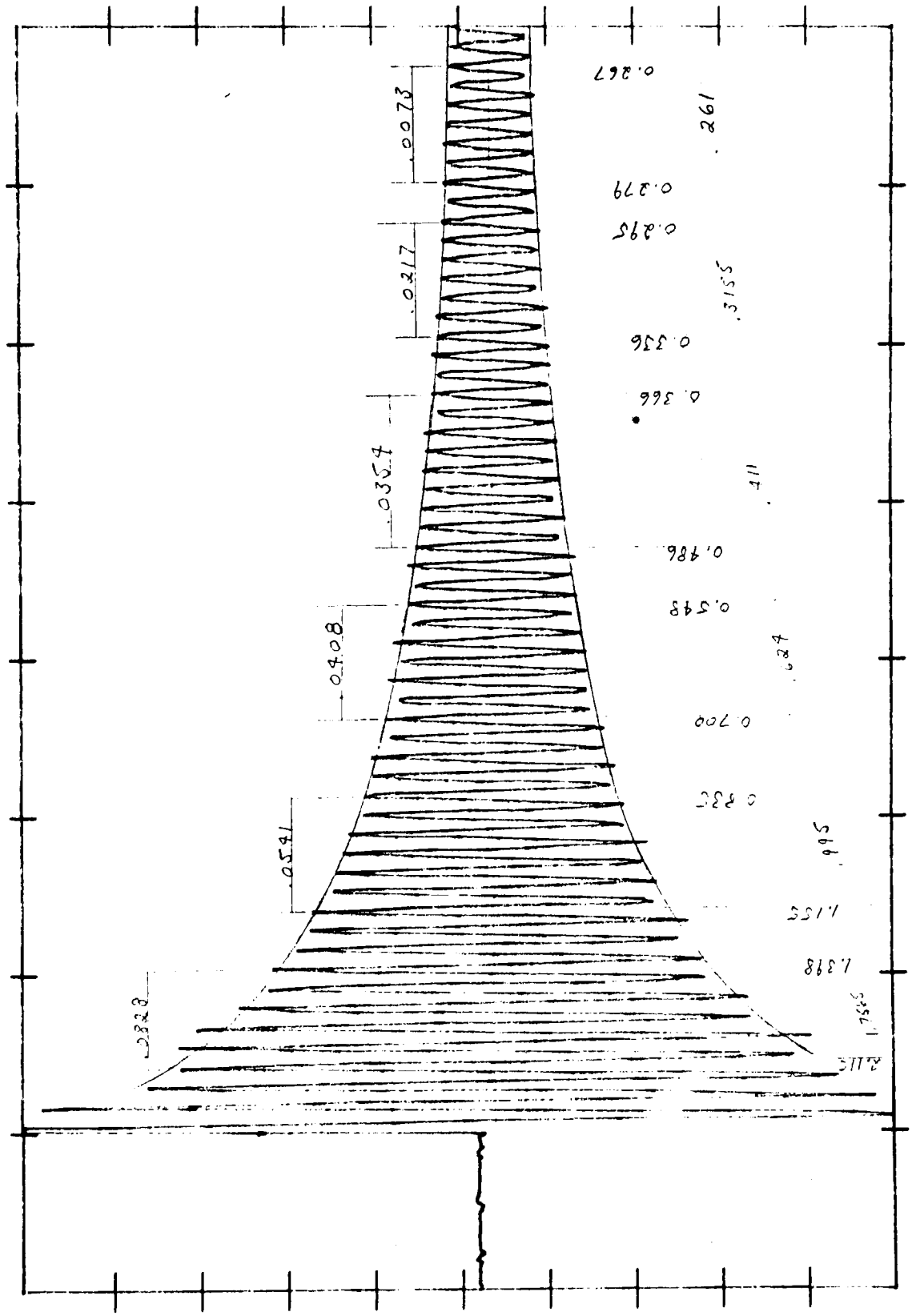

FIGURE 6.7 High Amplitude Impulse of Blade Group A-31 @ 2030 lbs Load

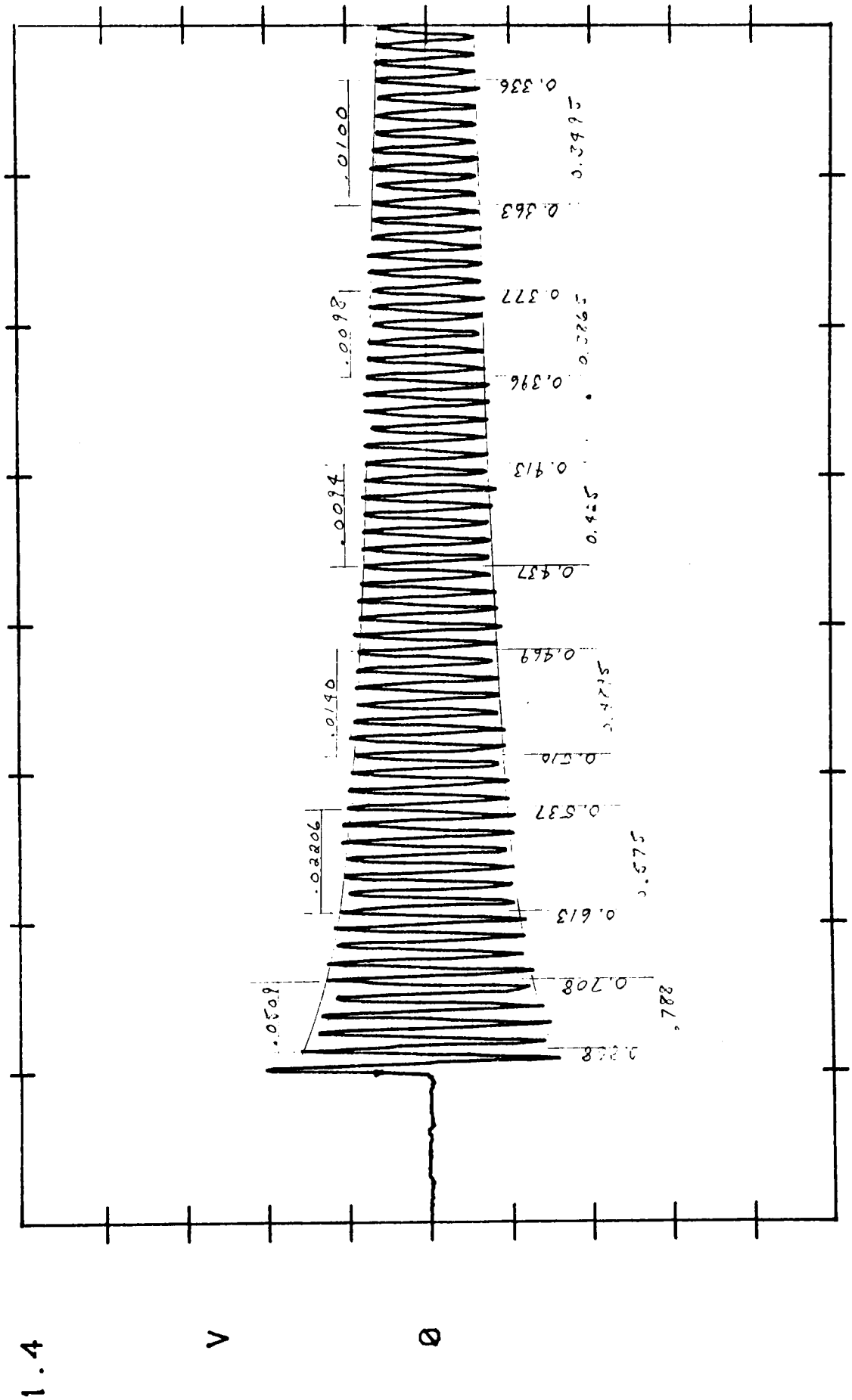

FIGURE 6.8 Low Amplitude Impulse of Blade Group A-31 @ 3100 lbs. Load

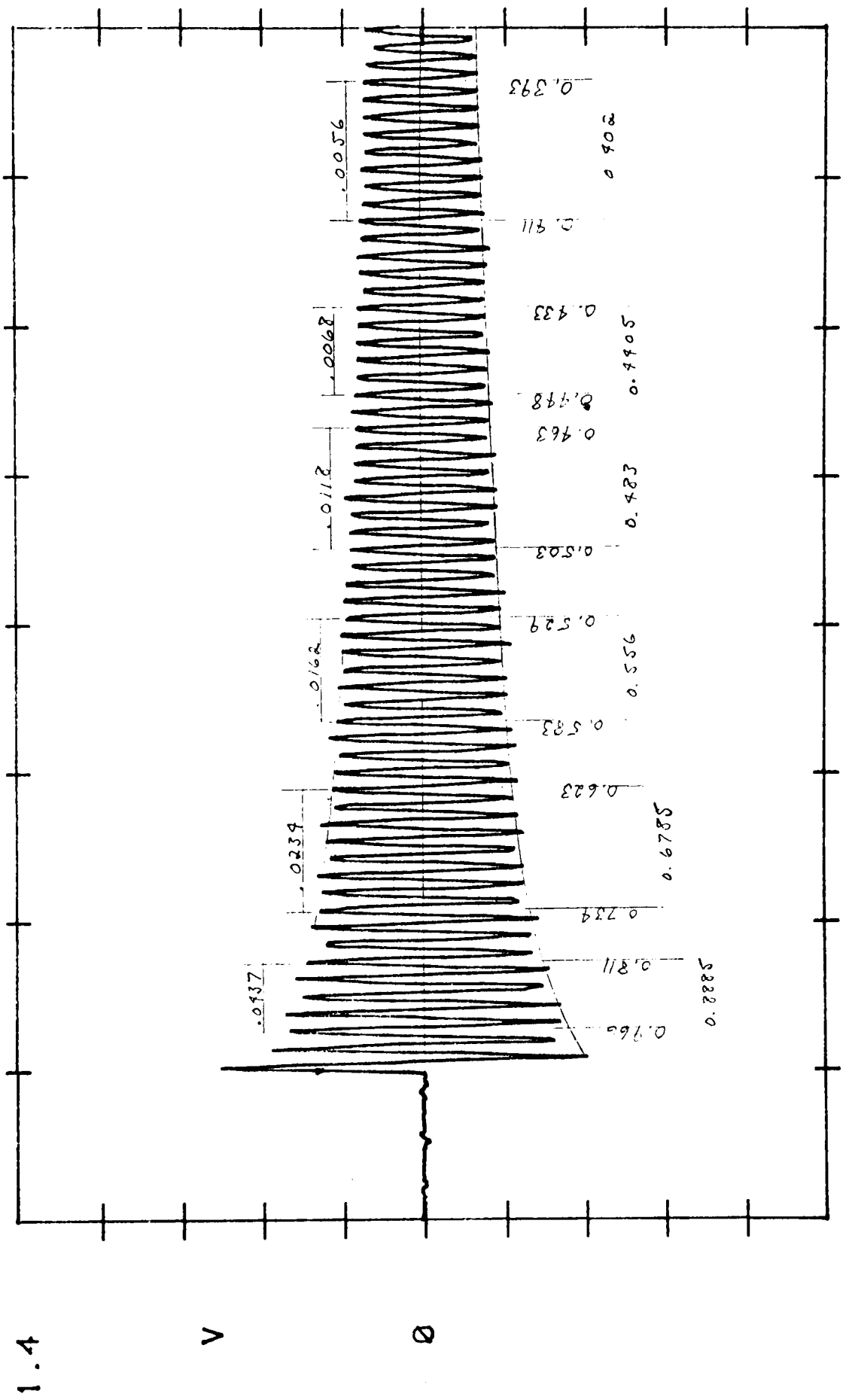

FIGURE 6.9 Low Amplitude Impulse of Blade Group A-31 @ 3100 lbs. Load

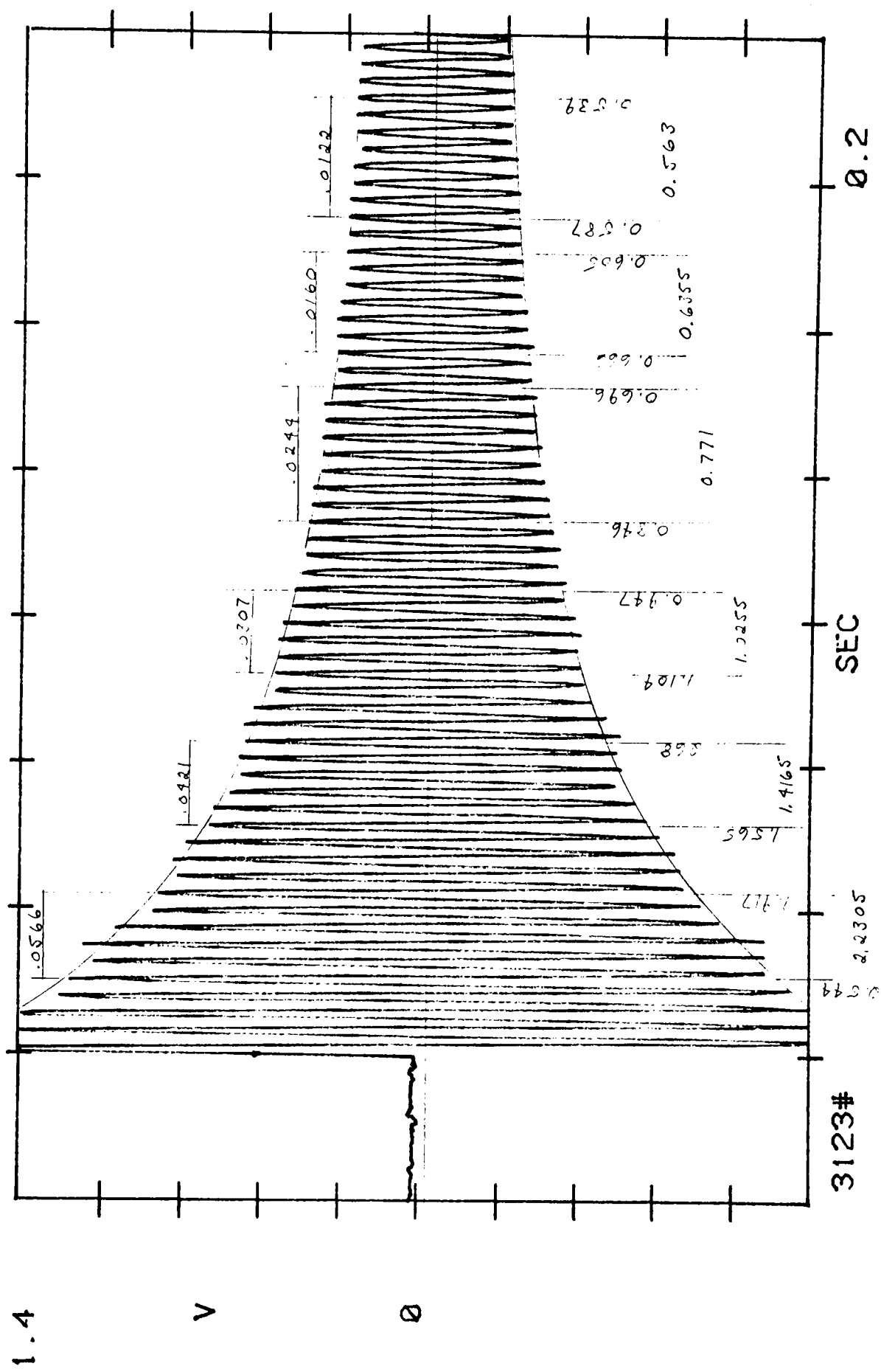

FIGURE 6.10 High Amplitude Impulse of Blade Group A-31 @ 3100 lbs. Load

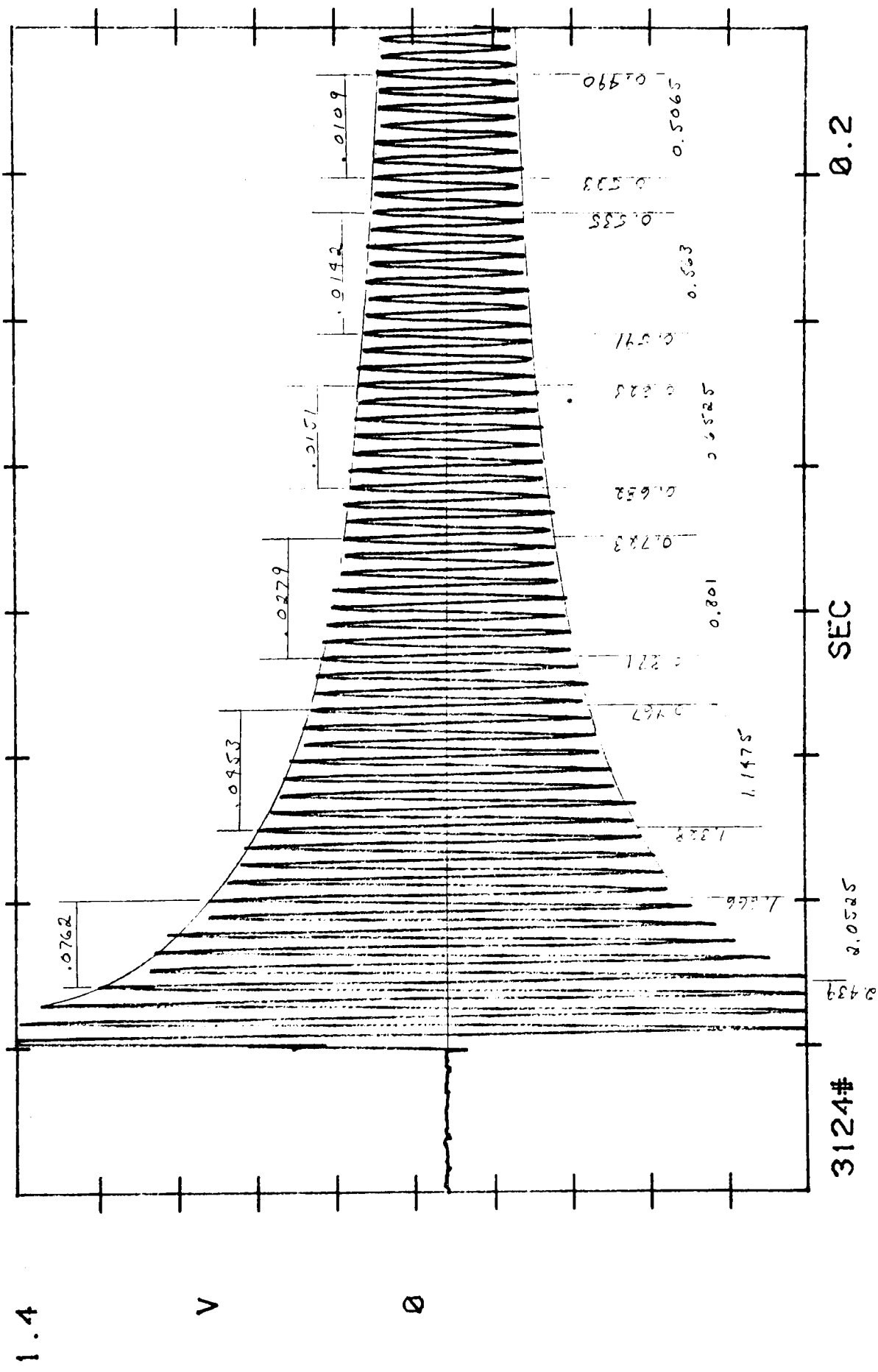

FIGURE 6.11 High Amplitude Impulse of Blade Group A-31 @ 3100 lbs. Load

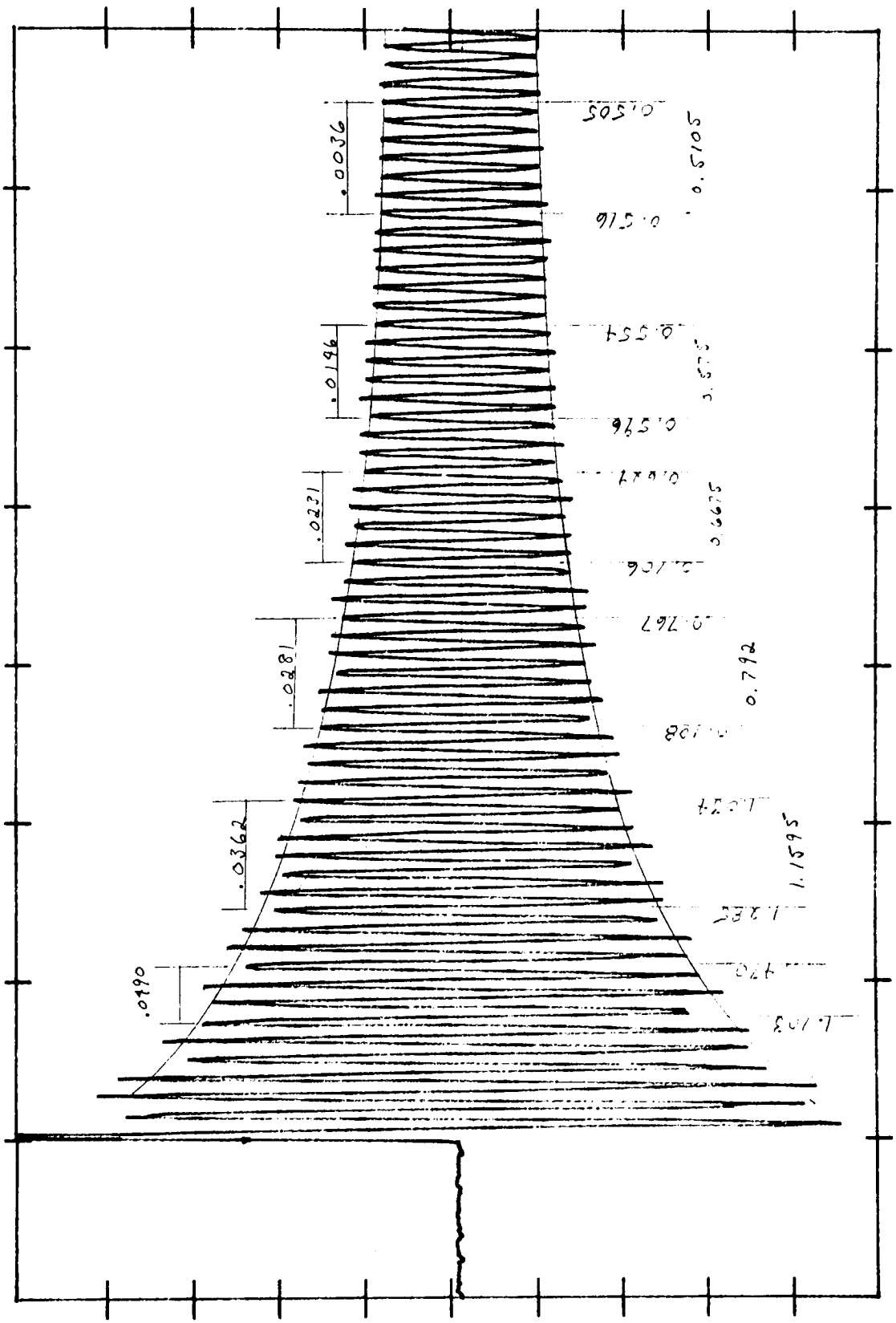

FIGURE 6.12 Medium Amplitude Impulse of Blade Group A-31 @ 3100 lbs. Load

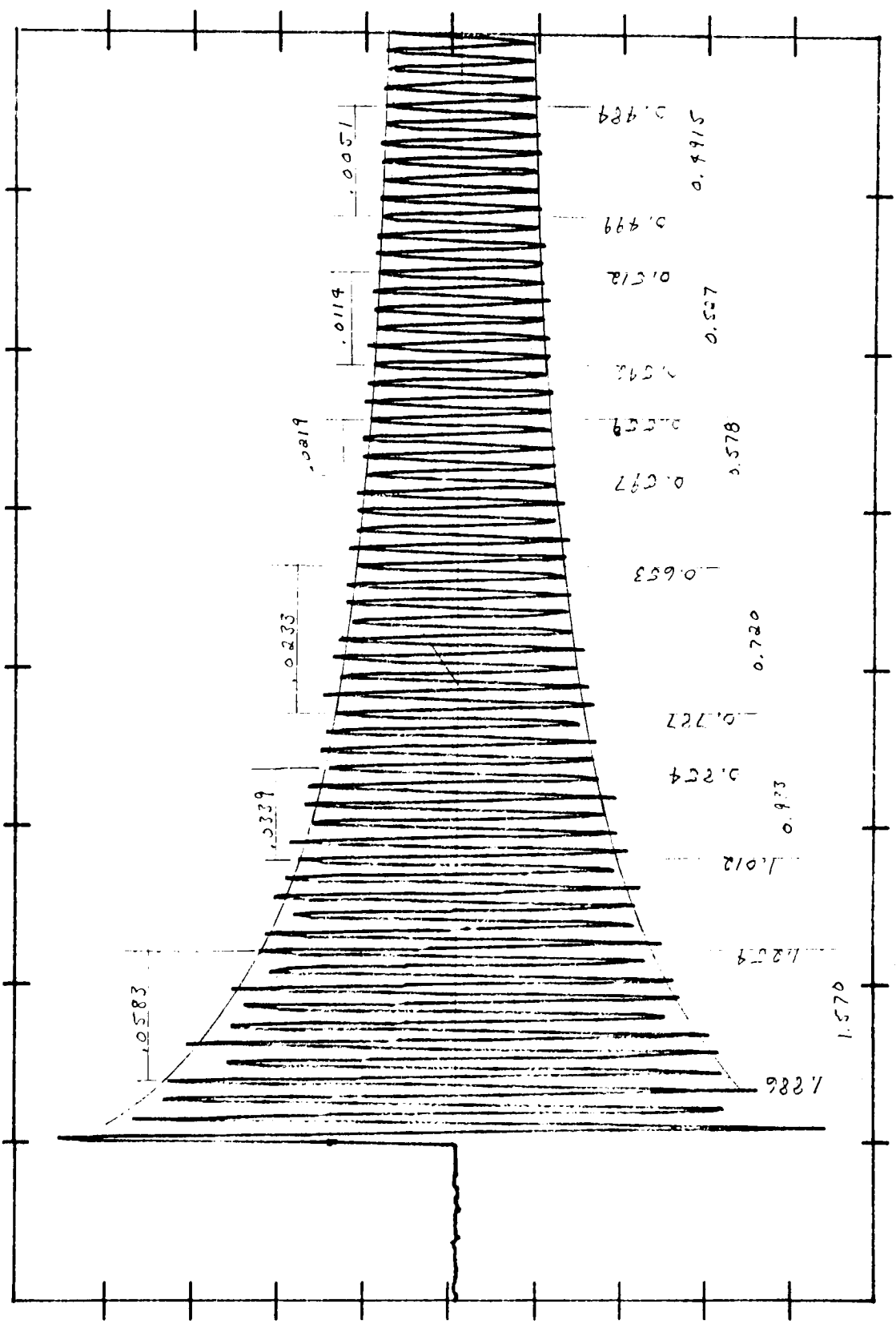

FIGURE 6.13 Medium Amplitude Impulse of Blade Group A-31 @ 3100 lbs. Load

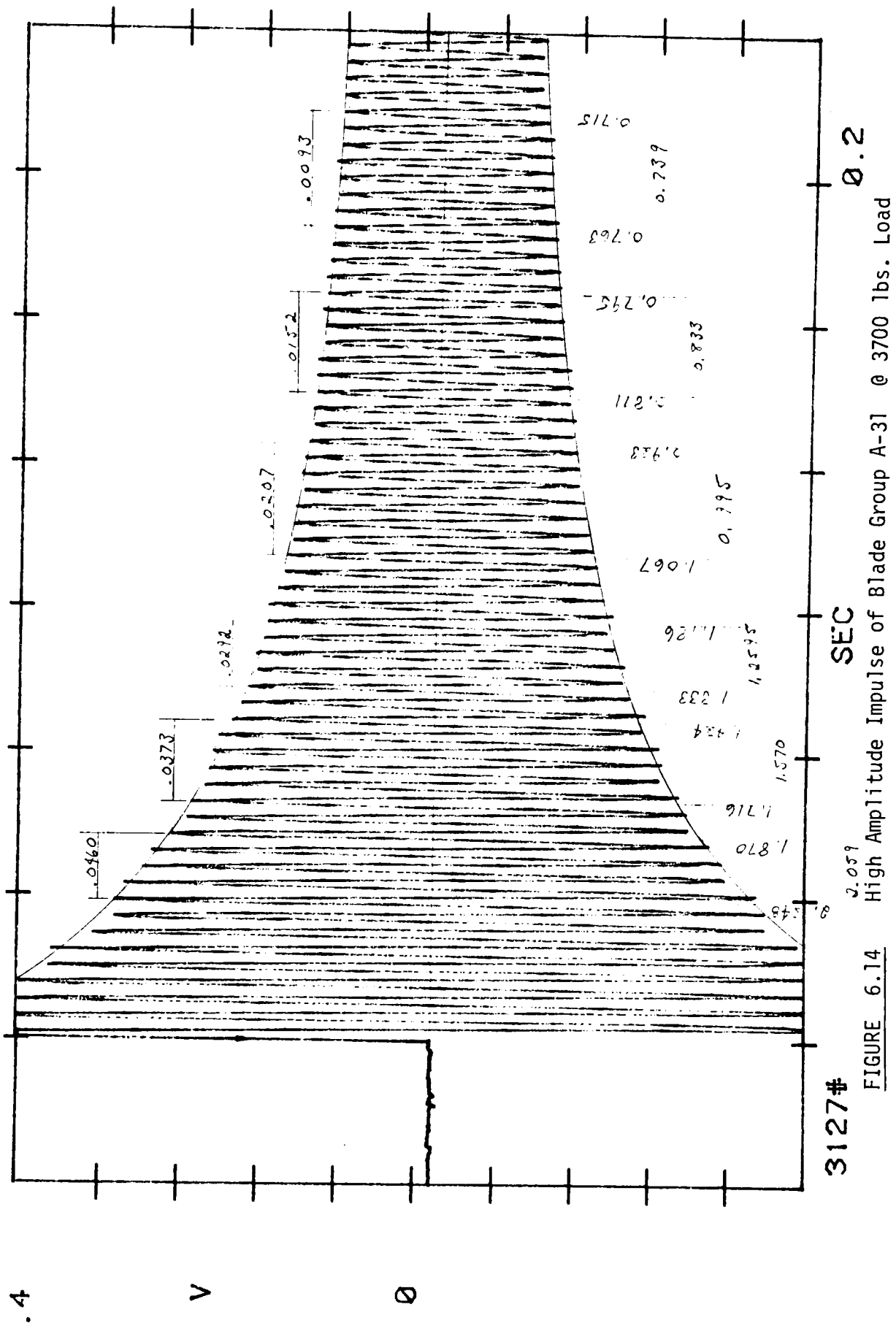

FIGURE 6.14 High Amplitude Impulse of Blade Group A-31 @ 3700 lbs. Load

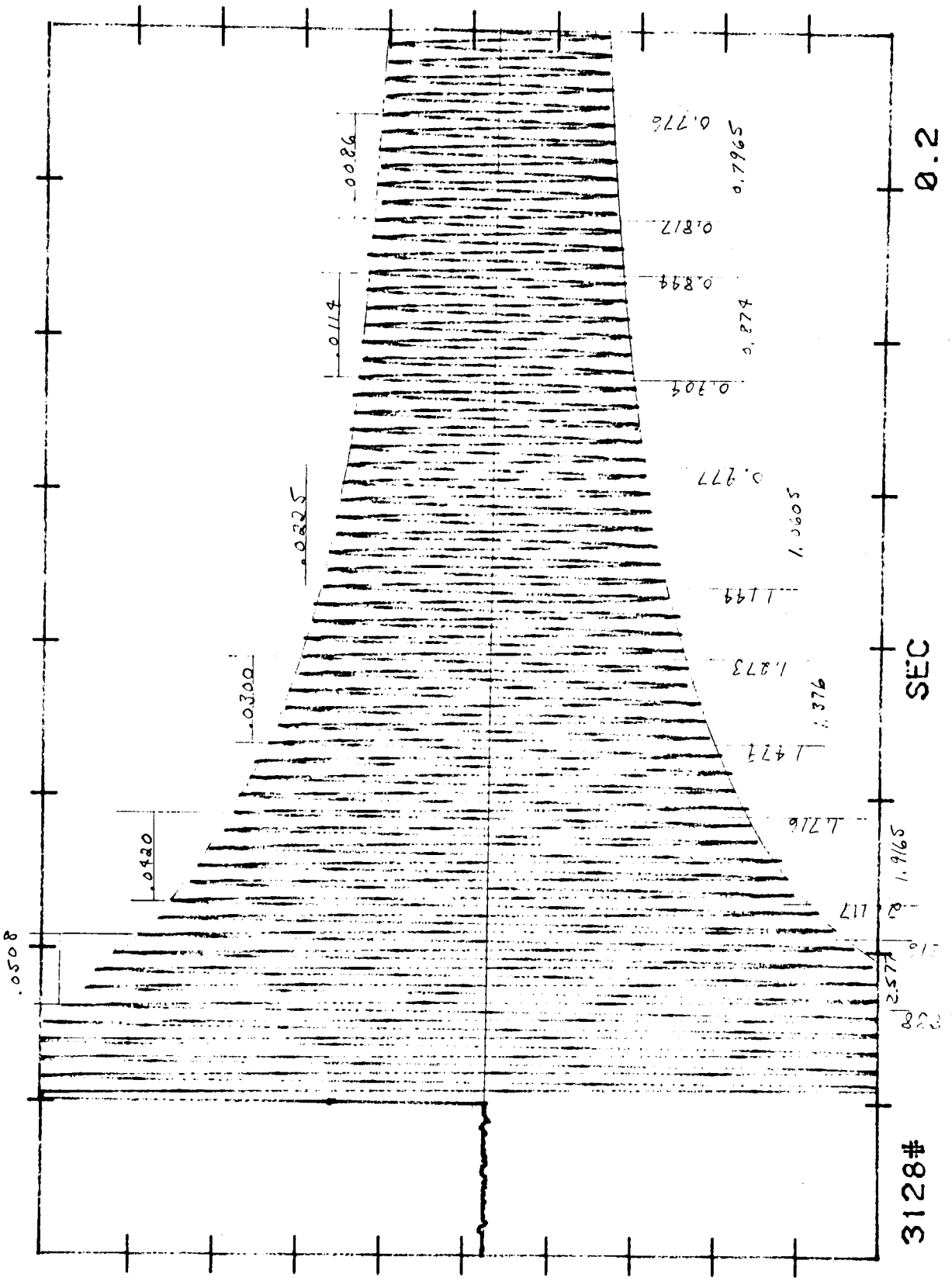

FIGURE 6.15 High Amplitude Impulse of Blade Group A-31 @ 3700 lbs. Load

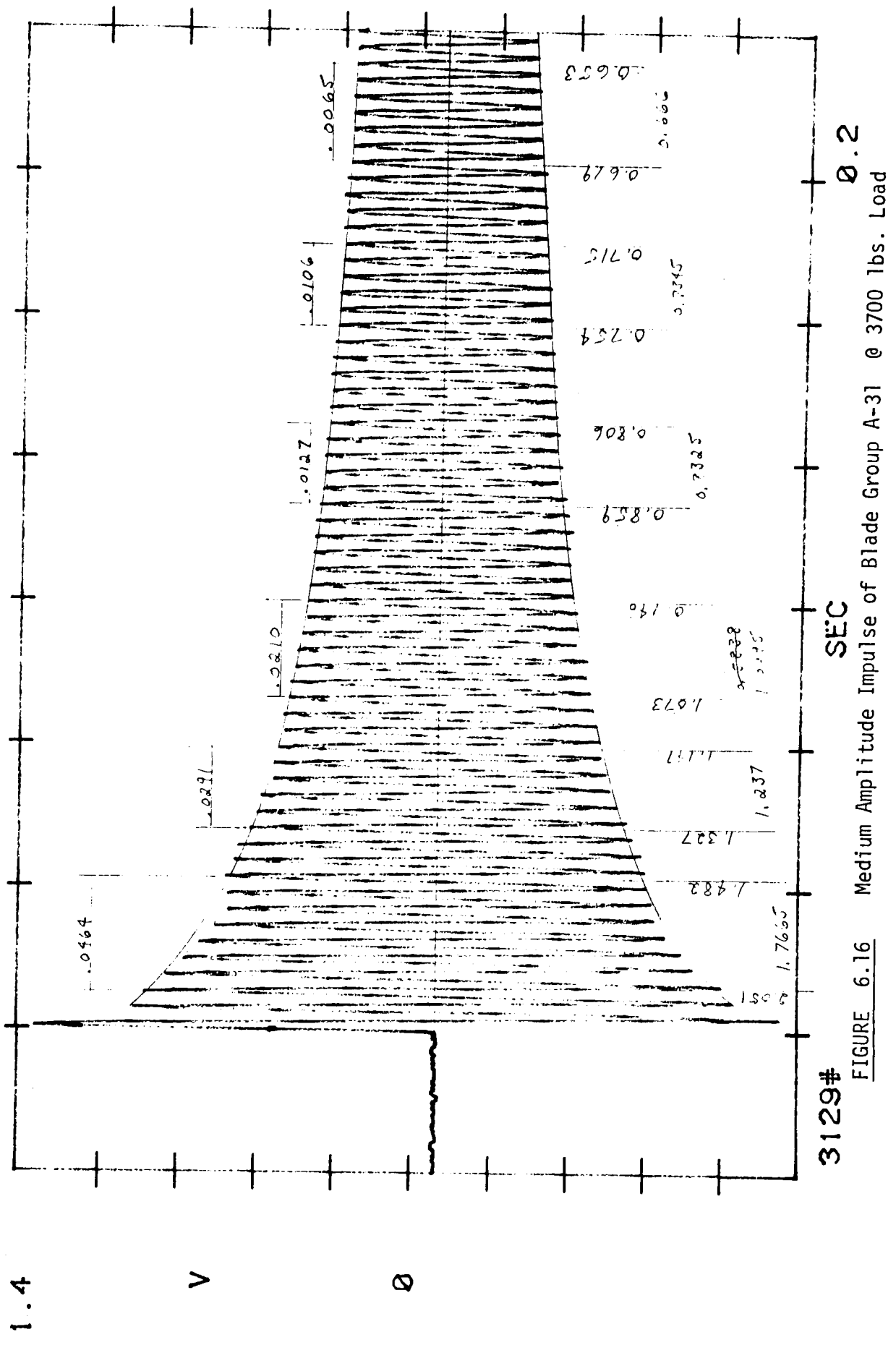

FIGURE 6.16 Medium Amplitude Impulse of Blade Group A-31 @ 3700 lbs. Load

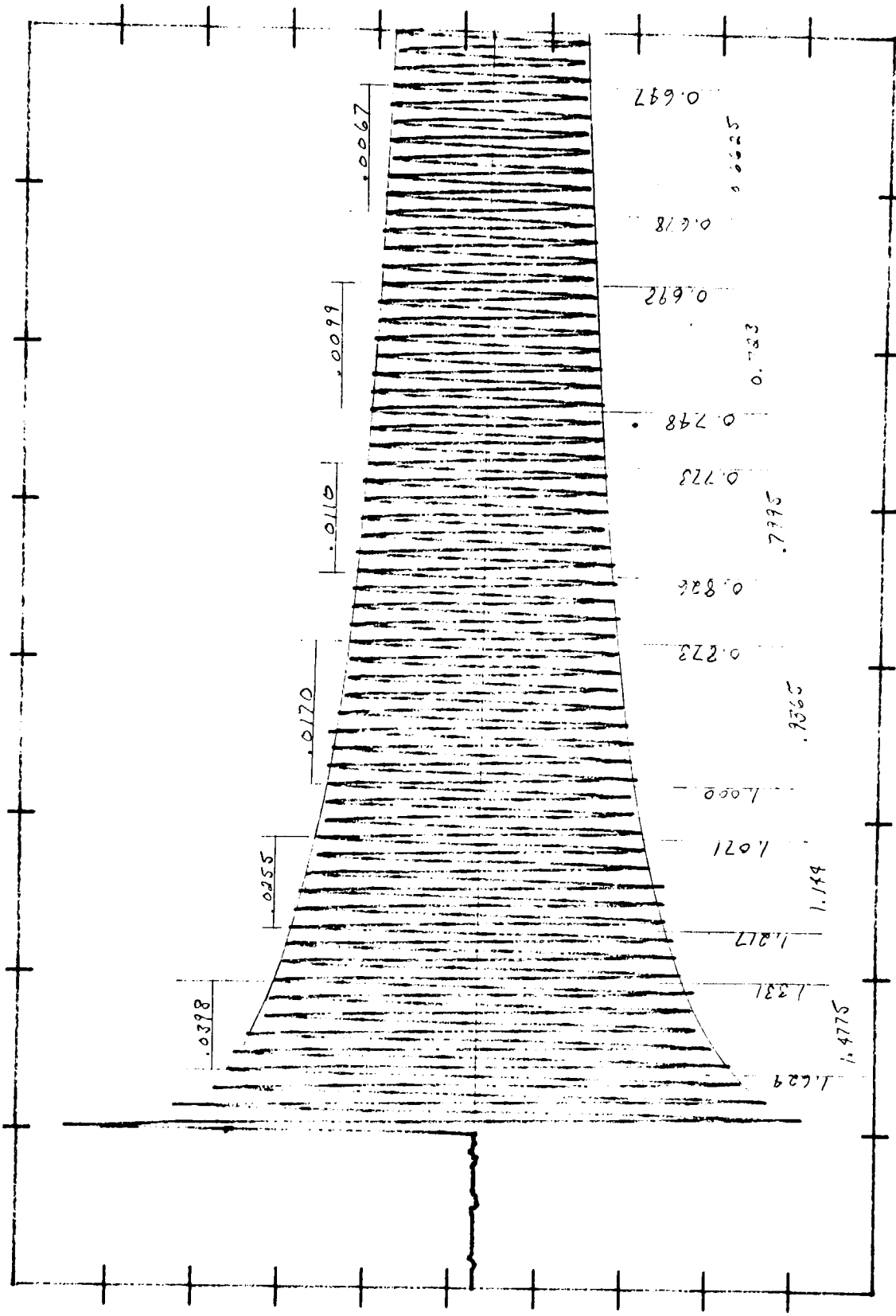

FIGURE 6.17 Medium Amplitude Impulse of Blade Group A-31 @ 3700 lbs. Load

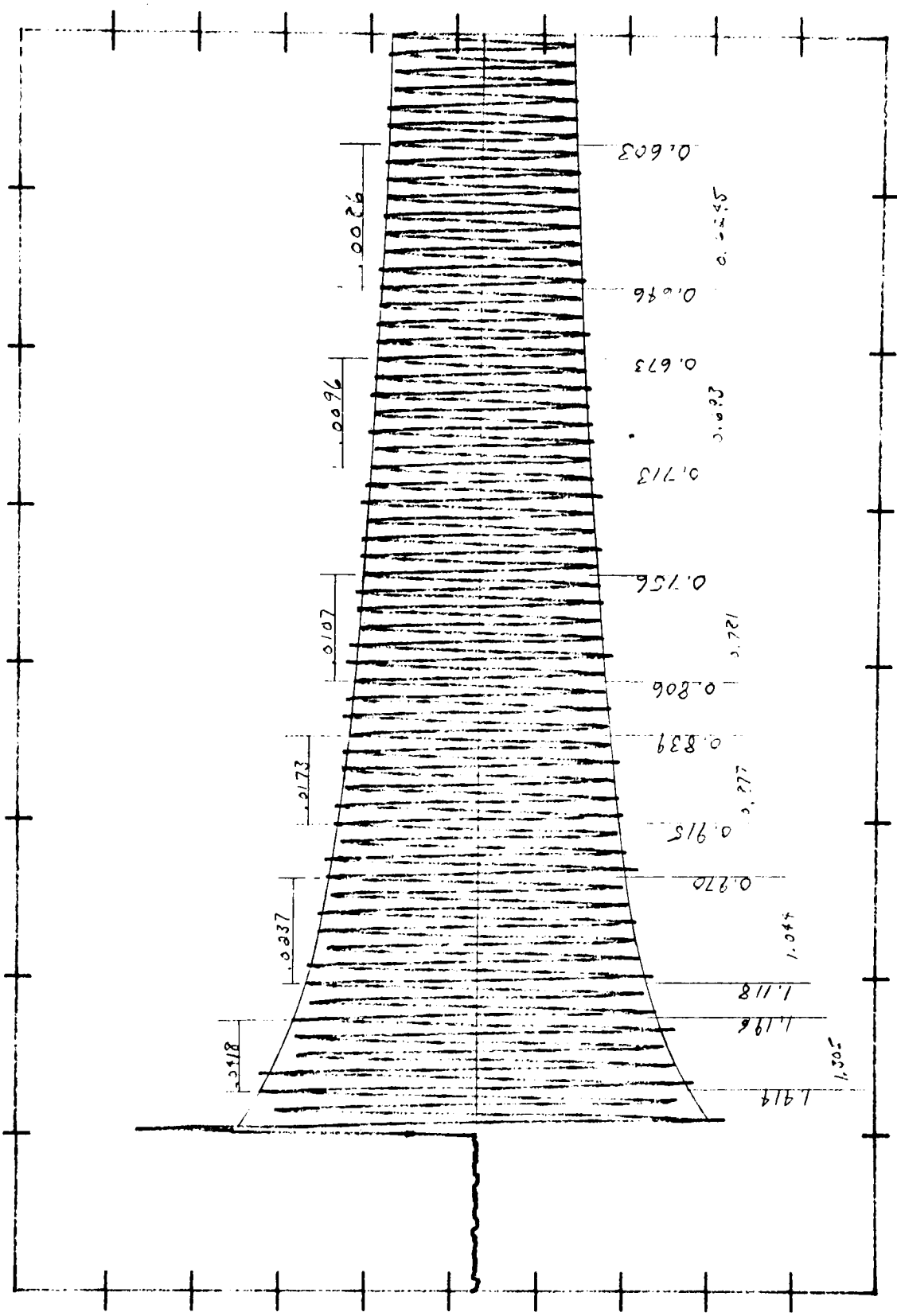

FIGURE 6.18 Low Amplitude Impulse of Blade Group A-31 @ 3700 lbs. Load

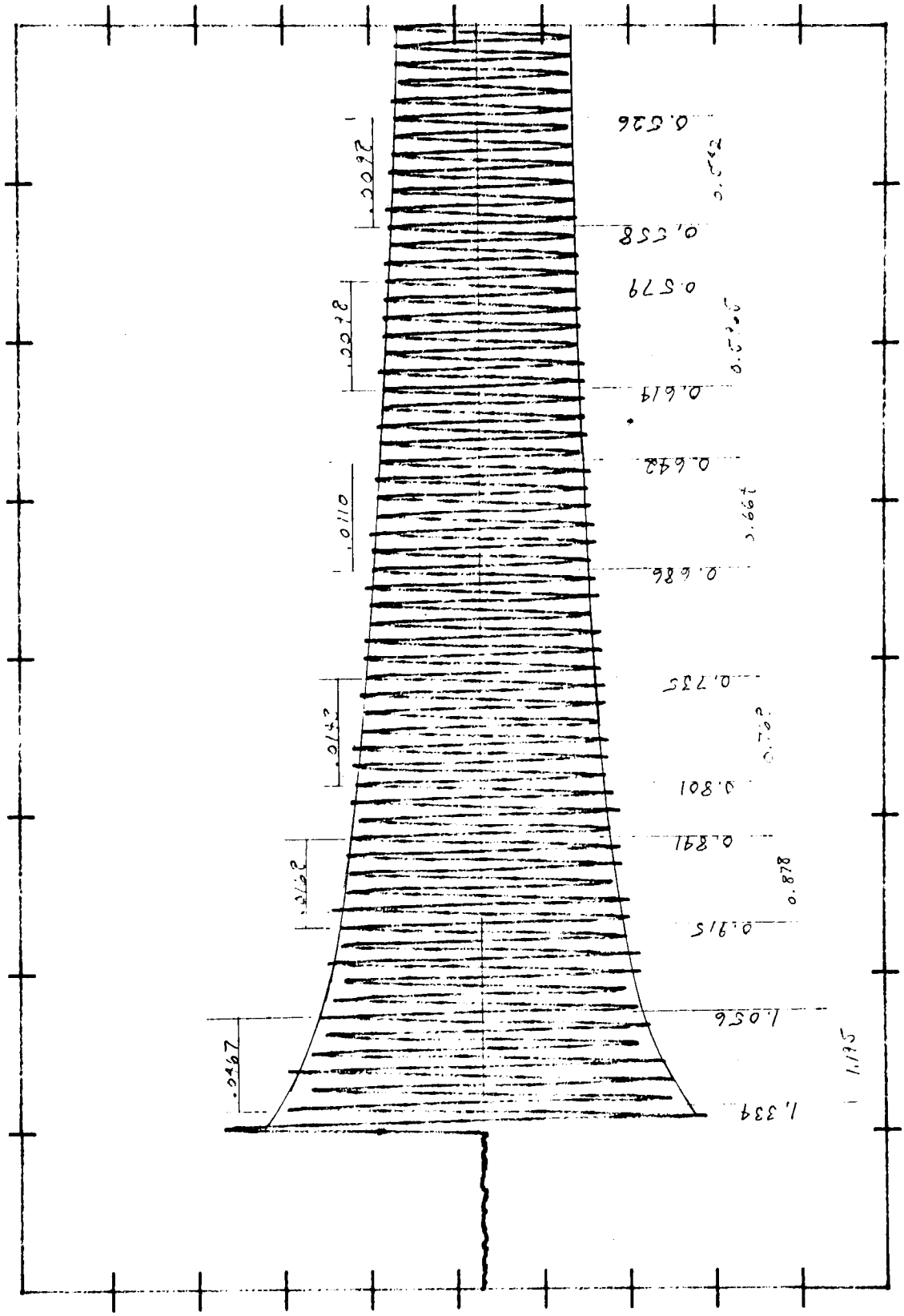

FIGURE 6.19 Low Amplitude Impulse of Blade Group A-31 @ 3700 lbs. Load

FIGURE 6.20

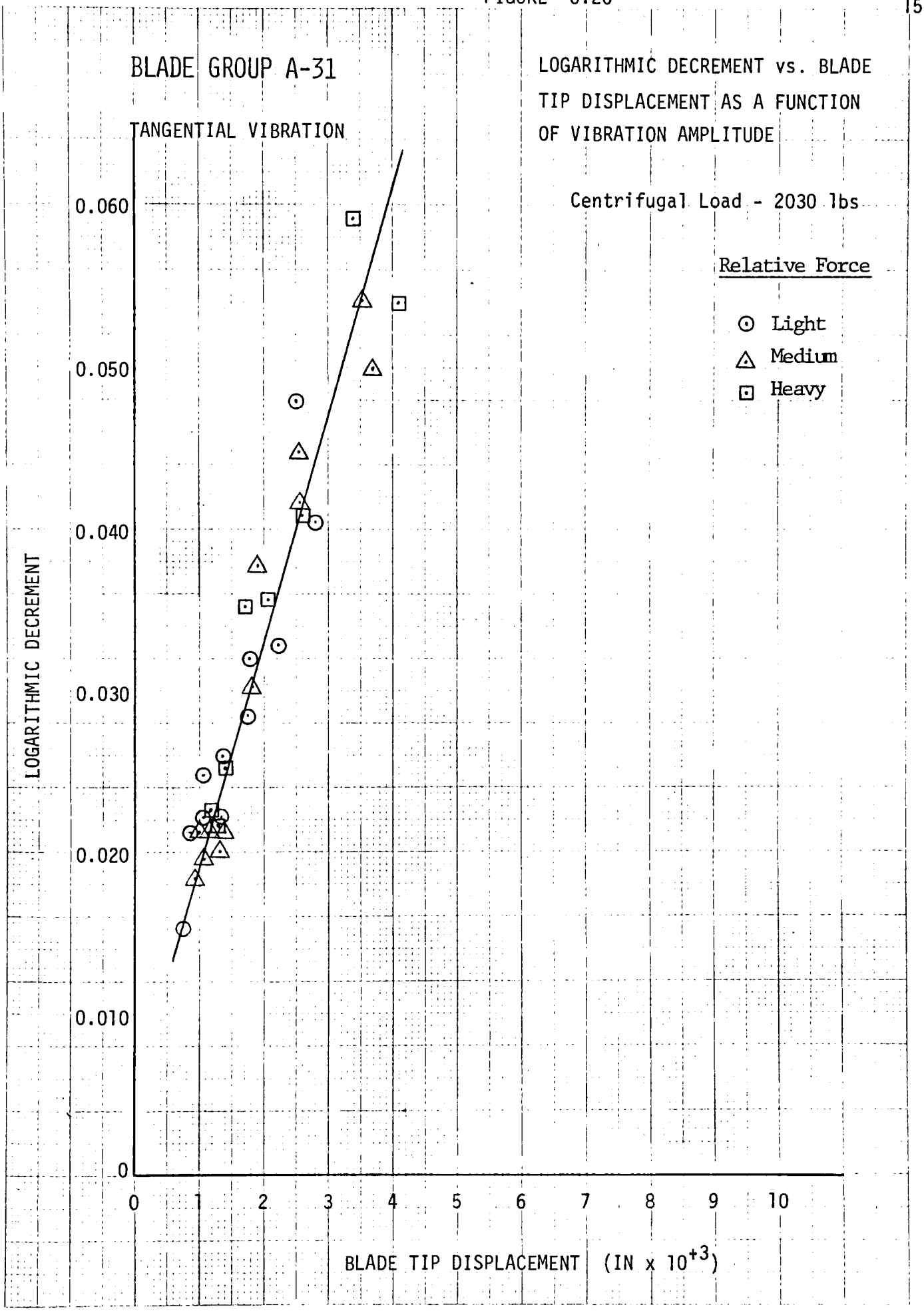

FIGURE 6.21

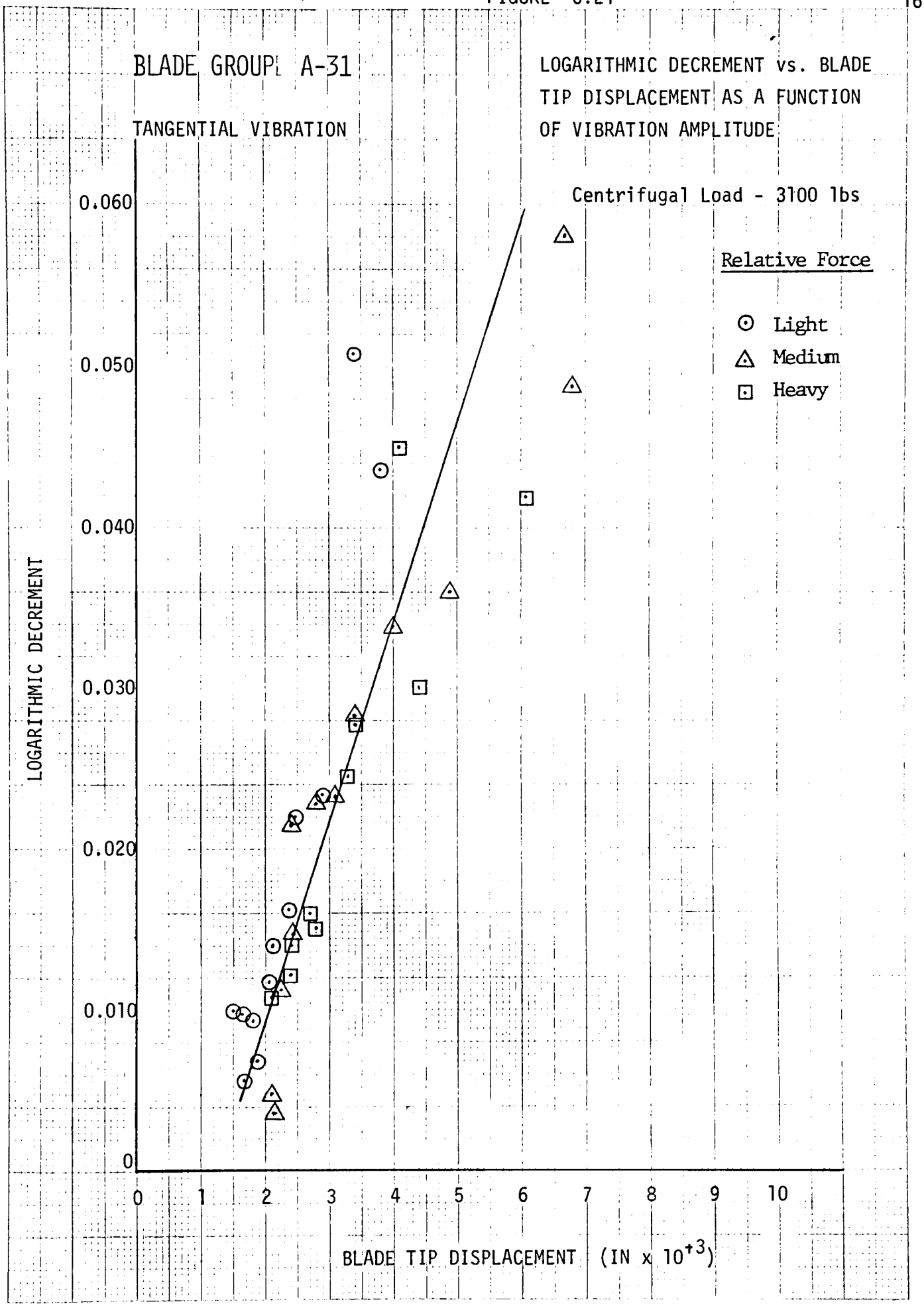

FIGURE 6.22

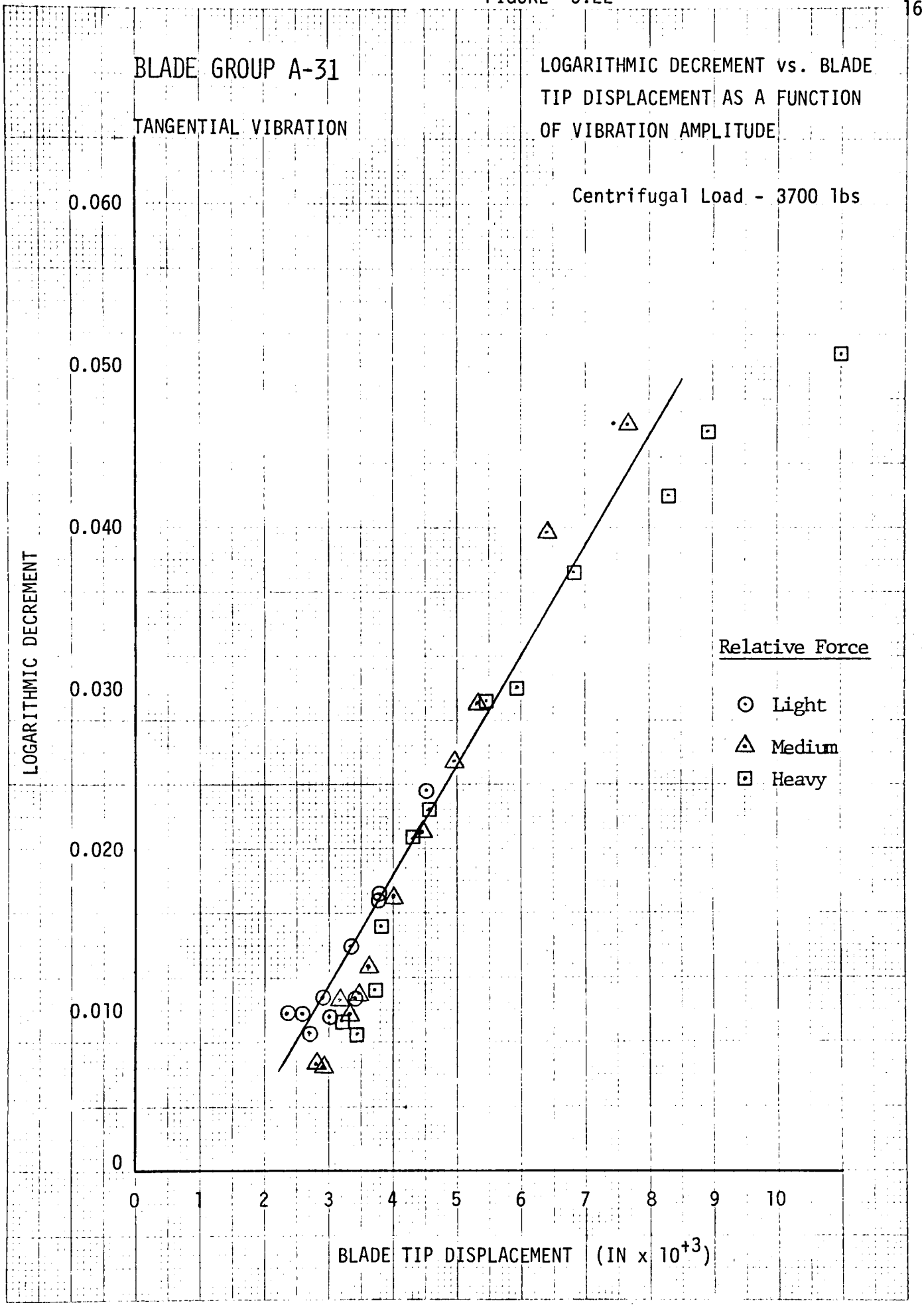
BLADE GROUP A-31
TANGENTIAL VIBRATION
LOGARITHMIC DECREMENT vs. BLADE TIP DISPLACEMENT AS A FUNCTION OF VIBRATION AMPLITUDE
Centrifugal Load - 3700 lbs
LOGARITHMIC DECREMENT
0.060
0.050
0.040
0.030
0.020
0.010
0
0 1 2 3 4 5 6 7 8 9 10
BLADE TIP DISPLACEMENT (IN x 10^{+3})
Relative Force
Light
Medium
Heavy

BLADE GROUP 12

Tangential Vibration
4037 lbs. Centrifugal Load
1" on Calibration Plot = 0.00418" Blade Tip Displacement

Plot Number	Decay Amplitude (in)	Blade Tip Disp. (in x 10^{-3})	Logarithmic Decrement
1211	2.008	8.390	0.0254
"	1.615	6.750	0.0194
"	1.365	5.710	0.0139
"	1.195	5.000	0.0096
"	1.100	4.600	0.0078
"	1.020	4.260	0.0098
1212	2.215	9.260	0.0280
"	1.828	7.640	0.0202
"	1.515	6.330	0.0162
"	1.310	5.480	0.0098
"	1.190	4.970	0.0084
"	1.085	4.540	0.0081
1213	1.538	6.430	0.0200
"	1.293	5.400	0.0150
"	1.140	4.770	0.0107
"	1.033	4.320	0.0079
"	0.948	3.960	0.0068
"	0.860	3.590	0.0091

FIGURE 6.23 Example of Calibration-Regression Analysis Input Data

BLADE GROUP A-12 Regression Analysis

4037 lbs. Centrifugal Load

A_0	A_1	A_2	A_3	A_4	A_5	C_c	C_d	ξ_s
-8.6952 E-3	3.9705 E-3					0.9165	0.9574	1.933 E-3
-3.8958 E-3	2.3380 E-3	1.2914 E-4				0.9191	0.9537	1.966 E-3
0.043147	-0.021972	4.1329 E-3	-2.0998 E-4			0.9348	0.9668	1.827 E-3
0.198880	-0.130629	0.031612	-3.1957 E-3	1.1775 E-4		0.9462	0.9727	1.722 E-3
0.252123	-0.177266	0.047505	-5.8304 E-3	3.3042 E-4	-6.6951 E-6	0.9463	0.9728	1.791 E-3

$$y = A_0 + A_1x + A_2x^2 + A_3x^3 + ... + A_nx^n$$

Best Fit Curve Maximizes C_d and Minimizes ξ_s; Maximizes Convergance and Minimizes Std. Deviation.

FIGURE 6.24 Example of Regression Analysis Output for Best Fit Curve

FIGURE 6.25

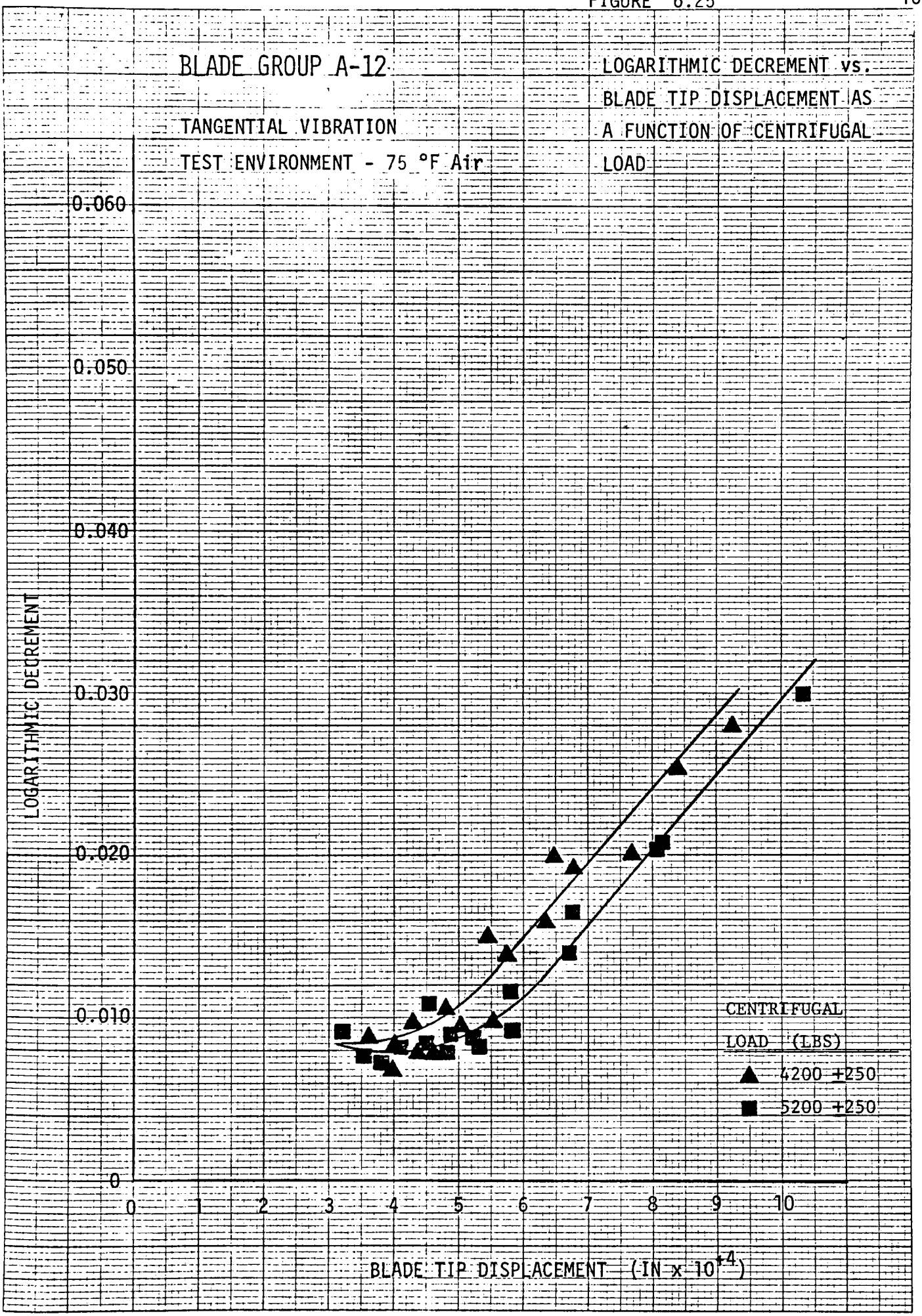
BLADE GROUP A-12
TANGENTIAL VIBRATION
TEST ENVIRONMENT - 75 °F Air
LOGARITHMIC DECREMENT vs. BLADE TIP DISPLACEMENT AS A FUNCTION OF CENTRIFUGAL LOAD
0.060
0.050
0.040
0.030
0.020
0.010
0
LOGARITHMIC DECREMENT
0
1
2
3
4
5
6
7
8
9
10
BLADE TIP DISPLACEMENT (IN x 10+4)
CENTRIFUGAL LOAD (LBS)
4200 ±250
5200 ±250

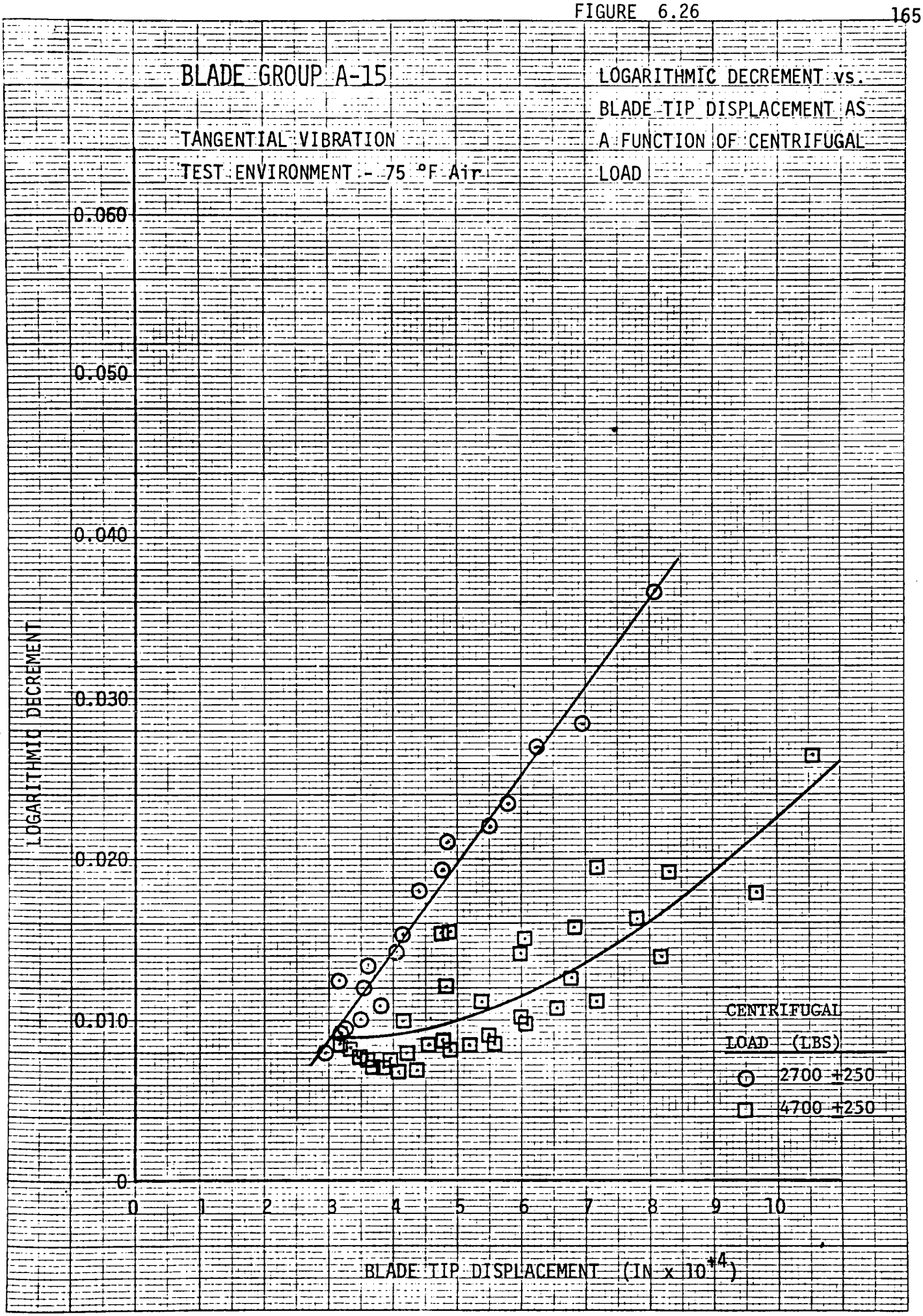
BLADE GROUP A-15
TANGENTIAL VIBRATION
TEST ENVIRONMENT - 75 °F Air
LOGARITHMIC DECREMENT vs. BLADE TIP DISPLACEMENT AS A FUNCTION OF CENTRIFUGAL LOAD
0.060
0.050
0.040
0.030
0.020
0.010
0
LOGARITHMIC DECREMENT
0
1
2
3
4
5
6
7
8
9
10
BLADE TIP DISPLACEMENT (IN x 10**4)
CENTRIFUGAL LOAD (LBS)
2700 ±250
4700 ±250

BLADE GROUP A-16

TANGENTIAL VIBRATION

TEST ENVIRONMENT - 75 °F Air

LOGARITHMIC DECREMENT vs. BLADE TIP DISPLACEMENT AS A FUNCTION OF CENTRIFUGAL LOAD

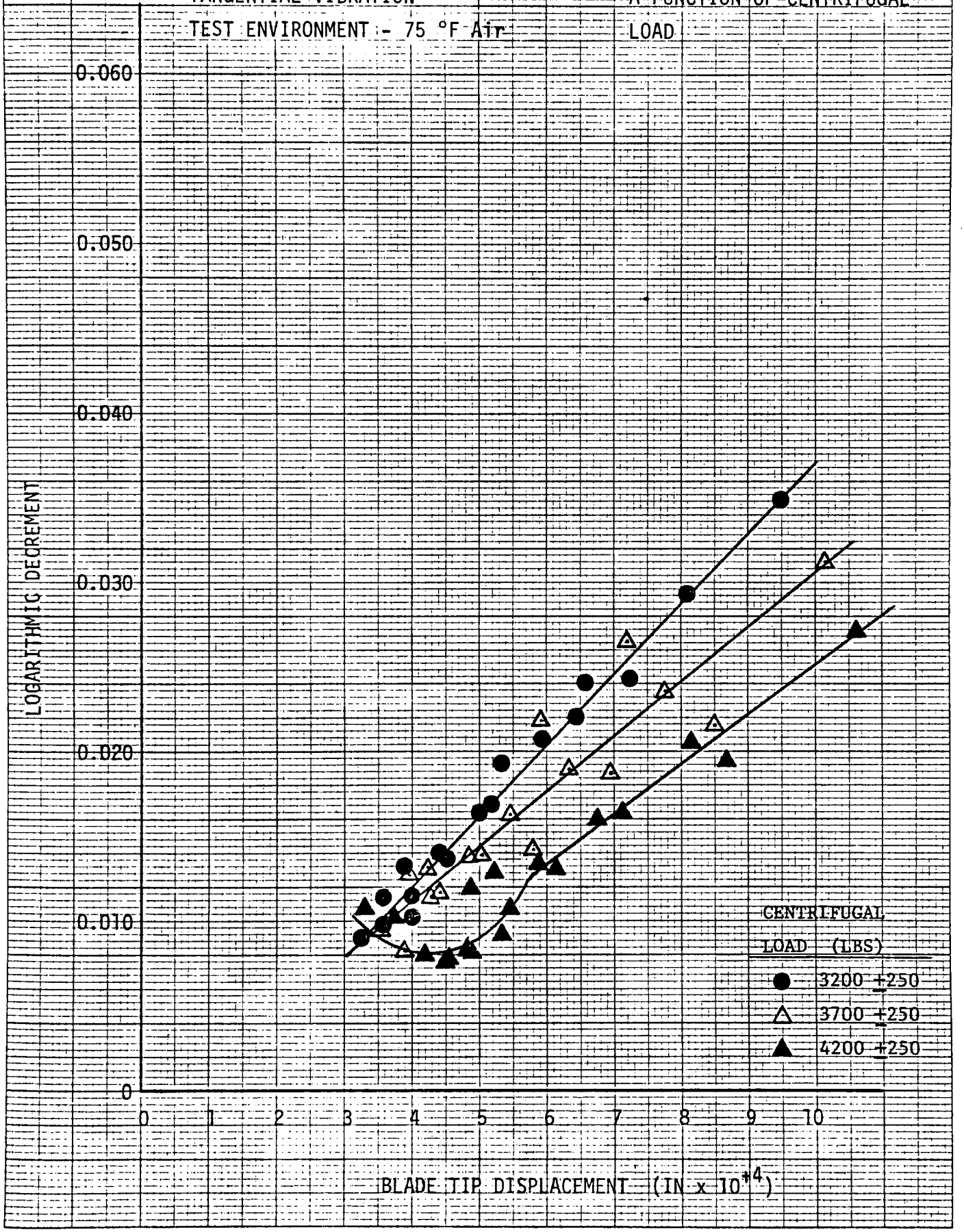

FIGURE 6.28

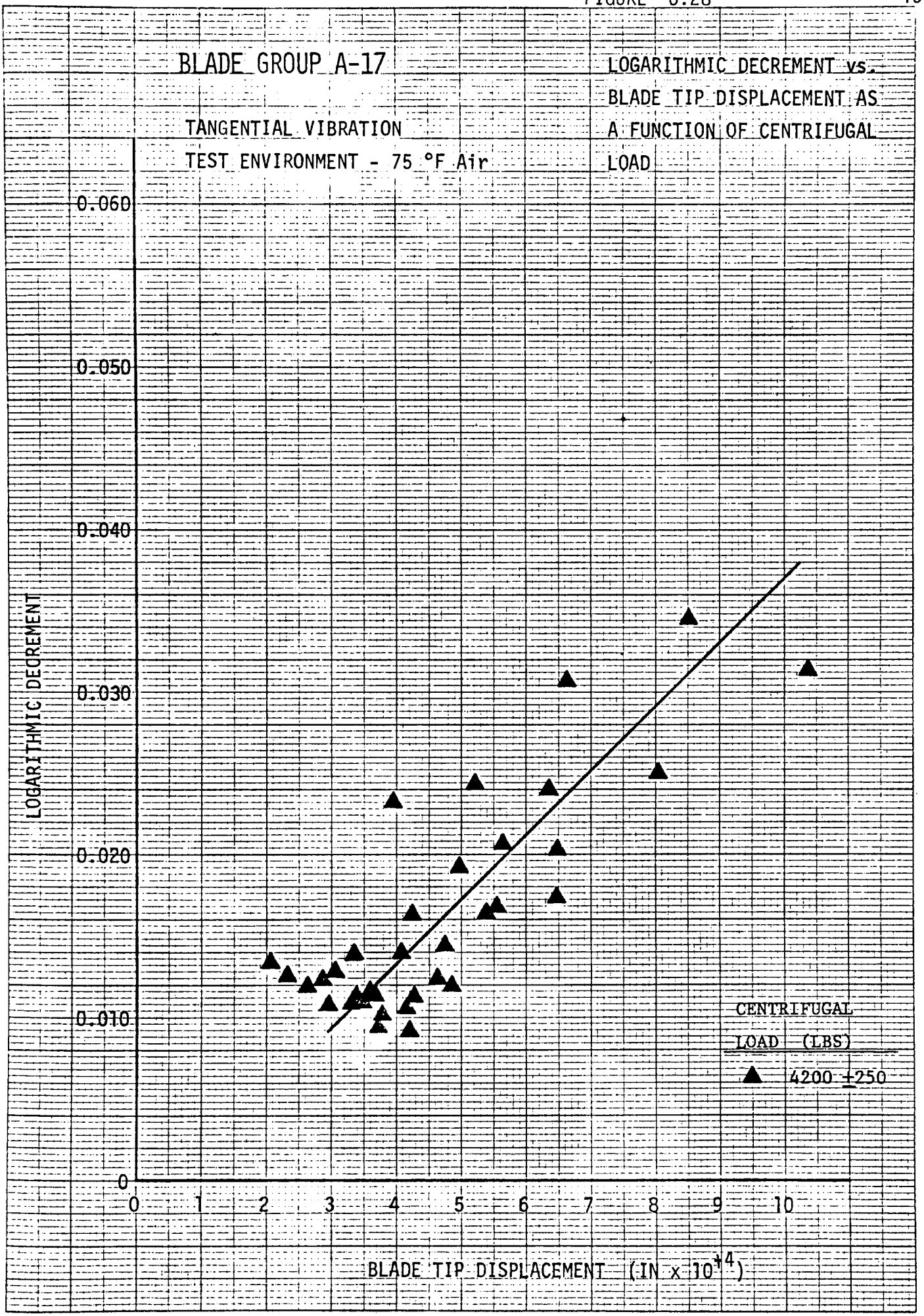
BLADE GROUP A-17
TANGENTIAL VIBRATION
TEST ENVIRONMENT - 75 °F Air
LOGARITHMIC DECREMENT vs. BLADE TIP DISPLACEMENT AS A FUNCTION OF CENTRIFUGAL LOAD
0.060
0.050
0.040
0.030
0.020
0.010
0
LOGARITHMIC DECREMENT
0 1 2 3 4 5 6 7 8 9 10
BLADE TIP DISPLACEMENT (IN x 10^-4)
CENTRIFUGAL LOAD (LBS)
4200 ±250

FIGURE 6.29

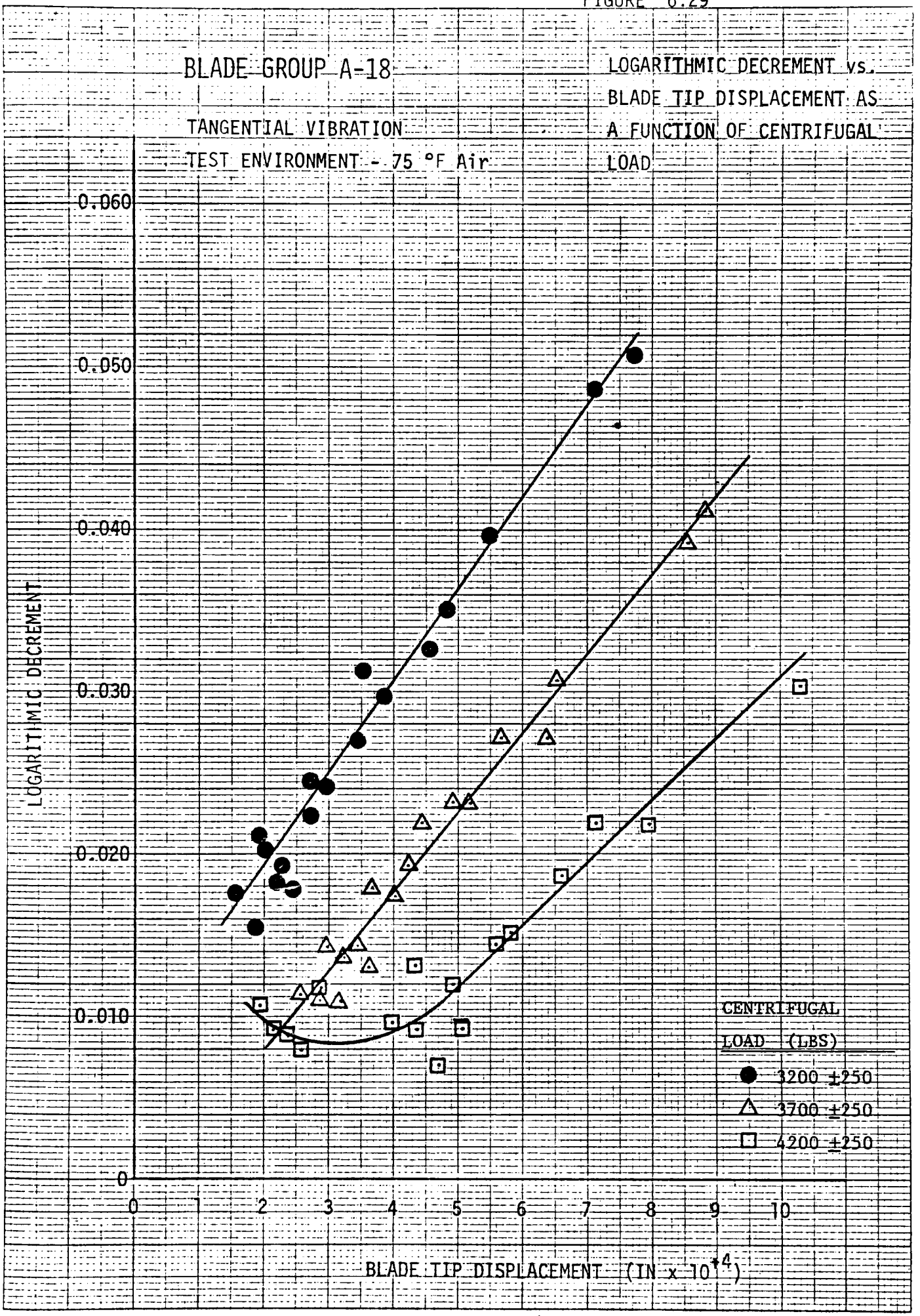
BLADE GROUP A-18
TANGENTIAL VIBRATION
TEST ENVIRONMENT - 75 °F Air
LOGARITHMIC DECREMENT vs. BLADE TIP DISPLACEMENT AS A FUNCTION OF CENTRIFUGAL LOAD
LOGARITHMIC DECREMENT
0.060
0.050
0.040
0.030
0.020
0.010
0
0
2
3
4
5
6
7
8
9
10
BLADE TIP DISPLACEMENT (IN x 10+4)
CENTRIFUGAL LOAD (LBS)
3200 ±250
3700 ±250
4200 ±250

FIGURE 6.30

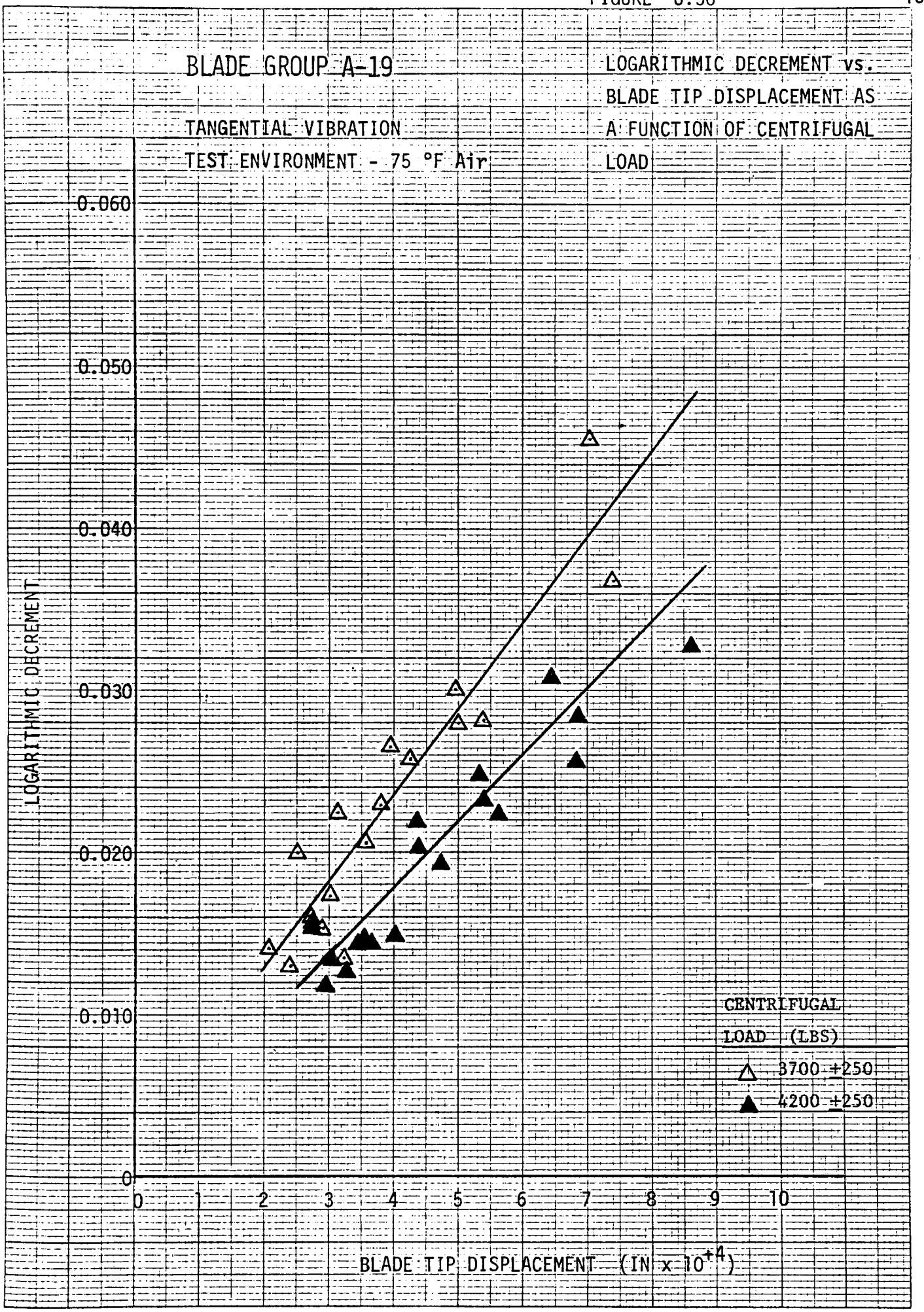
BLADE GROUP A-19
TANGENTIAL VIBRATION
TEST ENVIRONMENT - 75 °F Air
LOGARITHMIC DECREMENT vs. BLADE TIP DISPLACEMENT AS A FUNCTION OF CENTRIFUGAL LOAD
LOGARITHMIC DECREMENT
0.060
0.050
0.040
0.030
0.020
0.010
0
0 1 2 3 4 5 6 7 8 9 10
BLADE TIP DISPLACEMENT (IN x 10^{+4})
CENTRIFUGAL LOAD (LBS)
△ 3700 ±250
▲ 4200 ±250

FIGURE 6.31

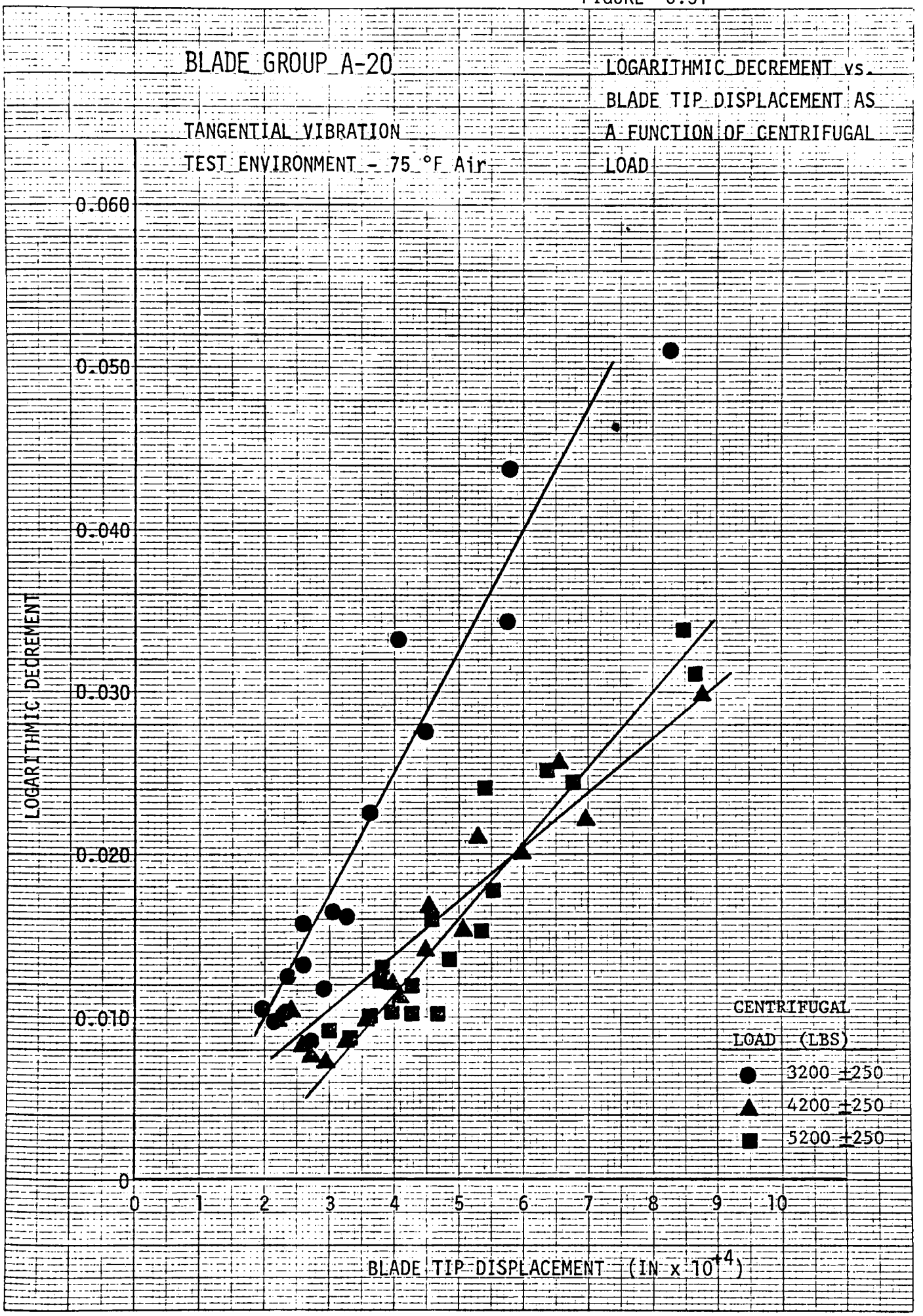

uares to the

FIGURE 6.32

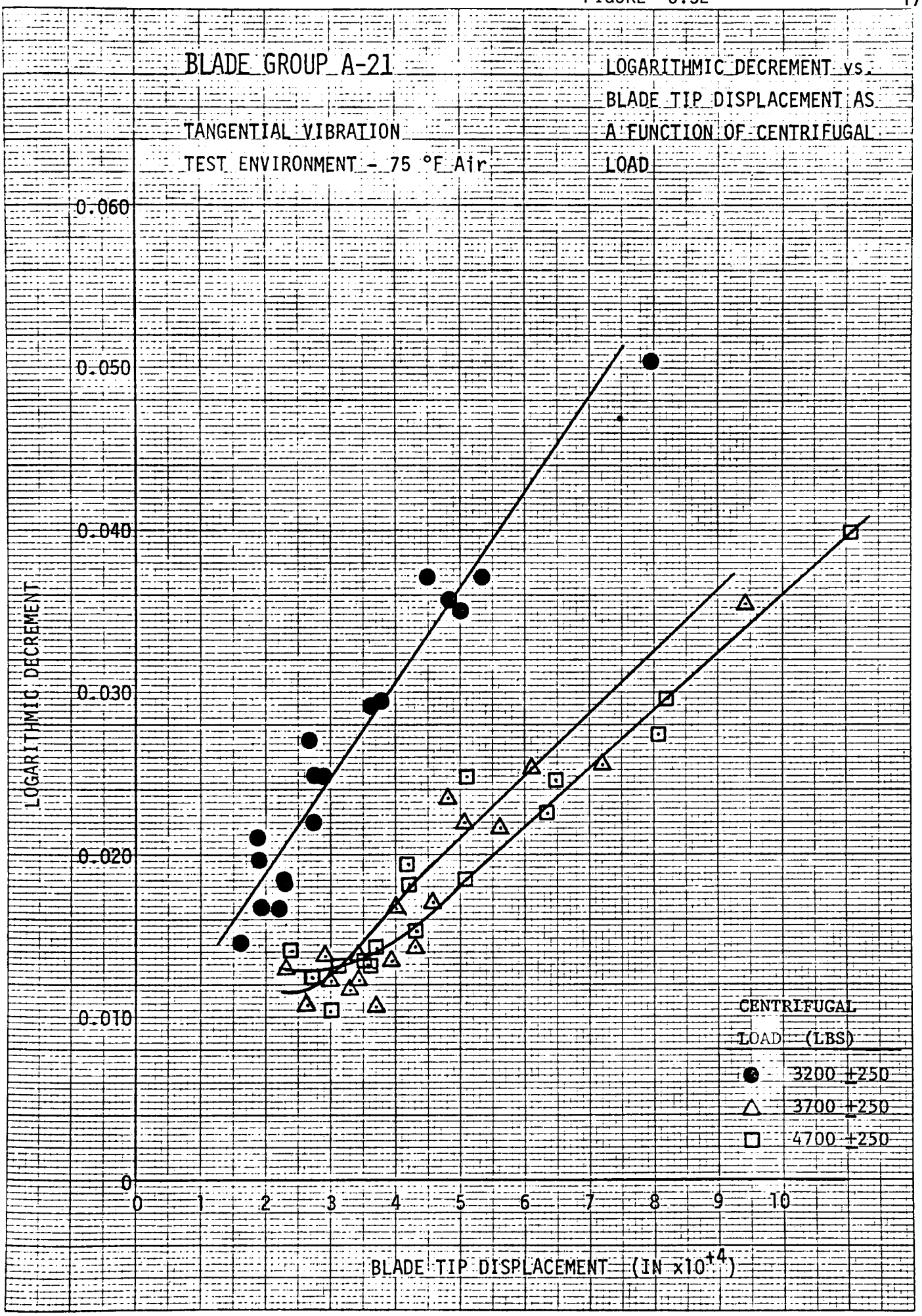
BLADE GROUP A-21
TANGENTIAL VIBRATION
TEST ENVIRONMENT - 75 °F Air
LOGARITHMIC DECREMENT vs. BLADE TIP DISPLACEMENT AS A FUNCTION OF CENTRIFUGAL LOAD
LOGARITHMIC DECREMENT
0.060
0.050
0.040
0.030
0.020
0.010
0
0 1 2 3 4 5 6 7 8 9 10
BLADE TIP DISPLACEMENT (IN x10+4)
CENTRIFUGAL LOAD (LBS)
3200 ±250
3700 ±250
4700 ±250

FIGURE 6.33

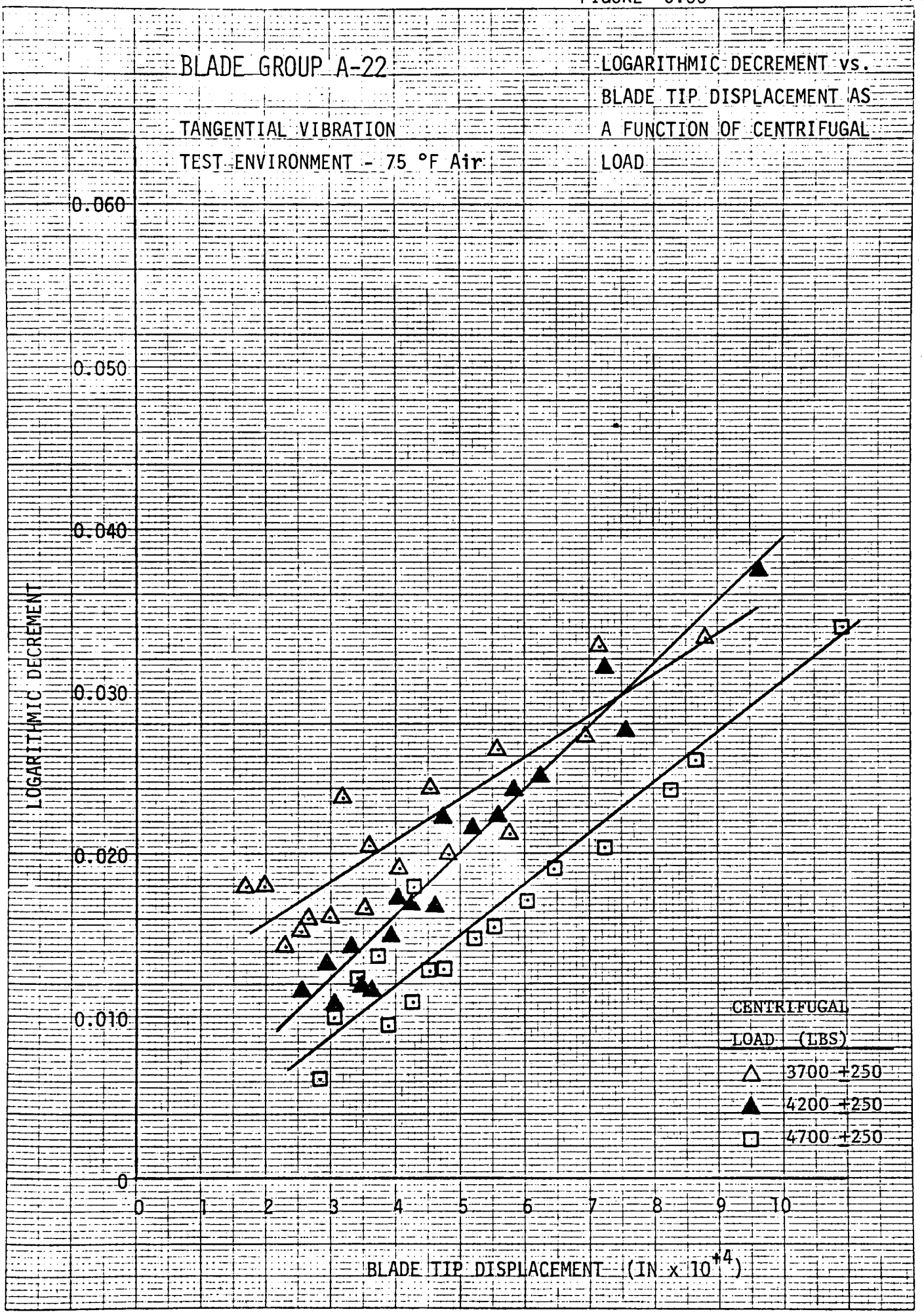
BLADE GROUP A-22
TANGENTIAL VIBRATION
TEST ENVIRONMENT - 75 °F Air
LOGARITHMIC DECREMENT vs. BLADE TIP DISPLACEMENT AS A FUNCTION OF CENTRIFUGAL LOAD
0.060
0.050
0.040
0.030
0.020
0.010
0
LOGARITHMIC DECREMENT
0 1 2 3 4 5 6 7 8 9 10
BLADE TIP DISPLACEMENT (IN x 10+4)
CENTRIFUGAL LOAD (LBS)
3700 ±250
4200 ±250
4700 ±250

FIGURE 6.34

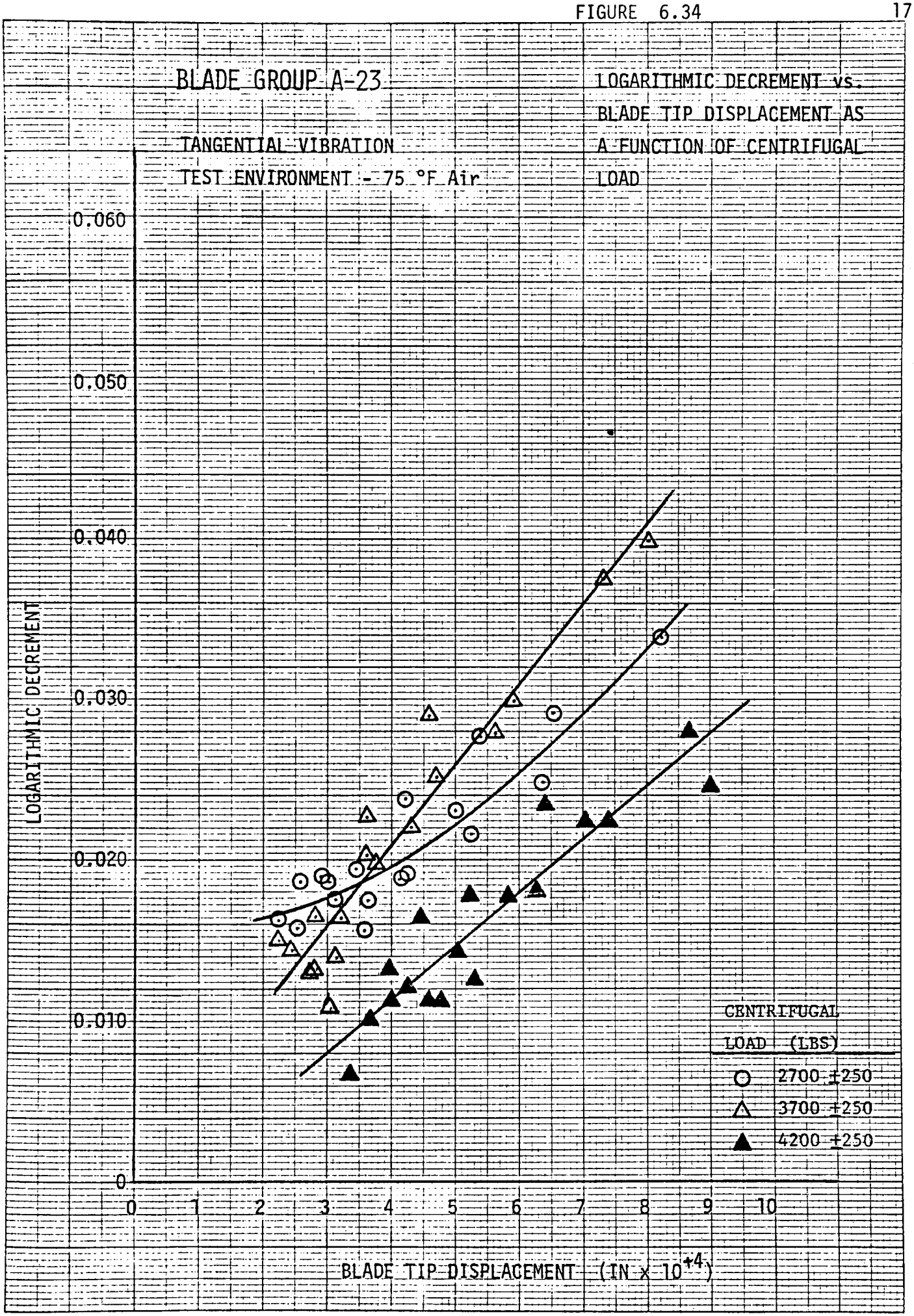
BLADE GROUP A-23
TANGENTIAL VIBRATION
TEST ENVIRONMENT - 75 °F Air
LOGARITHMIC DECREMENT vs. BLADE TIP DISPLACEMENT AS A FUNCTION OF CENTRIFUGAL LOAD
LOGARITHMIC DECREMENT
0.060
0.050
0.040
0.030
0.020
0.010
0
0 1 2 3 4 5 6 7 8 9 10
BLADE TIP DISPLACEMENT (IN x 10+4)
CENTRIFUGAL LOAD (LBS)
2700 ±250
3700 ±250
4200 ±250

FIGURE 6.35

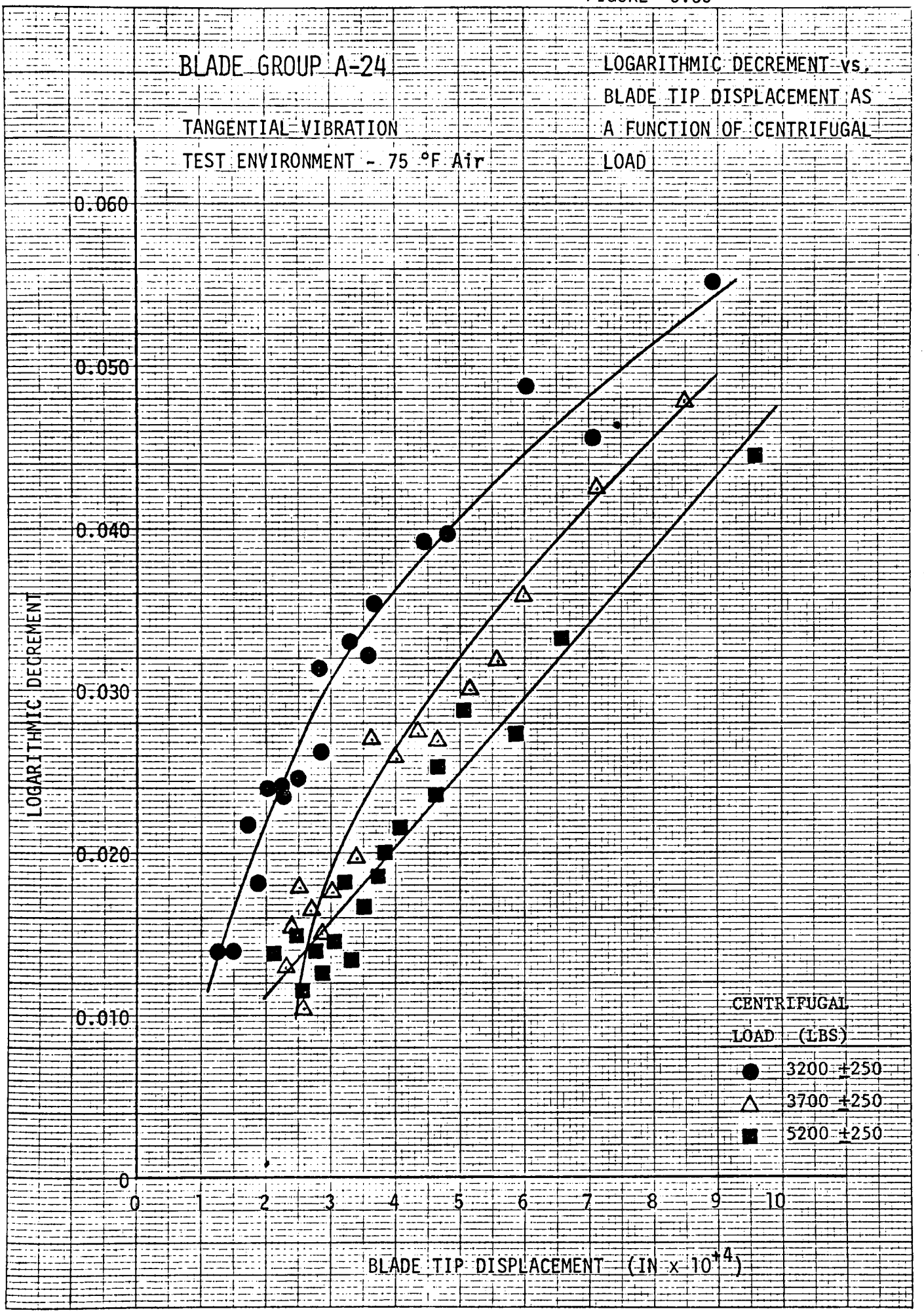
BLADE GROUP A-24
TANGENTIAL VIBRATION
TEST ENVIRONMENT - 75 °F Air
LOGARITHMIC DECREMENT vs. BLADE TIP DISPLACEMENT AS A FUNCTION OF CENTRIFUGAL LOAD
LOGARITHMIC DECREMENT
0.060
0.050
0.040
0.030
0.020
0.010
0
0 1 2 3 4 5 6 7 8 9 10
BLADE TIP DISPLACEMENT (IN x 10+4)
CENTRIFUGAL LOAD (LBS)
3200 ±250
3700 ±250
5200 ±250

FIGURE 6.36

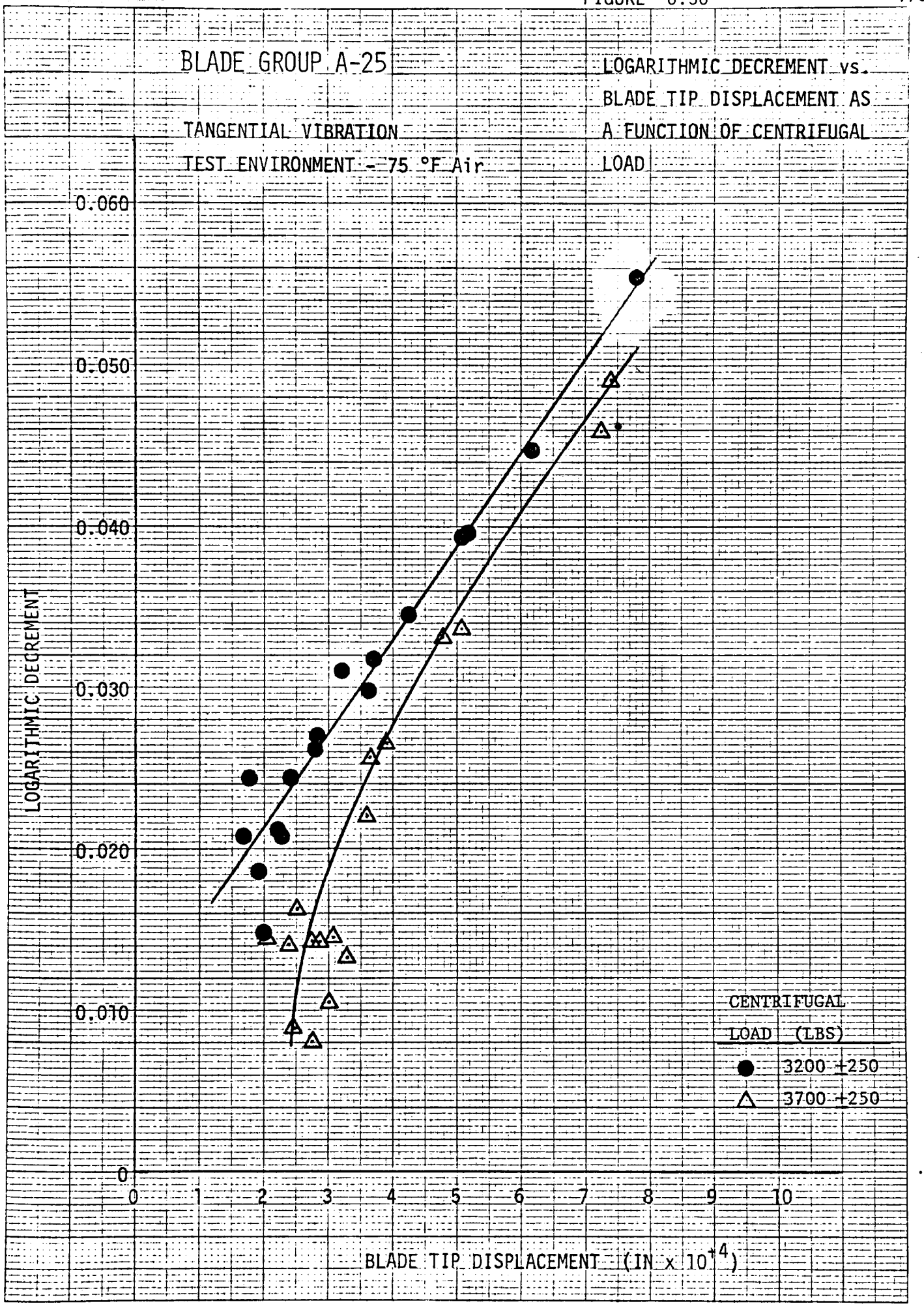

ares to the

FIGURE 6.37

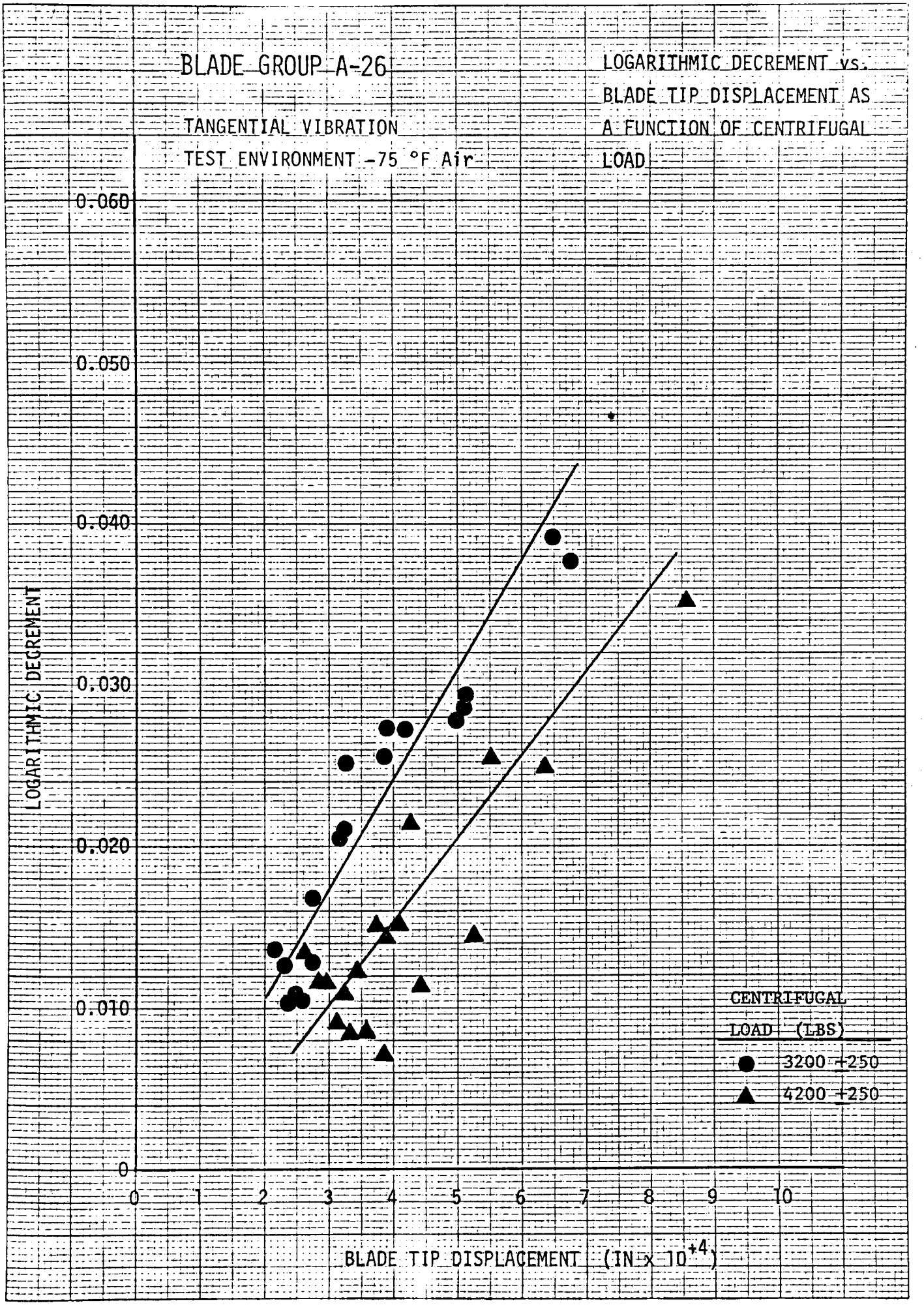
BLADE GROUP A-26
TANGENTIAL VIBRATION
TEST ENVIRONMENT -75 °F Air
LOGARITHMIC DECREMENT vs. BLADE TIP DISPLACEMENT AS A FUNCTION OF CENTRIFUGAL LOAD
0.060
0.050
0.040
0.030
0.020
0.010
0
LOGARITHMIC DECREMENT
0
1
2
3
4
5
6
7
8
9
10
BLADE TIP DISPLACEMENT (IN x 10+4)
CENTRIFUGAL LOAD (LBS)
3200 ±250
4200 ±250

FIGURE 6.38

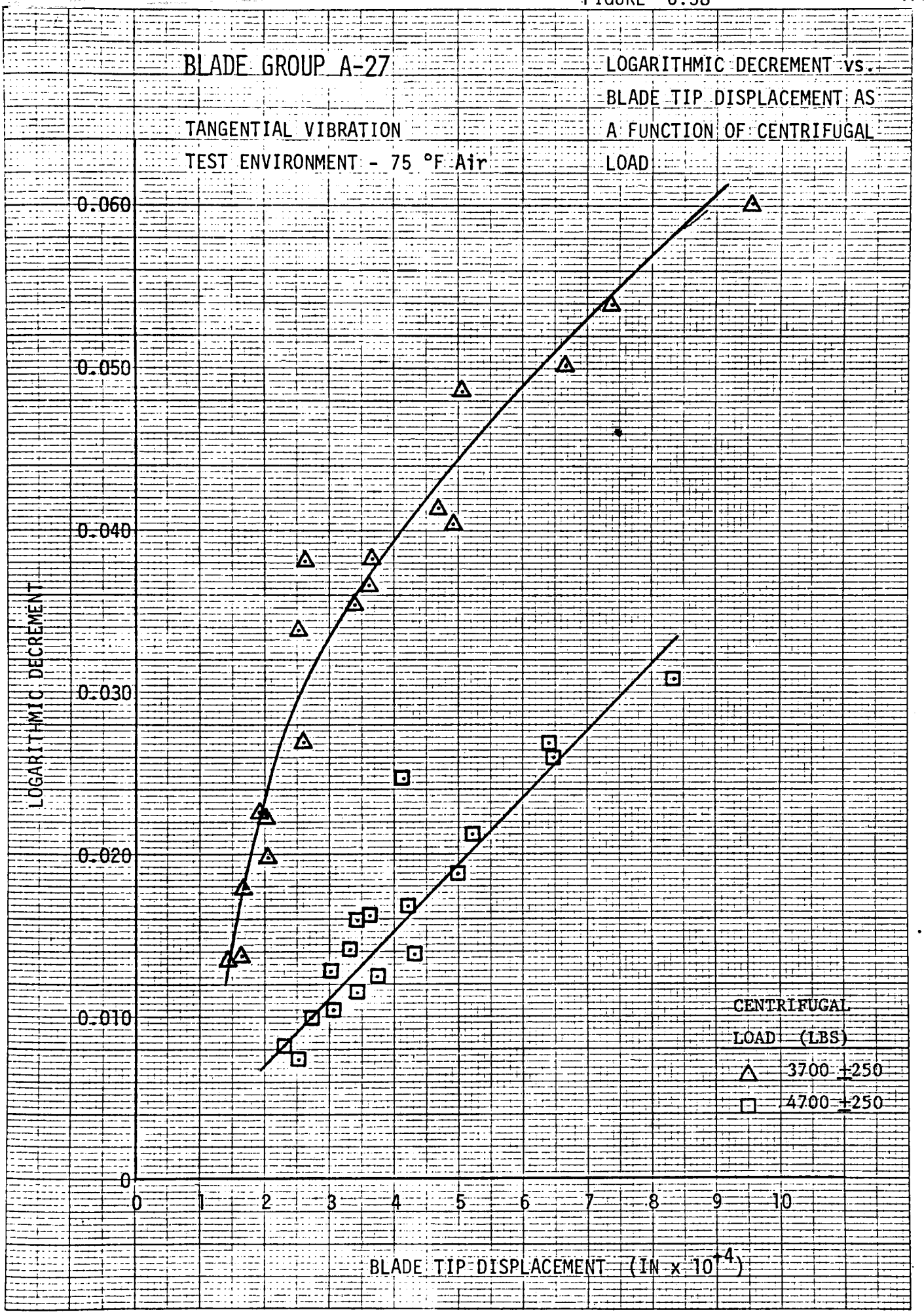

Marks to the

FIGURE 6.39

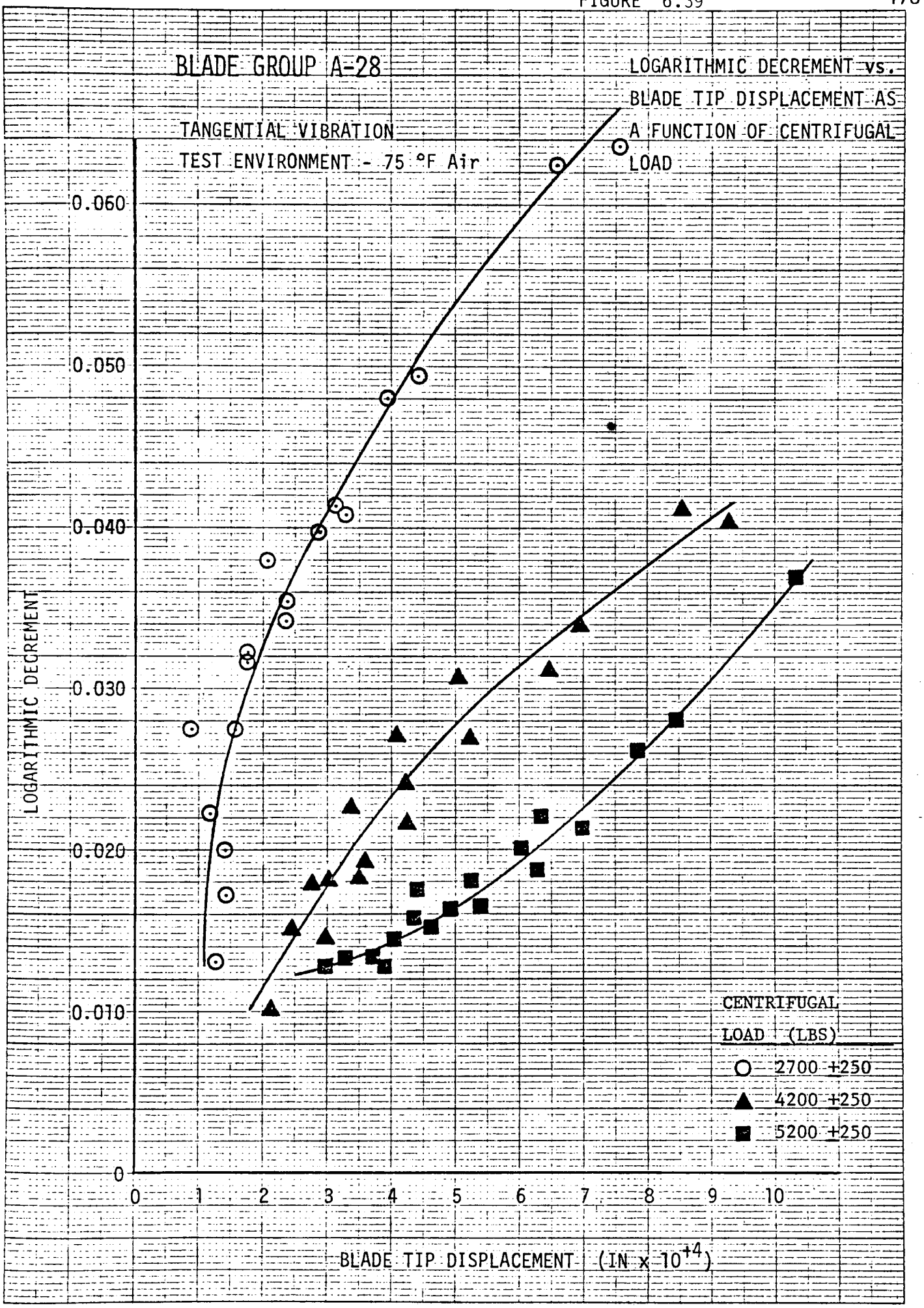
BLADE GROUP A-28
LOGARITHMIC DECREMENT vs. BLADE TIP DISPLACEMENT AS A FUNCTION OF CENTRIFUGAL LOAD
TANGENTIAL VIBRATION
TEST ENVIRONMENT - 75 °F Air
LOGARITHMIC DECREMENT
0.060
0.050
0.040
0.030
0.020
0.010
0
0 1 2 3 4 5 6 7 8 9 10
BLADE TIP DISPLACEMENT (IN x 10+4)
CENTRIFUGAL LOAD (LBS)
2700 ±250
4200 ±250
5200 ±250

FIGURE 6.40

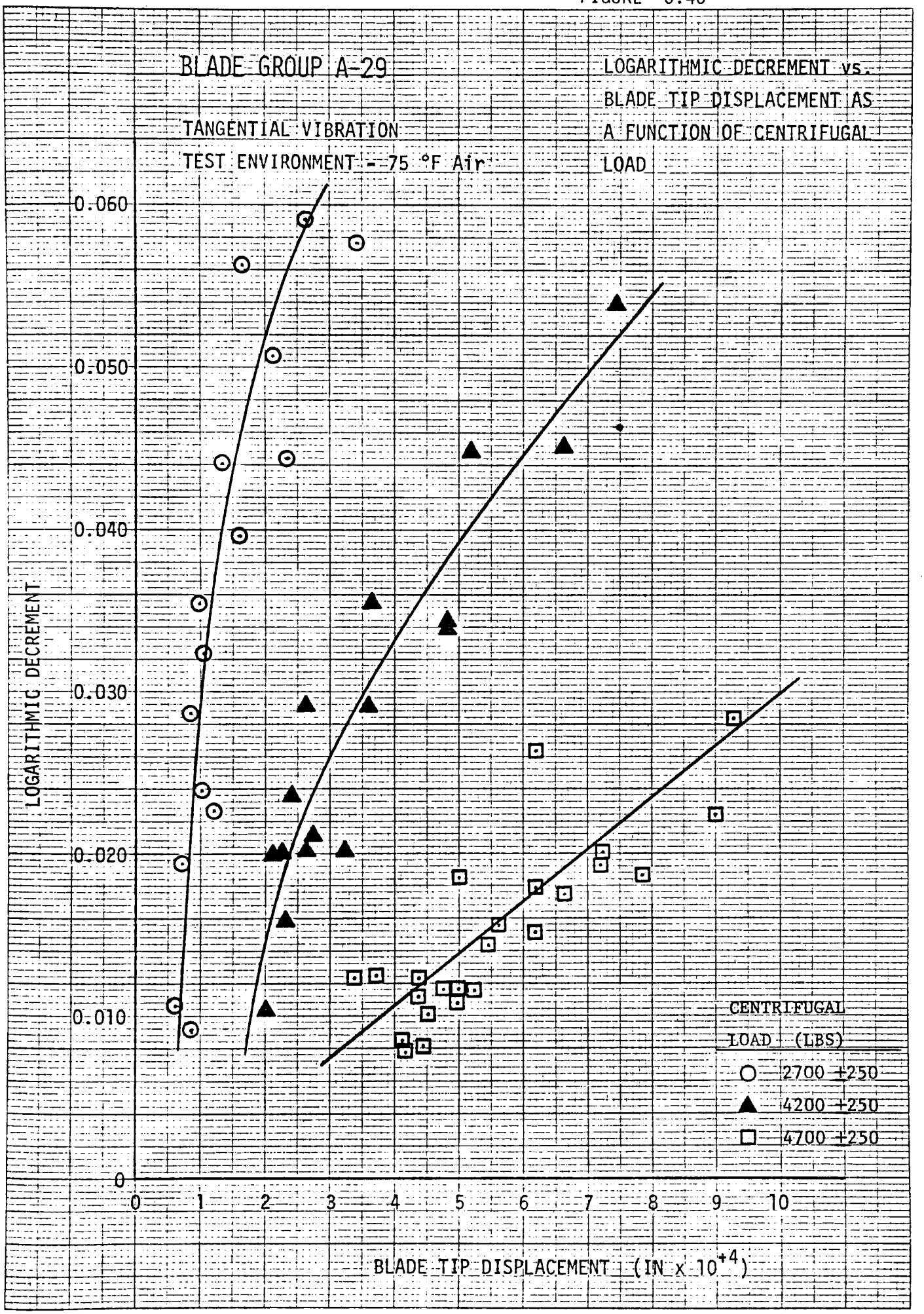
BLADE GROUP A-29
TANGENTIAL VIBRATION
TEST ENVIRONMENT - 75 °F Air
LOGARITHMIC DECREMENT vs. BLADE TIP DISPLACEMENT AS A FUNCTION OF CENTRIFUGAL LOAD
LOGARITHMIC DECREMENT
0.060
0.050
0.040
0.030
0.020
0.010
0
0 1 2 3 4 5 6 7 8 9 10
BLADE TIP DISPLACEMENT (IN x 10+4)
CENTRIFUGAL LOAD (LBS)
2700 ±250
4200 ±250
4700 ±250

FIGURE 6.41

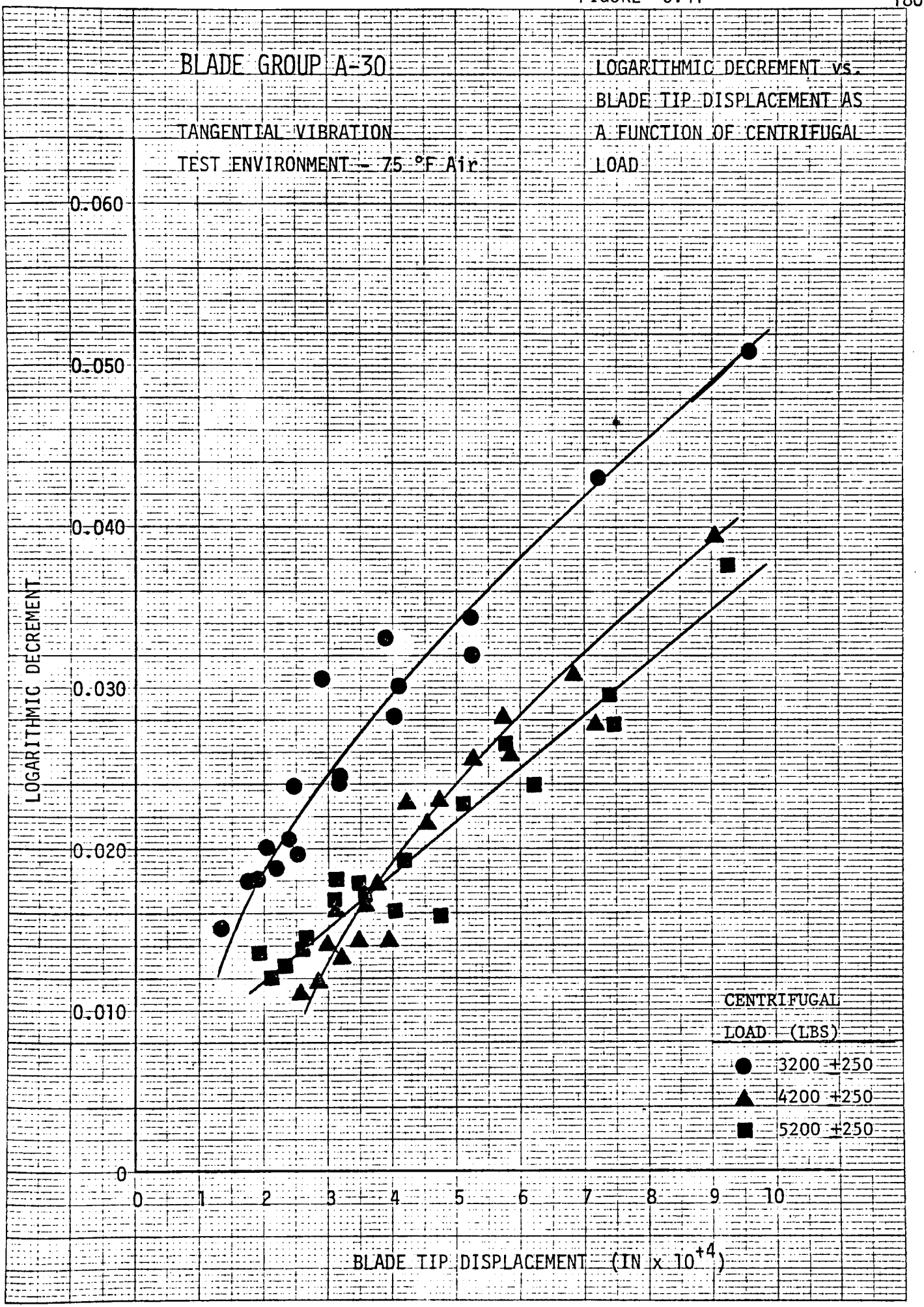
BLADE GROUP A-30
TANGENTIAL VIBRATION
TEST ENVIRONMENT – 75 °F Air
LOGARITHMIC DECREMENT vs. BLADE TIP DISPLACEMENT AS A FUNCTION OF CENTRIFUGAL LOAD
0.060
0.050
0.040
0.030
0.020
0.010
0
LOGARITHMIC DECREMENT
0
1
2
3
4
5
6
7
8
9
10
BLADE TIP DISPLACEMENT (IN x 10+4)
CENTRIFUGAL LOAD (LBS)
3200 ±250
4200 ±250
5200 ±250

FIGURE 6.42

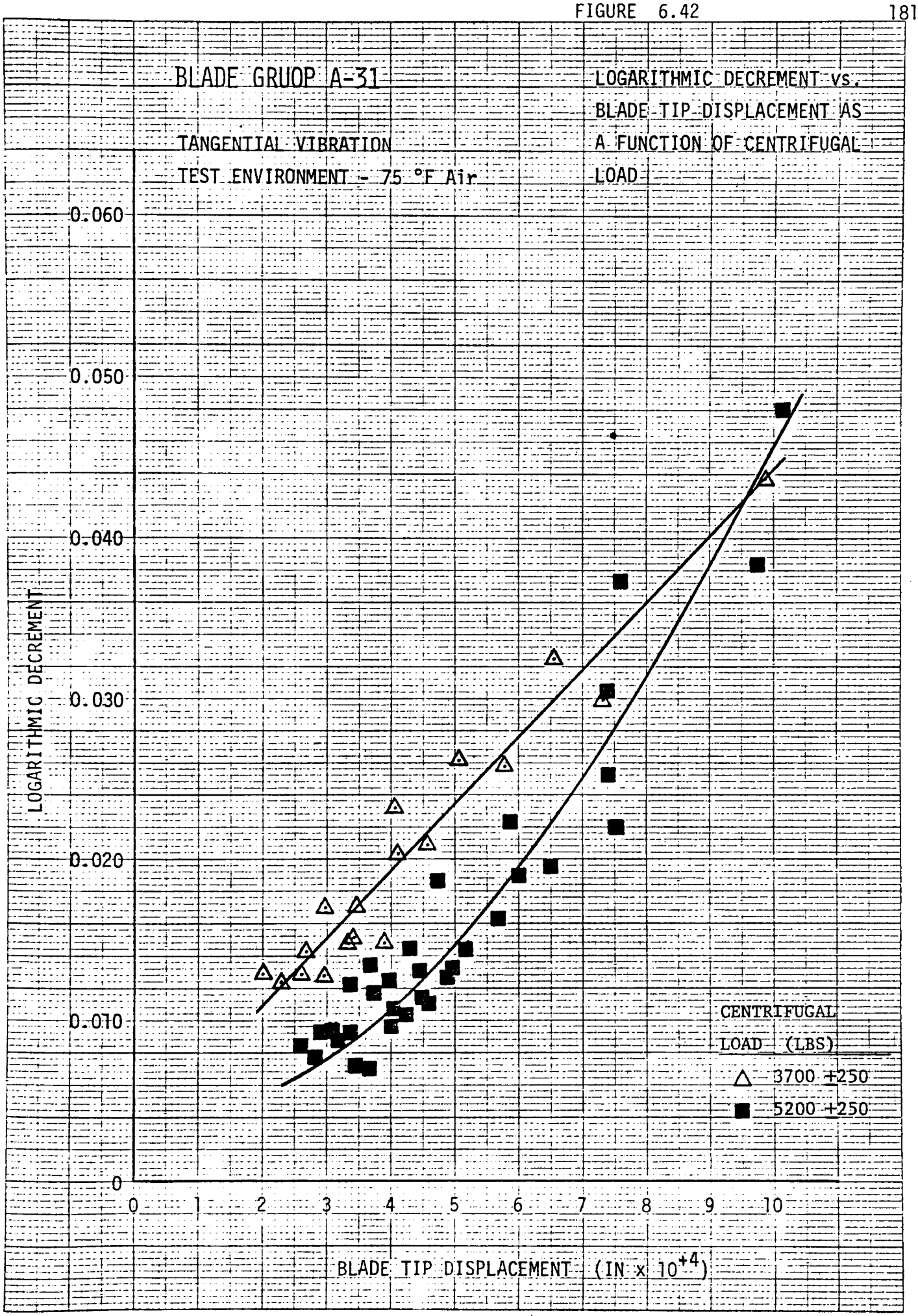
BLADE GRUOP A-31
TANGENTIAL VIBRATION
TEST ENVIRONMENT - 75 °F Air
LOGARITHMIC DECREMENT vs. BLADE TIP DISPLACEMENT AS A FUNCTION OF CENTRIFUGAL LOAD
0.060
0.050
0.040
0.030
0.020
0.010
0
LOGARITHMIC DECREMENT
0 1 2 3 4 5 6 7 8 9 10
BLADE TIP DISPLACEMENT (IN x 10+4)
CENTRIFUGAL LOAD (LBS)
3700 ±250
5200 ±250

FIGURE 6.43

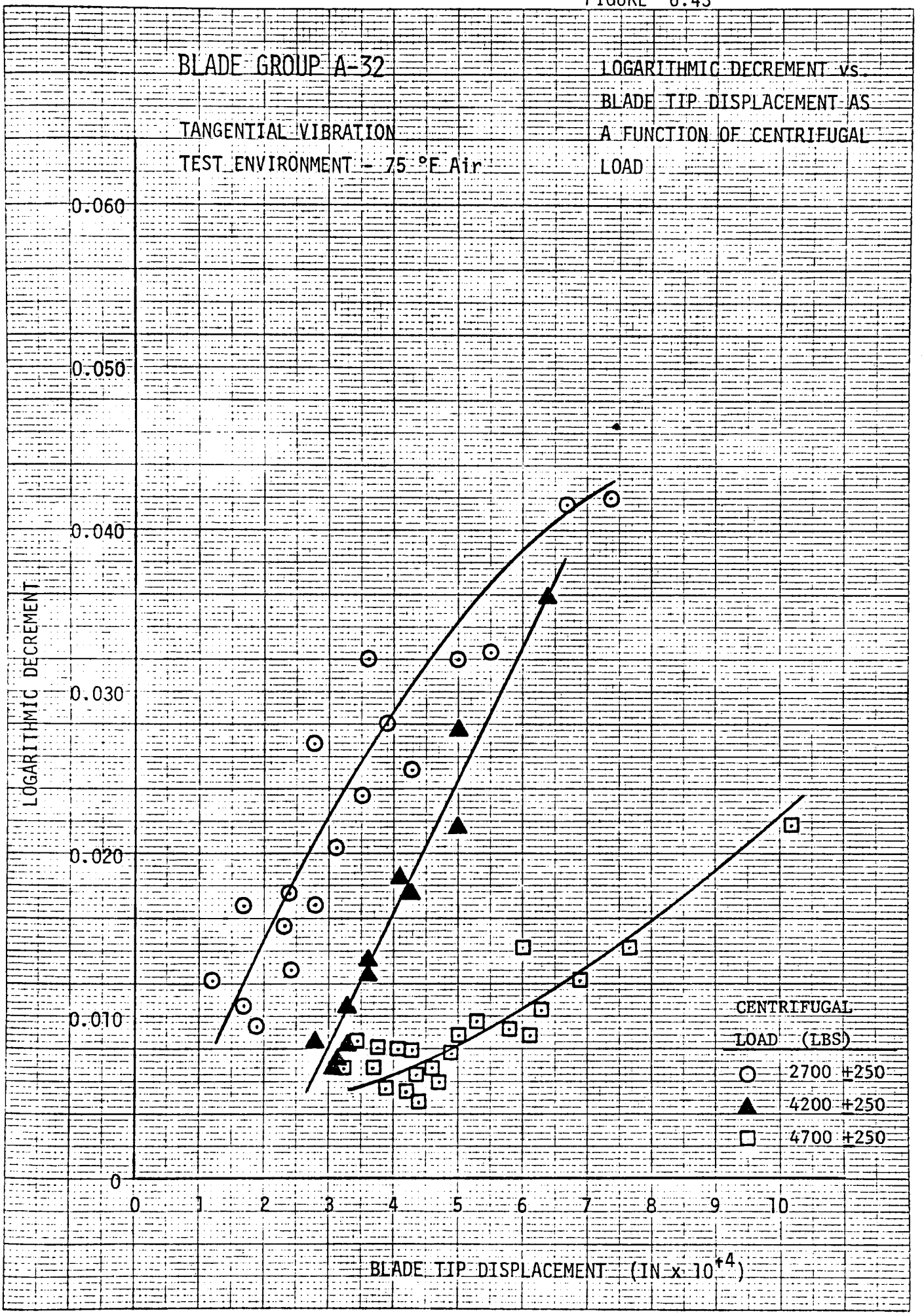
BLADE GROUP A-32
TANGENTIAL VIBRATION
TEST ENVIRONMENT - 75 °F Air
LOGARITHMIC DECREMENT vs. BLADE TIP DISPLACEMENT AS A FUNCTION OF CENTRIFUGAL LOAD
0.060
0.050
0.040
0.030
0.020
0.010
0
LOGARITHMIC DECREMENT
0
1
2
3
4
5
6
7
8
9
10
BLADE TIP DISPLACEMENT (IN x 10^+4)
CENTRIFUGAL LOAD (LBS)
2700 ±250
4200 ±250
4700 ±250

FIGURE 6.44

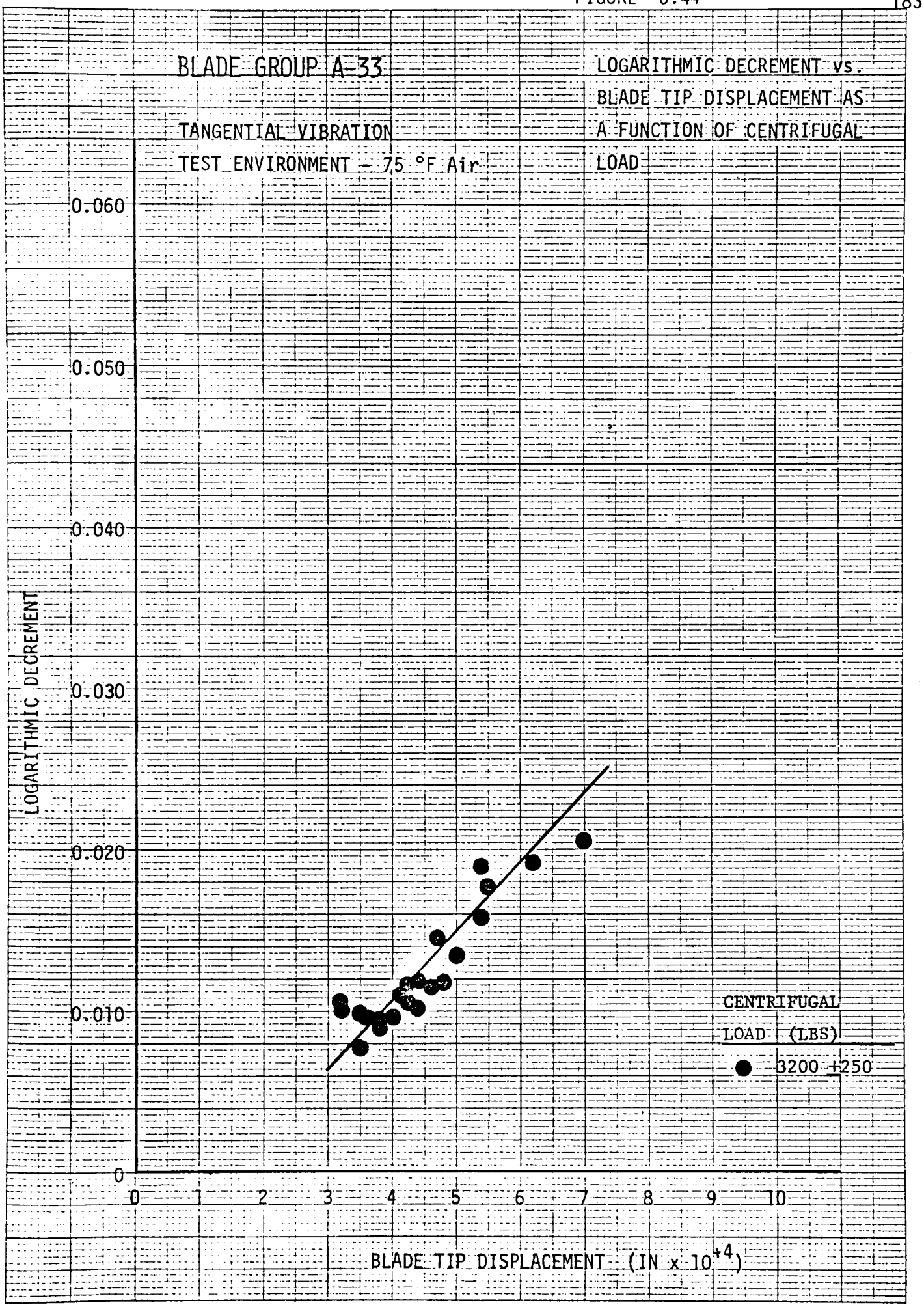

Squares to th

FIGURE 6.45

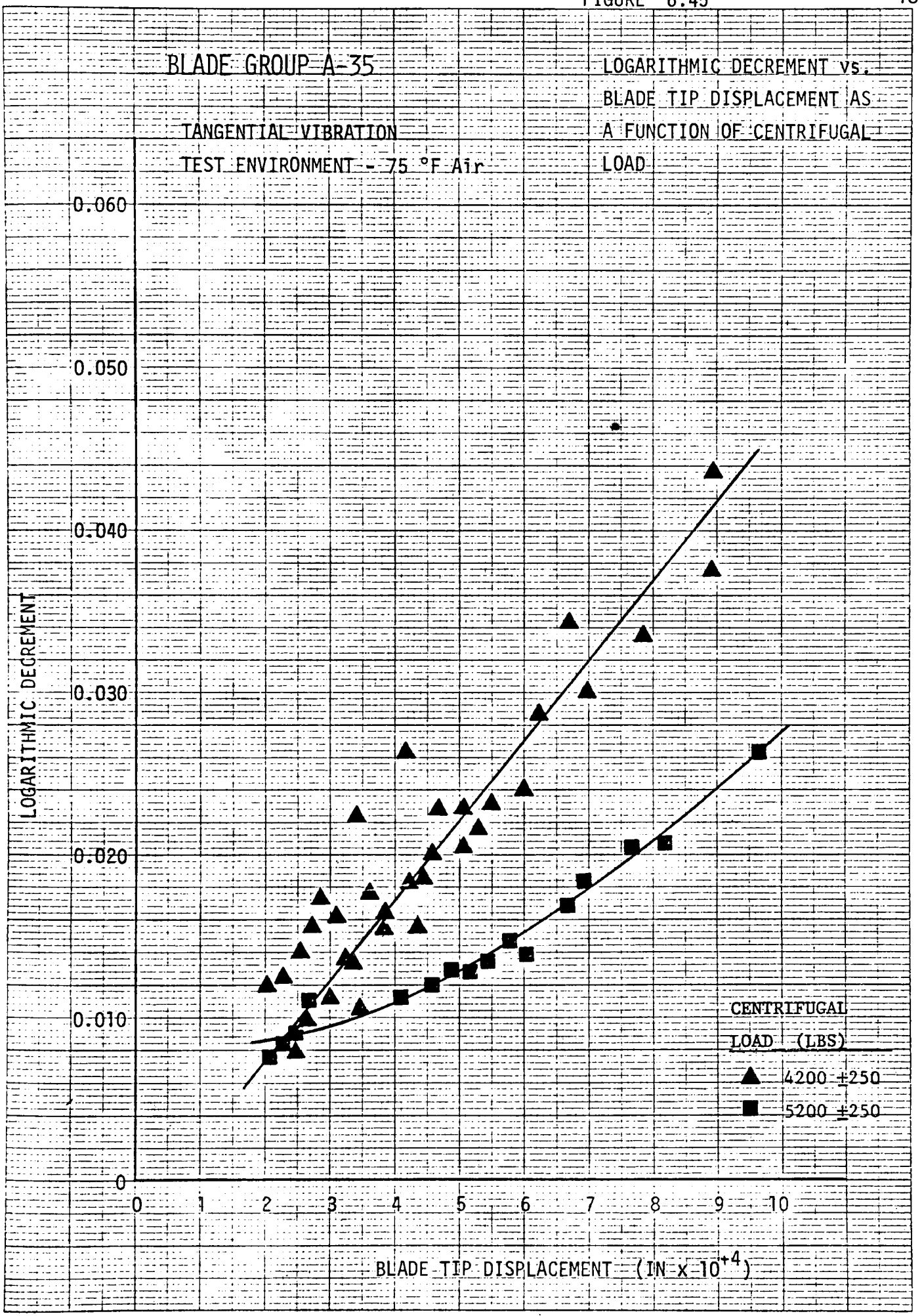
BLADE GROUP A-35
TANGENTIAL VIBRATION
TEST ENVIRONMENT - 75 °F Air
LOGARITHMIC DECREMENT vs. BLADE TIP DISPLACEMENT AS A FUNCTION OF CENTRIFUGAL LOAD
0.060
0.050
0.040
0.030
0.020
0.010
0
LOGARITHMIC DECREMENT
0
1
2
3
4
5
6
7
8
9
10
BLADE TIP DISPLACEMENT (IN x 10+4)
CENTRIFUGAL LOAD (LBS)
4200 ±250
5200 ±250

FIGURE 6.46

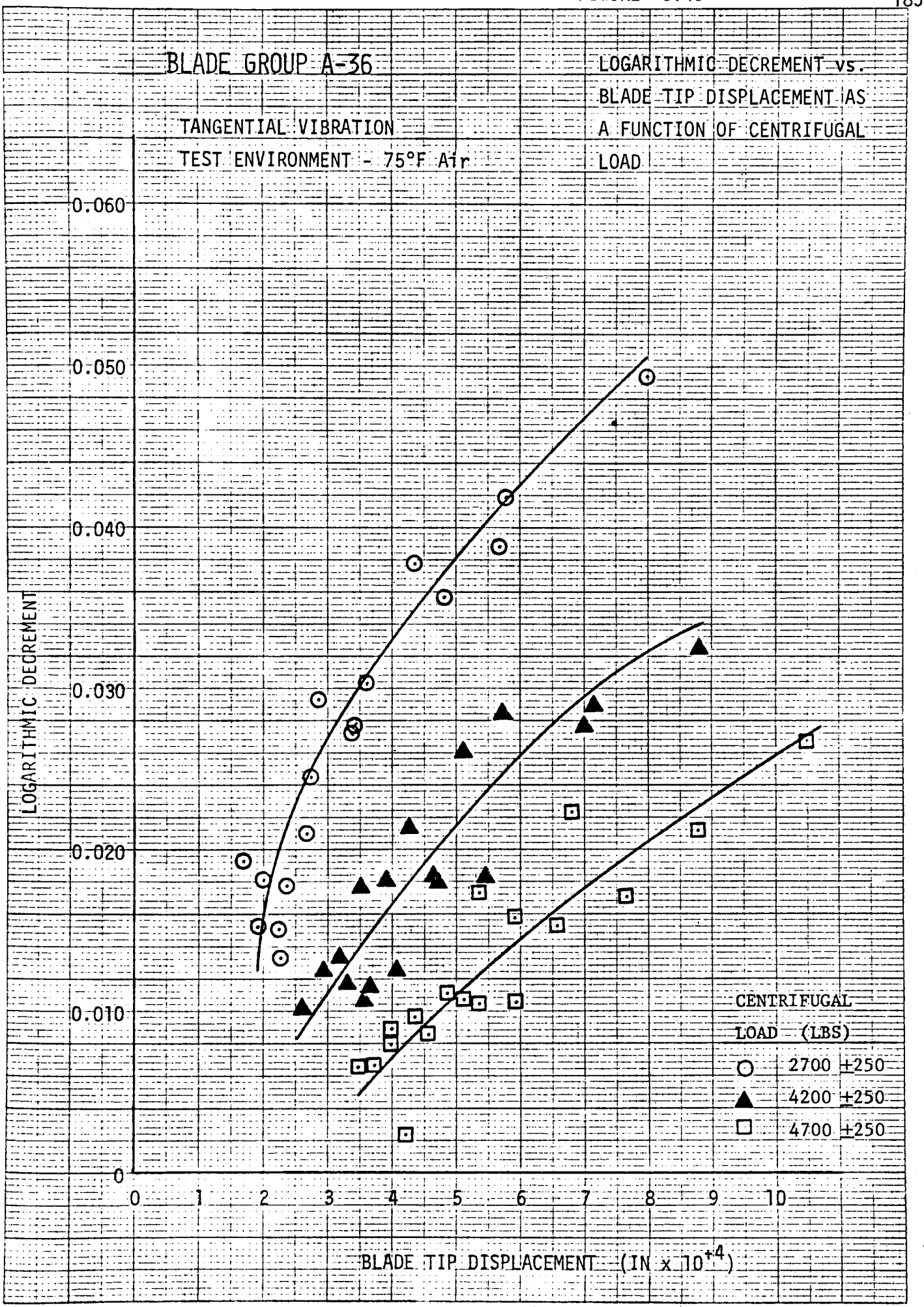
BLADE GROUP A-36
TANGENTIAL VIBRATION
TEST ENVIRONMENT - 75°F Air
LOGARITHMIC DECREMENT vs. BLADE TIP DISPLACEMENT AS A FUNCTION OF CENTRIFUGAL LOAD
LOGARITHMIC DECREMENT
0.060
0.050
0.040
0.030
0.020
0.010
0
0 1 2 3 4 5 6 7 8 9 10
BLADE TIP DISPLACEMENT (IN x 10+4)
CENTRIFUGAL LOAD (LBS)
2700 ±250
4200 ±250
4700 ±250

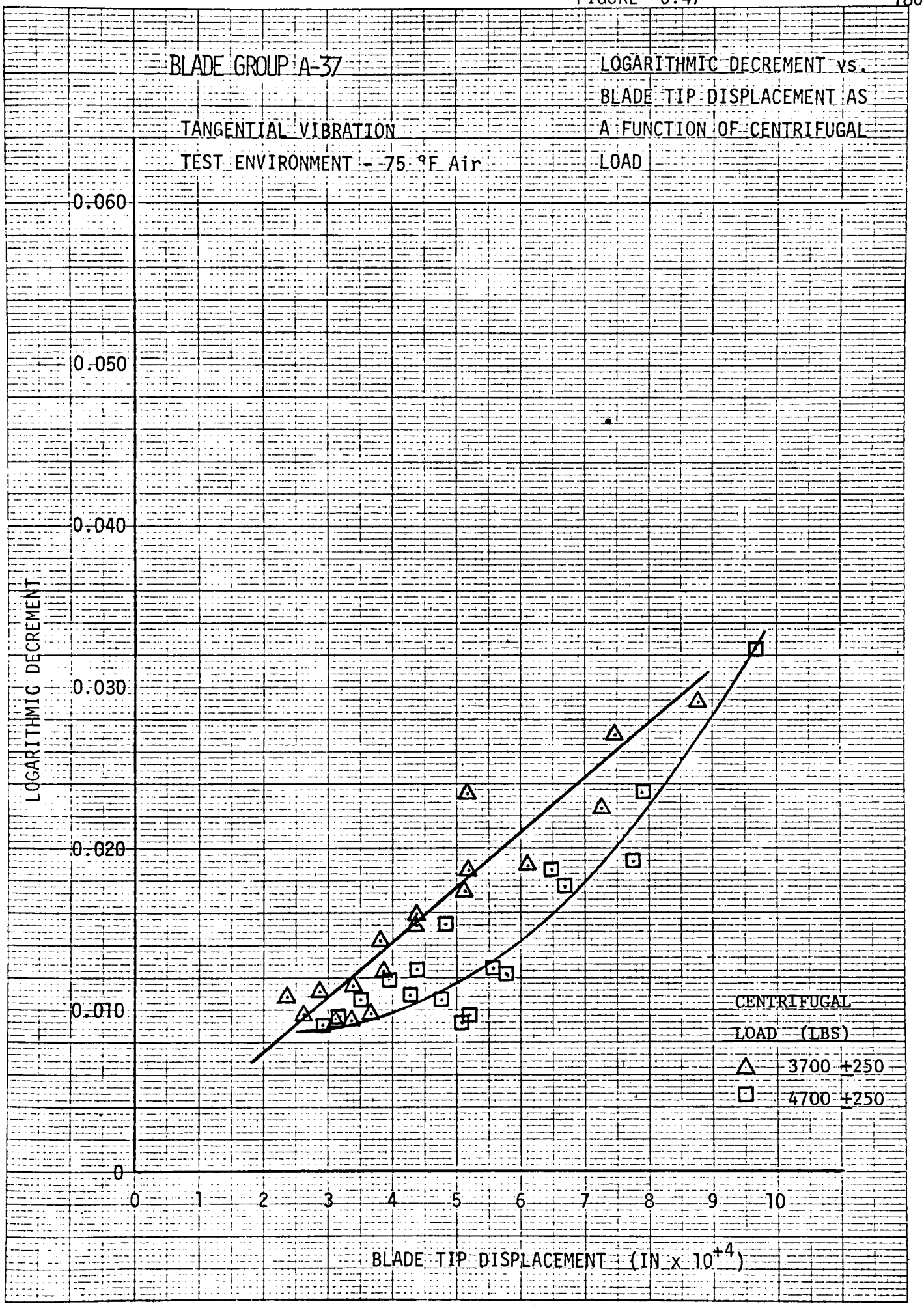
BLADE GROUP A-37
TANGENTIAL VIBRATION
TEST ENVIRONMENT - 75 °F Air
LOGARITHMIC DECREMENT vs. BLADE TIP DISPLACEMENT AS A FUNCTION OF CENTRIFUGAL LOAD
0.060
0.050
0.040
0.030
0.020
0.010
0
LOGARITHMIC DECREMENT
0 1 2 3 4 5 6 7 8 9 10
BLADE TIP DISPLACEMENT (IN x 10+4)
CENTRIFUGAL LOAD (LBS)
3700 ±250
4700 ±250

FIGURE 6.48

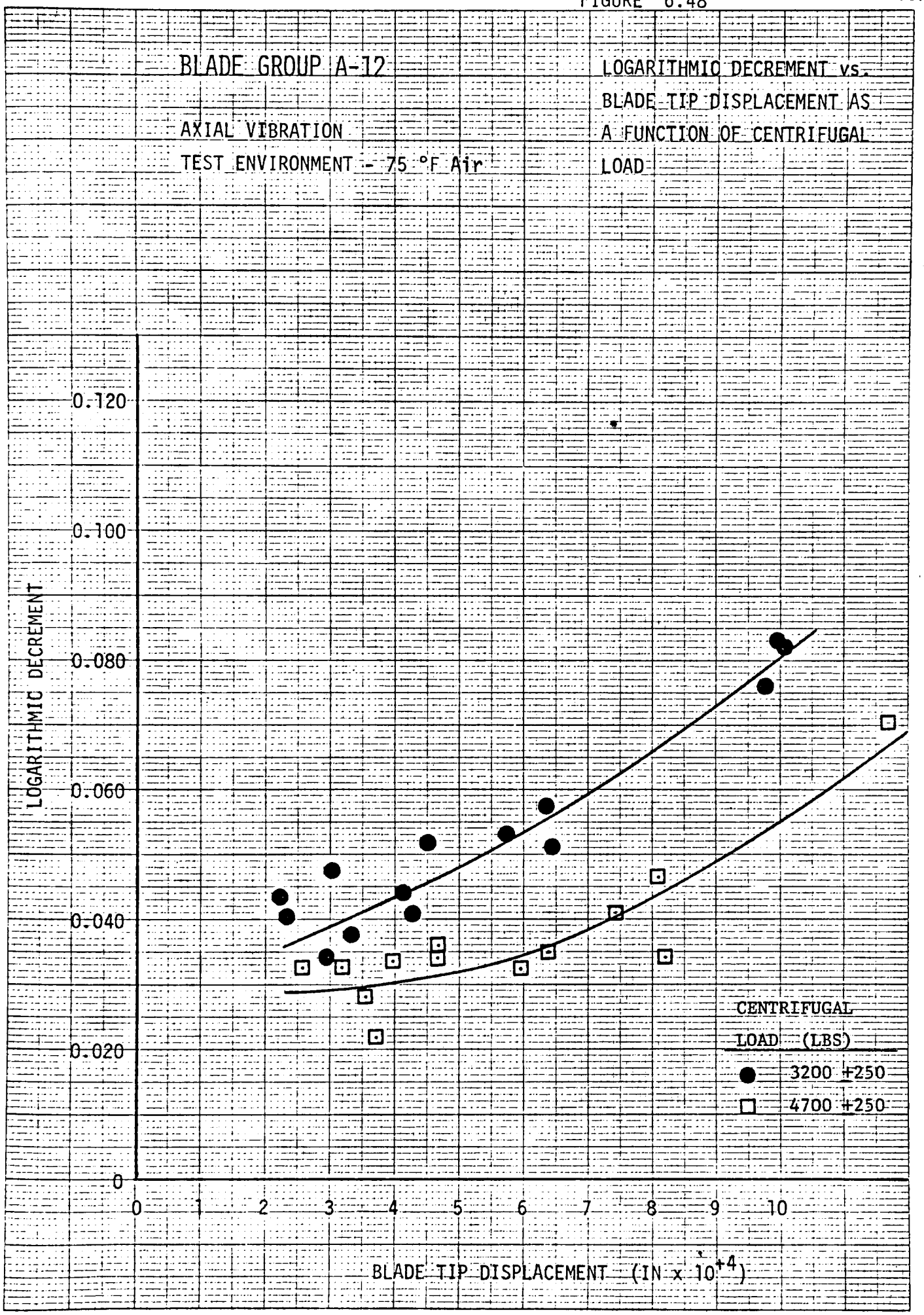
BLADE GROUP A-12
AXIAL VIBRATION
TEST ENVIRONMENT - 75 °F Air
LOGARITHMIC DECREMENT vs. BLADE TIP DISPLACEMENT AS A FUNCTION OF CENTRIFUGAL LOAD
LOGARITHMIC DECREMENT
0.120
0.100
0.080
0.060
0.040
0.020
0
0 1 2 3 4 5 6 7 8 9 10
BLADE TIP DISPLACEMENT (IN x 10+4)
CENTRIFUGAL LOAD (LBS)
3200 ±250
4700 ±250

FIGURE 6.49

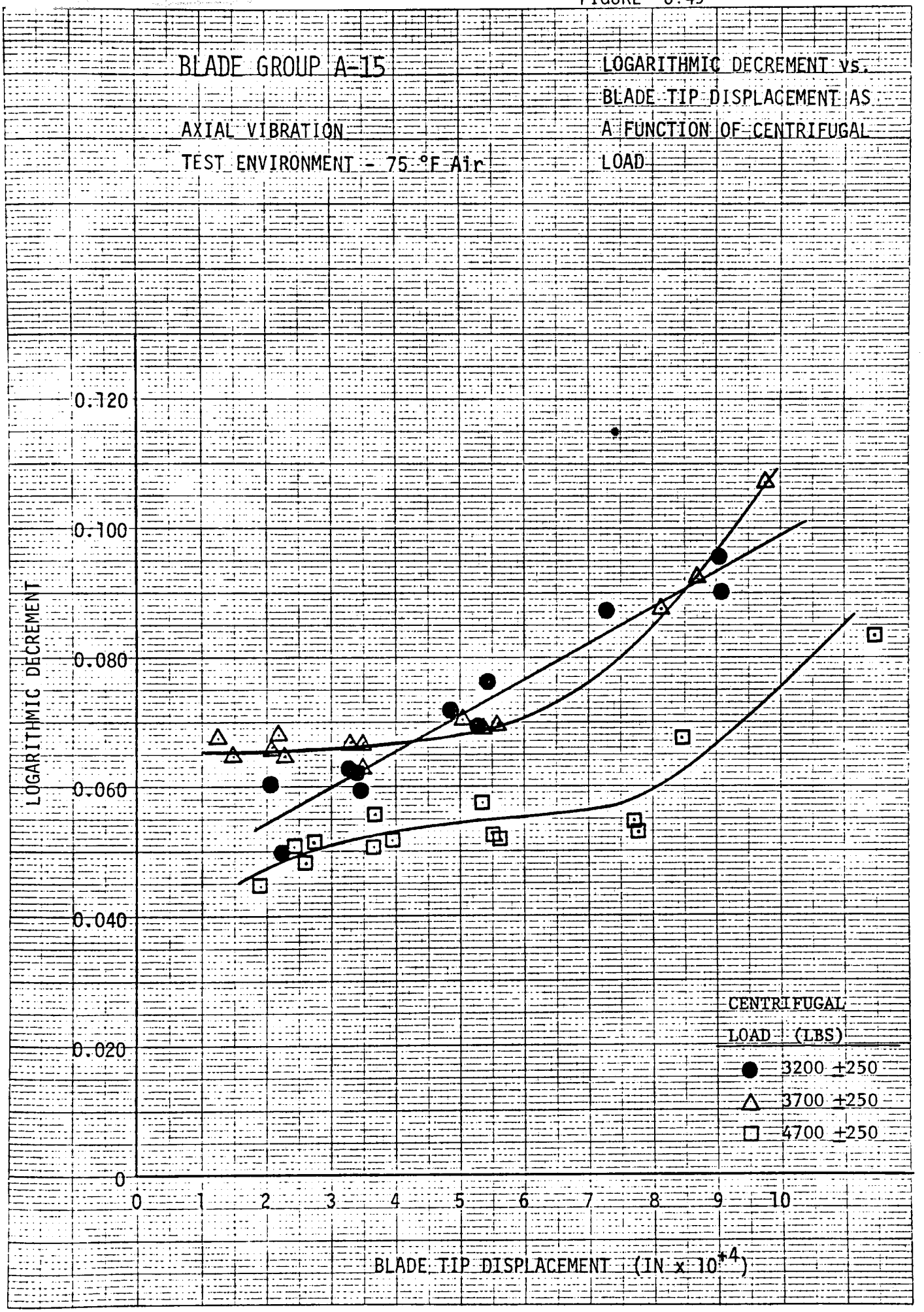

squares to th

FIGURE 6.50

BLADE GROUP A-18

AXIAL VIBRATION

TEST ENVIRONMENT - 75 °F Air

LOGARITHMIC DECREMENT vs. BLADE TIP DISPLACEMENT AS A FUNCTION OF CENTRIFUGAL LOAD

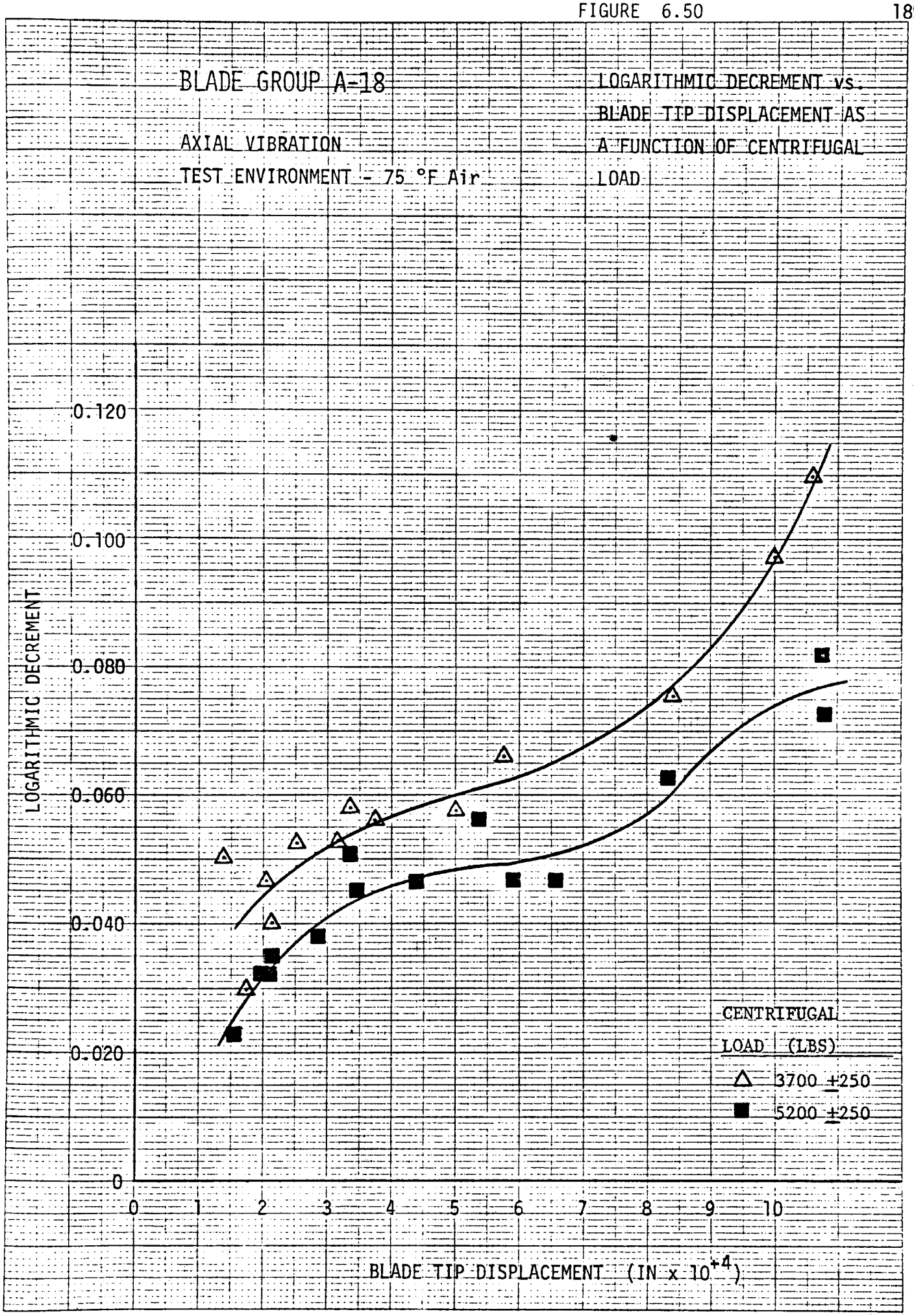

FIGURE 6.51

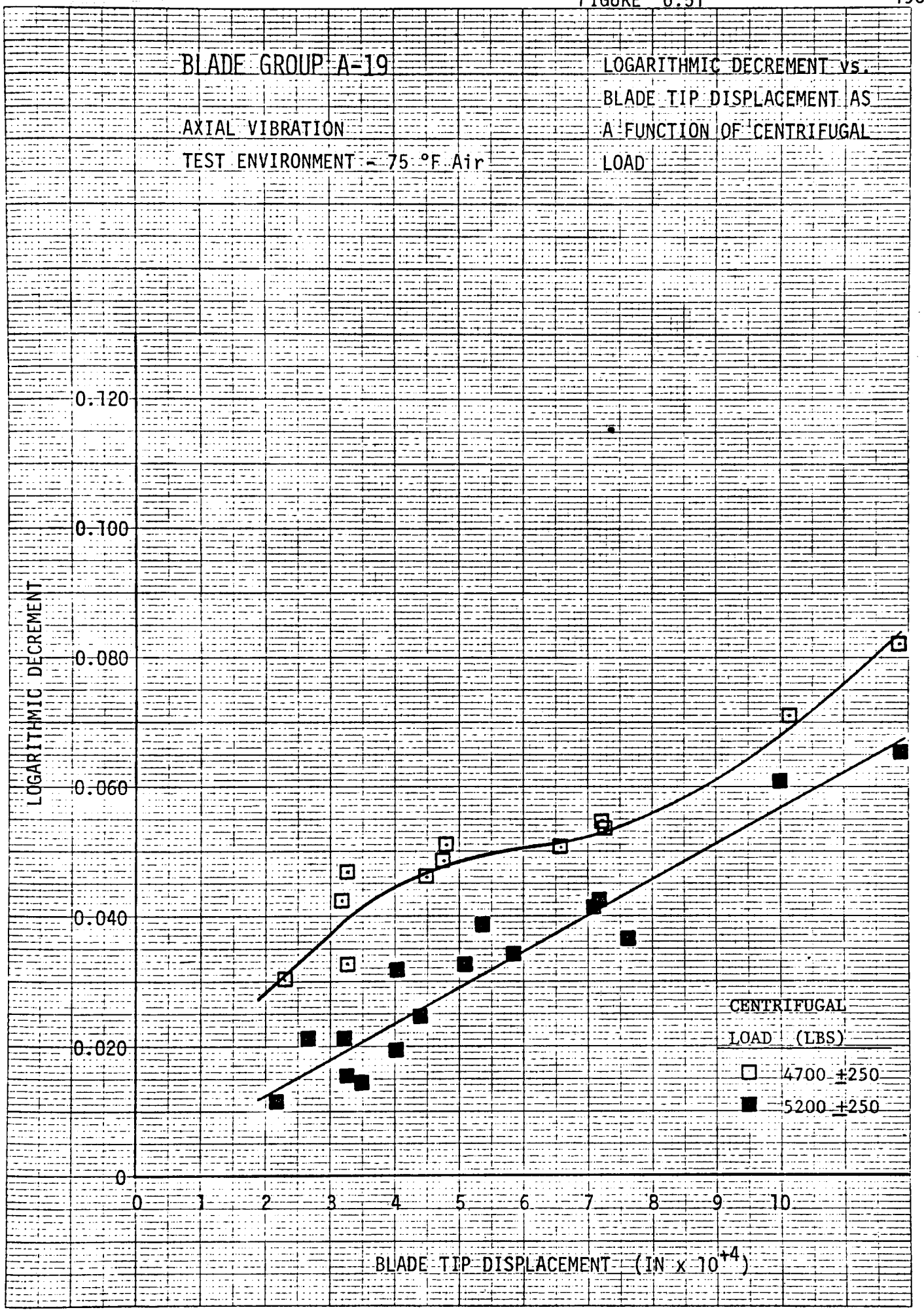
BLADE GROUP A-19
AXIAL VIBRATION
TEST ENVIRONMENT - 75 °F Air
LOGARITHMIC DECREMENT vs. BLADE TIP DISPLACEMENT AS A FUNCTION OF CENTRIFUGAL LOAD
LOGARITHMIC DECREMENT
0.120
0.100
0.080
0.060
0.040
0.020
0
0
1
2
3
4
5
6
7
8
9
10
BLADE TIP DISPLACEMENT (IN x 10+4)
CENTRIFUGAL LOAD (LBS)
4700 ±250
5200 ±250

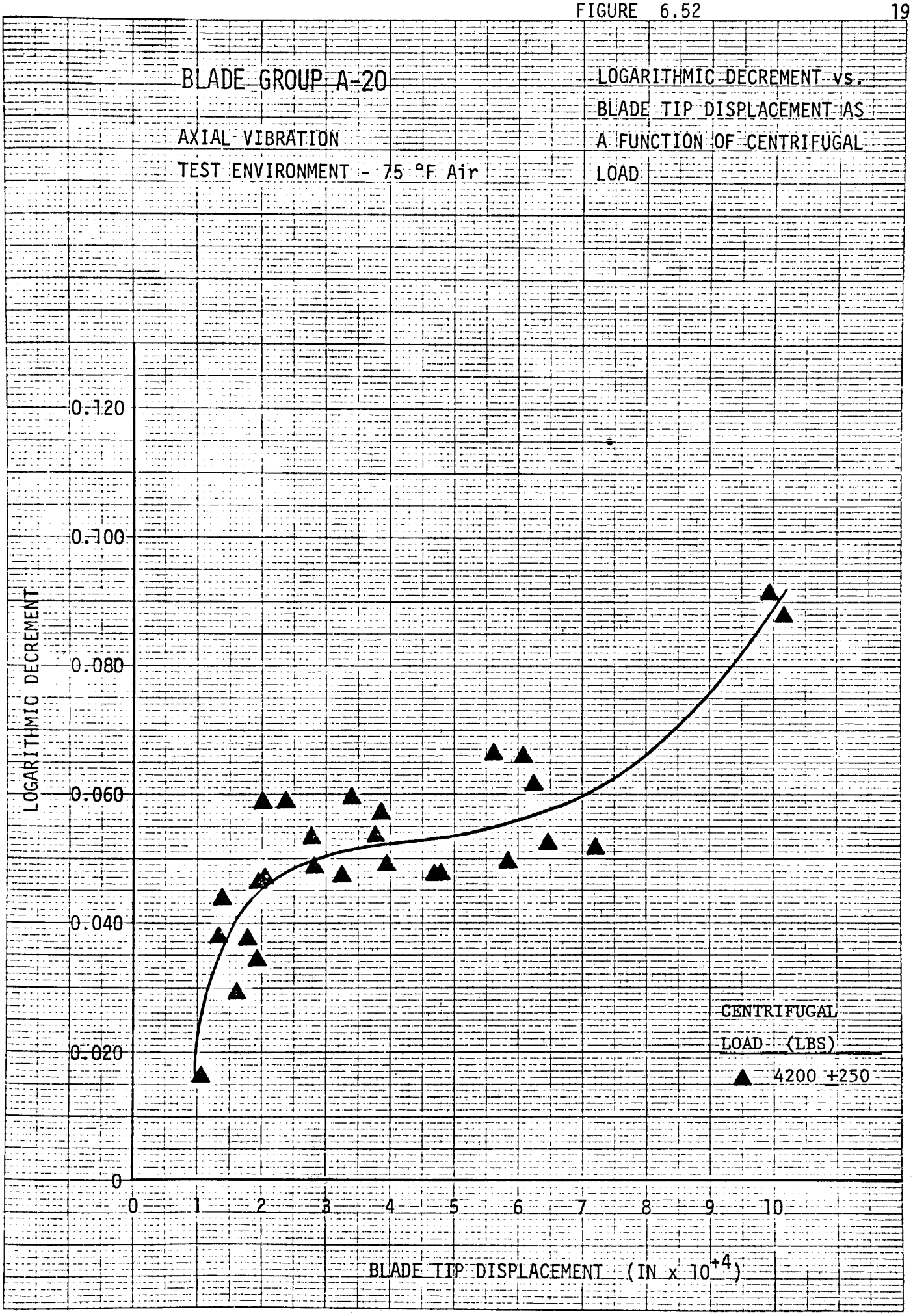
BLADE GROUP A-20
AXIAL VIBRATION
TEST ENVIRONMENT - 75 °F Air
LOGARITHMIC DECREMENT vs. BLADE TIP DISPLACEMENT AS A FUNCTION OF CENTRIFUGAL LOAD
LOGARITHMIC DECREMENT
0.120
0.100
0.080
0.060
0.040
0.020
0
0 1 2 3 4 5 6 7 8 9 10
BLADE TIP DISPLACEMENT (IN x 10+4)
CENTRIFUGAL LOAD (LBS)
4200 ±250

FIGURE 6.53

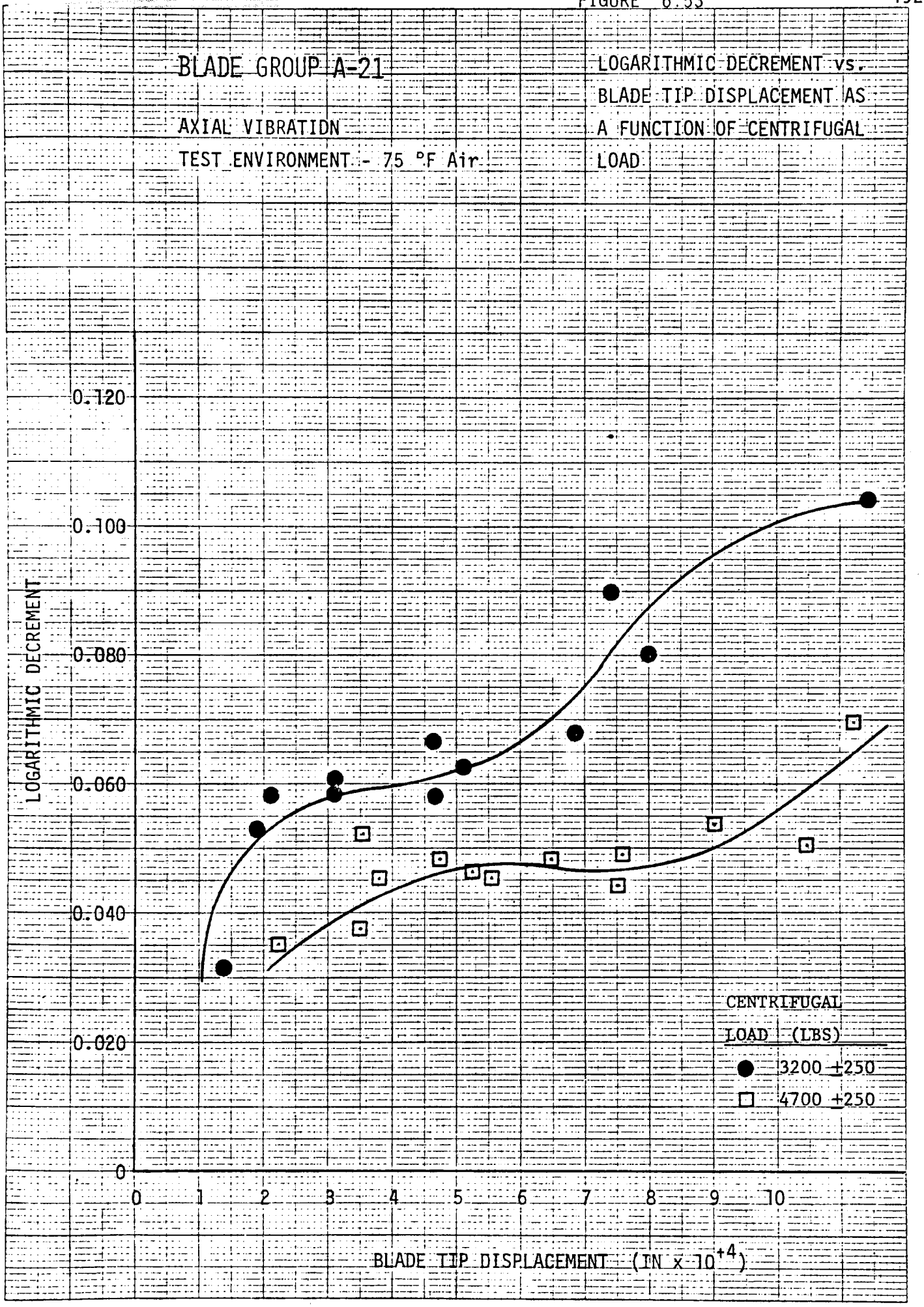
BLADE GROUP A-21
AXIAL VIBRATION
TEST ENVIRONMENT - 75 °F Air
LOGARITHMIC DECREMENT vs. BLADE TIP DISPLACEMENT AS A FUNCTION OF CENTRIFUGAL LOAD
LOGARITHMIC DECREMENT
0.120
0.100
0.080
0.060
0.040
0.020
0
0 1 2 3 4 5 6 7 8 9 10
BLADE TIP DISPLACEMENT (IN x 10+4)
CENTRIFUGAL LOAD (LBS)
3200 ±250
4700 ±250

FIGURE 6.54

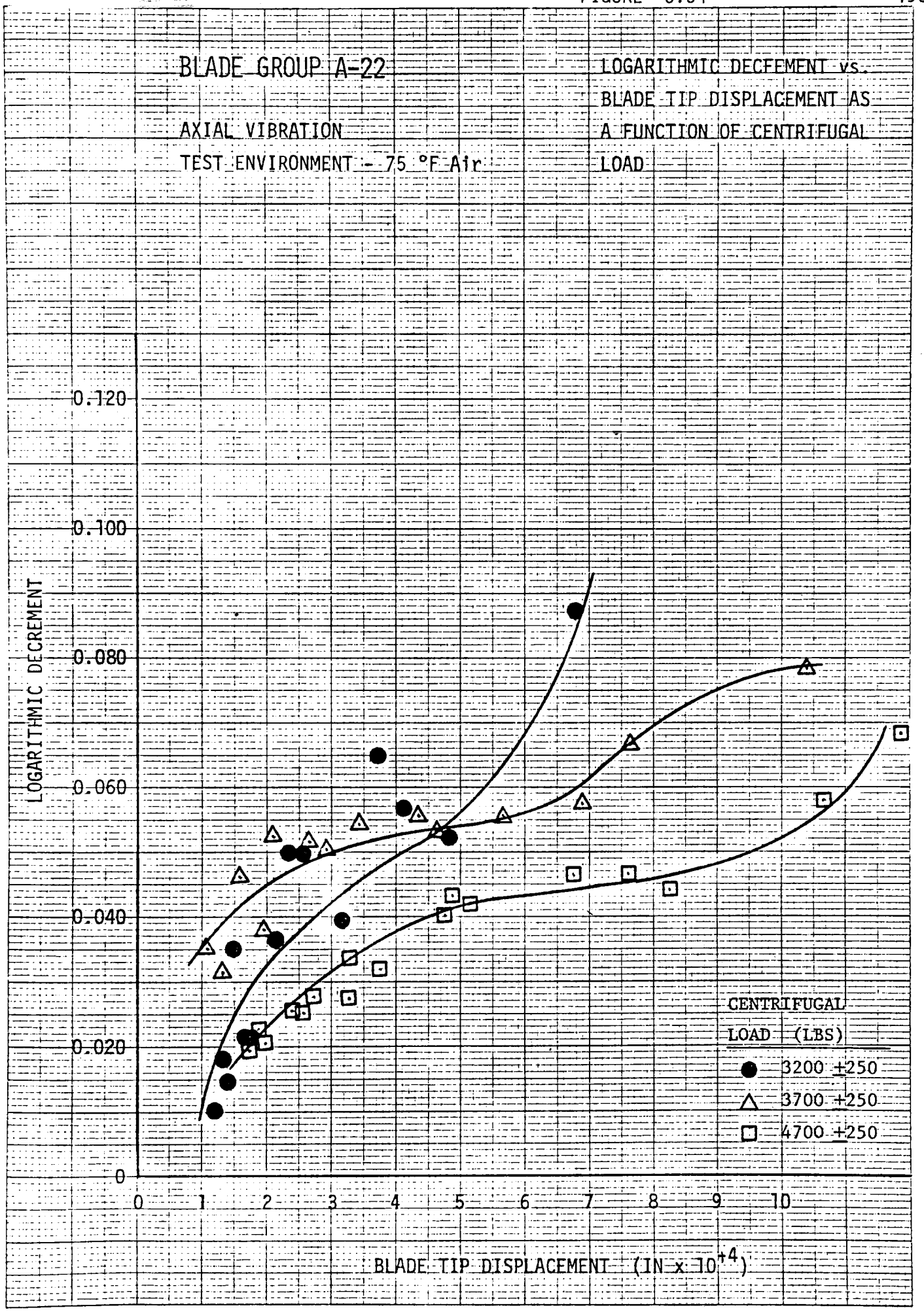
BLADE GROUP A-22
AXIAL VIBRATION
TEST ENVIRONMENT - 75 °F Air
LOGARITHMIC DECFEMENT vs. BLADE TIP DISPLACEMENT AS A FUNCTION OF CENTRIFUGAL LOAD
LOGARITHMIC DECREMENT
0.120
0.100
0.080
0.060
0.040
0.020
0
0 1 2 3 4 5 6 7 8 9 10
BLADE TIP DISPLACEMENT (IN x 10+4)
CENTRIFUGAL LOAD (LBS)
3200 ±250
3700 ±250
4700 ±250

FIGURE 6.55

BLADE GROUP A-24

AXIAL VIBRATION

TEST ENVITONMENT - 75 °F Air

LOGARITHMIC DECREMENT vs. BLADE TIP DISPLACEMENT AS A FUNCTION OF CENTRIFUGAL LOAD

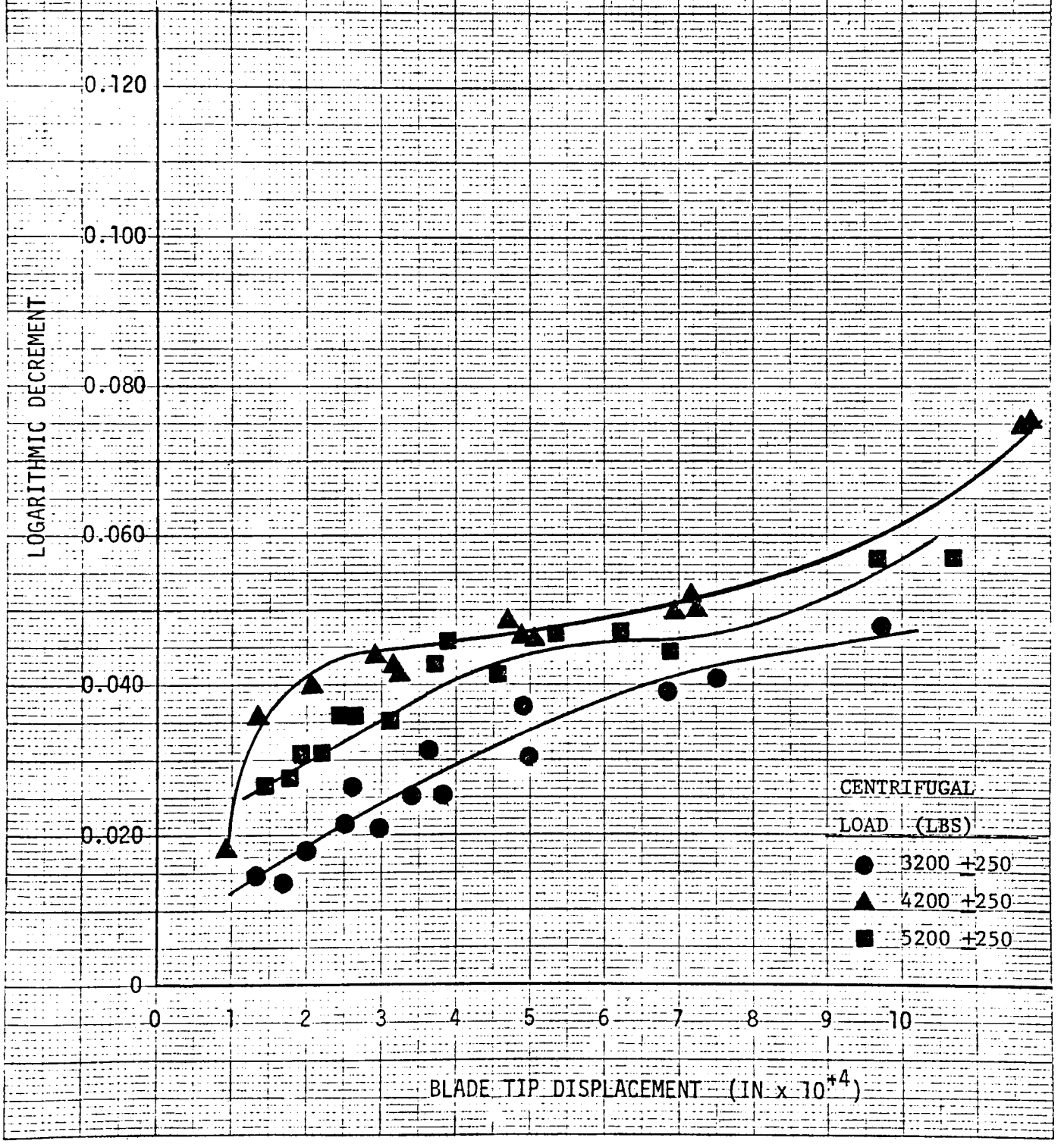

BLADE GROUP A-25

AXIAL VIBRATION

TEST ENVIRONMENT - 75 °F Air

LOGARITHMIC DECREMENT vs. BLADE TIP DISPLACEMENT AS A FUNCTION OF CENTRIFUGAL LOAD

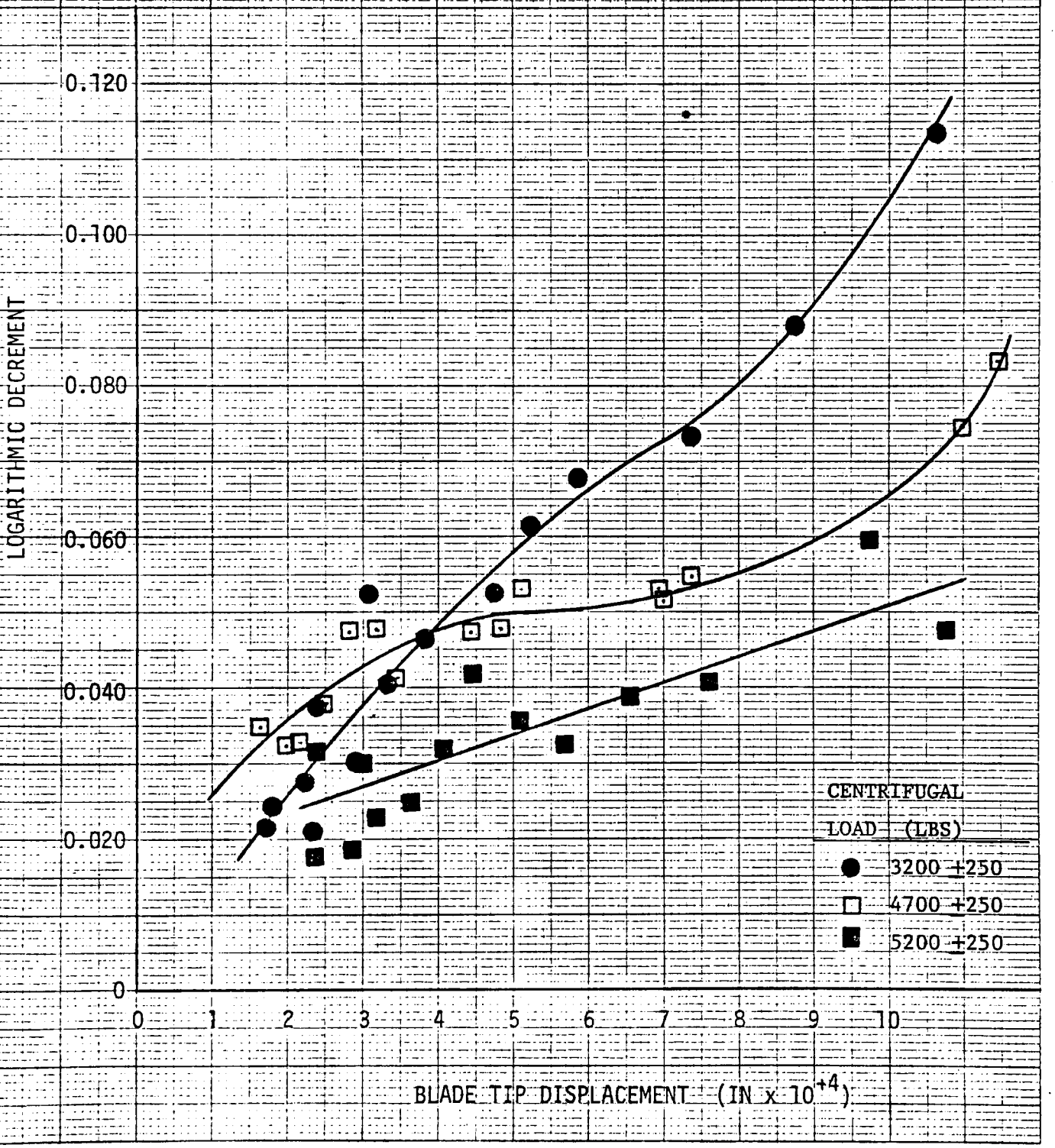

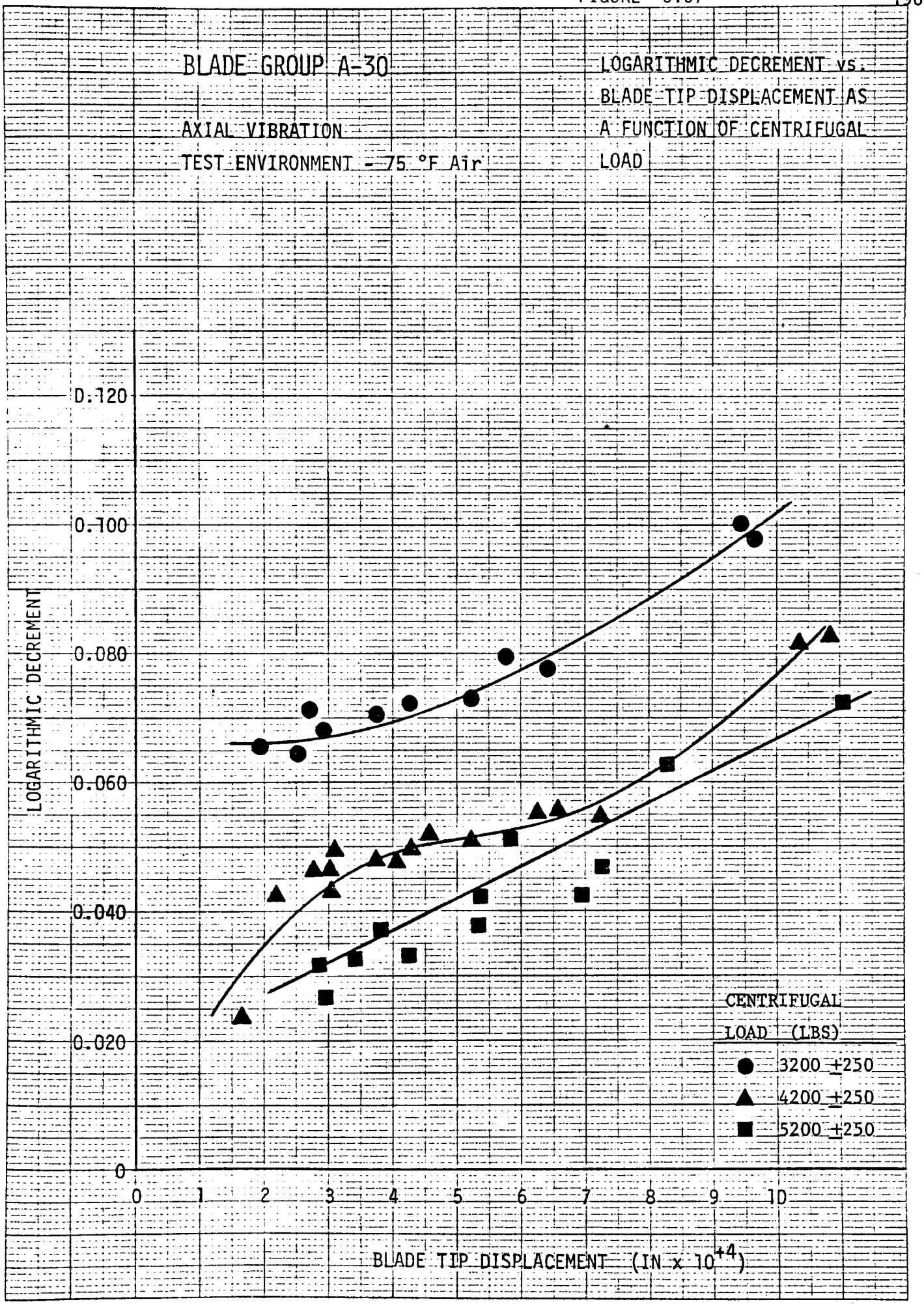
BLADE GROUP A-30
AXIAL VIBRATION
TEST ENVIRONMENT - 75 °F Air
LOGARITHMIC DECREMENT vs. BLADE TIP DISPLACEMENT AS A FUNCTION OF CENTRIFUGAL LOAD
LOGARITHMIC DECREMENT
0.120
0.100
0.080
0.060
0.040
0.020
0
0 1 2 3 4 5 6 7 8 9 10
BLADE TIP DISPLACEMENT (IN x 10+4)
CENTRIFUGAL LOAD (LBS)
3200 ±250
4200 ±250
5200 ±250

FIGURE 6.58

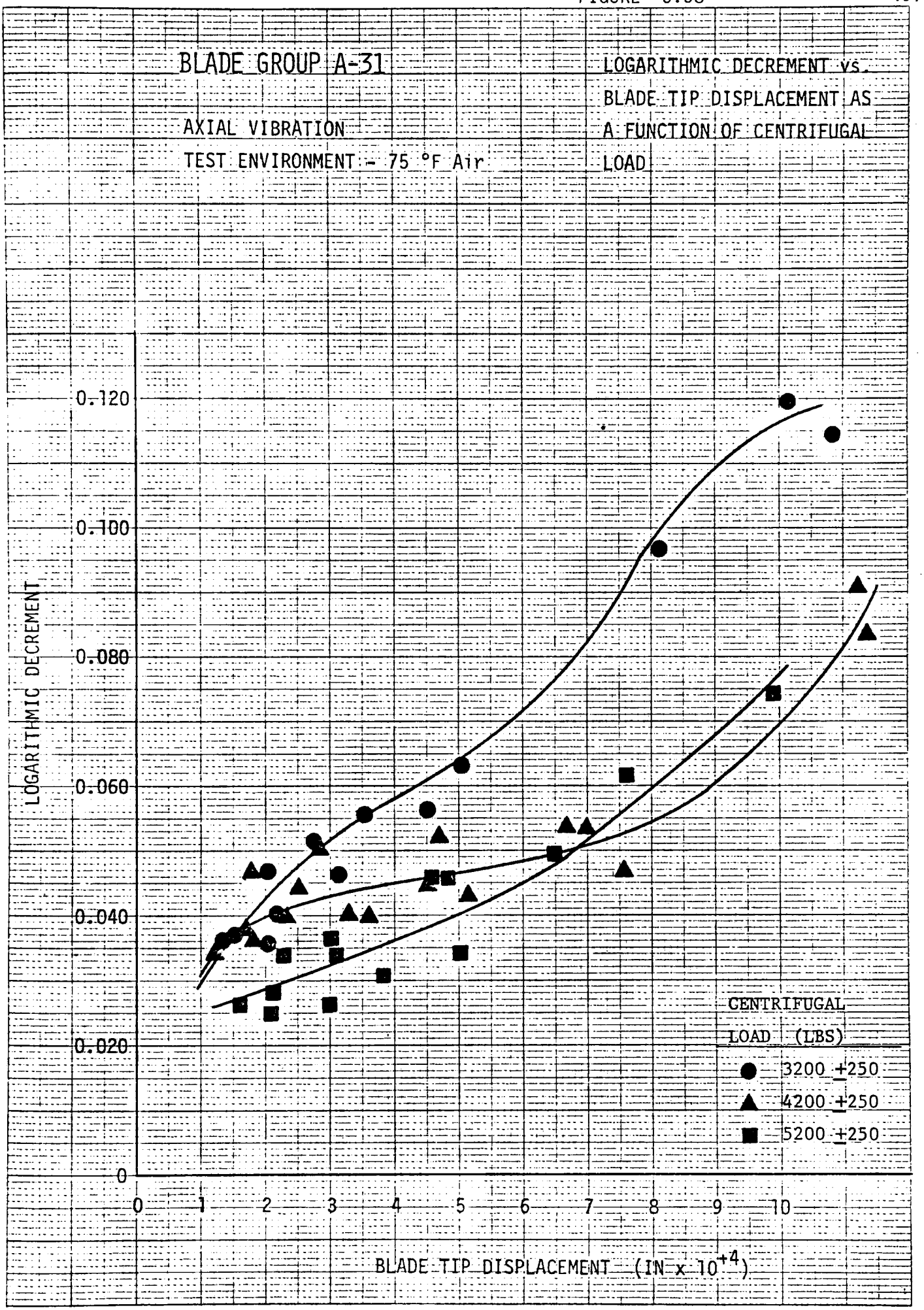
BLADE GROUP A-31
AXIAL VIBRATION
TEST ENVIRONMENT - 75 °F Air
LOGARITHMIC DECREMENT vs. BLADE TIP DISPLACEMENT AS A FUNCTION OF CENTRIFUGAL LOAD
LOGARITHMIC DECREMENT
0.120
0.100
0.080
0.060
0.040
0.020
0
0
1
2
3
4
5
6
7
8
9
10
BLADE TIP DISPLACEMENT (IN x 10^{+4})
CENTRIFUGAL LOAD (LBS)
3200 ±250
4200 ±250
5200 ±250

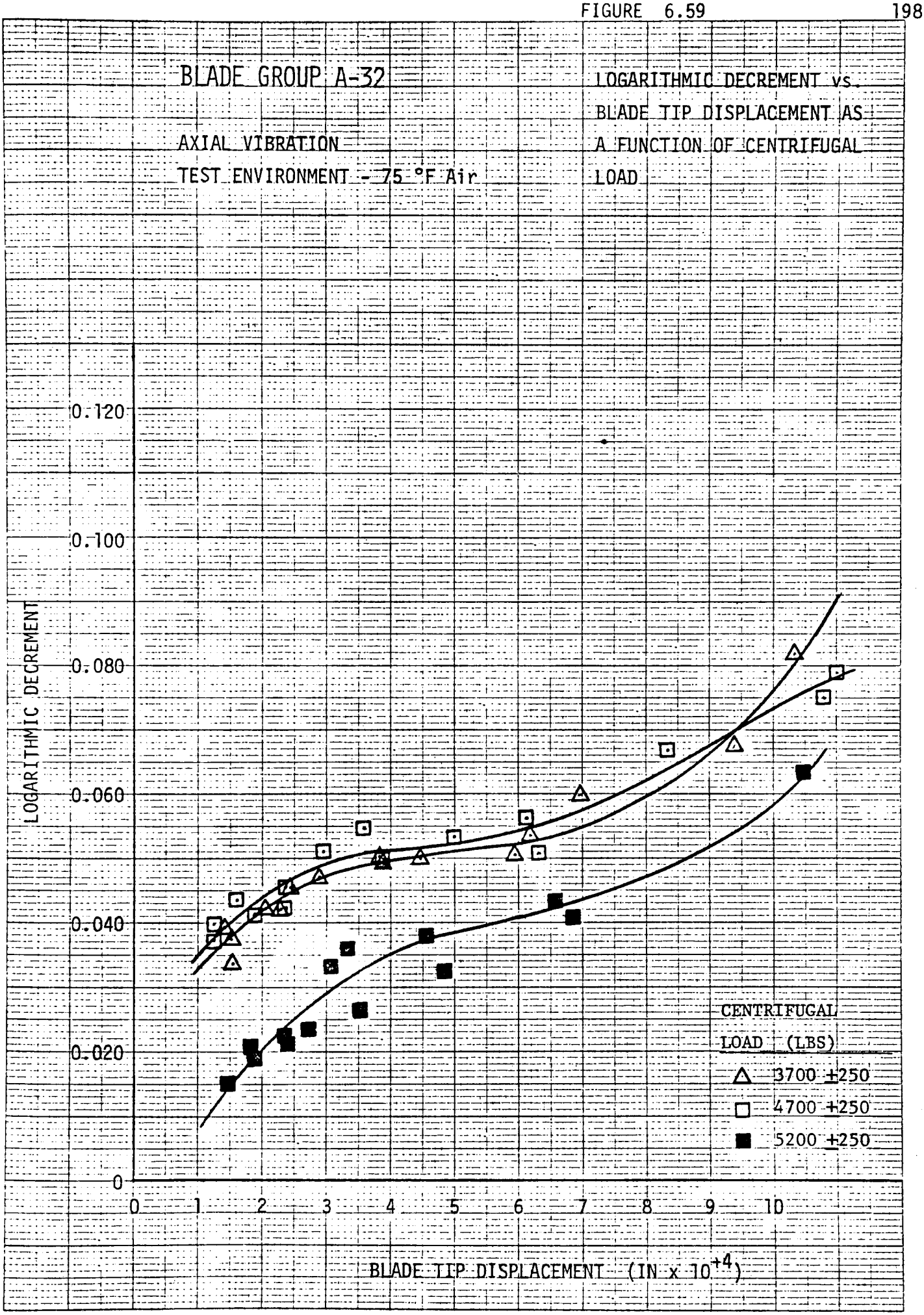
BLADE GROUP A-32
AXIAL VIBRATION
TEST ENVIRONMENT - 75 °F Air
LOGARITHMIC DECREMENT vs. BLADE TIP DISPLACEMENT AS A FUNCTION OF CENTRIFUGAL LOAD
LOGARITHMIC DECREMENT
0.120
0.100
0.080
0.060
0.040
0.020
0
0 1 2 3 4 5 6 7 8 9 10
BLADE TIP DISPLACEMENT (IN x 10+4)
CENTRIFUGAL LOAD (LBS)
3700 ±250
4700 ±250
5200 ±250

FIGURE 6.60

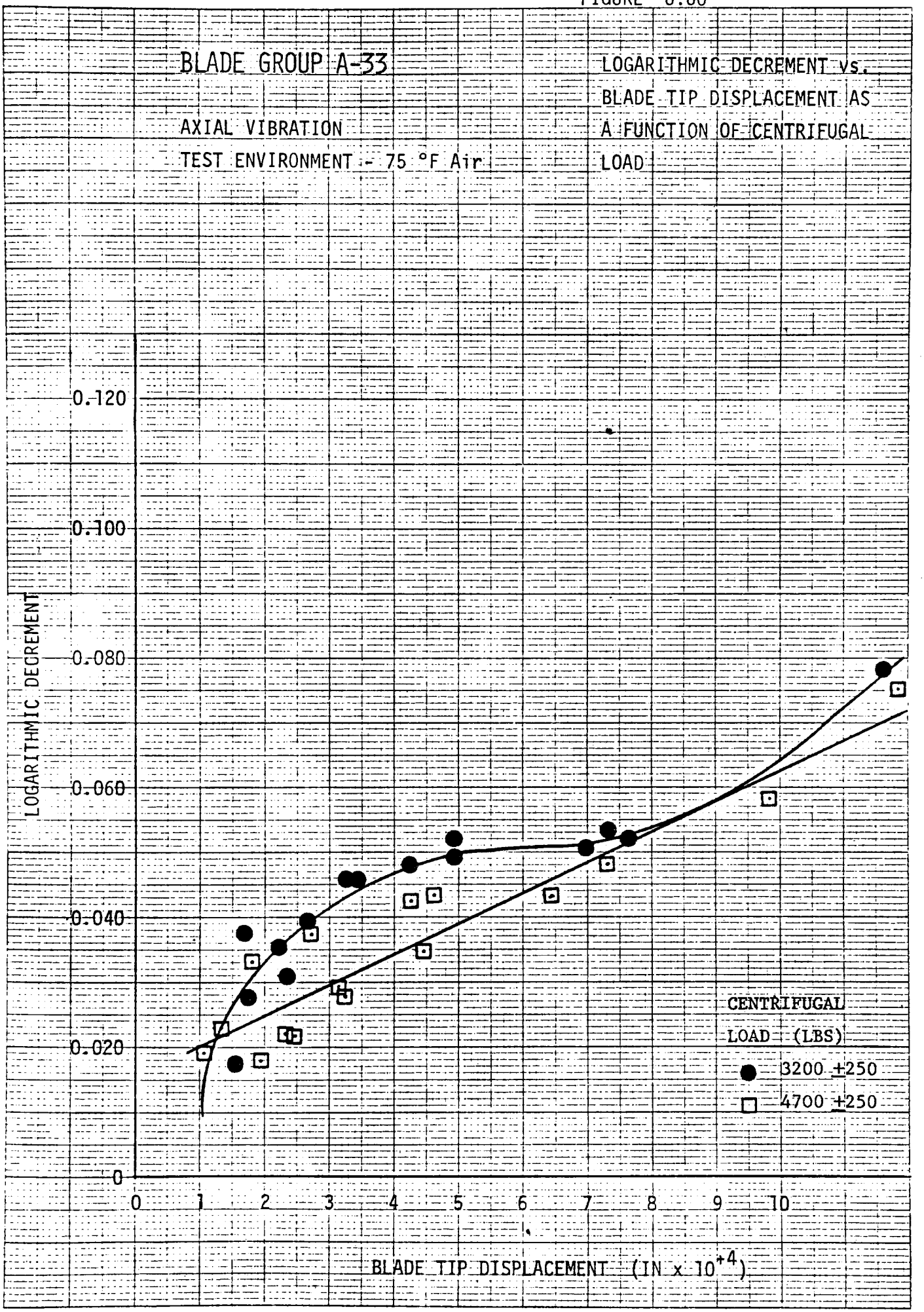
BLADE GROUP A-33
AXIAL VIBRATION
TEST ENVIRONMENT - 75 °F Air
LOGARITHMIC DECREMENT vs. BLADE TIP DISPLACEMENT AS A FUNCTION OF CENTRIFUGAL LOAD
LOGARITHMIC DECREMENT
0.120
0.100
0.080
0.060
0.040
0.020
0
0 1 2 3 4 5 6 7 8 9 10
BLADE TIP DISPLACEMENT (IN x 10^+4)
CENTRIFUGAL LOAD (LBS)
3200 ±250
4700 ±250

FIGURE 6.61

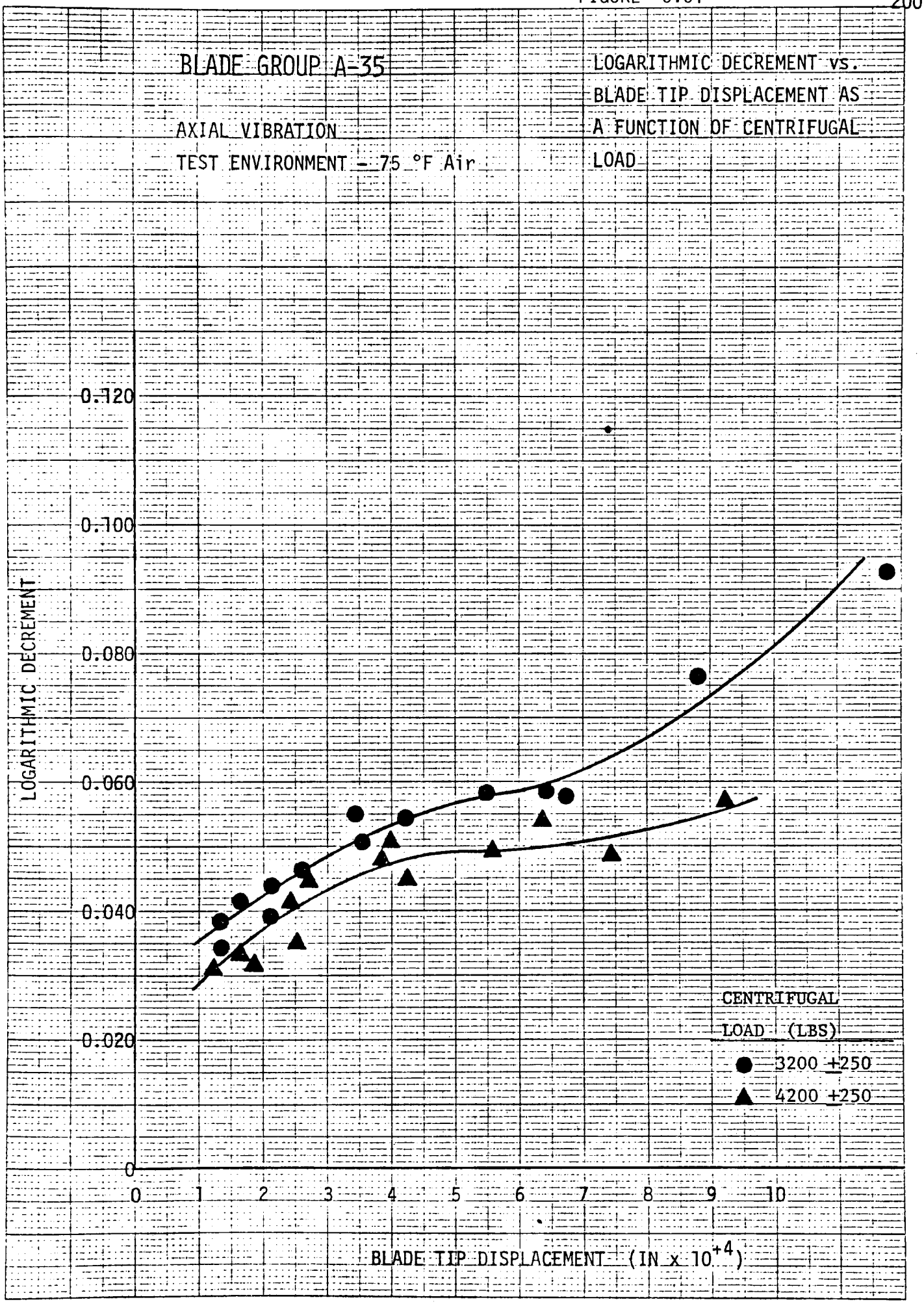
BLADE GROUP A-35
AXIAL VIBRATION
TEST ENVIRONMENT – 75 °F Air
LOGARITHMIC DECREMENT vs. BLADE TIP DISPLACEMENT AS A FUNCTION OF CENTRIFUGAL LOAD
LOGARITHMIC DECREMENT
0.120
0.100
0.080
0.060
0.040
0.020
0
0 1 2 3 4 5 6 7 8 9 10
BLADE TIP DISPLACEMENT (IN x 10+4)
CENTRIFUGAL LOAD (LBS)
3200 ±250
4200 ±250

FIGURE 6.62

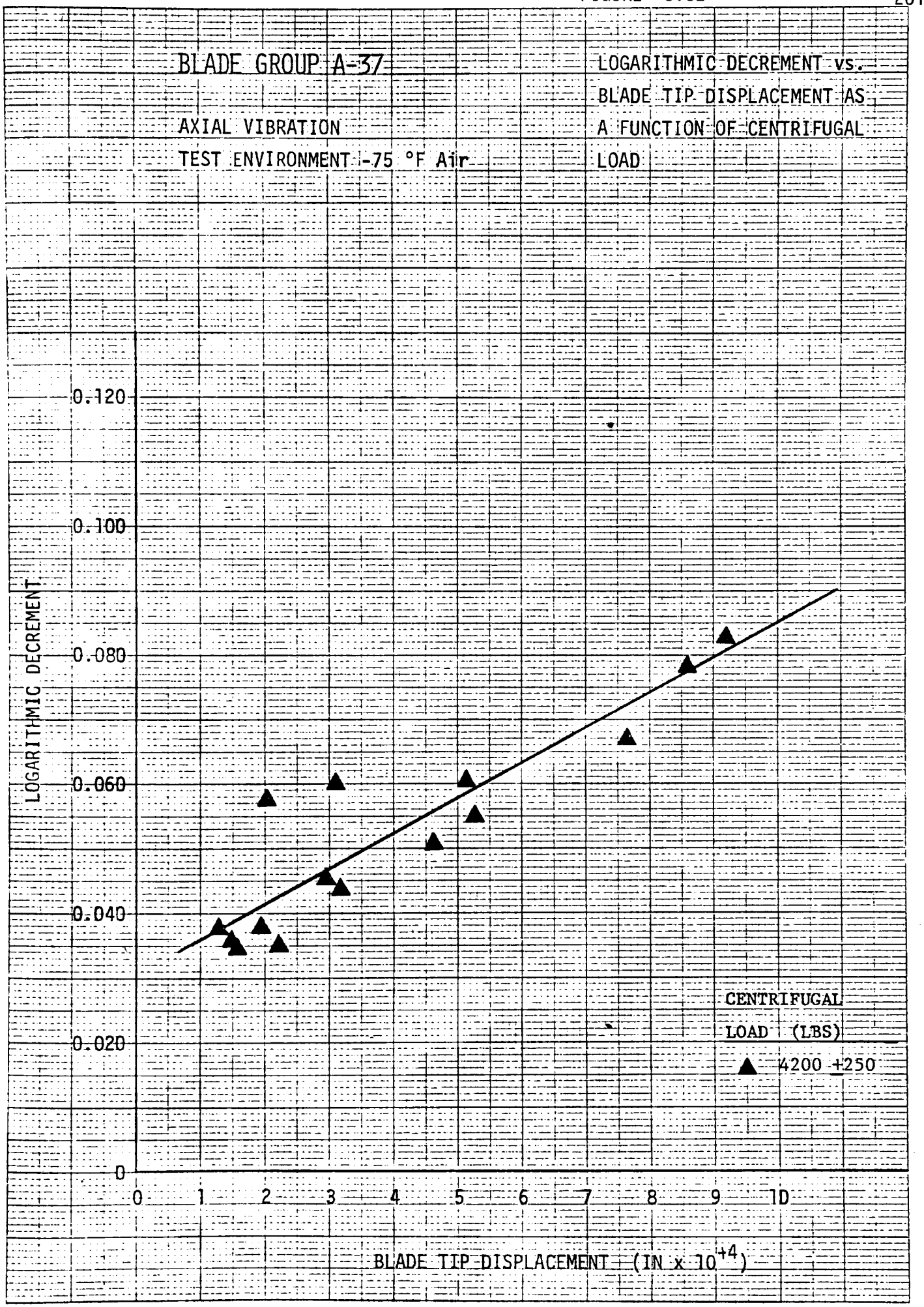
BLADE GROUP A-37
AXIAL VIBRATION
TEST ENVIRONMENT -75 °F Air
LOGARITHMIC DECREMENT vs. BLADE TIP DISPLACEMENT AS A FUNCTION OF CENTRIFUGAL LOAD
LOGARITHMIC DECREMENT
0.120
0.100
0.080
0.060
0.040
0.020
0
0
1
2
3
4
5
6
7
8
9
10
BLADE TIP DISPLACEMENT (IN x 10+4)
CENTRIFUGAL LOAD (LBS)
4200 ±250

FIGURE 6.63

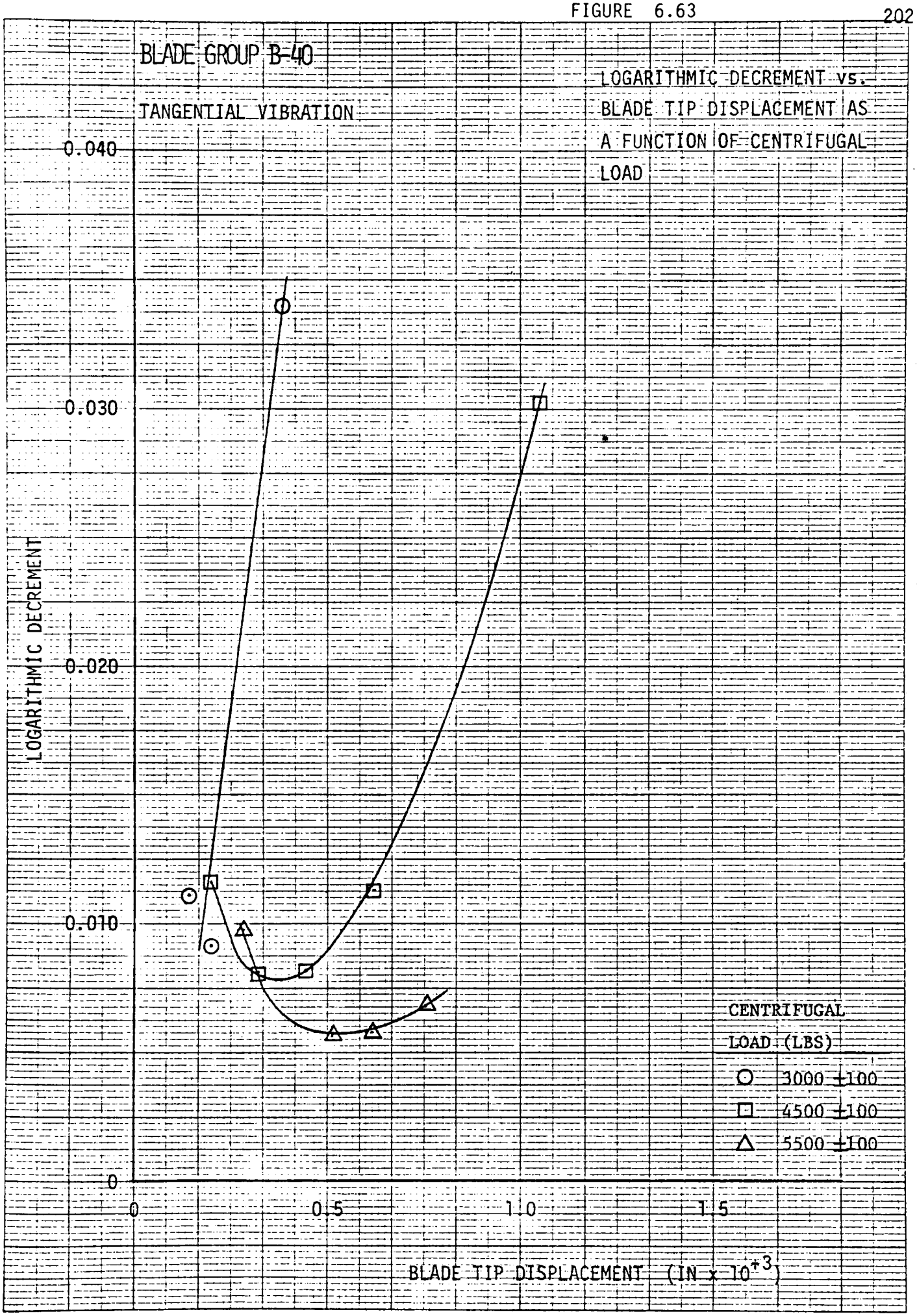
BLADE GROUP B-40
TANGENTIAL VIBRATION
LOGARITHMIC DECREMENT vs. BLADE TIP DISPLACEMENT AS A FUNCTION OF CENTRIFUGAL LOAD
0.040
0.030
0.020
0.010
0
LOGARITHMIC DECREMENT
0
0.5
1.0
1.5
BLADE TIP DISPLACEMENT (IN x 10^+3)
CENTRIFUGAL LOAD (LBS)
3000 ±100
4500 ±100
5500 ±100

FIGURE 6.64

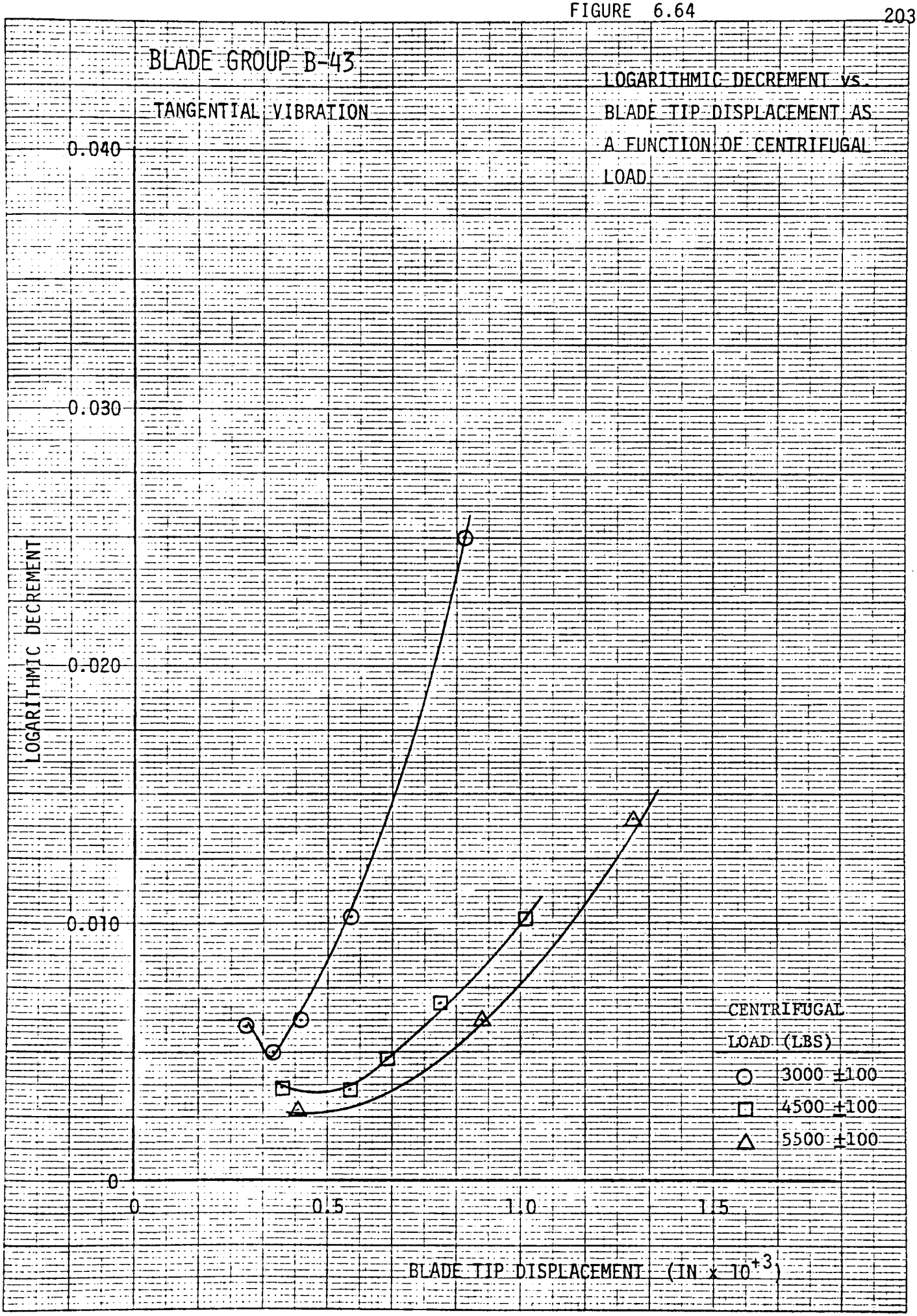
BLADE GROUP B-43
TANGENTIAL VIBRATION
LOGARITHMIC DECREMENT VS. BLADE TIP DISPLACEMENT AS A FUNCTION OF CENTRIFUGAL LOAD
0.040
0.030
0.020
0.010
0
LOGARITHMIC DECREMENT
0
0.5
1.0
1.5
BLADE TIP DISPLACEMENT (IN x 10+3)
CENTRIFUGAL LOAD (LBS)
3000 ±100
4500 ±100
5500 ±100

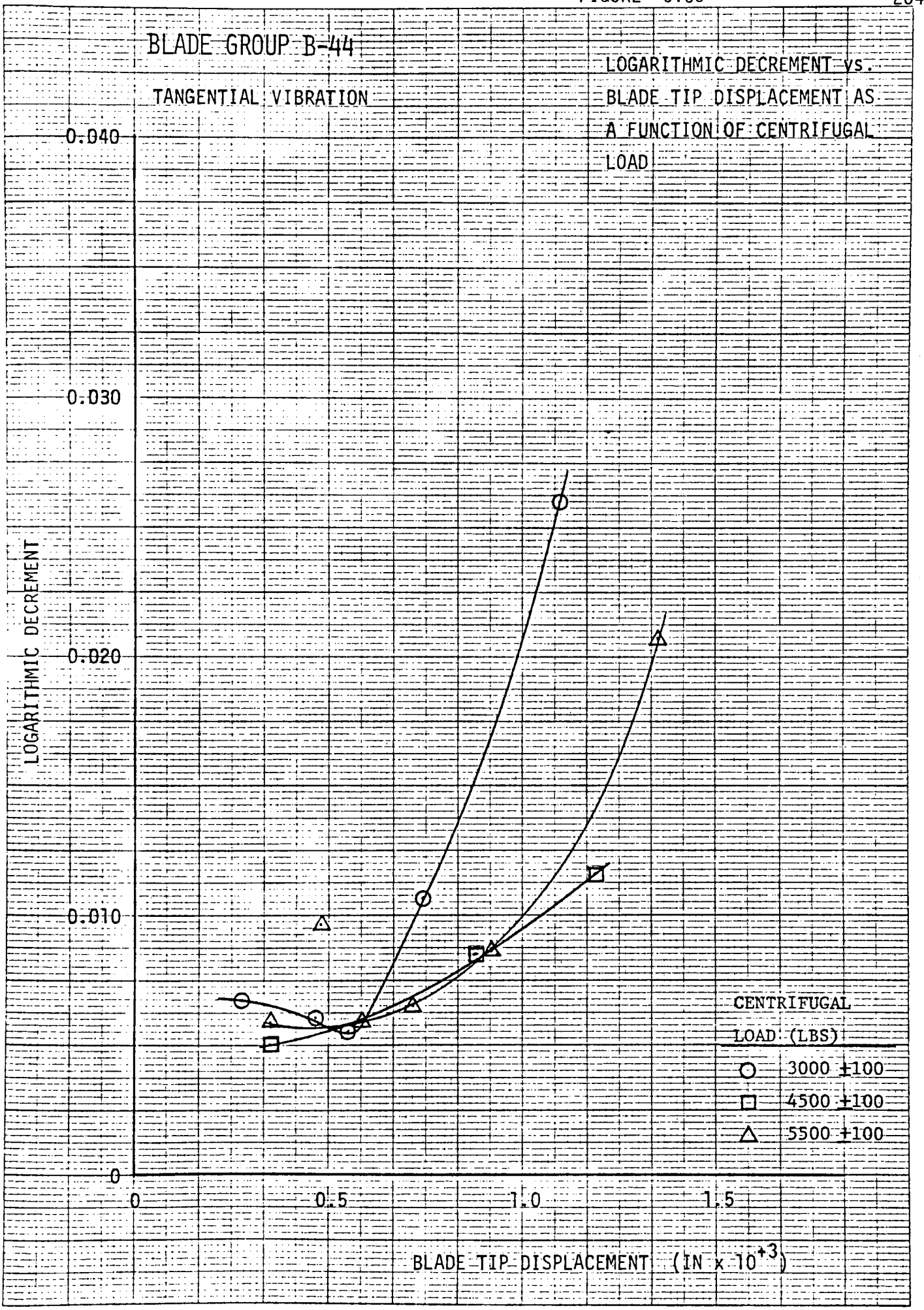
BLADE GROUP B-44
TANGENTIAL VIBRATION
LOGARITHMIC DECREMENT vs. BLADE TIP DISPLACEMENT AS A FUNCTION OF CENTRIFUGAL LOAD
0.040
0.030
0.020
0.010
0
LOGARITHMIC DECREMENT
0
0.5
1.0
1.5
BLADE TIP DISPLACEMENT (IN x 10+3)
CENTRIFUGAL LOAD (LBS)
3000 ±100
4500 ±100
5500 ±100

FIGURE 6.66

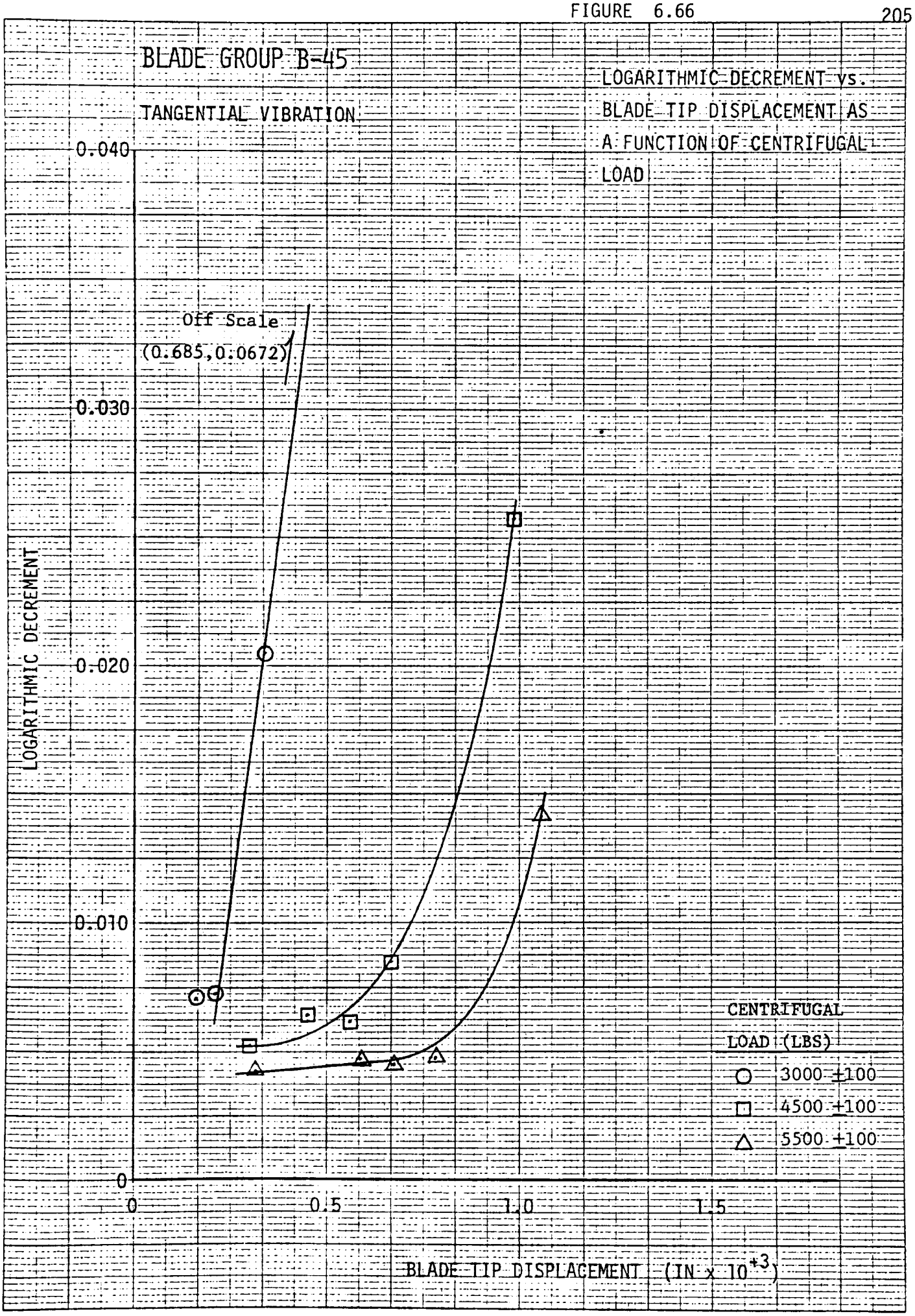
BLADE GROUP B-45
TANGENTIAL VIBRATION
LOGARITHMIC DECREMENT vs. BLADE TIP DISPLACEMENT AS A FUNCTION OF CENTRIFUGAL LOAD
0.040
0.030
0.020
0.010
0
Off Scale
(0.685, 0.0672)
LOGARITHMIC DECREMENT
0
0.5
1.0
1.5
BLADE TIP DISPLACEMENT (IN x 10+3)
CENTRIFUGAL LOAD (LBS)
3000 ±100
4500 ±100
5500 ±100

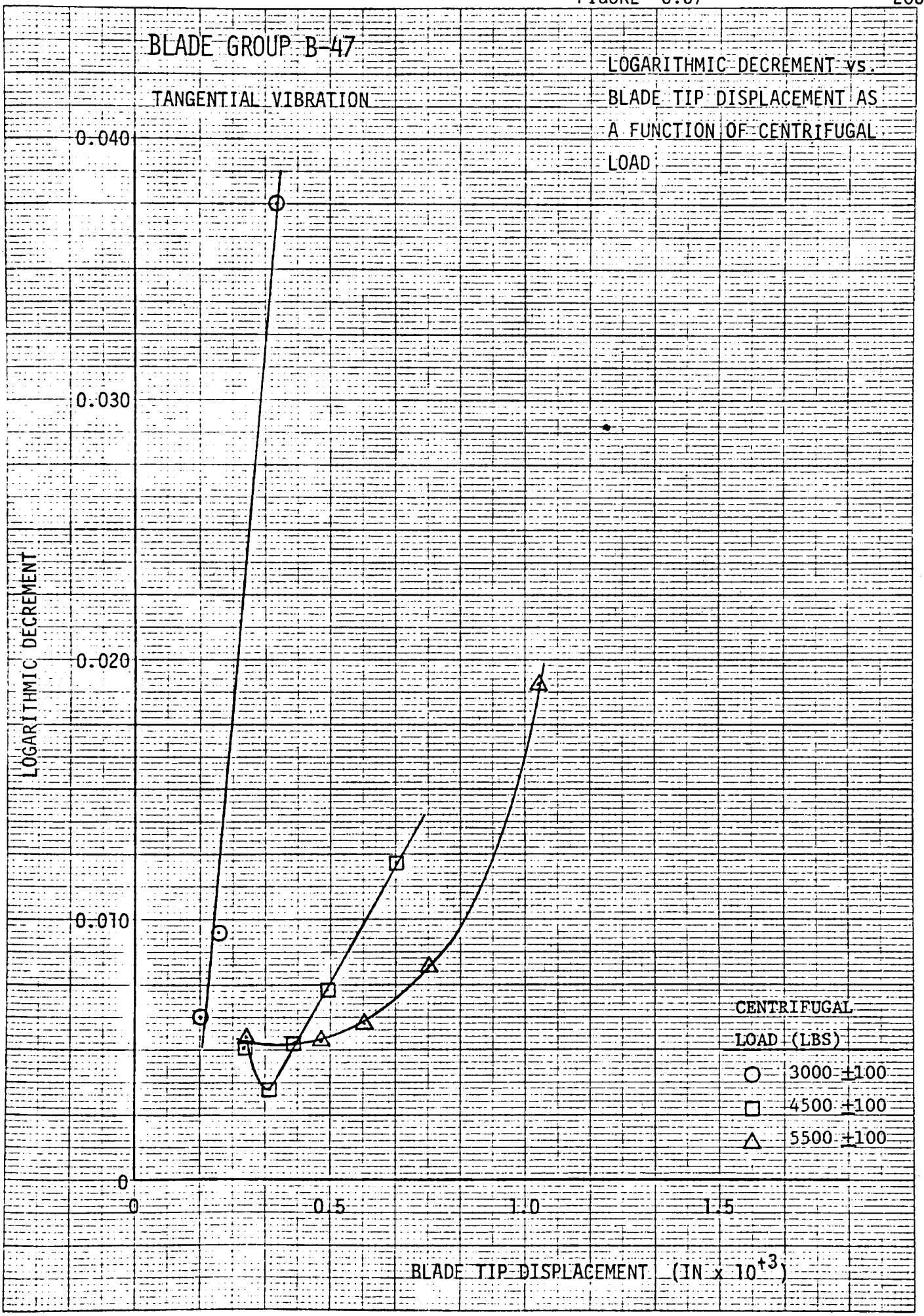
BLADE GROUP B-47
TANGENTIAL VIBRATION
LOGARITHMIC DECREMENT vs. BLADE TIP DISPLACEMENT AS A FUNCTION OF CENTRIFUGAL LOAD
LOGARITHMIC DECREMENT
0.040
0.030
0.020
0.010
0
0
0.5
1.0
1.5
BLADE TIP DISPLACEMENT (IN x 10+3)
CENTRIFUGAL LOAD (LBS)
3000 ±100
4500 ±100
5500 ±100

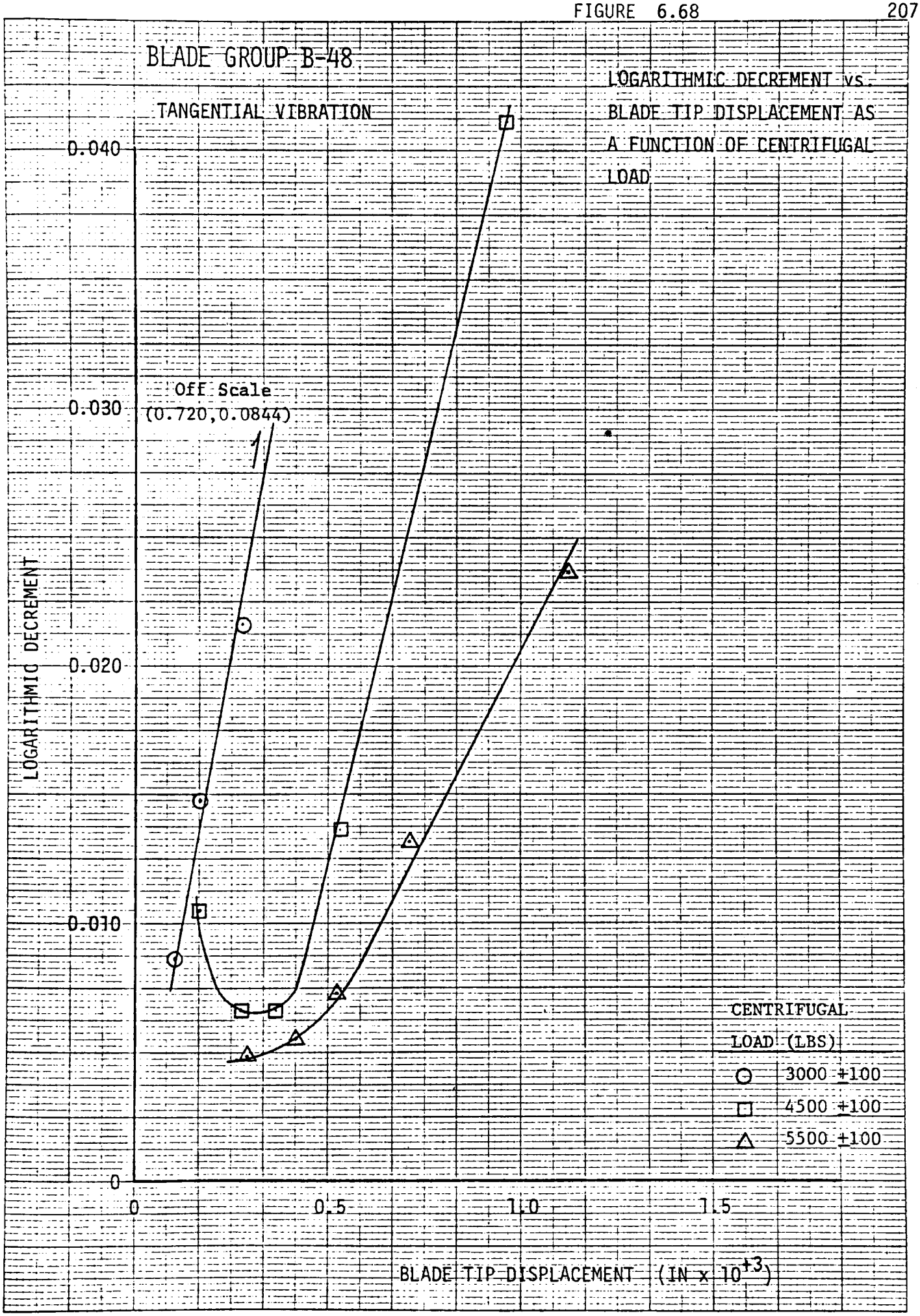
BLADE GROUP B-48
TANGENTIAL VIBRATION
LOGARITHMIC DECREMENT vs. BLADE TIP DISPLACEMENT AS A FUNCTION OF CENTRIFUGAL LOAD
0.040
0.030
0.020
0.010
0
Off Scale
(0.720,0.0844)
LOGARITHMIC DECREMENT
0
0.5
1.0
1.5
BLADE TIP DISPLACEMENT (IN x 10+3)
CENTRIFUGAL LOAD (LBS)
3000 ±100
4500 ±100
5500 ±100

FIGURE 6.69

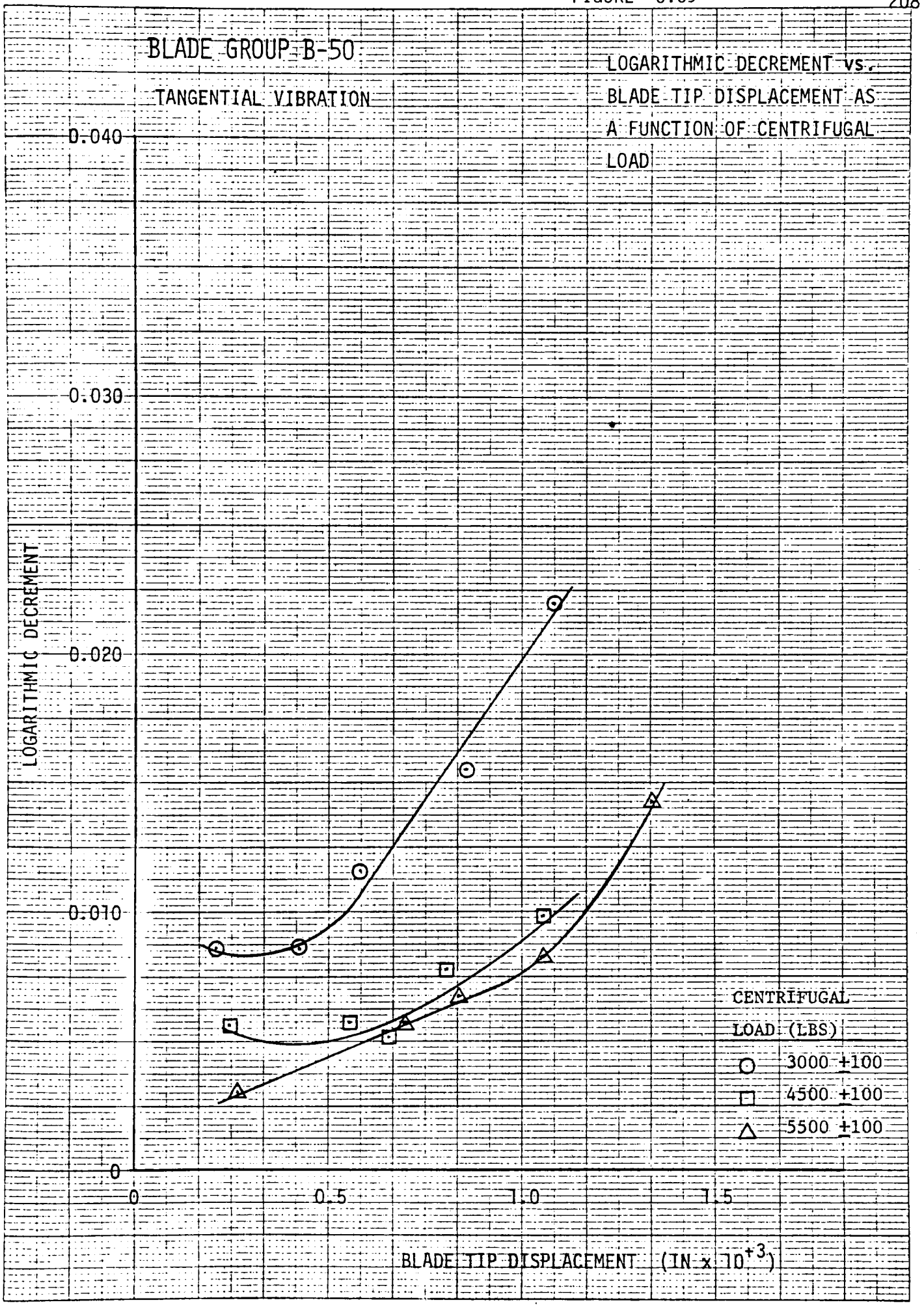
BLADE GROUP B-50
TANGENTIAL VIBRATION
LOGARITHMIC DECREMENT vs. BLADE TIP DISPLACEMENT AS A FUNCTION OF CENTRIFUGAL LOAD
0.040
0.030
0.020
0.010
0
LOGARITHMIC DECREMENT
0
0.5
1.0
1.5
BLADE TIP DISPLACEMENT (IN x 10+3)
CENTRIFUGAL LOAD (LBS)
3000 ±100
4500 ±100
5500 ±100

FIGURE 6.70

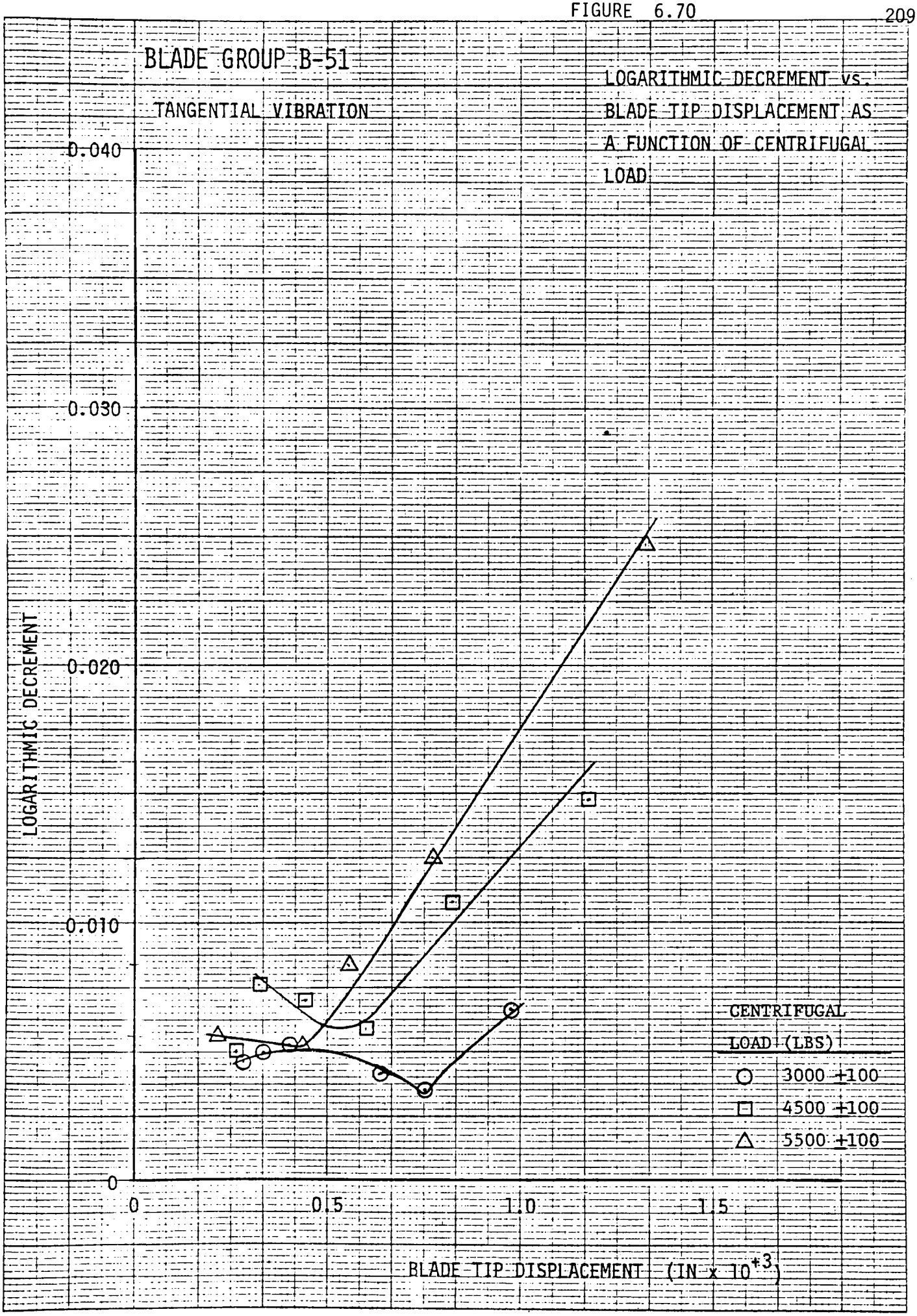
BLADE GROUP B-51
TANGENTIAL VIBRATION
LOGARITHMIC DECREMENT vs. BLADE TIP DISPLACEMENT AS A FUNCTION OF CENTRIFUGAL LOAD
0.040
0.030
0.020
0.010
0
LOGARITHMIC DECREMENT
0
0.5
1.0
1.5
BLADE TIP DISPLACEMENT (IN x 10+3)
CENTRIFUGAL LOAD (LBS)
3000 ±100
4500 ±100
5500 ±100

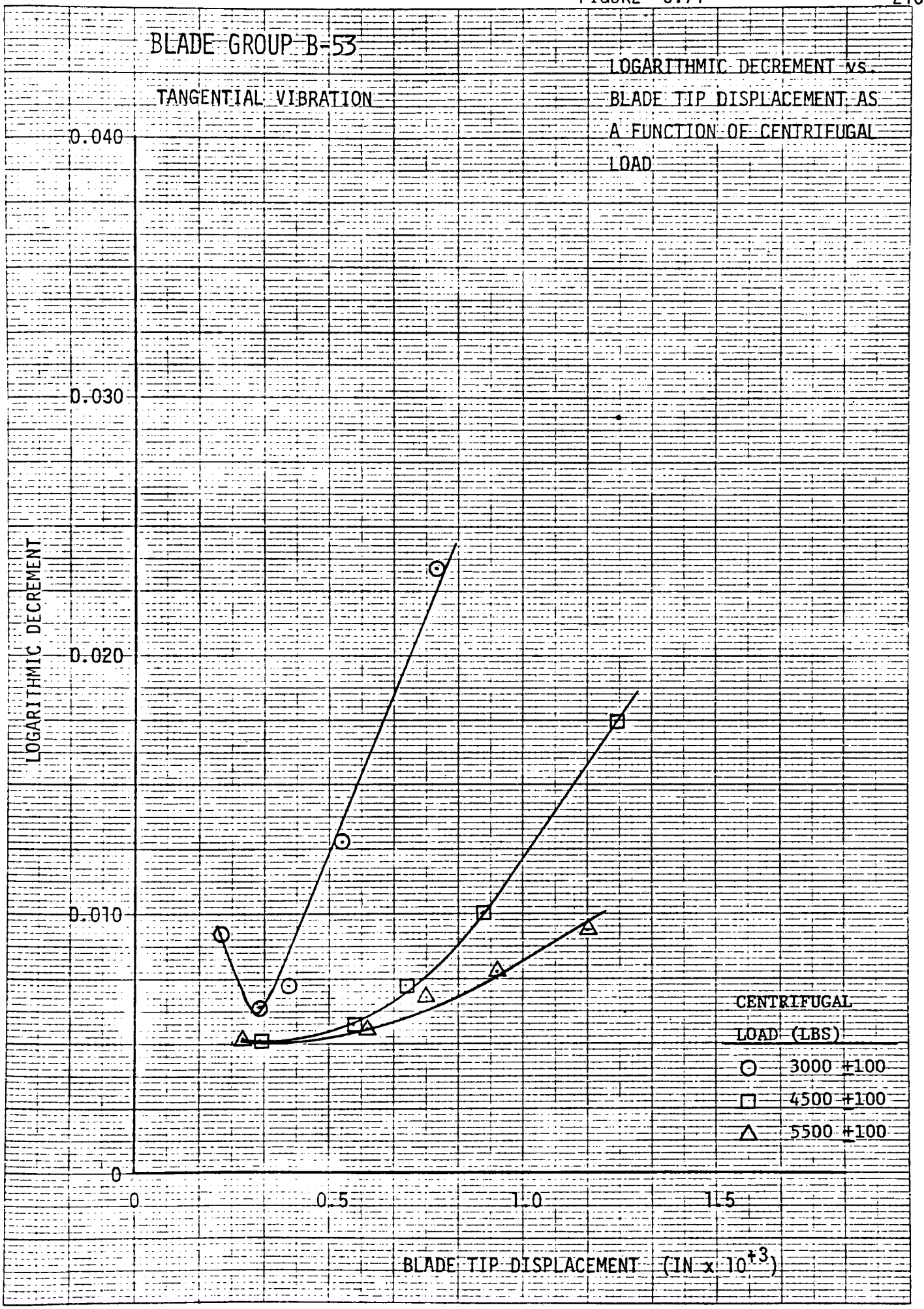
BLADE GROUP B=53
TANGENTIAL VIBRATION
LOGARITHMIC DECREMENT vs. BLADE TIP DISPLACEMENT AS A FUNCTION OF CENTRIFUGAL LOAD
0.040
0.030
0.020
0.010
0
LOGARITHMIC DECREMENT
0
0.5
1.0
1.5
BLADE TIP DISPLACEMENT (IN x 10+3)
CENTRIFUGAL LOAD (LBS)
3000 ±100
4500 ±100
5500 ±100

FIGURE 6.72

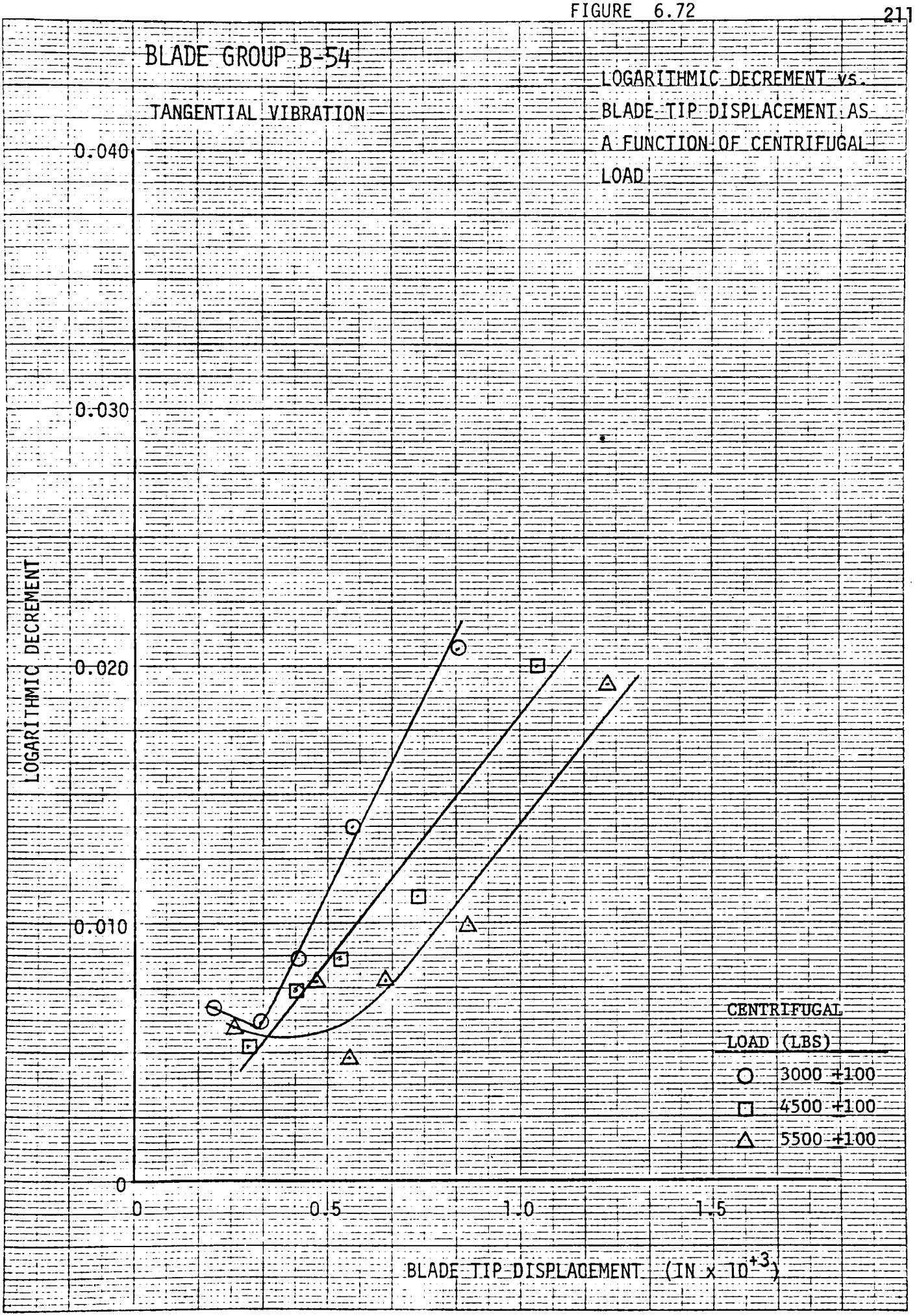
BLADE GROUP B-54
TANGENTIAL VIBRATION
LOGARITHMIC DECREMENT vs. BLADE TIP DISPLACEMENT AS A FUNCTION OF CENTRIFUGAL LOAD
0.040
0.030
0.020
0.010
0
LOGARITHMIC DECREMENT
0
0.5
1.0
1.5
BLADE TIP DISPLACEMENT (IN x 10+3)
CENTRIFUGAL LOAD (LBS)
3000 ±100
4500 ±100
5500 ±100

FIGURE 6.73

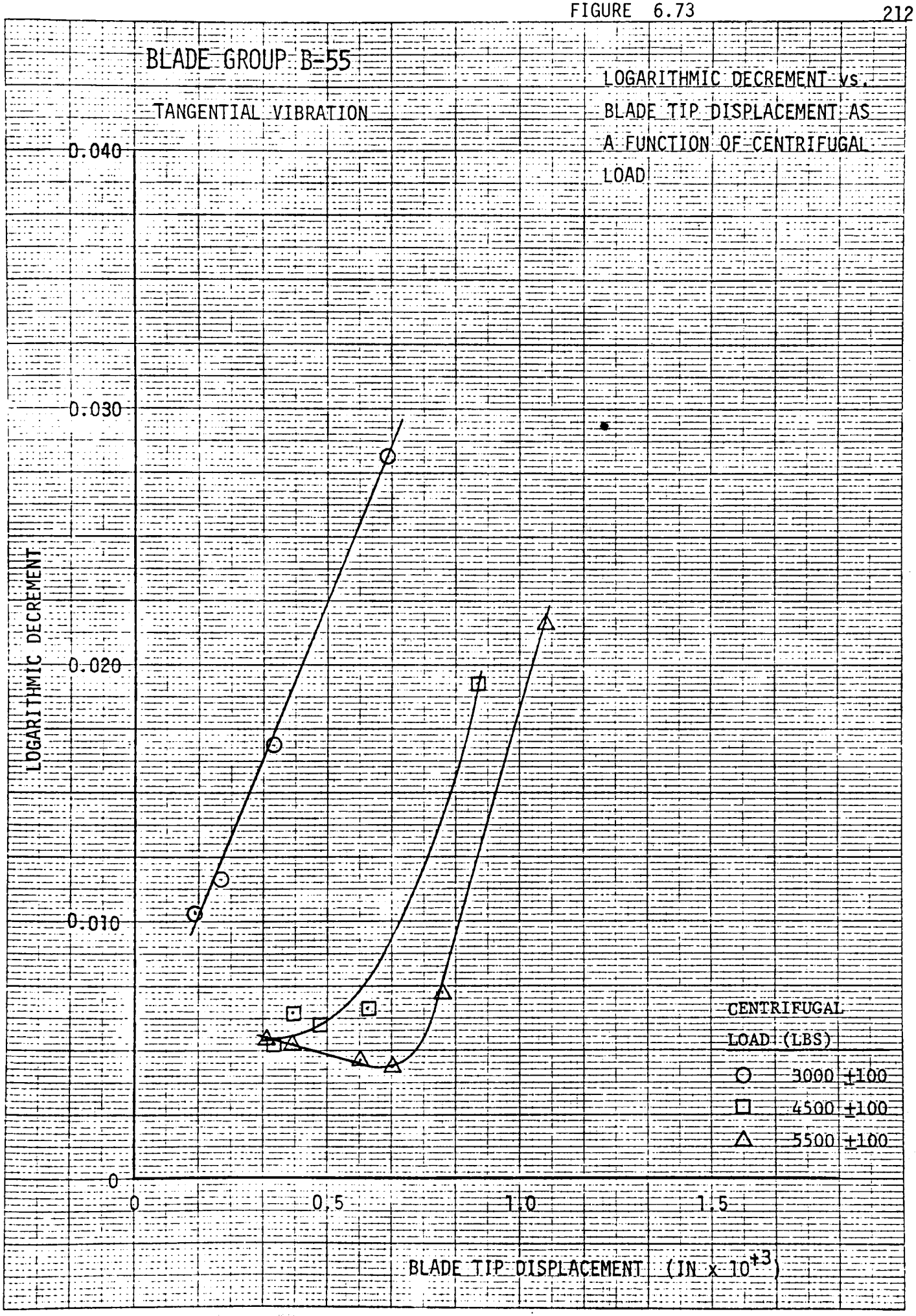
BLADE GROUP B-55
TANGENTIAL VIBRATION
LOGARITHMIC DECREMENT vs. BLADE TIP DISPLACEMENT AS A FUNCTION OF CENTRIFUGAL LOAD
0.040
0.030
0.020
0.010
0
LOGARITHMIC DECREMENT
0
0.5
1.0
1.5
BLADE TIP DISPLACEMENT (IN x 10+3)
CENTRIFUGAL LOAD (LBS)
3000 ±100
4500 ±100
5500 ±100

FIGURE 6.74

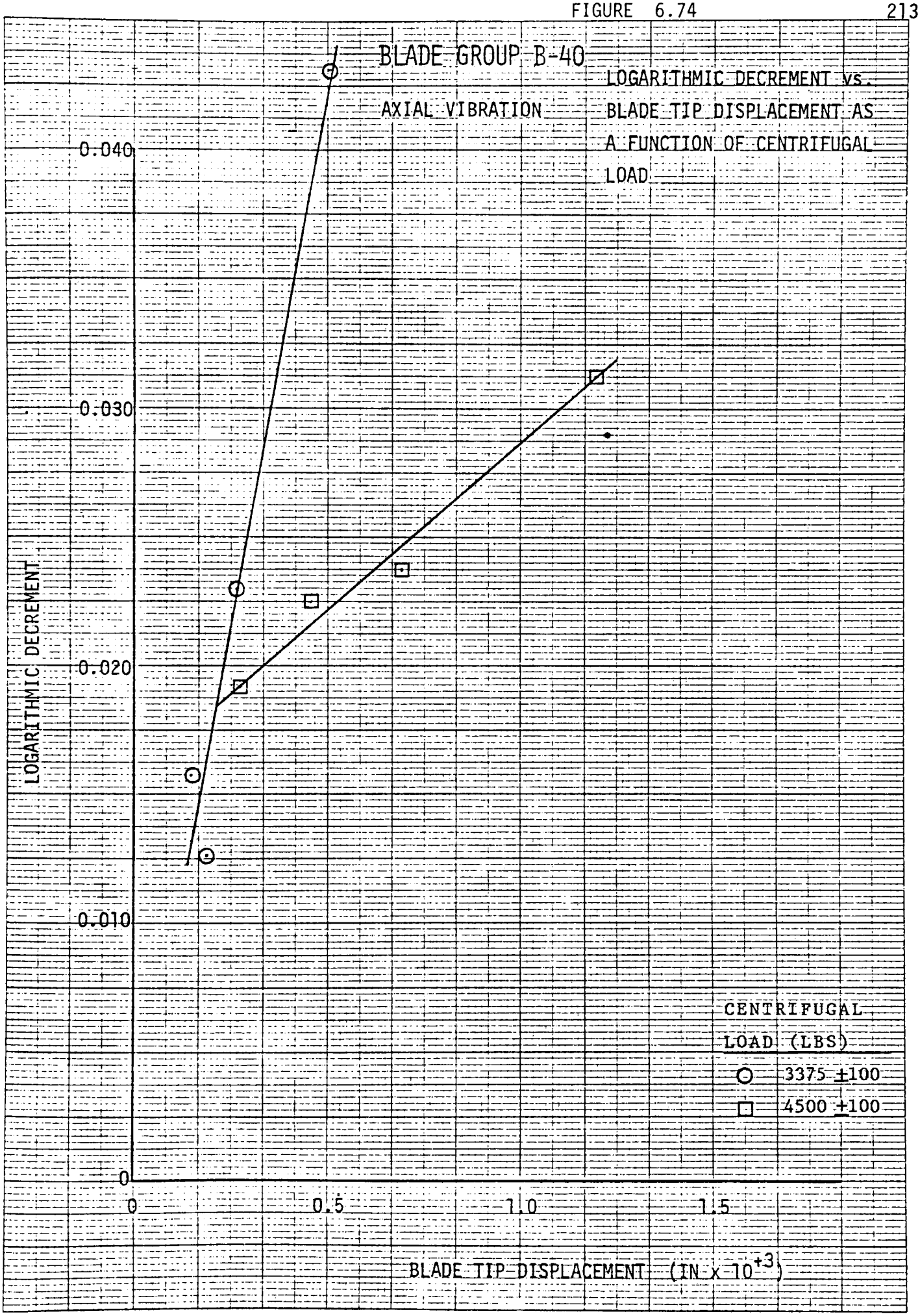
BLADE GROUP B-40
AXIAL VIBRATION
LOGARITHMIC DECREMENT vs. BLADE TIP DISPLACEMENT AS A FUNCTION OF CENTRIFUGAL LOAD
LOGARITHMIC DECREMENT
0.040
0.030
0.020
0.010
0
0
0.5
1.0
1.5
BLADE TIP DISPLACEMENT (IN x 10+3)
CENTRIFUGAL LOAD (LBS)
3375 ±100
4500 ±100

FIGURE 6.75

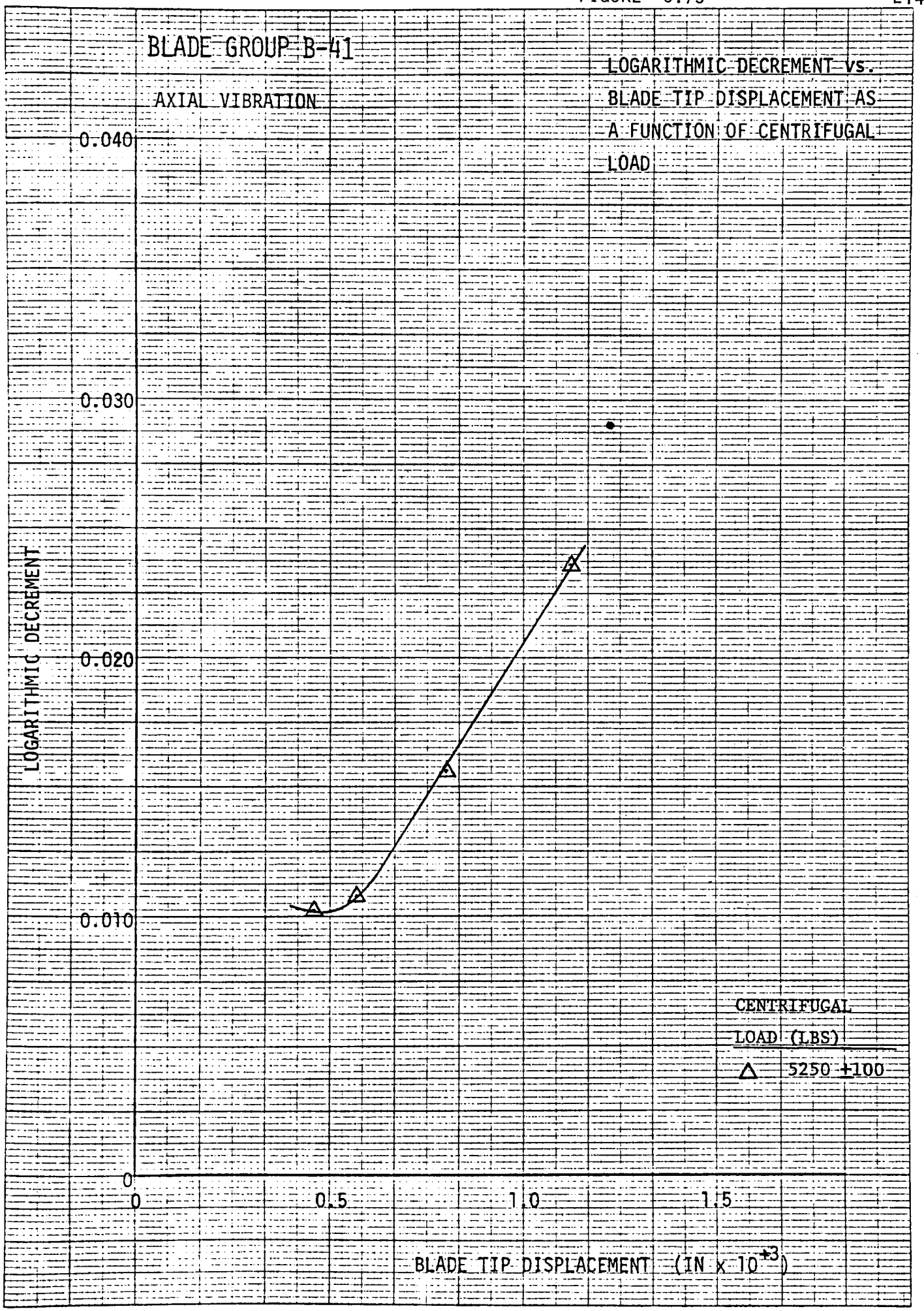
BLADE GROUP B-41
AXIAL VIBRATION
LOGARITHMIC DECREMENT vs. BLADE TIP DISPLACEMENT AS A FUNCTION OF CENTRIFUGAL LOAD
0.040
0.030
0.020
0.010
0
LOGARITHMIC DECREMENT
0
0.5
1.0
1.5
BLADE TIP DISPLACEMENT (IN x 10^-3)
CENTRIFUGAL LOAD (LBS)
△ 5250 ±100

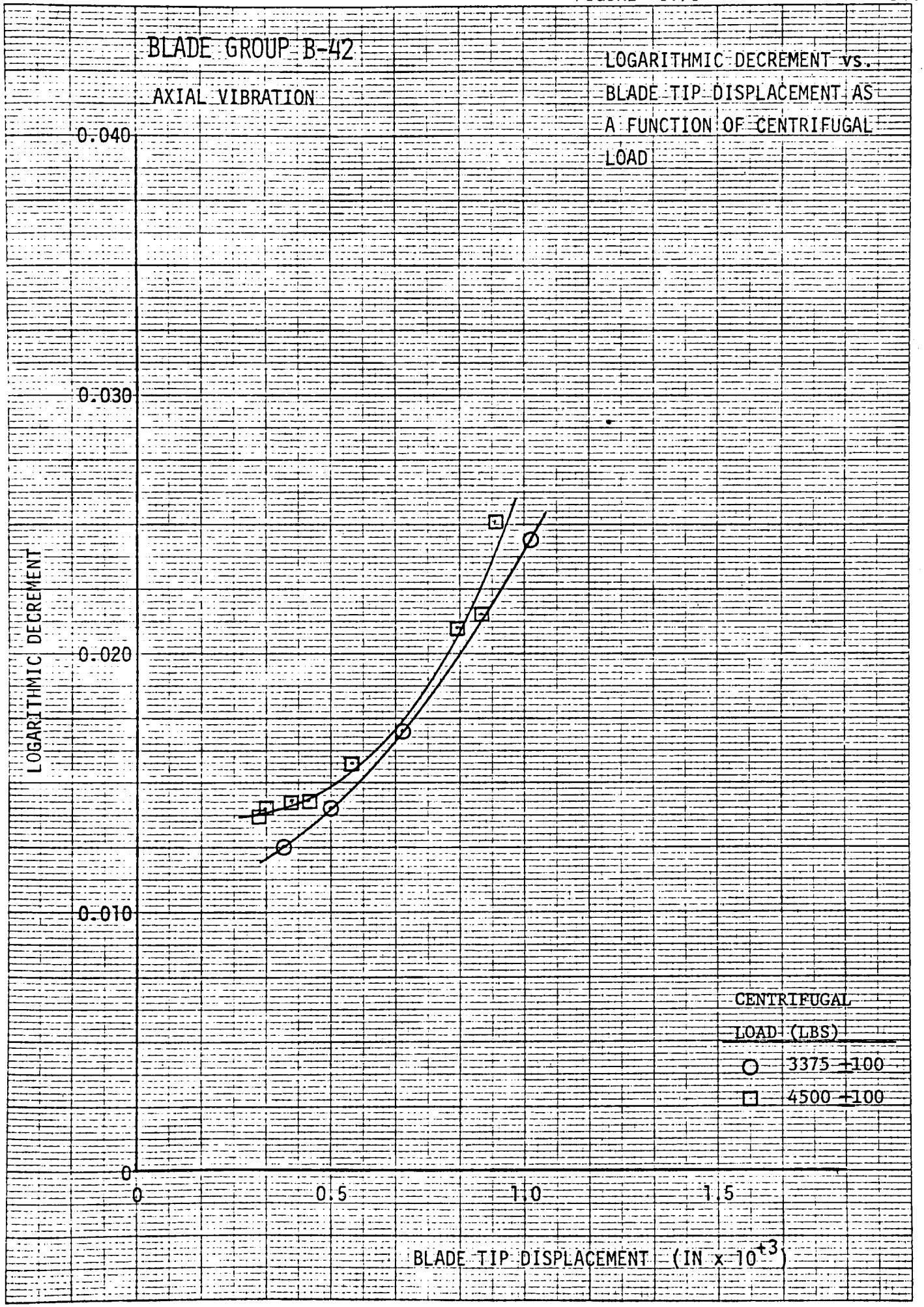
BLADE GROUP B-42
AXIAL VIBRATION
LOGARITHMIC DECREMENT vs. BLADE TIP DISPLACEMENT AS A FUNCTION OF CENTRIFUGAL LOAD
0.040
0.030
0.020
0.010
0
LOGARITHMIC DECREMENT
0
0.5
1.0
1.5
BLADE TIP DISPLACEMENT (IN x 10+3)
CENTRIFUGAL LOAD (LBS)
3375 ±100
4500 ±100

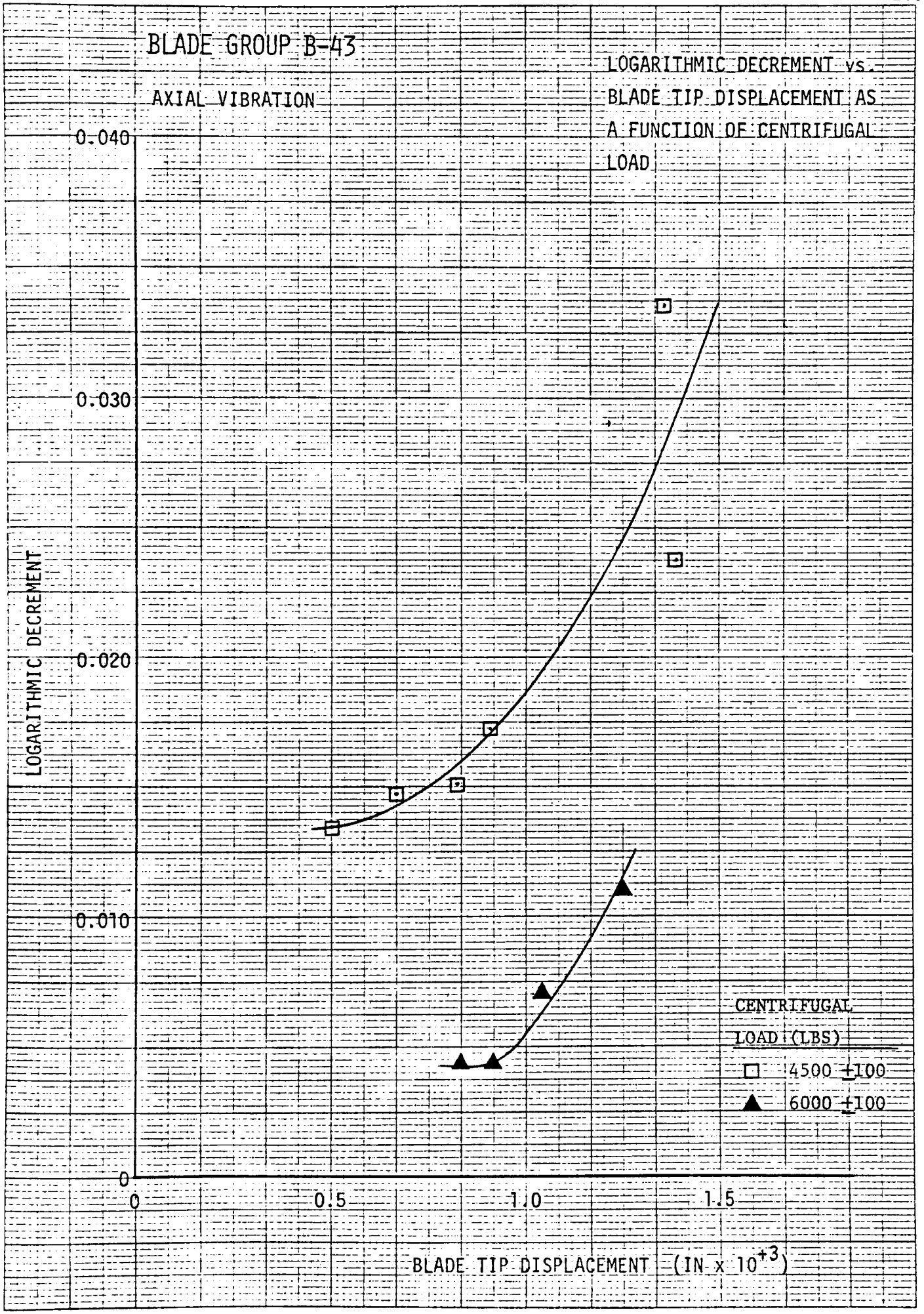
BLADE GROUP B-43
AXIAL VIBRATION
LOGARITHMIC DECREMENT vs. BLADE TIP DISPLACEMENT AS A FUNCTION OF CENTRIFUGAL LOAD
0.040
0.030
0.020
0.010
0
LOGARITHMIC DECREMENT
0
0.5
1.0
1.5
BLADE TIP DISPLACEMENT (IN x 10+3)
CENTRIFUGAL LOAD (LBS)
4500 ±100
6000 ±100

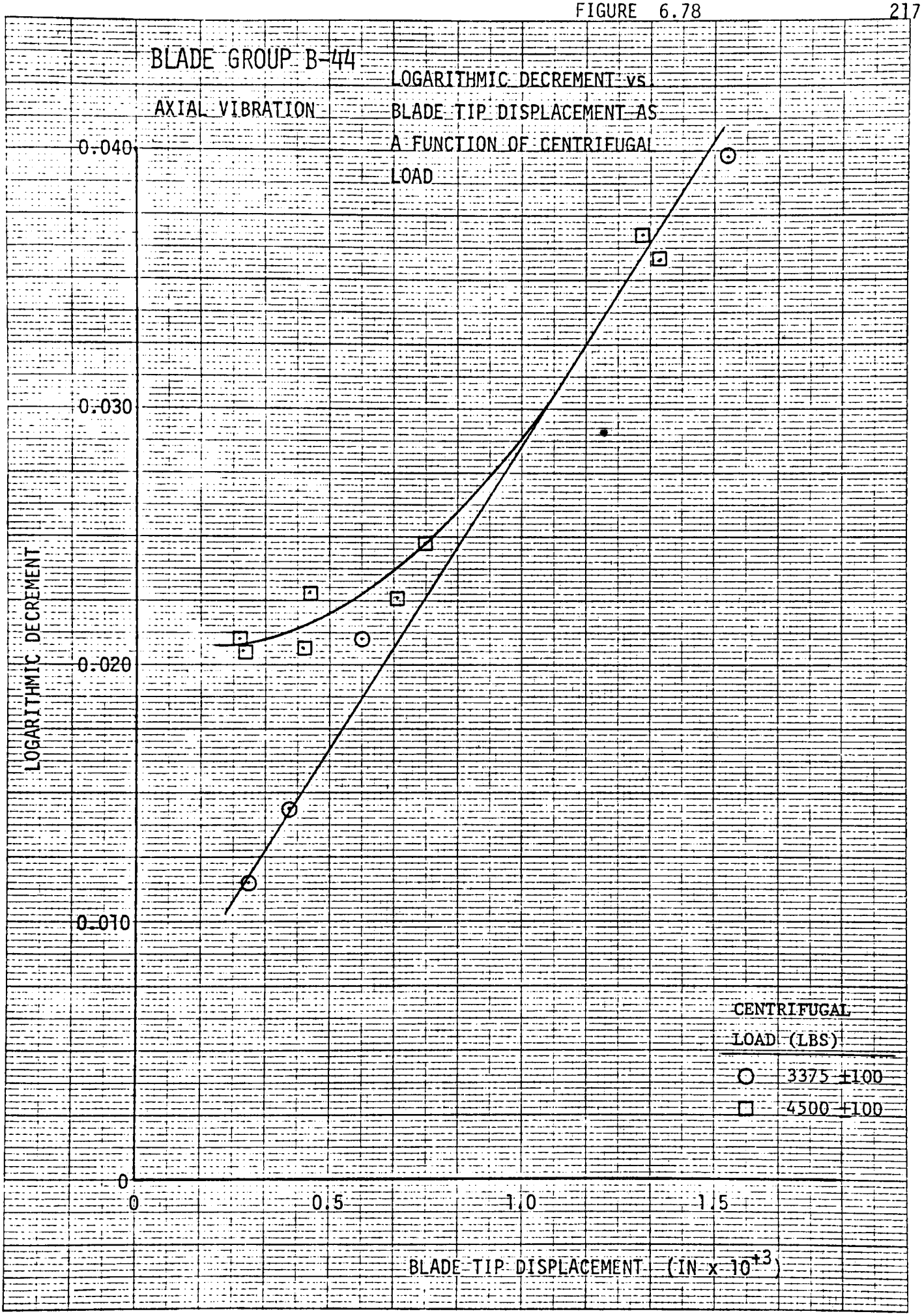
BLADE GROUP B-44
AXIAL VIBRATION
LOGARITHMIC DECREMENT vs. BLADE TIP DISPLACEMENT AS A FUNCTION OF CENTRIFUGAL LOAD
LOGARITHMIC DECREMENT
0.040
0.030
0.020
0.010
0
0
0.5
1.0
1.5
BLADE TIP DISPLACEMENT (IN x 10+3)
CENTRIFUGAL LOAD (LBS)
3375 ±100
4500 ±100

FIGURE 6.79

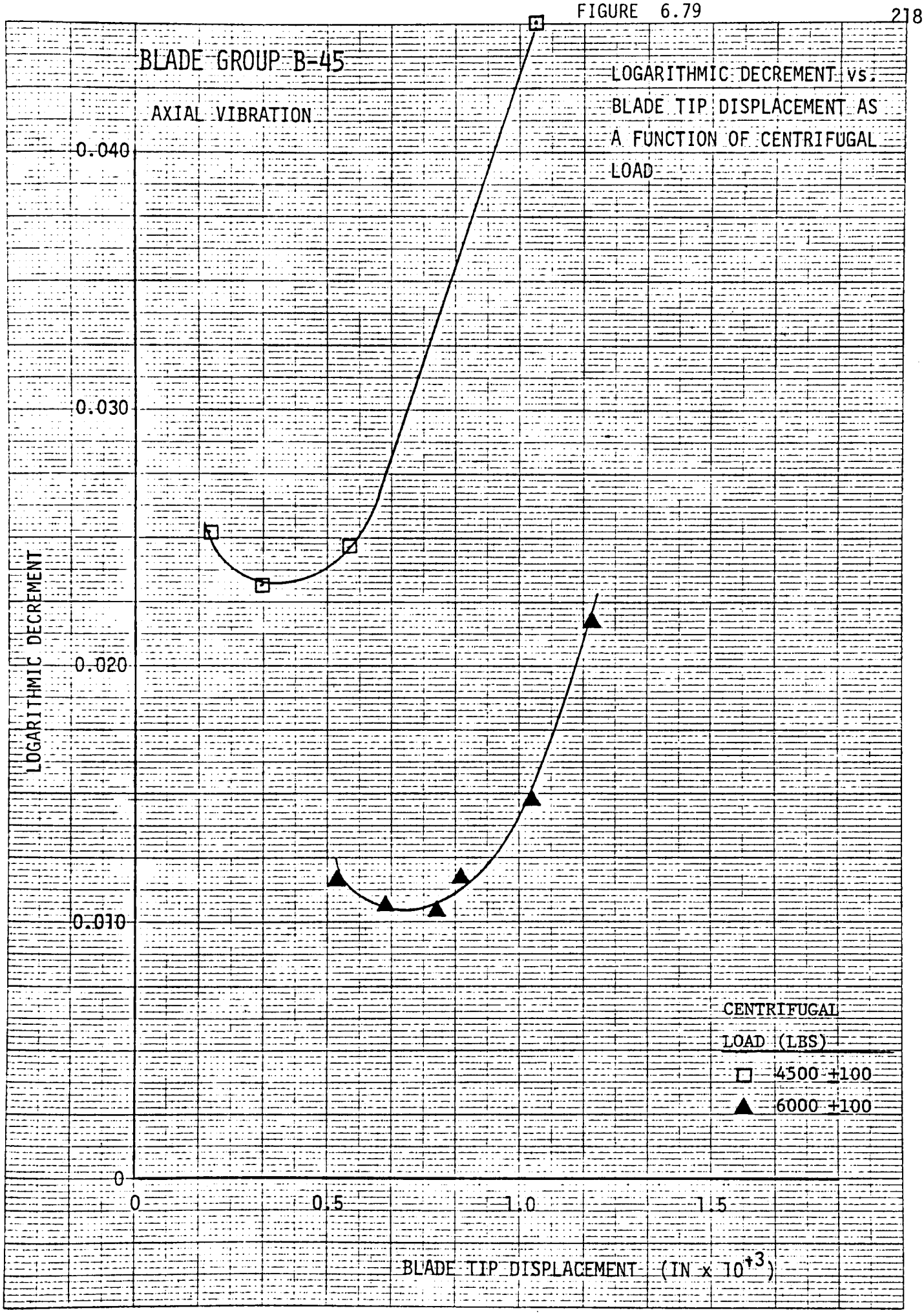
BLADE GROUP B-45
AXIAL VIBRATION
LOGARITHMIC DECREMENT vs. BLADE TIP DISPLACEMENT AS A FUNCTION OF CENTRIFUGAL LOAD
0.040
0.030
0.020
0.010
0
LOGARITHMIC DECREMENT
0
0.5
1.0
1.5
BLADE TIP DISPLACEMENT (IN x 10+3)
CENTRIFUGAL LOAD (LBS)
4500 ±100
6000 ±100

FIGURE 6.80

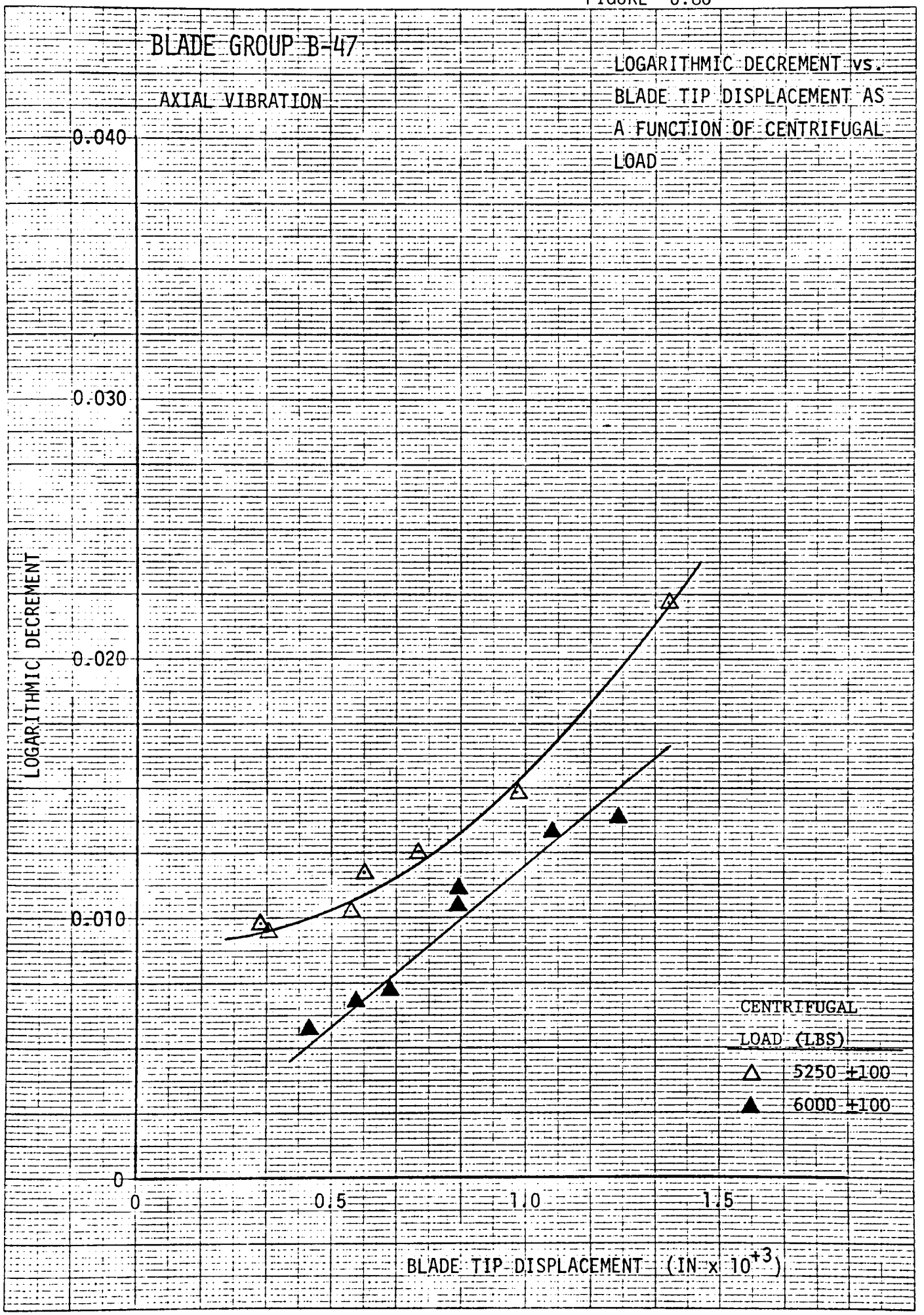
BLADE GROUP B-47
AXIAL VIBRATION
LOGARITHMIC DECREMENT vs. BLADE TIP DISPLACEMENT AS A FUNCTION OF CENTRIFUGAL LOAD
0.040
0.030
0.020
0.010
0
LOGARITHMIC DECREMENT
0
0.5
1.0
1.5
BLADE TIP DISPLACEMENT (IN x 10^{+3})
CENTRIFUGAL LOAD (LBS)
△ 5250 ±100
▲ 6000 ±100

FIGURE 6.81

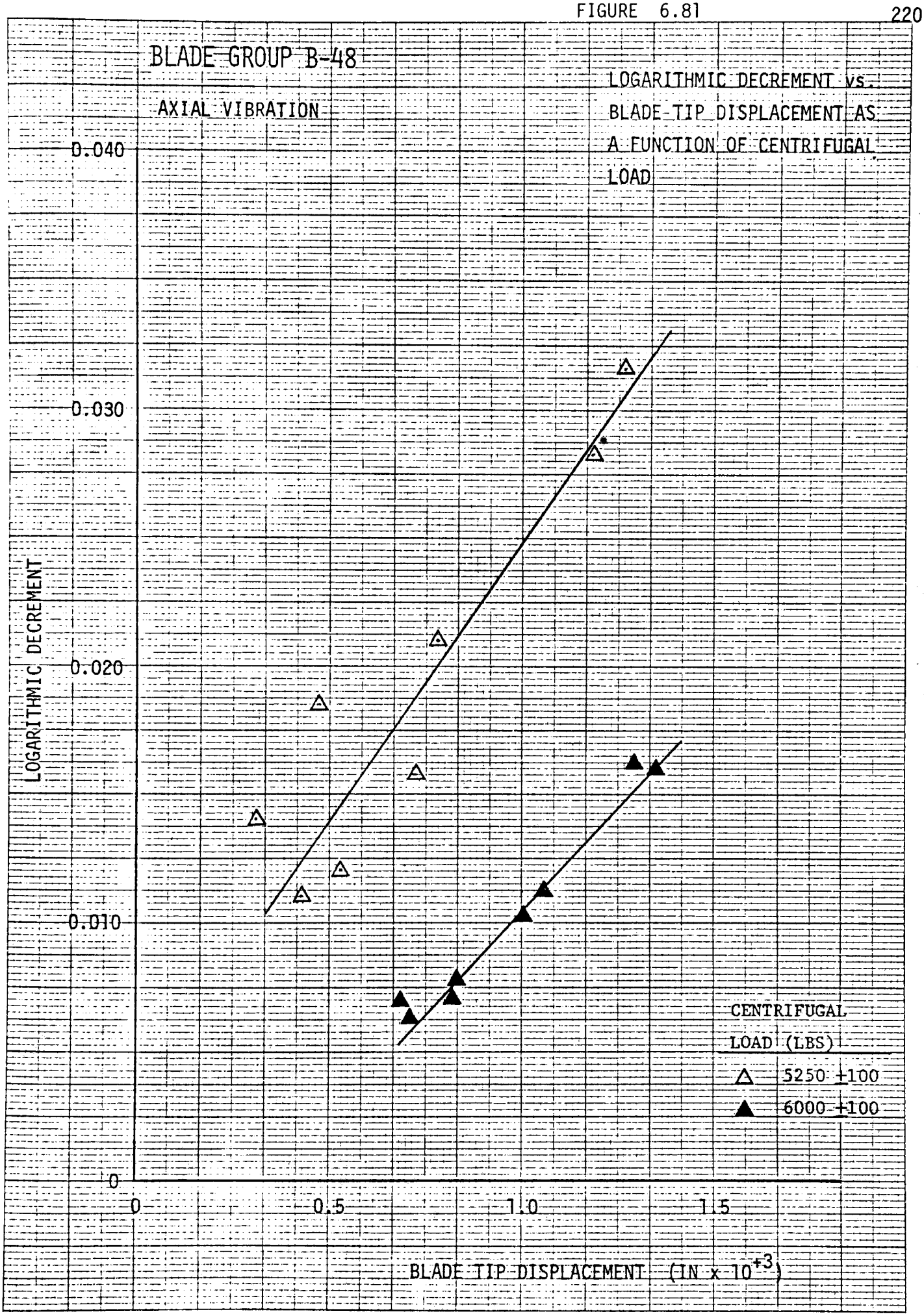
BLADE GROUP B-48
AXIAL VIBRATION
LOGARITHMIC DECREMENT vs. BLADE TIP DISPLACEMENT AS A FUNCTION OF CENTRIFUGAL LOAD
LOGARITHMIC DECREMENT
0.040
0.030
0.020
0.010
0
0
0.5
1.0
1.5
BLADE TIP DISPLACEMENT (IN x 10^{+3})
CENTRIFUGAL LOAD (LBS)
△ 5250 ±100
▲ 6000 ±100

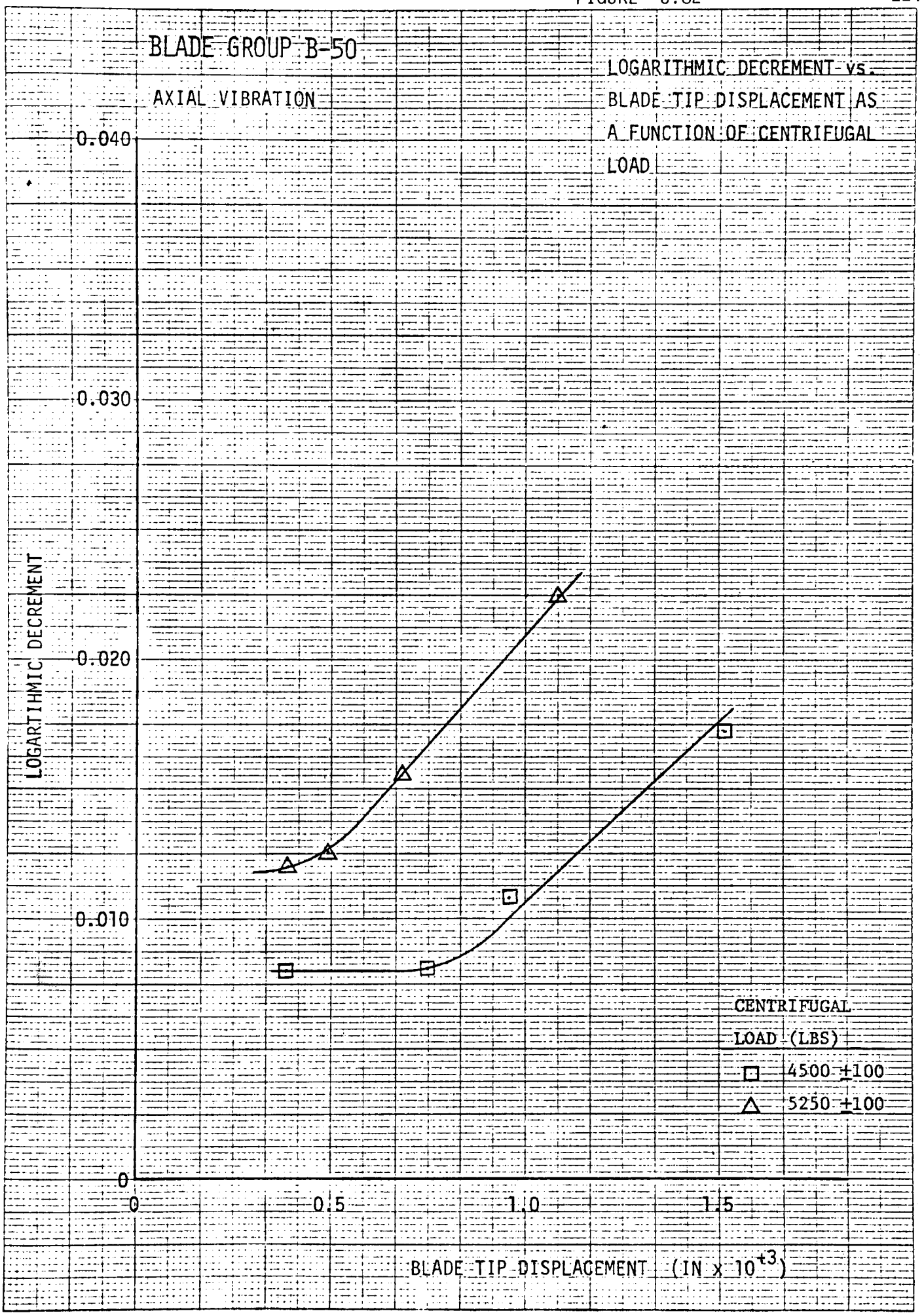
BLADE GROUP B-50
AXIAL VIBRATION
LOGARITHMIC DECREMENT vs. BLADE TIP DISPLACEMENT AS A FUNCTION OF CENTRIFUGAL LOAD
0.040
0.030
0.020
0.010
0
LOGARITHMIC DECREMENT
0
0.5
1.0
1.5
BLADE TIP DISPLACEMENT (IN x 10^+3)
CENTRIFUGAL LOAD (LBS)
4500 ±100
5250 ±100

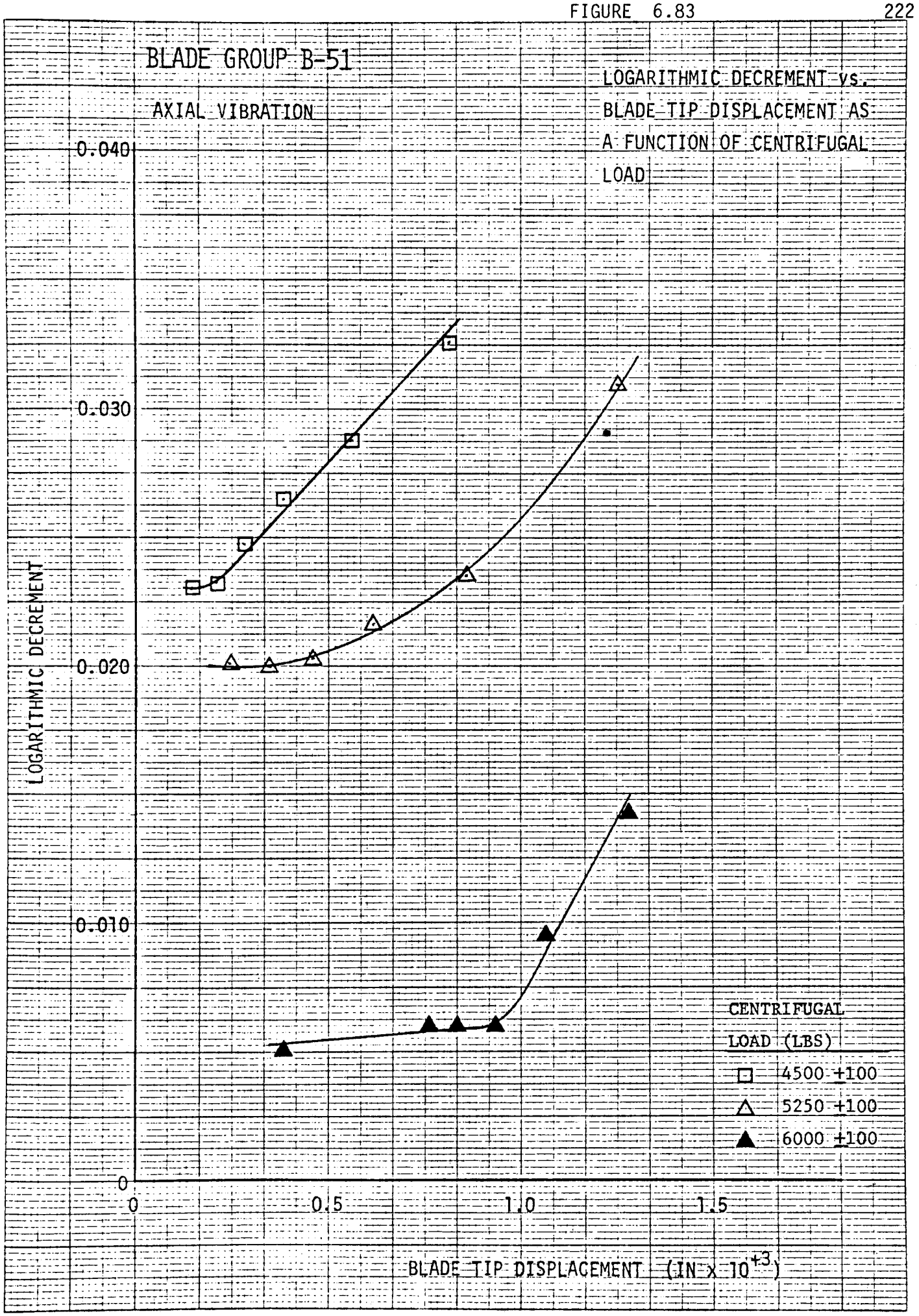
BLADE GROUP B-51
AXIAL VIBRATION
LOGARITHMIC DECREMENT vs. BLADE TIP DISPLACEMENT AS A FUNCTION OF CENTRIFUGAL LOAD
0.040
0.030
0.020
0.010
0
LOGARITHMIC DECREMENT
0
0.5
1.0
1.5
BLADE TIP DISPLACEMENT (IN x 10+3)
CENTRIFUGAL LOAD (LBS)
4500 ±100
5250 ±100
6000 ±100

FIGURE 6.84

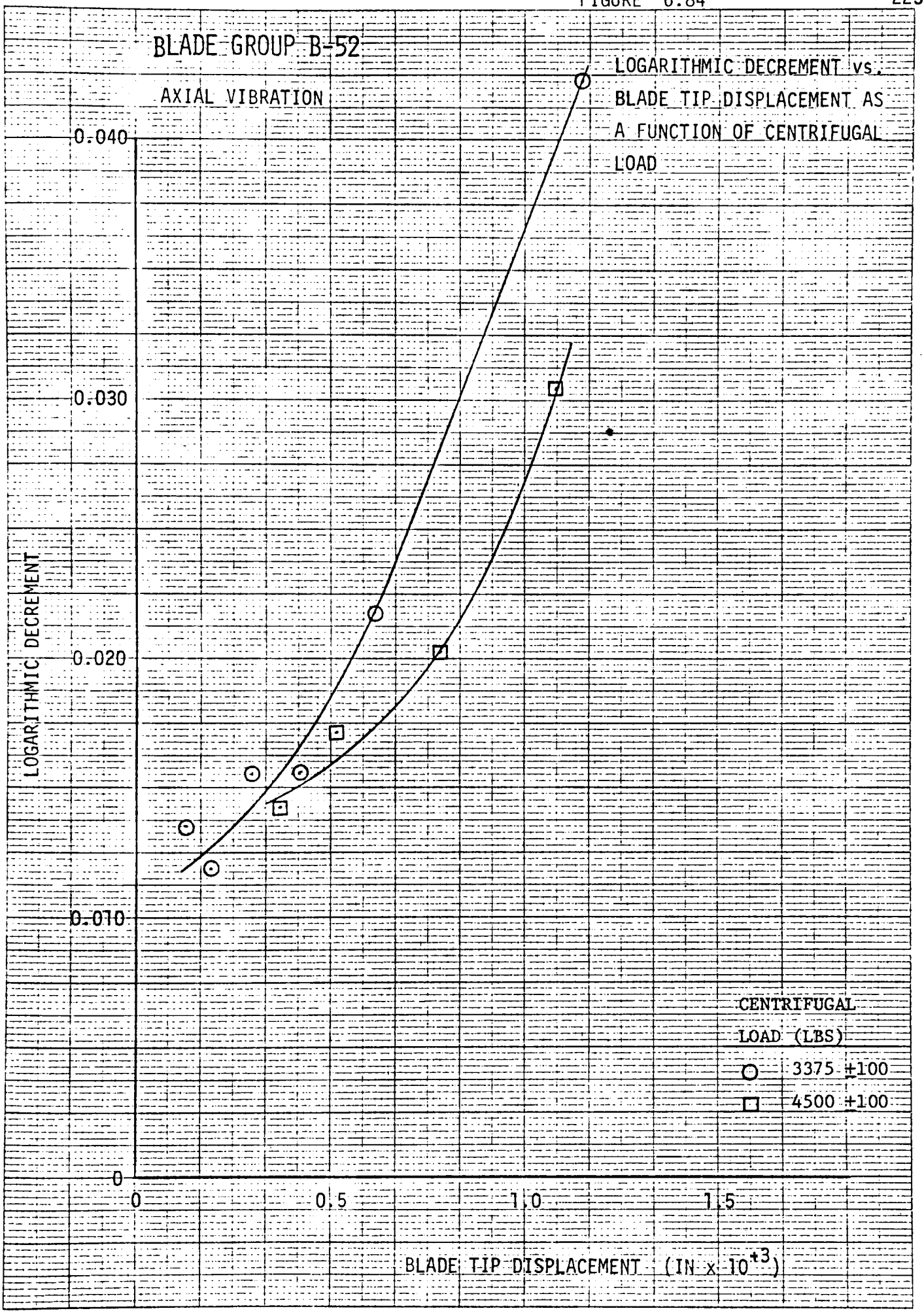
BLADE GROUP B-52
AXIAL VIBRATION
LOGARITHMIC DECREMENT vs. BLADE TIP DISPLACEMENT AS A FUNCTION OF CENTRIFUGAL LOAD
LOGARITHMIC DECREMENT
0.040
0.030
0.020
0.010
0
0
0.5
1.0
1.5
BLADE TIP DISPLACEMENT (IN x 10+3)
CENTRIFUGAL LOAD (LBS)
3375 ±100
4500 ±100

FIGURE 6.85

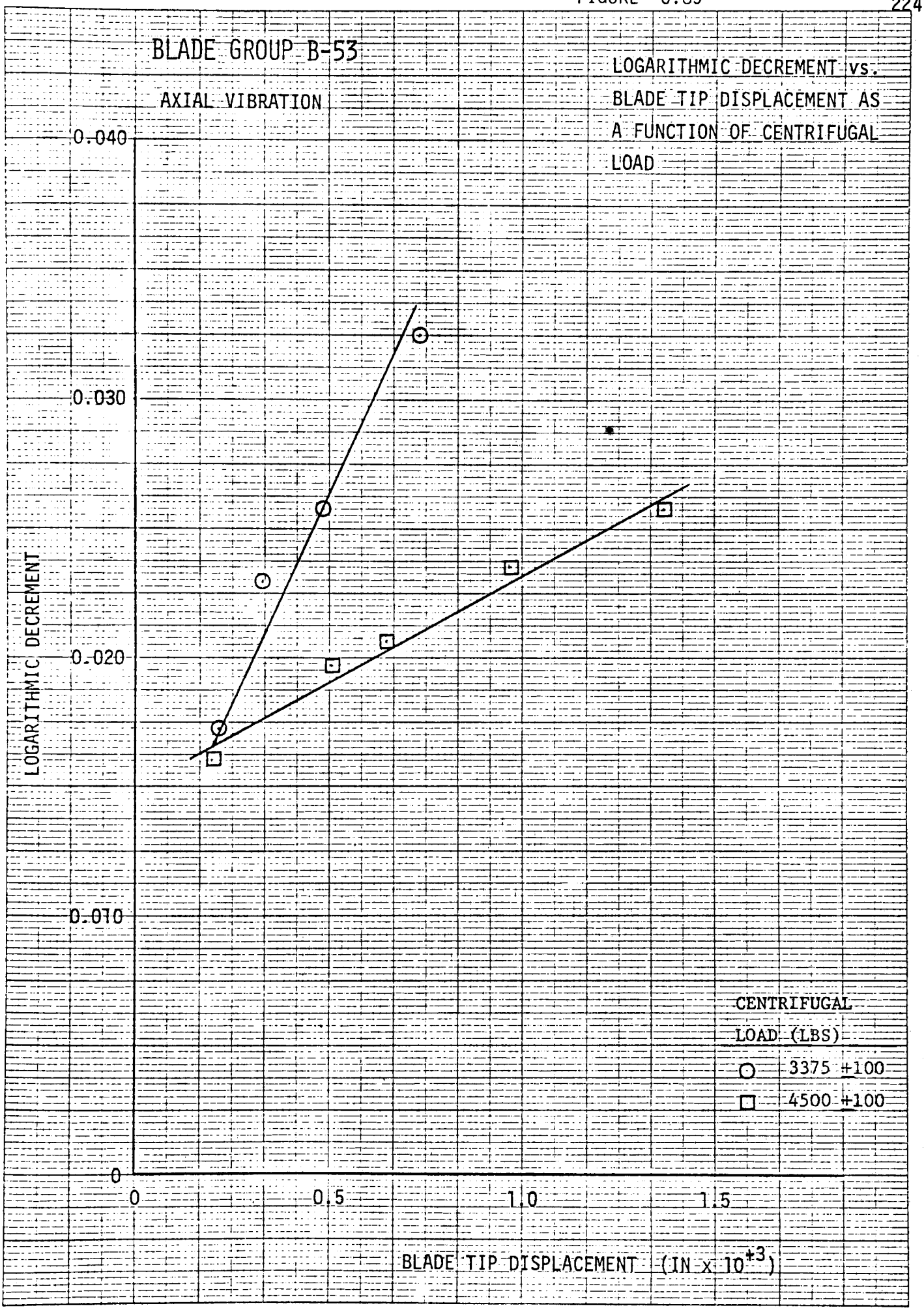
BLADE GROUP B-53
AXIAL VIBRATION
LOGARITHMIC DECREMENT vs. BLADE TIP DISPLACEMENT AS A FUNCTION OF CENTRIFUGAL LOAD
0.040
0.030
0.020
0.010
0
LOGARITHMIC DECREMENT
0
0.5
1.0
1.5
BLADE TIP DISPLACEMENT (IN x 10+3)
CENTRIFUGAL LOAD (LBS)
3375 ±100
4500 ±100

FIGURE 6.86

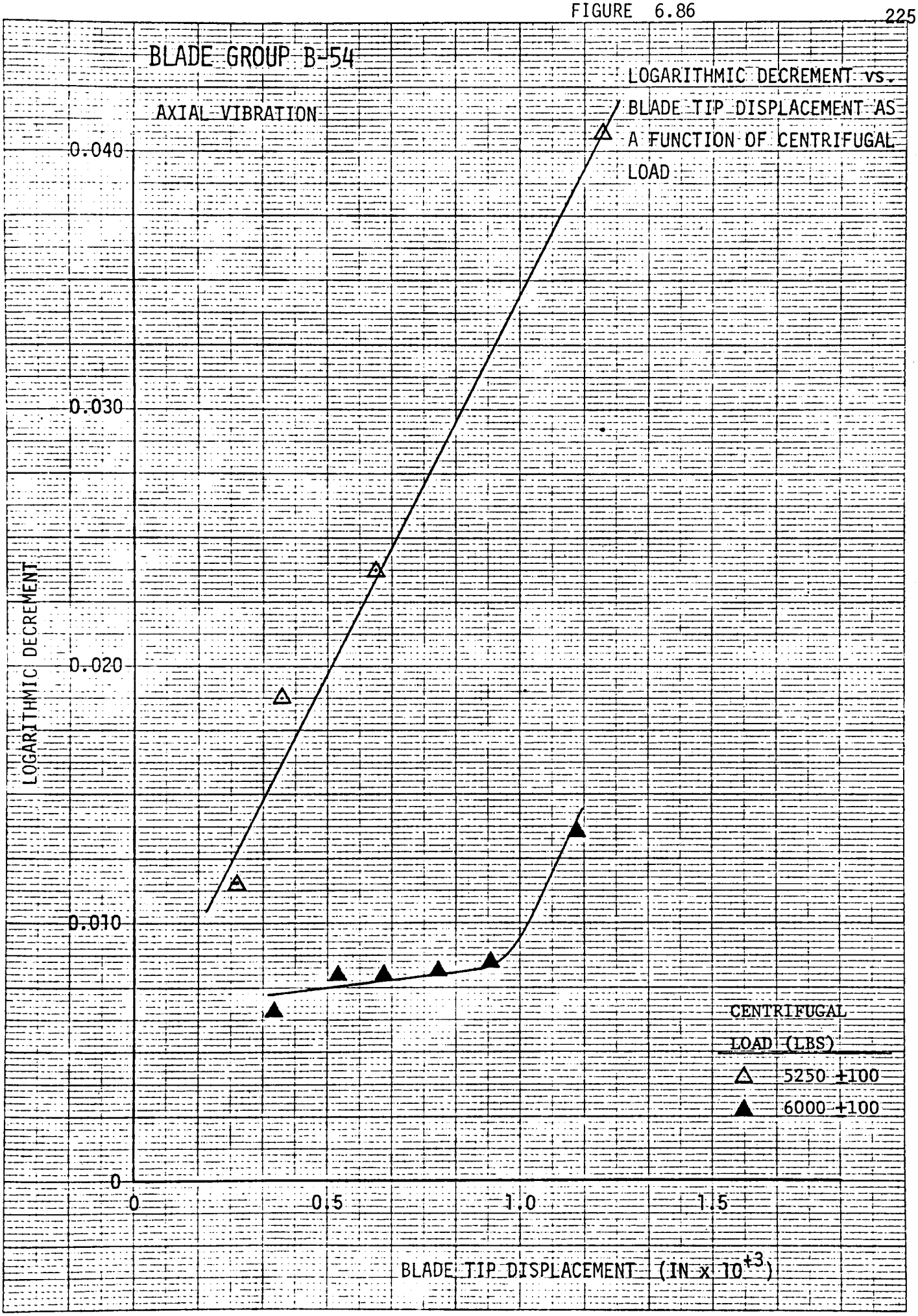
BLADE GROUP B-54
AXIAL VIBRATION
LOGARITHMIC DECREMENT vs. BLADE TIP DISPLACEMENT AS A FUNCTION OF CENTRIFUGAL LOAD
0.040
0.030
0.020
0.010
0
LOGARITHMIC DECREMENT
0
0.5
1.0
1.5
BLADE TIP DISPLACEMENT (IN x 10+3)
CENTRIFUGAL LOAD (LBS)
△ 5250 ±100
▲ 6000 ±100

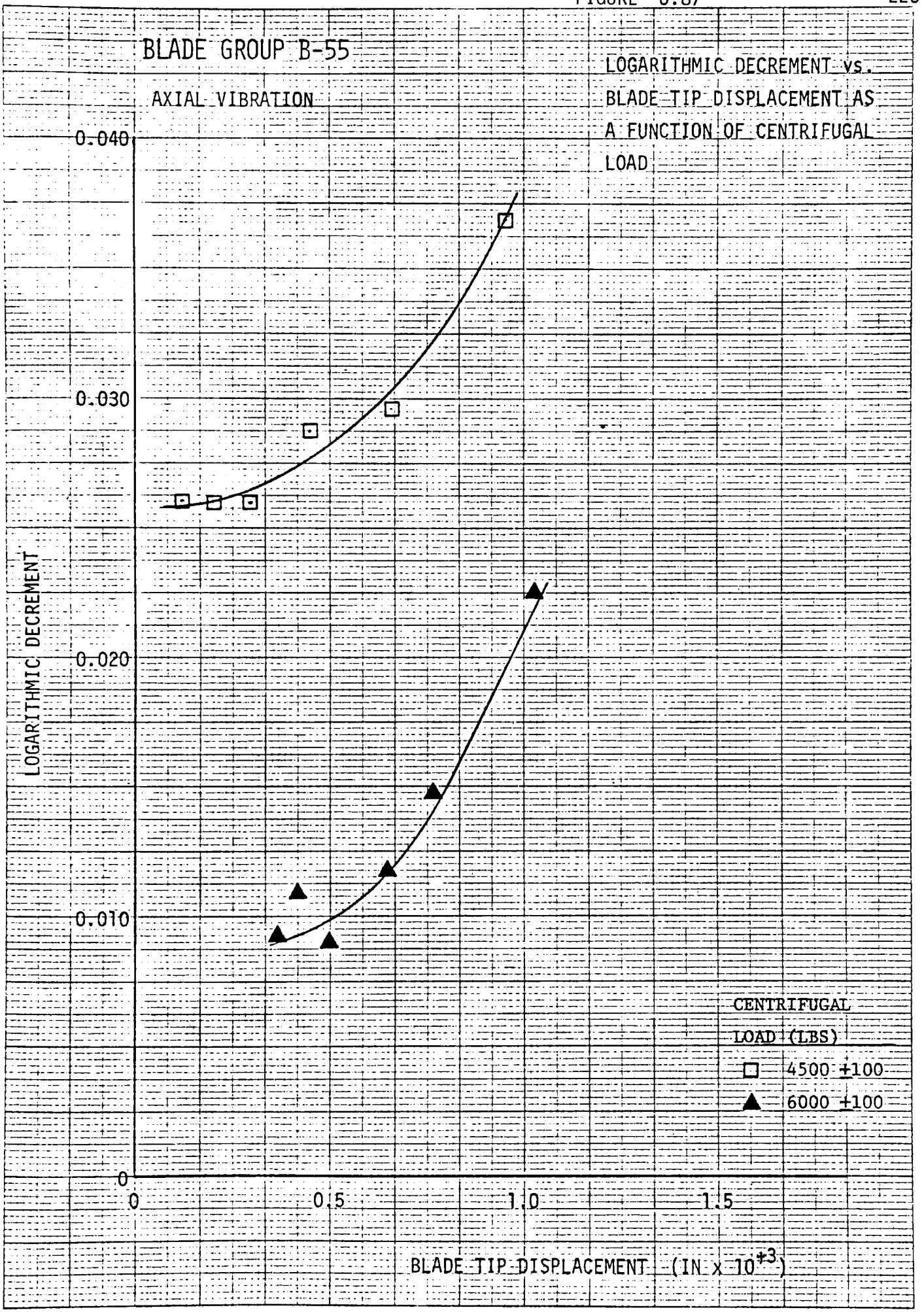
BLADE GROUP B-55
AXIAL VIBRATION
LOGARITHMIC DECREMENT vs. BLADE TIP DISPLACEMENT AS A FUNCTION OF CENTRIFUGAL LOAD
0.040
0.030
0.020
0.010
0
LOGARITHMIC DECREMENT
0
0.5
1.0
1.5
BLADE TIP DISPLACEMENT (IN x 10+3)
CENTRIFUGAL LOAD (LBS)
4500 ±100
6000 ±100

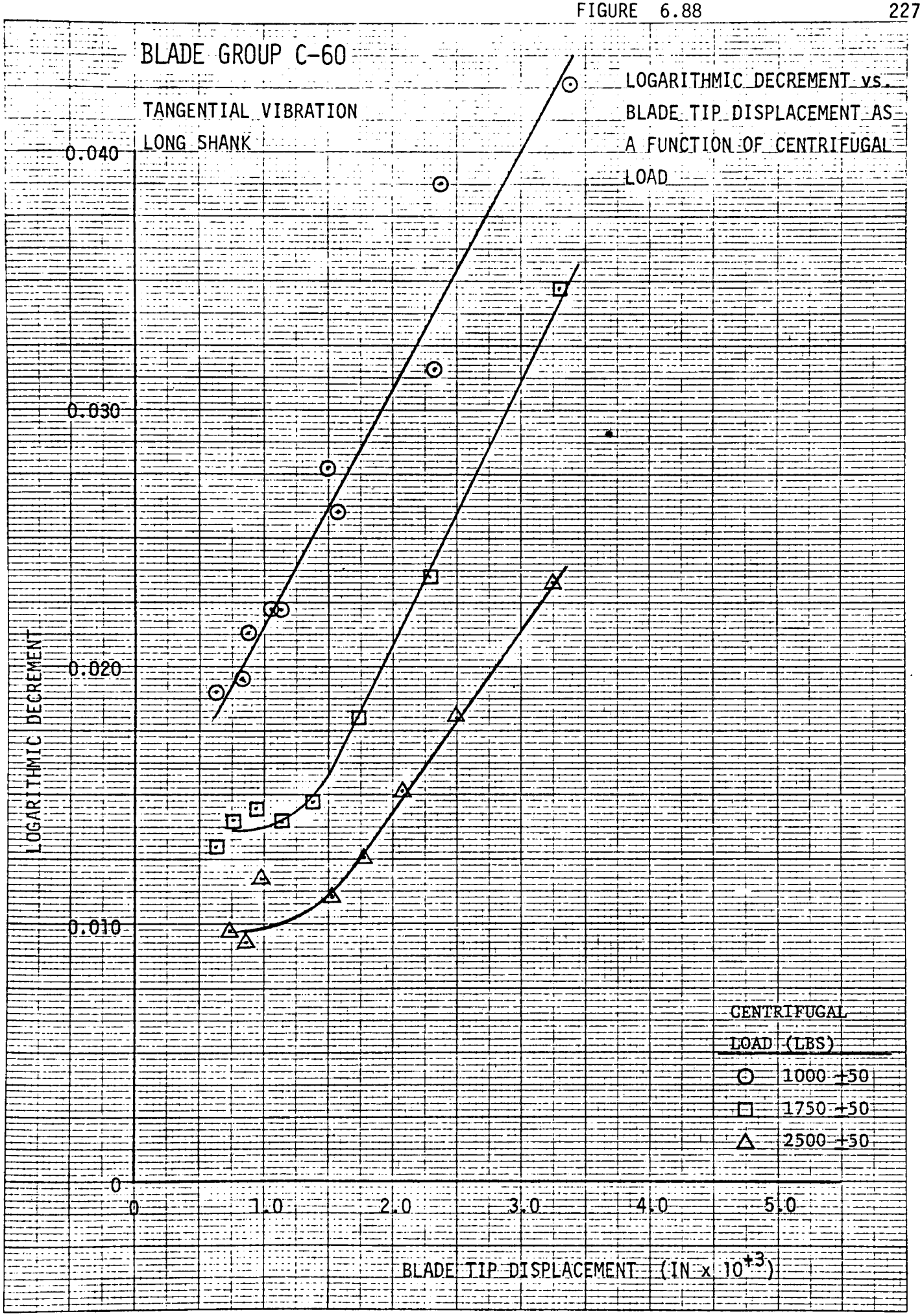
BLADE GROUP C-60
TANGENTIAL VIBRATION
LONG SHANK
LOGARITHMIC DECREMENT vs. BLADE TIP DISPLACEMENT AS A FUNCTION OF CENTRIFUGAL LOAD
0.040
0.030
0.020
0.010
0
LOGARITHMIC DECREMENT
0
1.0
2.0
3.0
4.0
5.0
BLADE TIP DISPLACEMENT (IN x 10+3)
CENTRIFUGAL LOAD (LBS)
1000 ±50
1750 ±50
2500 ±50

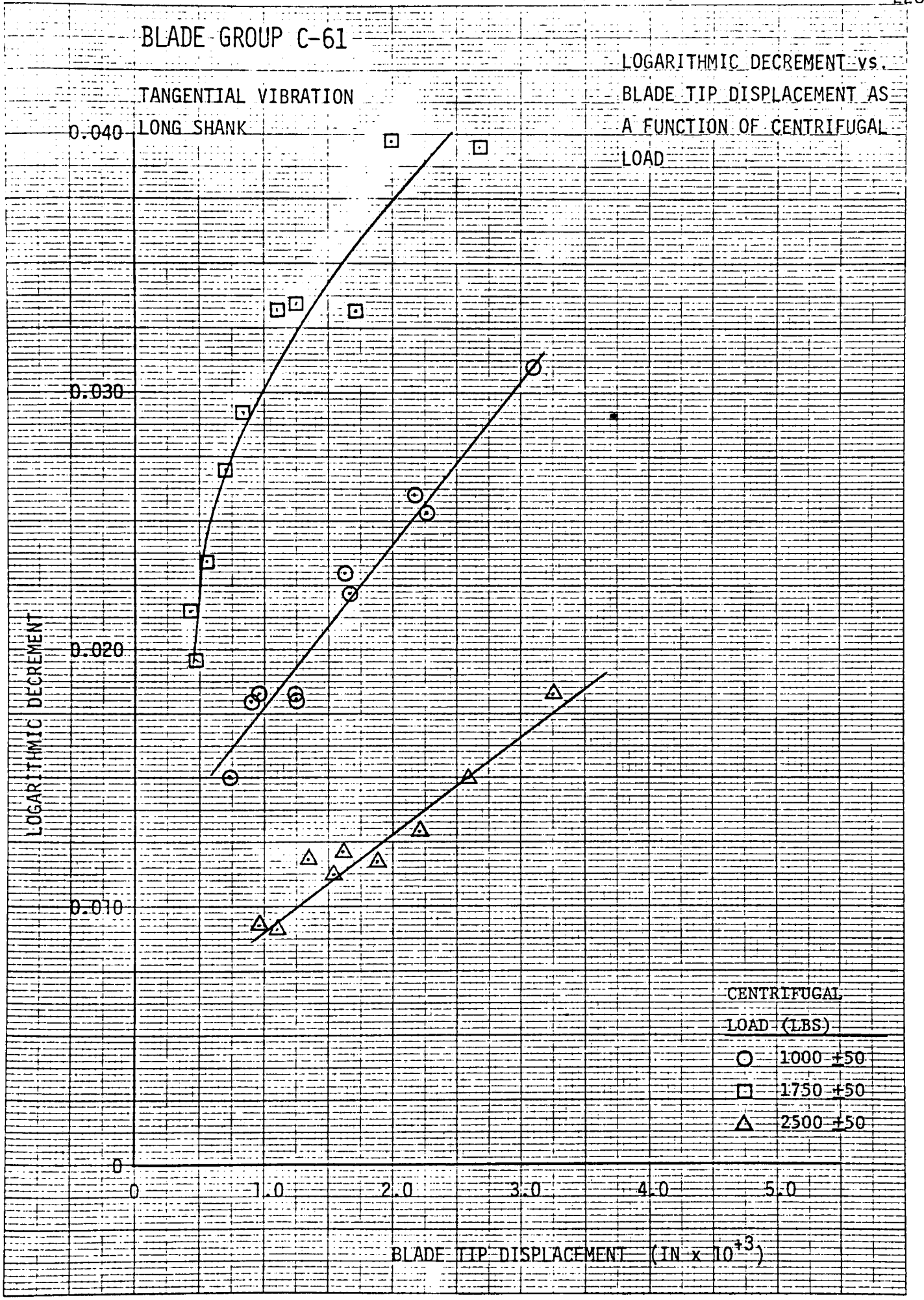
BLADE GROUP C-61
TANGENTIAL VIBRATION
LONG SHANK
LOGARITHMIC DECREMENT vs. BLADE TIP DISPLACEMENT AS A FUNCTION OF CENTRIFUGAL LOAD
0.040
0.030
0.020
0.010
0
LOGARITHMIC DECREMENT
0
1.0
2.0
3.0
4.0
5.0
BLADE TIP DISPLACEMENT (IN x 10+3)
CENTRIFUGAL LOAD (LBS)
1000 ±50
1750 ±50
2500 ±50

FIGURE 6.90

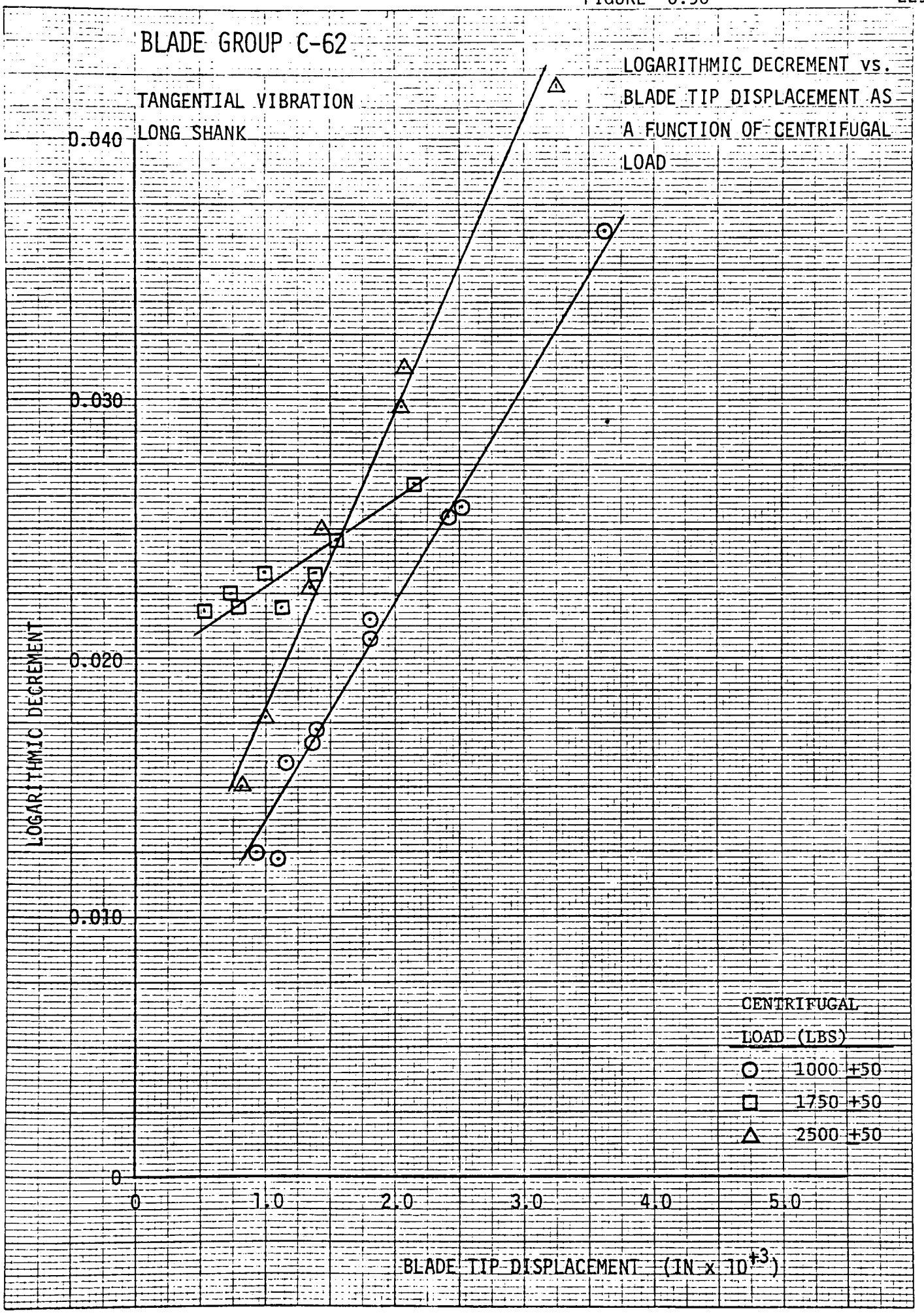
BLADE GROUP C-62
TANGENTIAL VIBRATION
LONG SHANK
LOGARITHMIC DECREMENT vs. BLADE TIP DISPLACEMENT AS A FUNCTION OF CENTRIFUGAL LOAD
0.040
0.030
0.020
0.010
0
LOGARITHMIC DECREMENT
0
1.0
2.0
3.0
4.0
5.0
BLADE TIP DISPLACEMENT (IN x 10+3)
CENTRIFUGAL LOAD (LBS)
1000 ±50
1750 ±50
2500 ±50

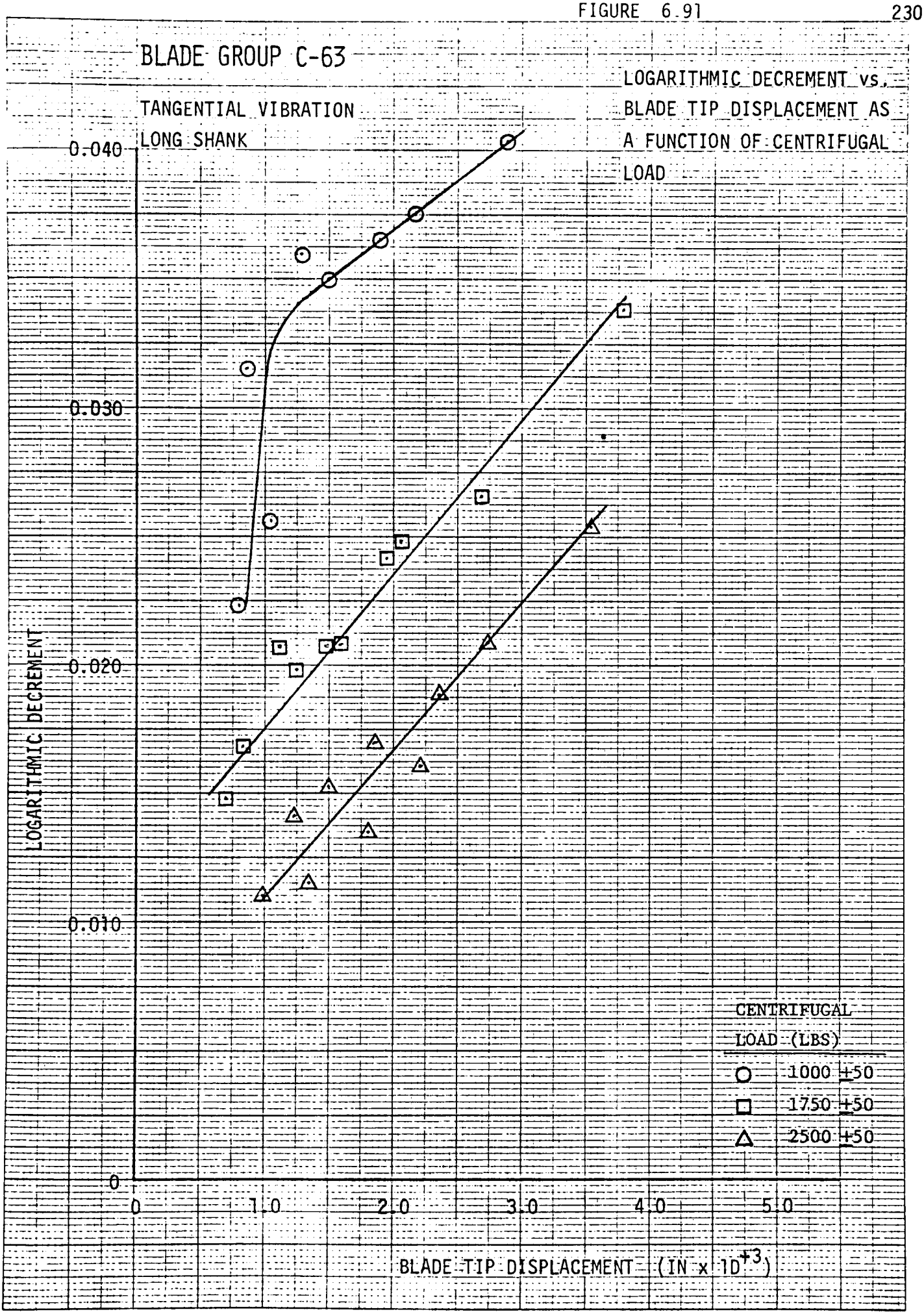
BLADE GROUP C-63
TANGENTIAL VIBRATION
LONG SHANK
LOGARITHMIC DECREMENT vs. BLADE TIP DISPLACEMENT AS A FUNCTION OF CENTRIFUGAL LOAD
LOGARITHMIC DECREMENT
0.040
0.030
0.020
0.010
0
0
1.0
2.0
3.0
4.0
5.0
BLADE TIP DISPLACEMENT (IN x 10+3)
CENTRIFUGAL LOAD (LBS)
1000 ±50
1750 ±50
2500 ±50

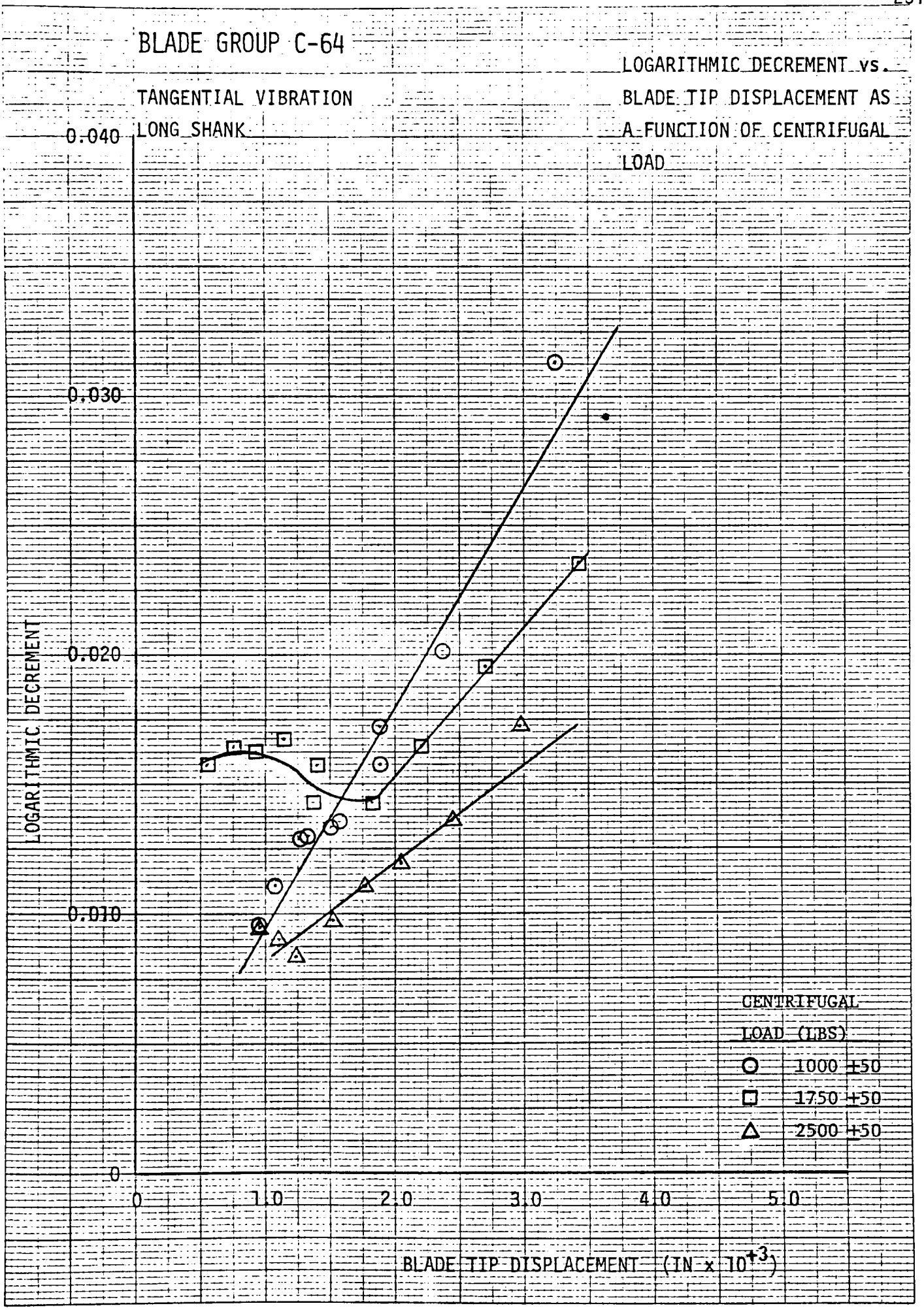
BLADE GROUP C-64
TANGENTIAL VIBRATION
LONG SHANK
LOGARITHMIC DECREMENT vs. BLADE TIP DISPLACEMENT AS A FUNCTION OF CENTRIFUGAL LOAD
0.040
0.030
0.020
0.010
0
LOGARITHMIC DECREMENT
0
1.0
2.0
3.0
4.0
5.0
BLADE TIP DISPLACEMENT (IN x 10+3)
CENTRIFUGAL LOAD (LBS)
1000 ±50
1750 ±50
2500 ±50

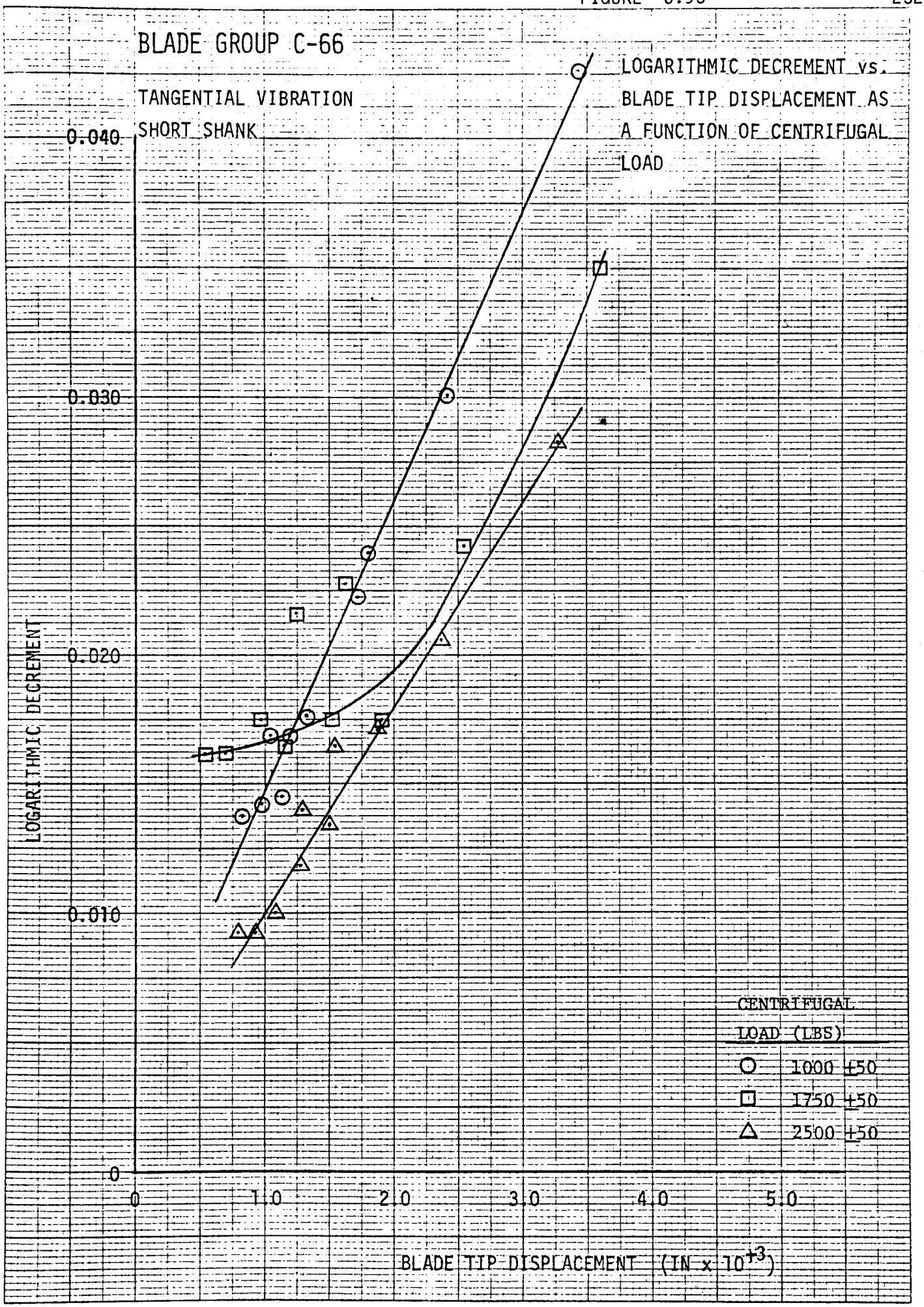
BLADE GROUP C-66
TANGENTIAL VIBRATION
SHORT SHANK
LOGARITHMIC DECREMENT vs. BLADE TIP DISPLACEMENT AS A FUNCTION OF CENTRIFUGAL LOAD
LOGARITHMIC DECREMENT
0.040
0.030
0.020
0.010
0
0
1.0
2.0
3.0
4.0
5.0
BLADE TIP DISPLACEMENT (IN x 10+3)
CENTRIFUGAL LOAD (LBS)
1000 ±50
1750 ±50
2500 ±50

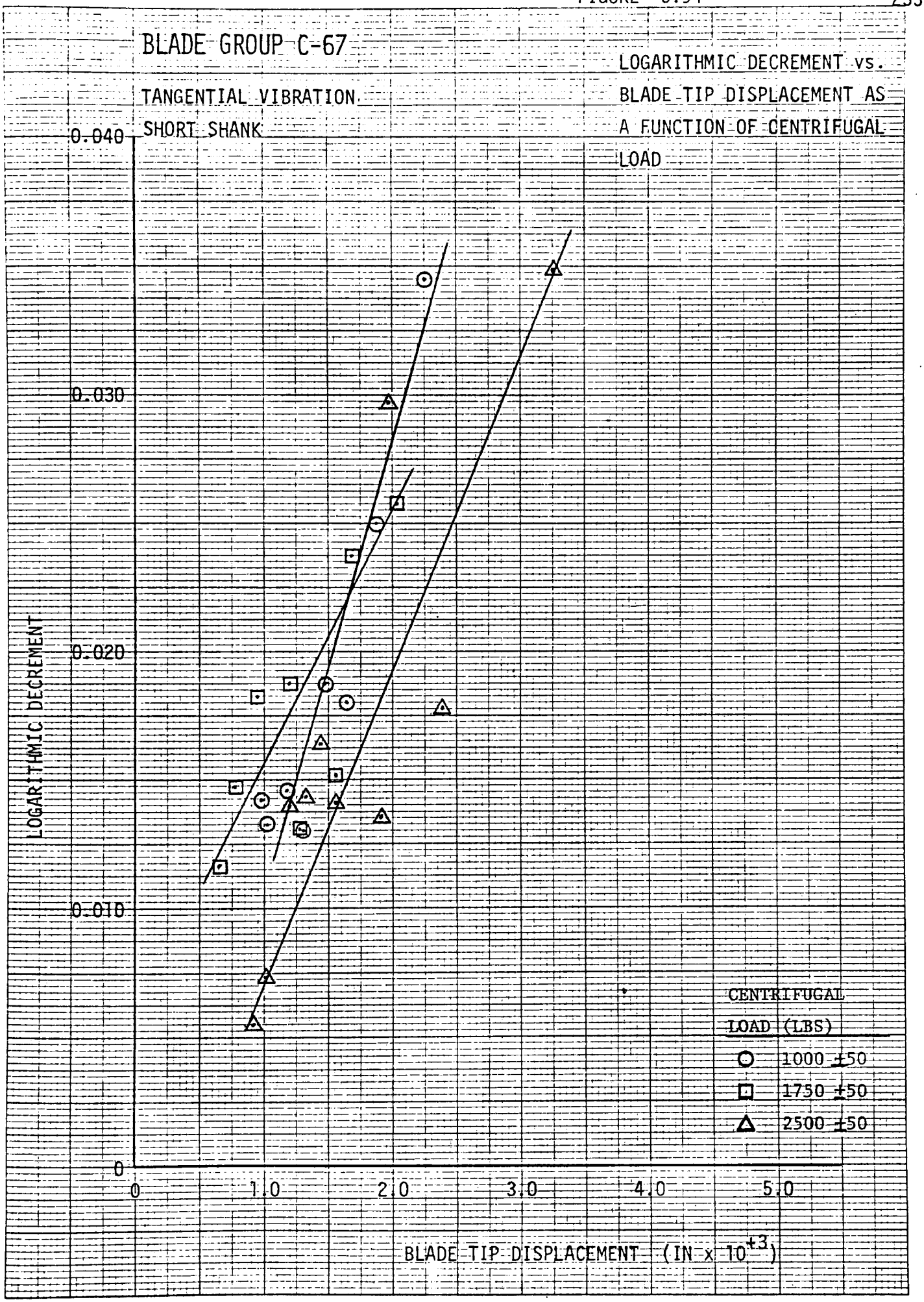
BLADE GROUP C-67
TANGENTIAL VIBRATION
SHORT SHANK
LOGARITHMIC DECREMENT vs. BLADE TIP DISPLACEMENT AS A FUNCTION OF CENTRIFUGAL LOAD
0.040
0.030
0.020
0.010
0
LOGARITHMIC DECREMENT
0
1.0
2.0
3.0
4.0
5.0
BLADE TIP DISPLACEMENT (IN x 10+3)
CENTRIFUGAL LOAD (LBS)
1000 ±50
1750 ±50
2500 ±50

FIGURE 6.95

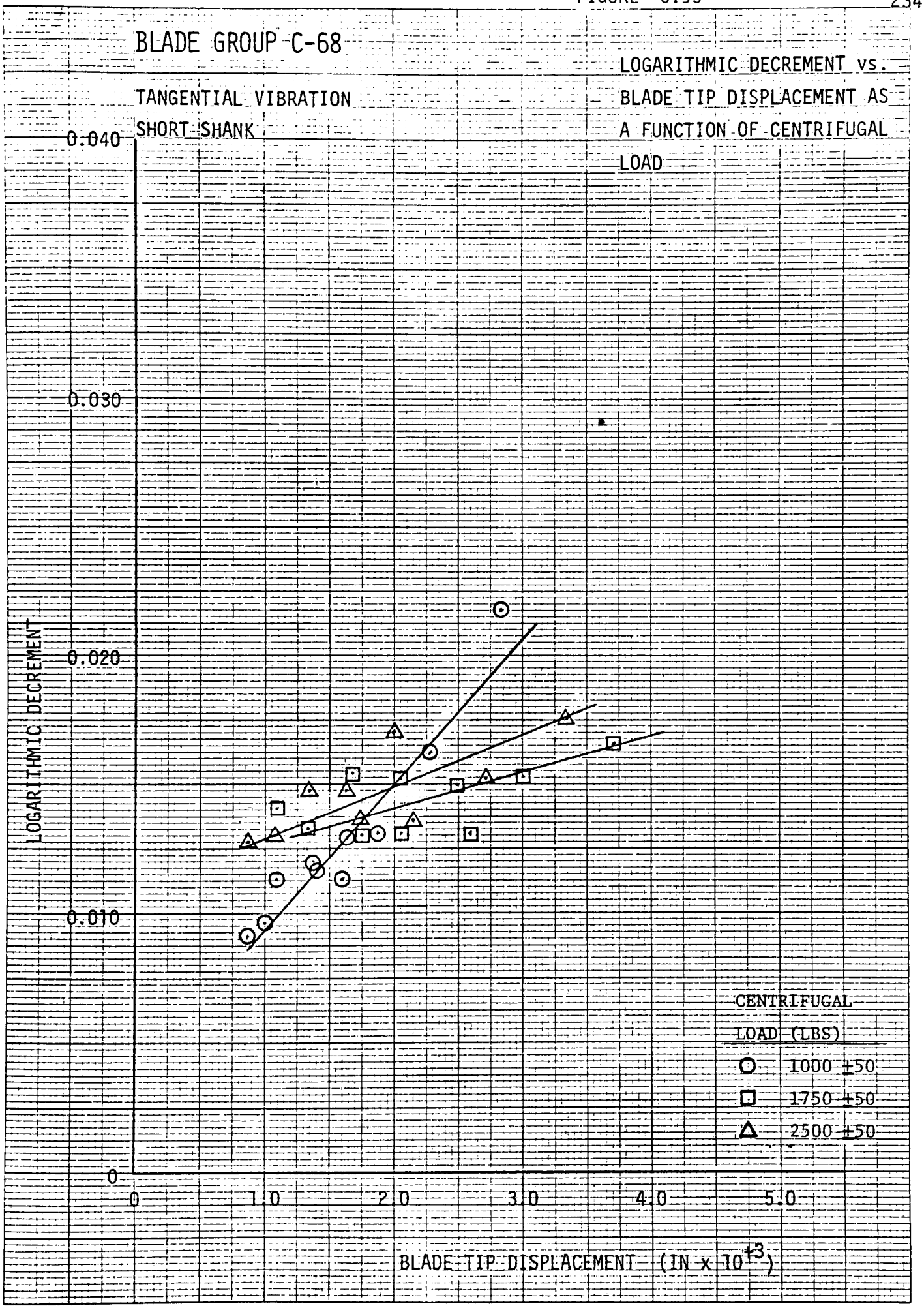
BLADE GROUP C-68
TANGENTIAL VIBRATION
SHORT SHANK
LOGARITHMIC DECREMENT vs. BLADE TIP DISPLACEMENT AS A FUNCTION OF CENTRIFUGAL LOAD
0.040
0.030
0.020
0.010
0
LOGARITHMIC DECREMENT
0
1.0
2.0
3.0
4.0
5.0
BLADE TIP DISPLACEMENT (IN x 10+3)
CENTRIFUGAL LOAD (LBS)
1000 ±50
1750 ±50
2500 ±50

FIGURE 6.96

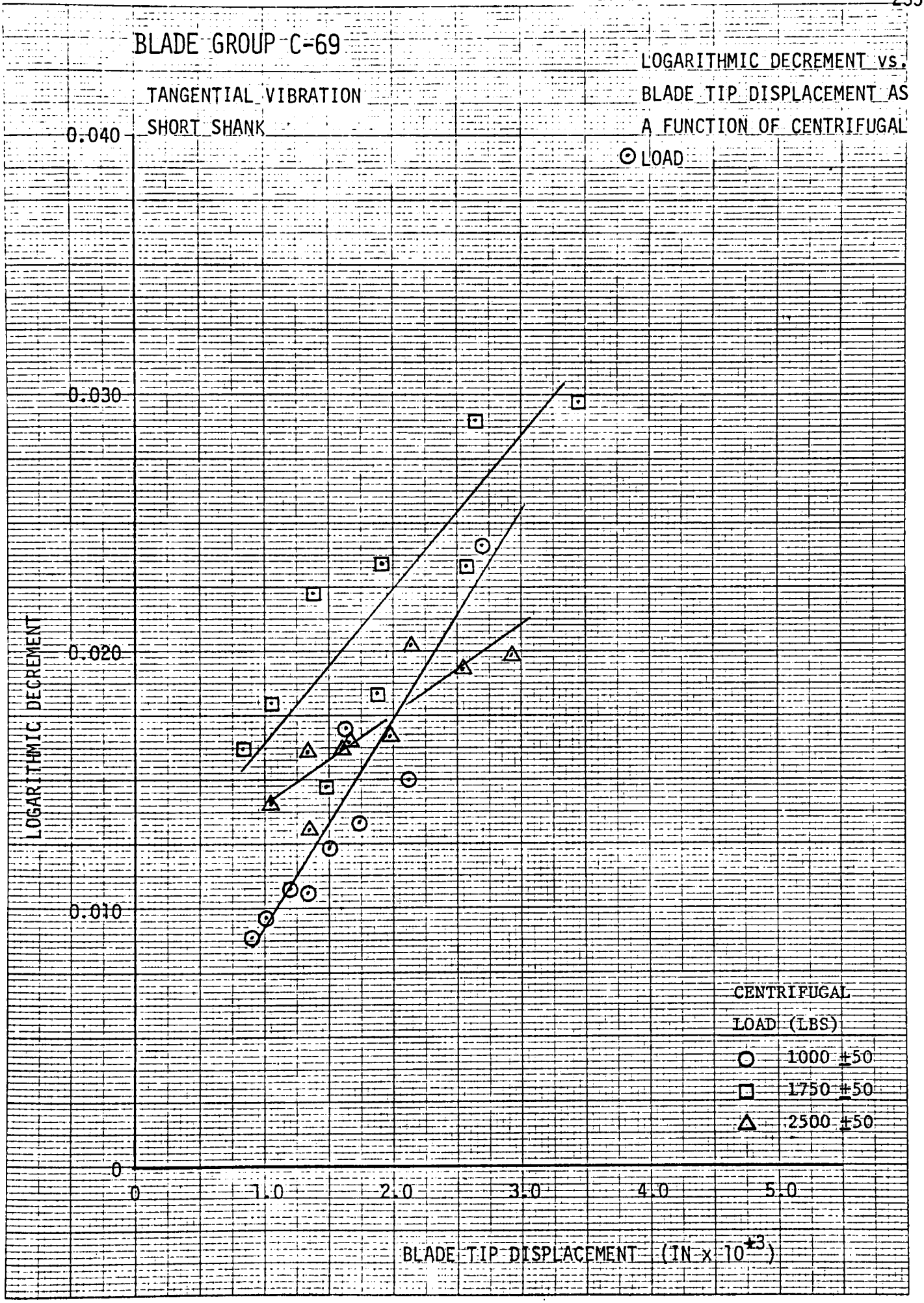
BLADE GROUP C-69
TANGENTIAL VIBRATION
SHORT SHANK
LOGARITHMIC DECREMENT vs.
BLADE TIP DISPLACEMENT AS
A FUNCTION OF CENTRIFUGAL
LOAD
0.040
0.030
0.020
0.010
0
LOGARITHMIC DECREMENT
0
1.0
2.0
3.0
4.0
5.0
BLADE TIP DISPLACEMENT (IN x 10**3)
CENTRIFUGAL
LOAD (LBS)
1000 ±50
1750 ±50
2500 ±50

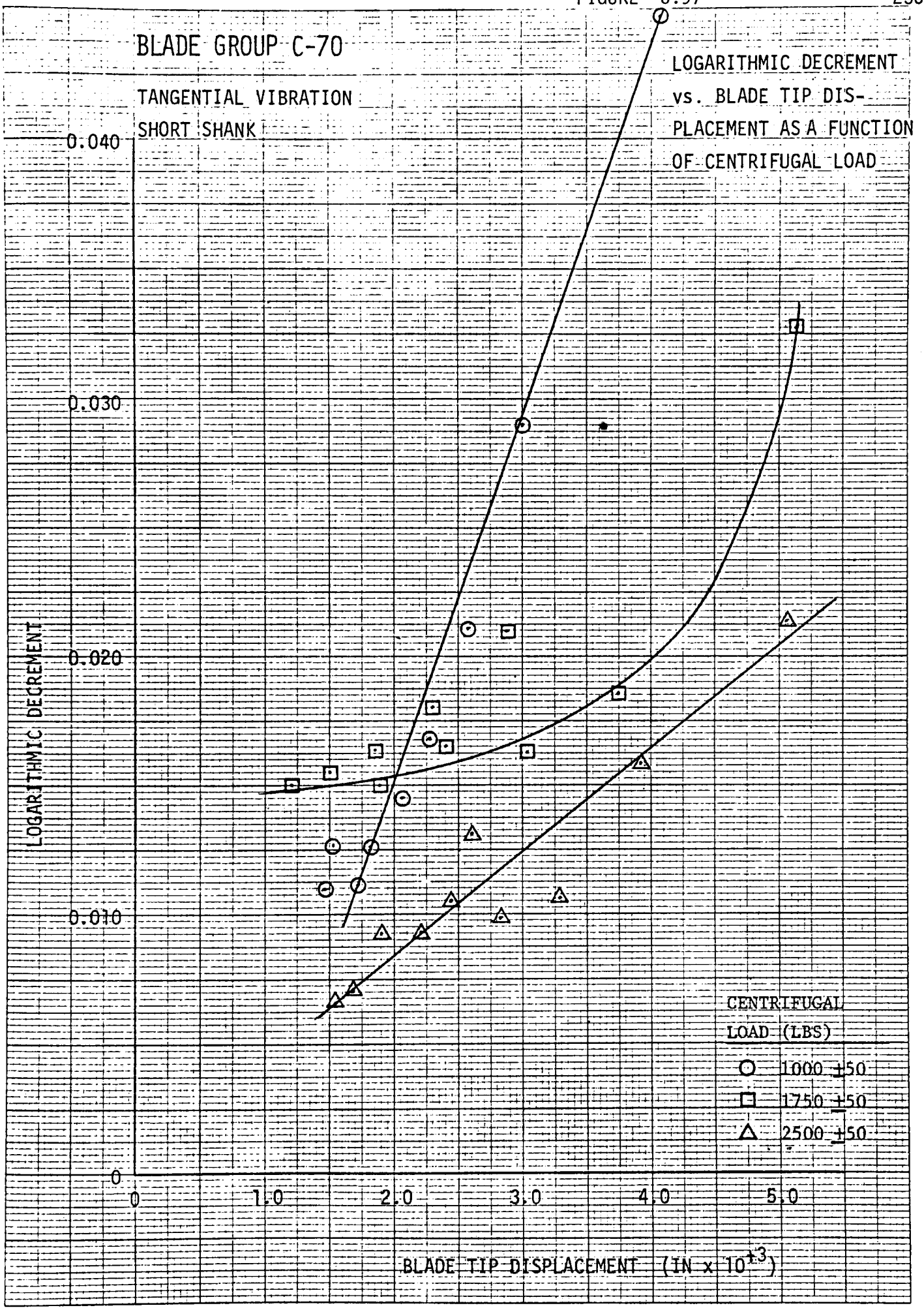
BLADE GROUP C-70
TANGENTIAL VIBRATION
SHORT SHANK
LOGARITHMIC DECREMENT vs. BLADE TIP DISPLACEMENT AS A FUNCTION OF CENTRIFUGAL LOAD
LOGARITHMIC DECREMENT
0.040
0.030
0.020
0.010
0
0
1.0
2.0
3.0
4.0
5.0
BLADE TIP DISPLACEMENT (IN x 10+3)
CENTRIFUGAL LOAD (LBS)
1000 ±50
1750 ±50
2500 ±50

FIGURE 6.98

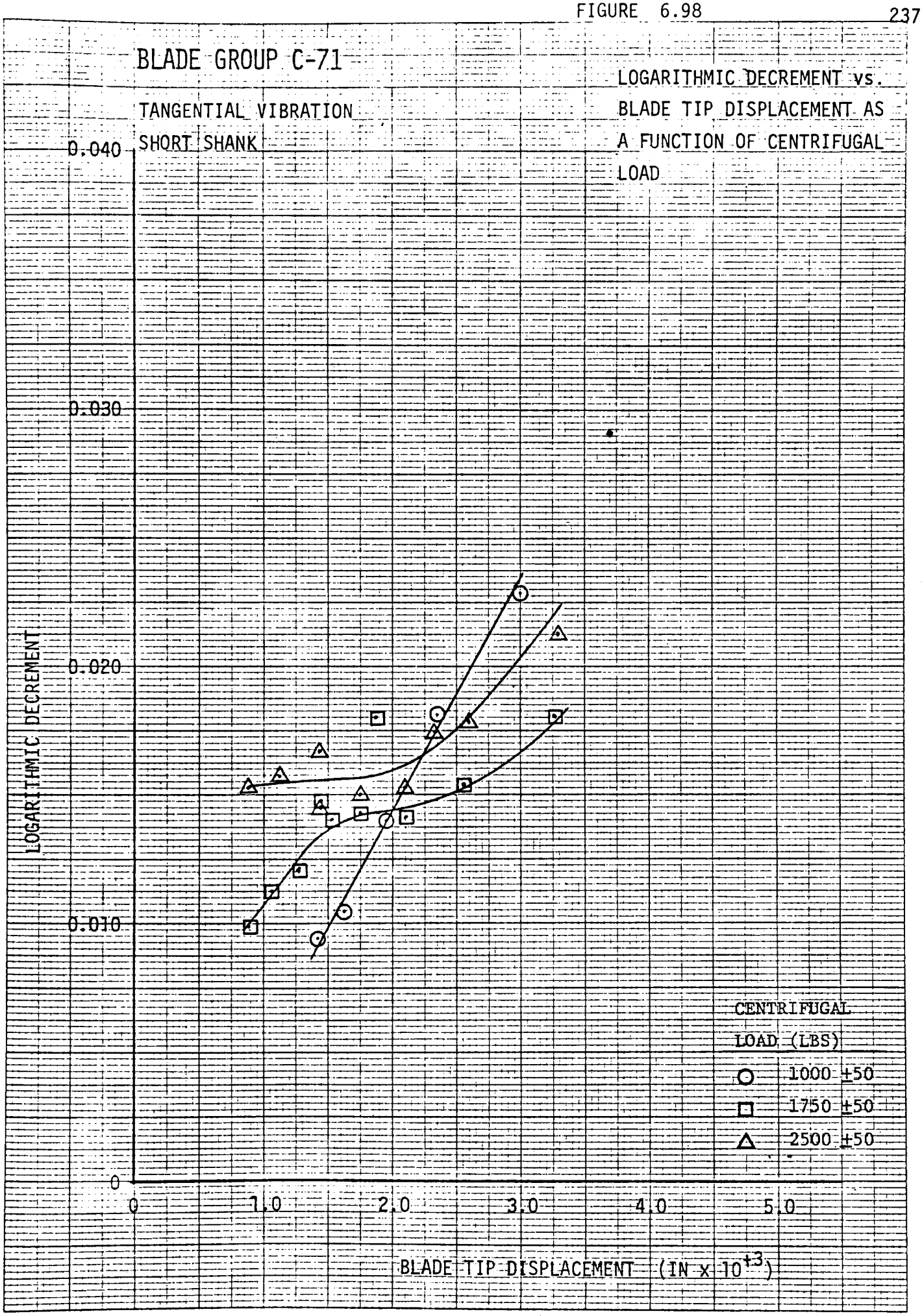
BLADE GROUP C-71
TANGENTIAL VIBRATION
SHORT SHANK
LOGARITHMIC DECREMENT vs. BLADE TIP DISPLACEMENT AS A FUNCTION OF CENTRIFUGAL LOAD
0.040
0.030
0.020
0.010
0
LOGARITHMIC DECREMENT
0
1.0
2.0
3.0
4.0
5.0
BLADE TIP DISPLACEMENT (IN x 10+3)
CENTRIFUGAL LOAD (LBS)
1000 ±50
1750 ±50
2500 ±50

FIGURE 6.99

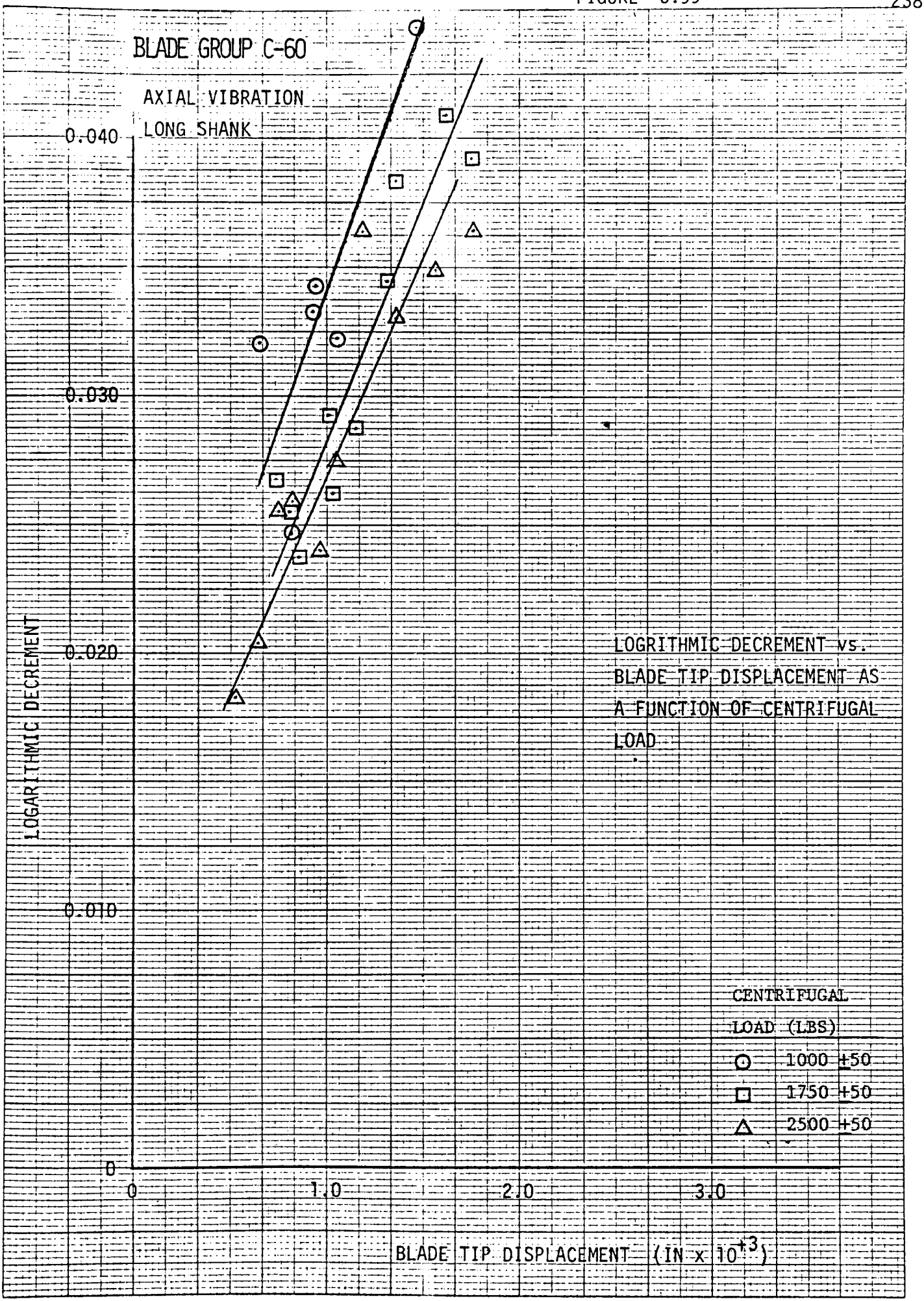

LOGRITHMIC DECREMENT vs. BLADE TIP DISPLACEMENT AS A FUNCTION OF CENTRIFUGAL LOAD

FIGURE 6.100

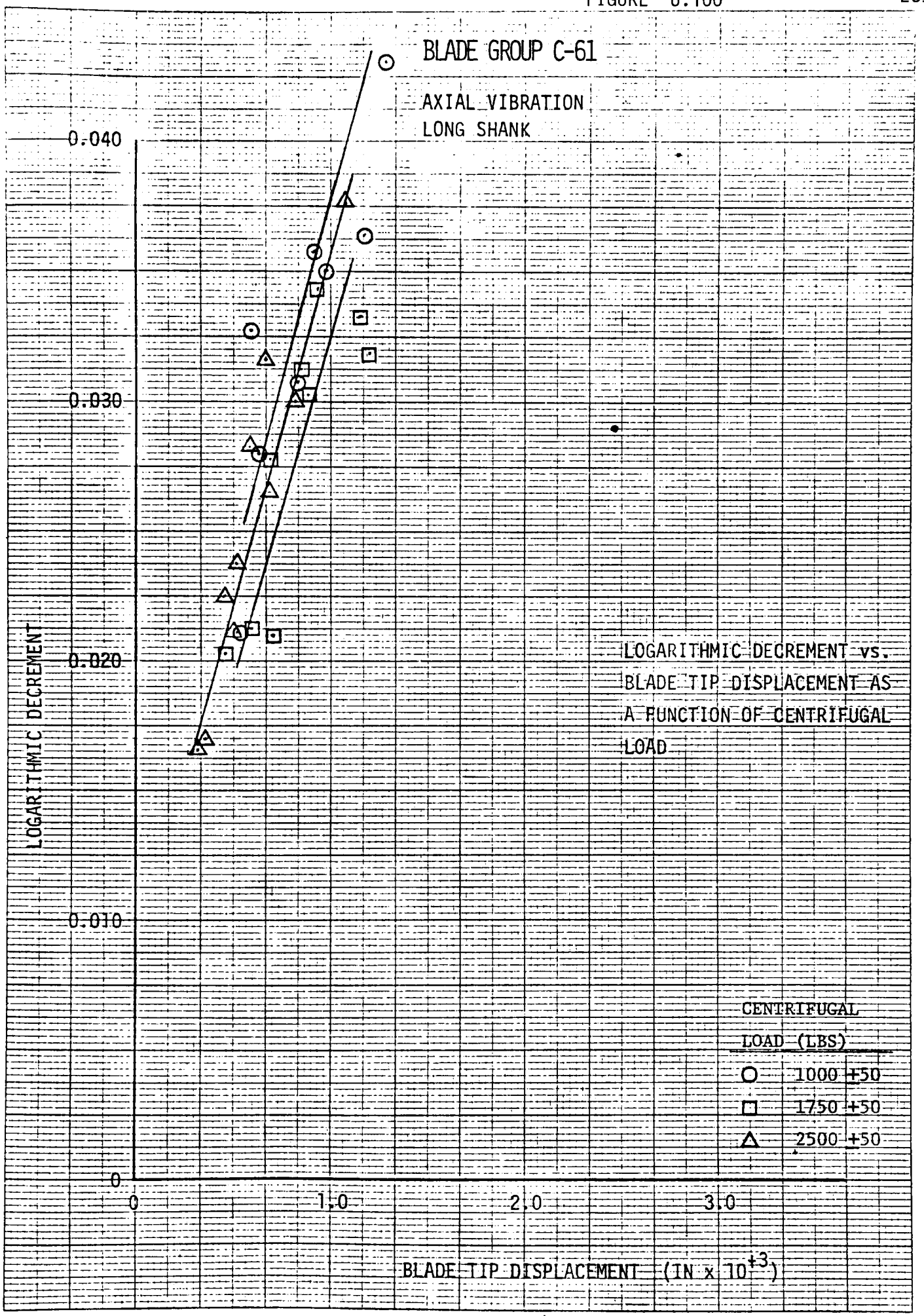
BLADE GROUP C-61
AXIAL VIBRATION
LONG SHANK
0.040
0.030
0.020
0.010
0
LOGARITHMIC DECREMENT
0
1.0
2.0
3.0
BLADE TIP DISPLACEMENT (IN x 10+3)
LOGARITHMIC DECREMENT vs. BLADE TIP DISPLACEMENT AS A FUNCTION OF CENTRIFUGAL LOAD
CENTRIFUGAL LOAD (LBS)
1000 +50
1750 +50
2500 +50

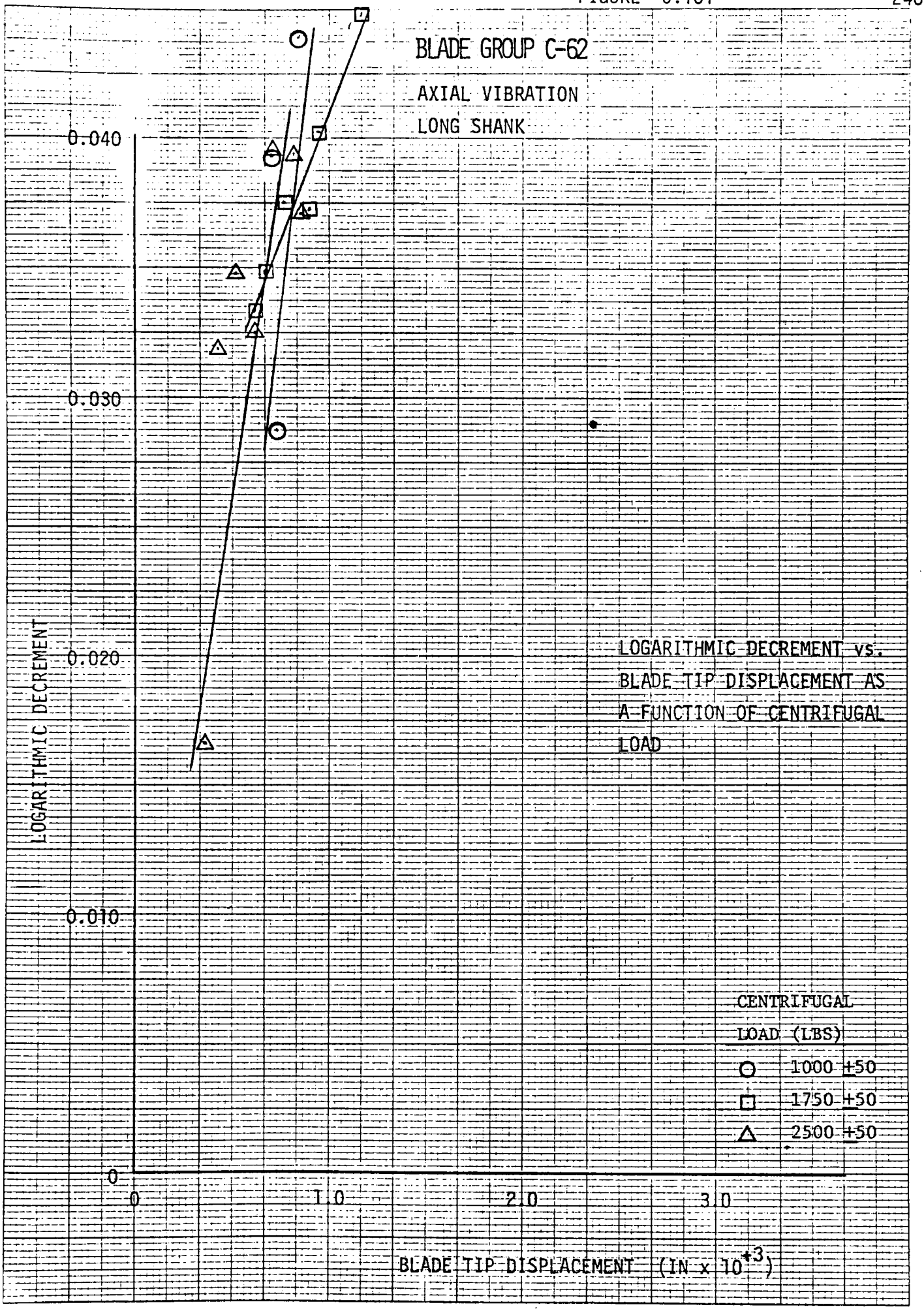
BLADE GROUP C-62
AXIAL VIBRATION
LONG SHANK
0.040
0.030
0.020
0.010
0
LOGARITHMIC DECREMENT
LOGARITHMIC DECREMENT vs. BLADE TIP DISPLACEMENT AS A FUNCTION OF CENTRIFUGAL LOAD
CENTRIFUGAL LOAD (LBS)
1000 ±50
1750 ±50
2500 ±50
0
1.0
2.0
3.0
BLADE TIP DISPLACEMENT (IN x 10+3)

FIGURE 6.102

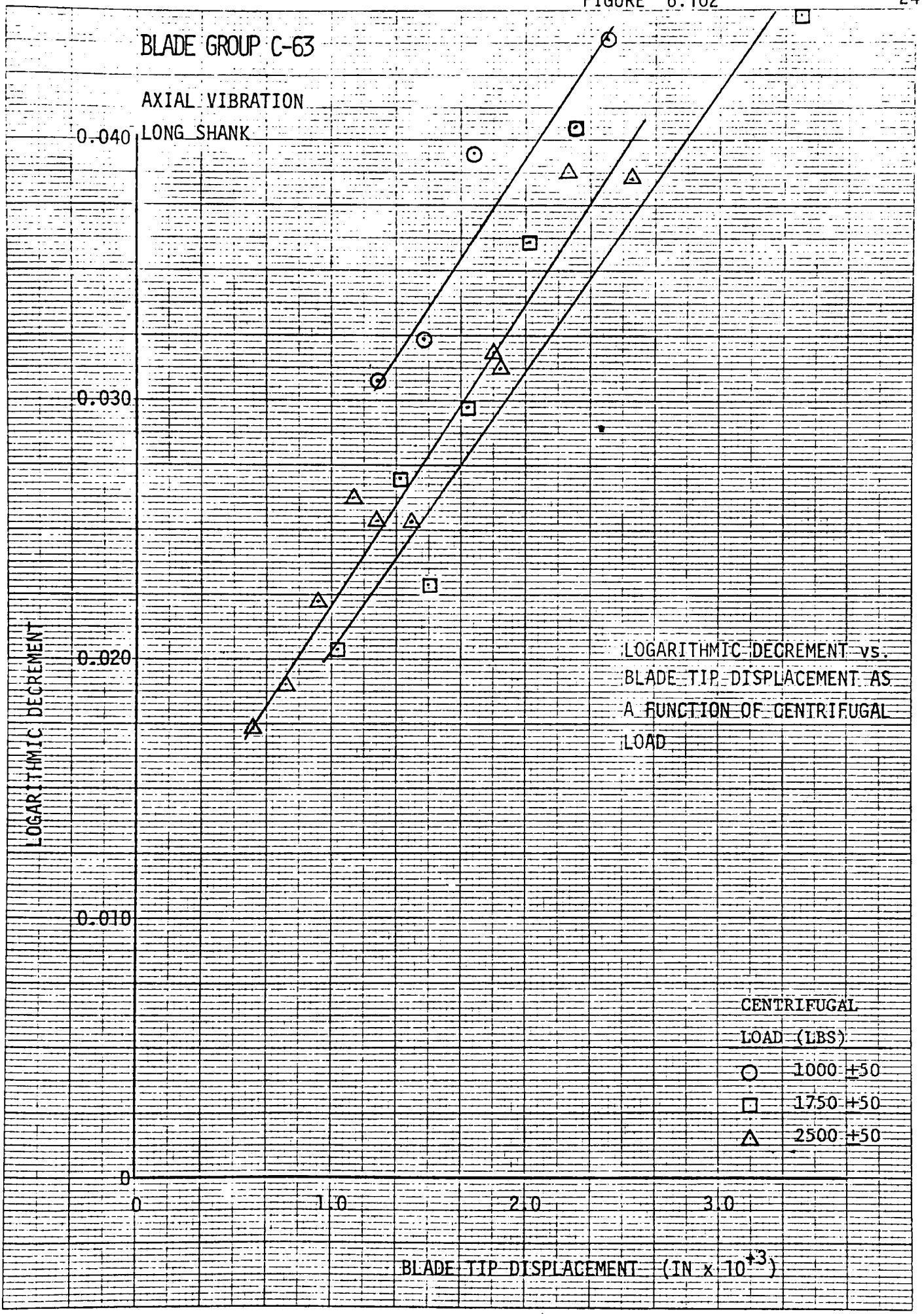
BLADE GROUP C-63
AXIAL VIBRATION
LONG SHANK
0.040
0.030
0.020
0.010
0
LOGARITHMIC DECREMENT
0
1.0
2.0
3.0
BLADE TIP DISPLACEMENT (IN x 10+3)
LOGARITHMIC DECREMENT vs. BLADE TIP DISPLACEMENT AS A FUNCTION OF CENTRIFUGAL LOAD
CENTRIFUGAL LOAD (LBS)
1000 ±50
1750 ±50
2500 ±50

FIGURE 6.103

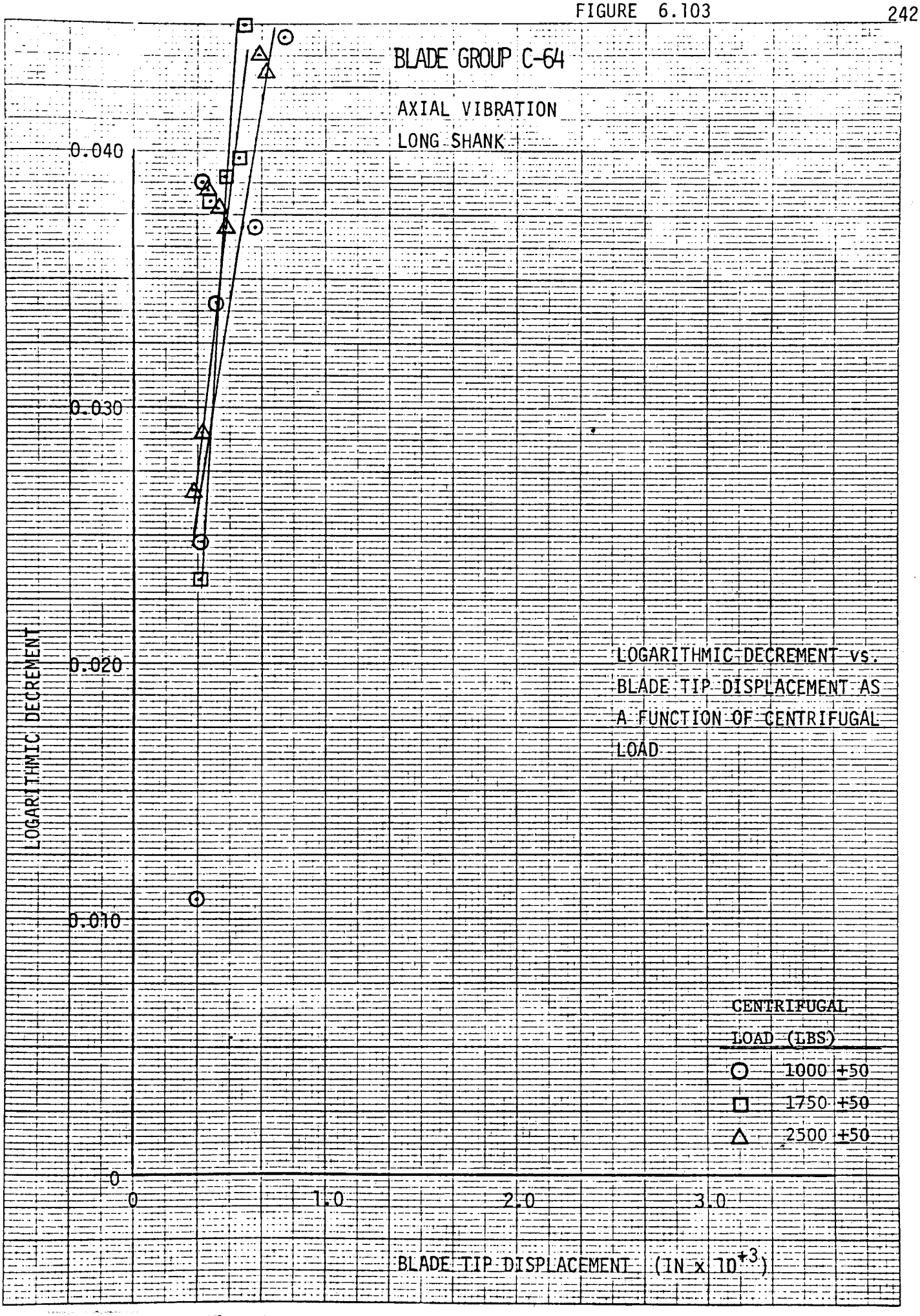
BLADE GROUP C-64
AXIAL VIBRATION
LONG SHANK
0.040
0.030
0.020
0.010
0
LOGARITHMIC DECREMENT
LOGARITHMIC DECREMENT vs. BLADE TIP DISPLACEMENT AS A FUNCTION OF CENTRIFUGAL LOAD
CENTRIFUGAL LOAD (LBS)
1000 ±50
1750 ±50
2500 ±50
0
1.0
2.0
3.0
BLADE TIP DISPLACEMENT (IN x 10+3)

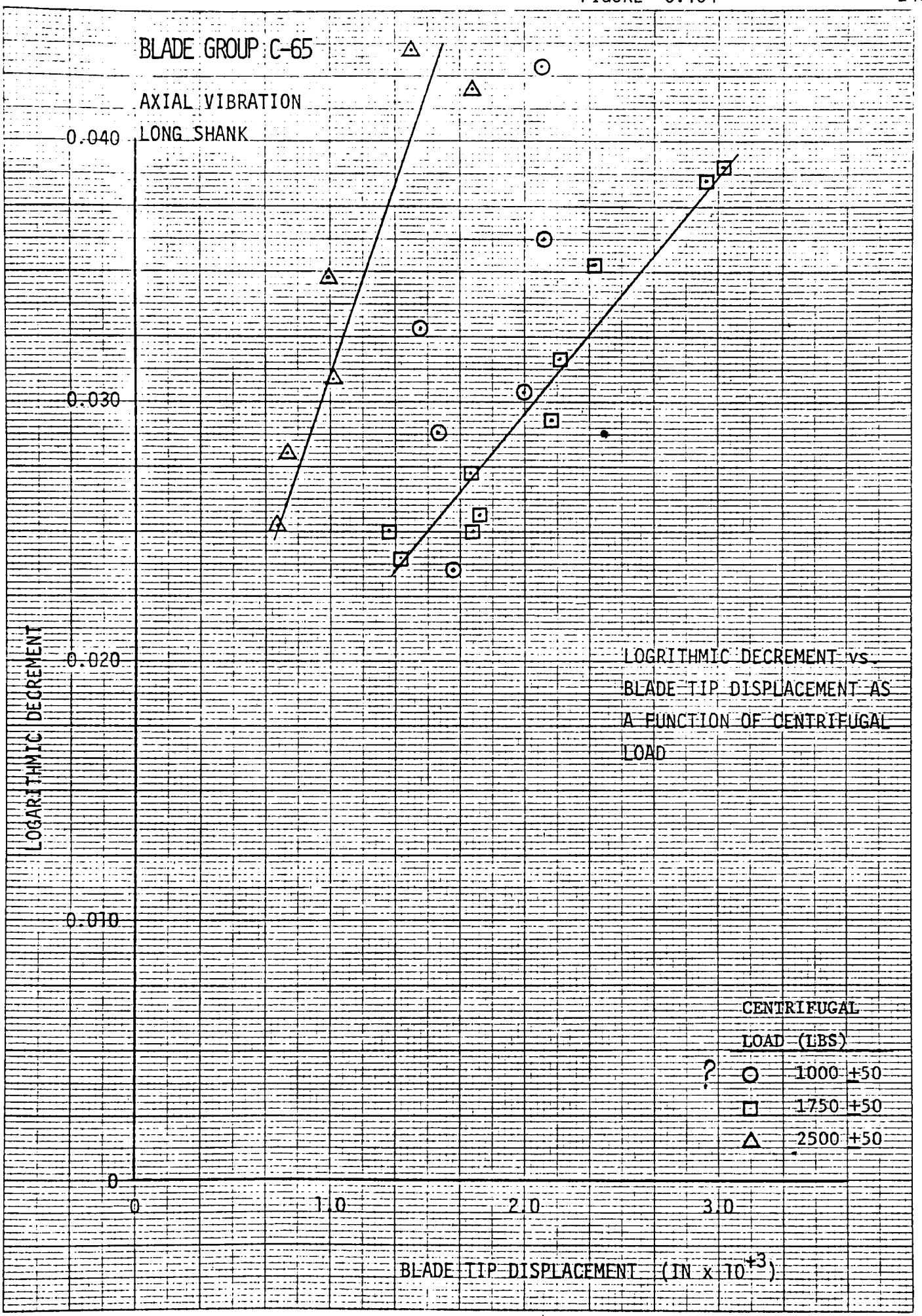
BLADE GROUP C-65
AXIAL VIBRATION
LONG SHANK
0.040
0.030
0.020
0.010
0
LOGARITHMIC DECREMENT
0
1.0
2.0
3.0
BLADE TIP DISPLACEMENT (IN x 10+3)
LOGRITHMIC DECREMENT vs. BLADE TIP DISPLACEMENT AS A FUNCTION OF CENTRIFUGAL LOAD
CENTRIFUGAL LOAD (LBS)
1000 ±50
1750 ±50
2500 ±50

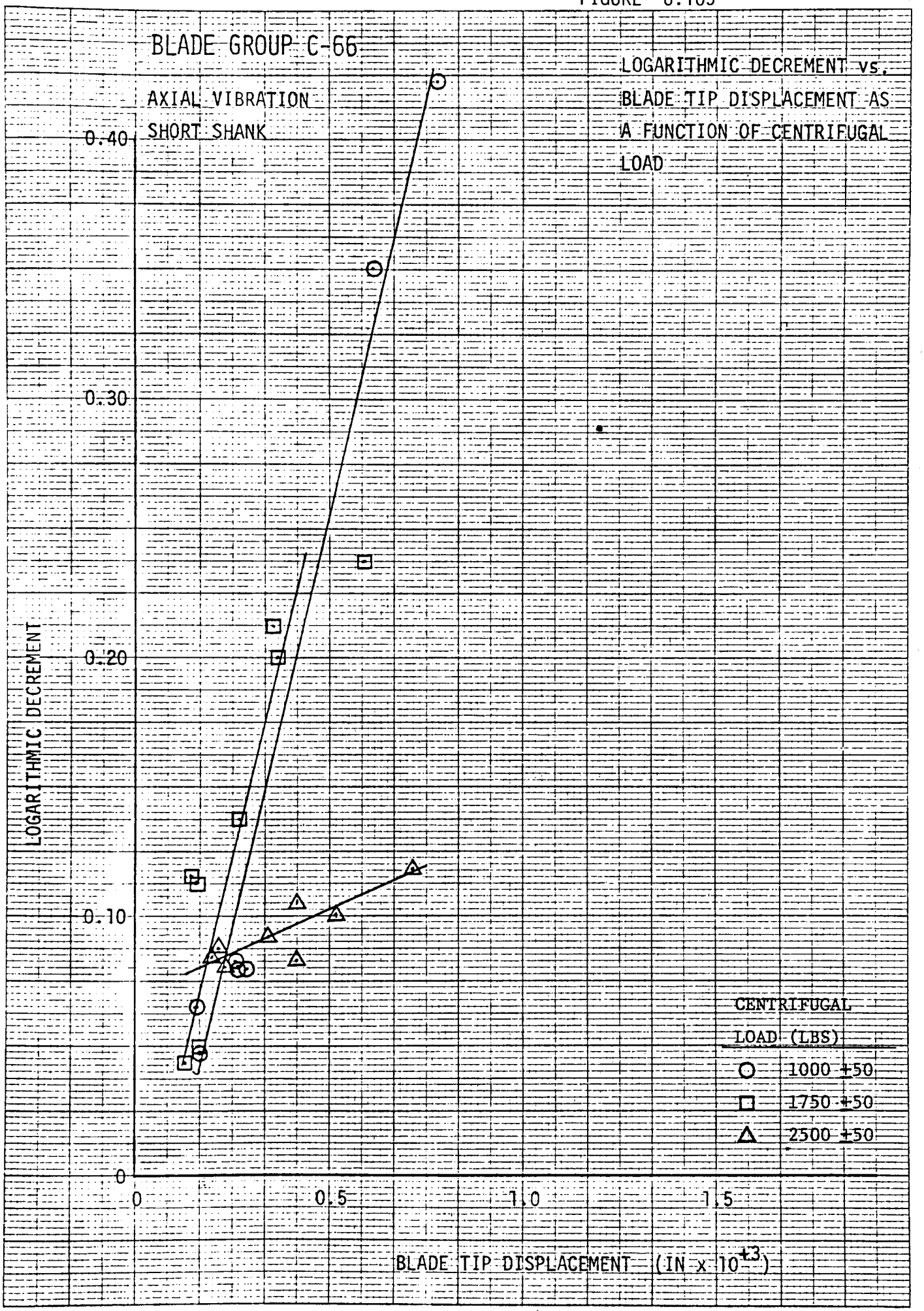
BLADE GROUP C-66
AXIAL VIBRATION
SHORT SHANK
LOGARITHMIC DECREMENT vs. BLADE TIP DISPLACEMENT AS A FUNCTION OF CENTRIFUGAL LOAD
LOGARITHMIC DECREMENT
0.40
0.30
0.20
0.10
0
0
0.5
1.0
1.5
BLADE TIP DISPLACEMENT (IN x 10+3)
CENTRIFUGAL LOAD (LBS)
1000 ±50
1750 ±50
2500 ±50

FIGURE 6.106

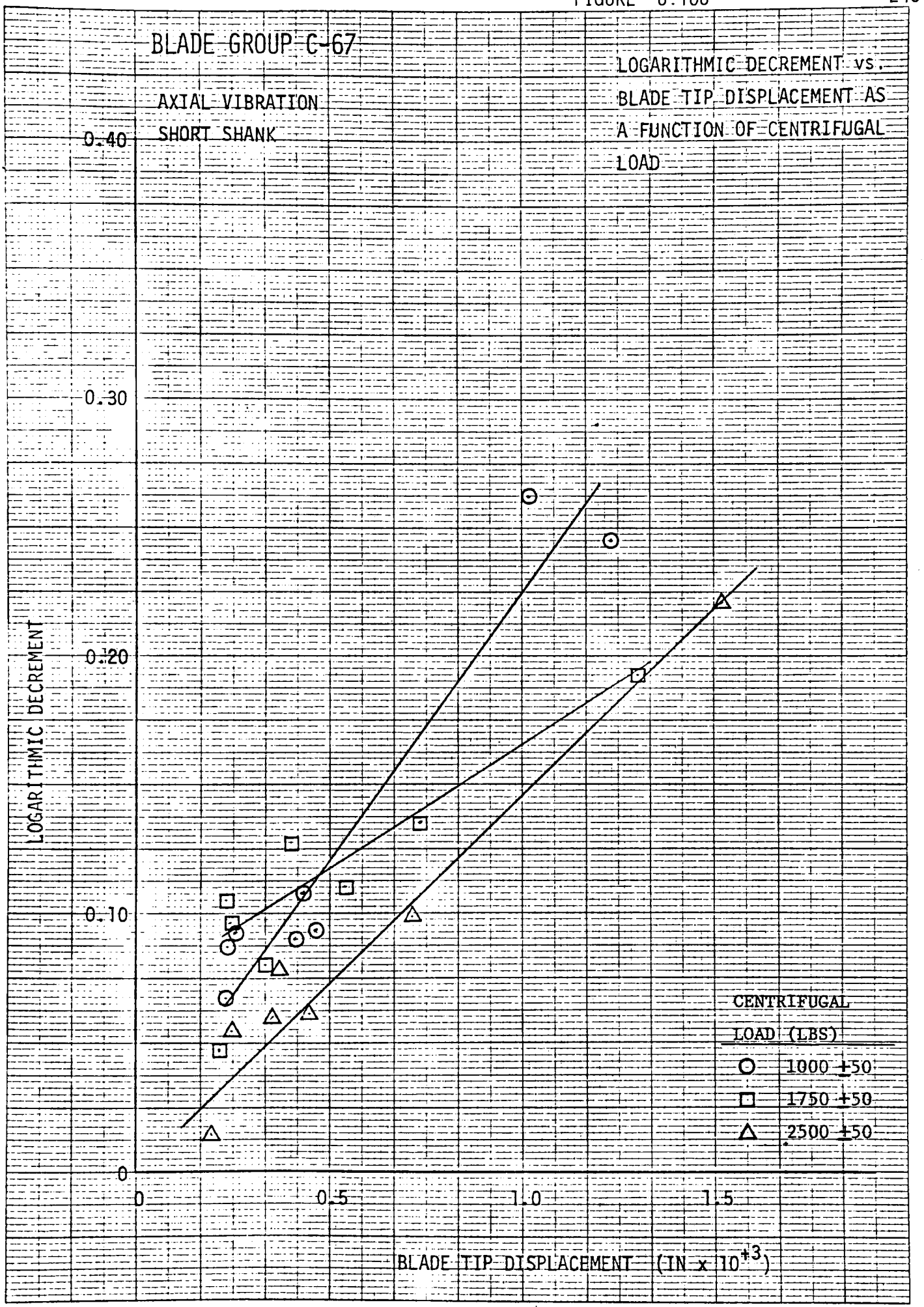
BLADE GROUP C-67
AXIAL VIBRATION
SHORT SHANK
LOGARITHMIC DECREMENT vs. BLADE TIP DISPLACEMENT AS A FUNCTION OF CENTRIFUGAL LOAD
LOGARITHMIC DECREMENT
0.40
0.30
0.20
0.10
0
0
0.5
1.0
1.5
BLADE TIP DISPLACEMENT (IN x 10+3)
CENTRIFUGAL LOAD (LBS)
1000 ±50
1750 ±50
2500 ±50

FIGURE 6.107

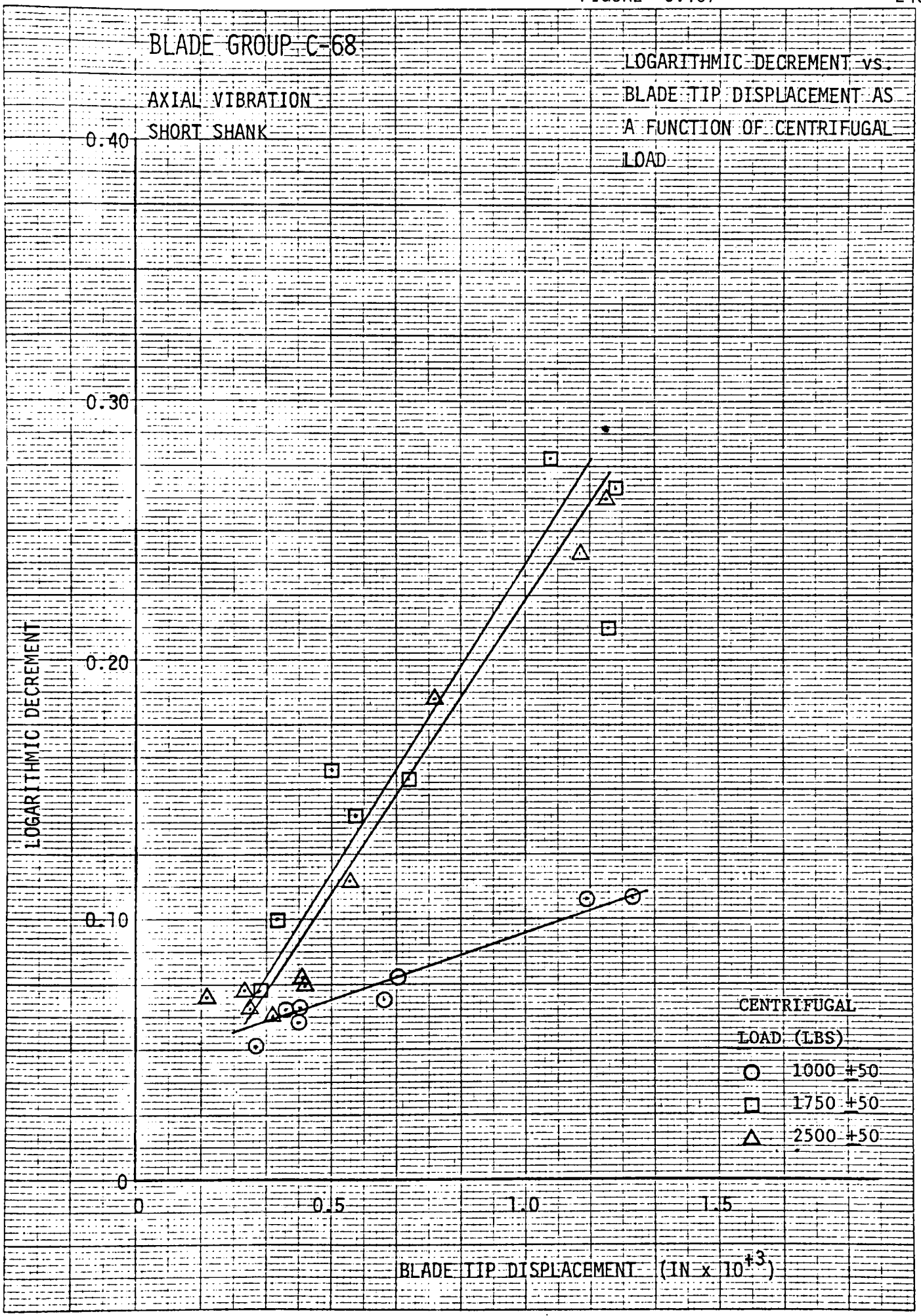
BLADE GROUP C-68
AXIAL VIBRATION
SHORT SHANK
LOGARITHMIC DECREMENT vs. BLADE TIP DISPLACEMENT AS A FUNCTION OF CENTRIFUGAL LOAD
LOGARITHMIC DECREMENT
0.40
0.30
0.20
0.10
0
0
0.5
1.0
1.5
BLADE TIP DISPLACEMENT (IN x 10+3)
CENTRIFUGAL LOAD (LBS)
1000 ±50
1750 ±50
2500 ±50

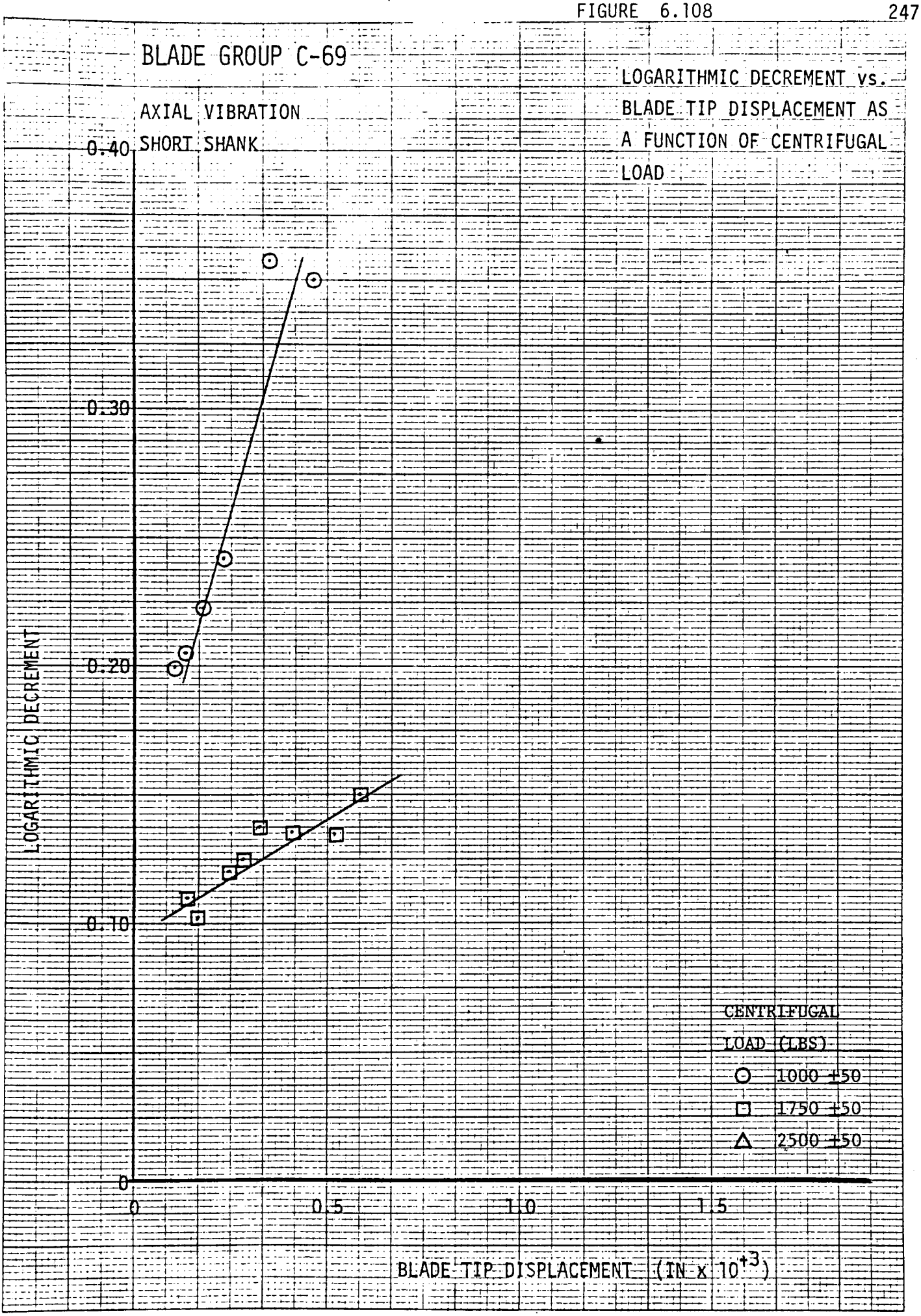
BLADE GROUP C-69
AXIAL VIBRATION
SHORT SHANK
LOGARITHMIC DECREMENT vs. BLADE TIP DISPLACEMENT AS A FUNCTION OF CENTRIFUGAL LOAD
0.40
0.30
0.20
0.10
0
LOGARITHMIC DECREMENT
0
0.5
1.0
1.5
BLADE TIP DISPLACEMENT (IN x 10+3)
CENTRIFUGAL LOAD (LBS)
1000 ±50
1750 ±50
2500 ±50

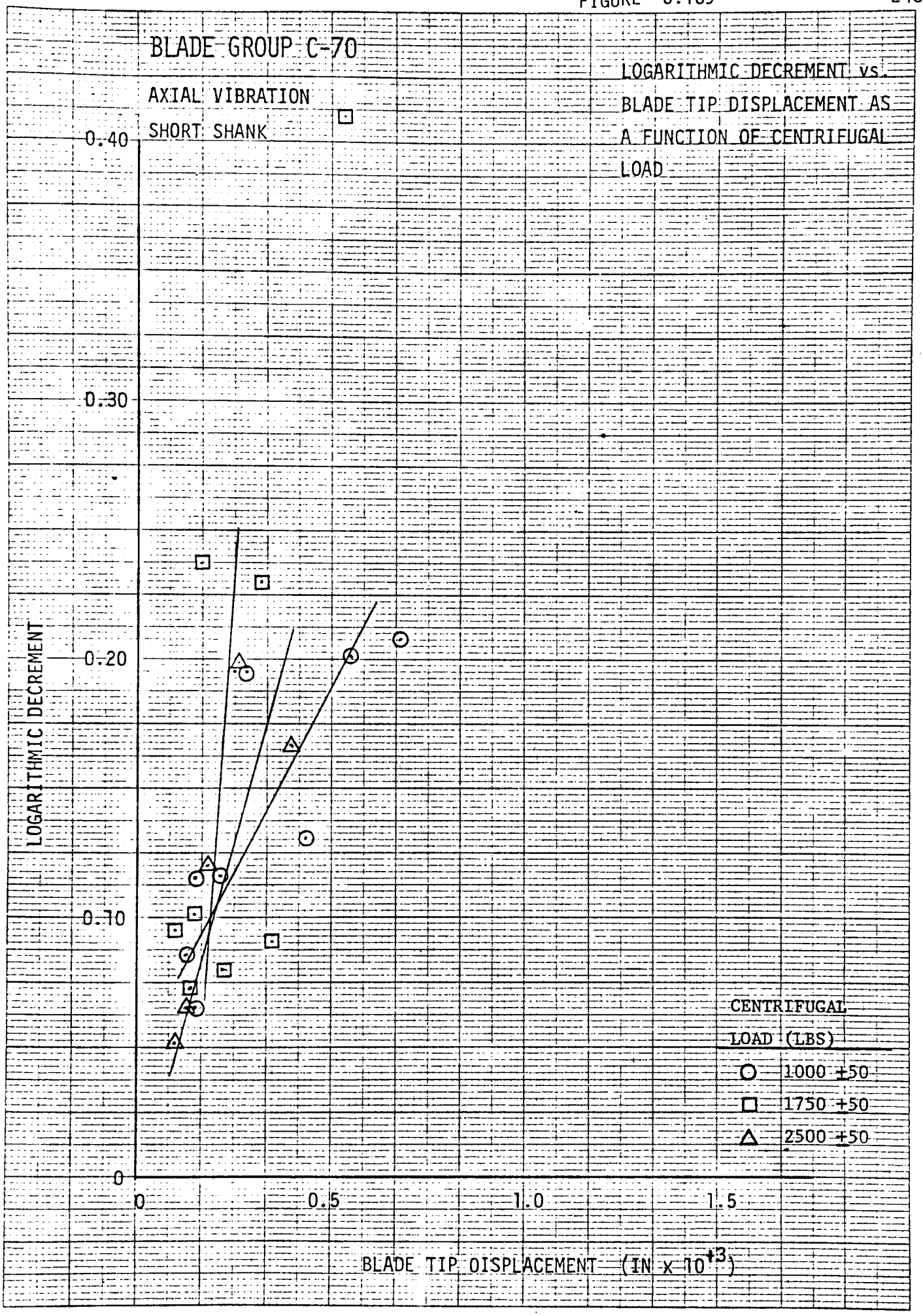
BLADE GROUP C-70
AXIAL VIBRATION
SHORT SHANK
LOGARITHMIC DECREMENT vs. BLADE TIP DISPLACEMENT AS A FUNCTION OF CENTRIFUGAL LOAD
LOGARITHMIC DECREMENT
0.40
0.30
0.20
0.10
0
0
0.5
1.0
1.5
BLADE TIP DISPLACEMENT (IN x 10+3)
CENTRIFUGAL LOAD (LBS)
1000 ±50
1750 ±50
2500 ±50

FIGURE 6.110

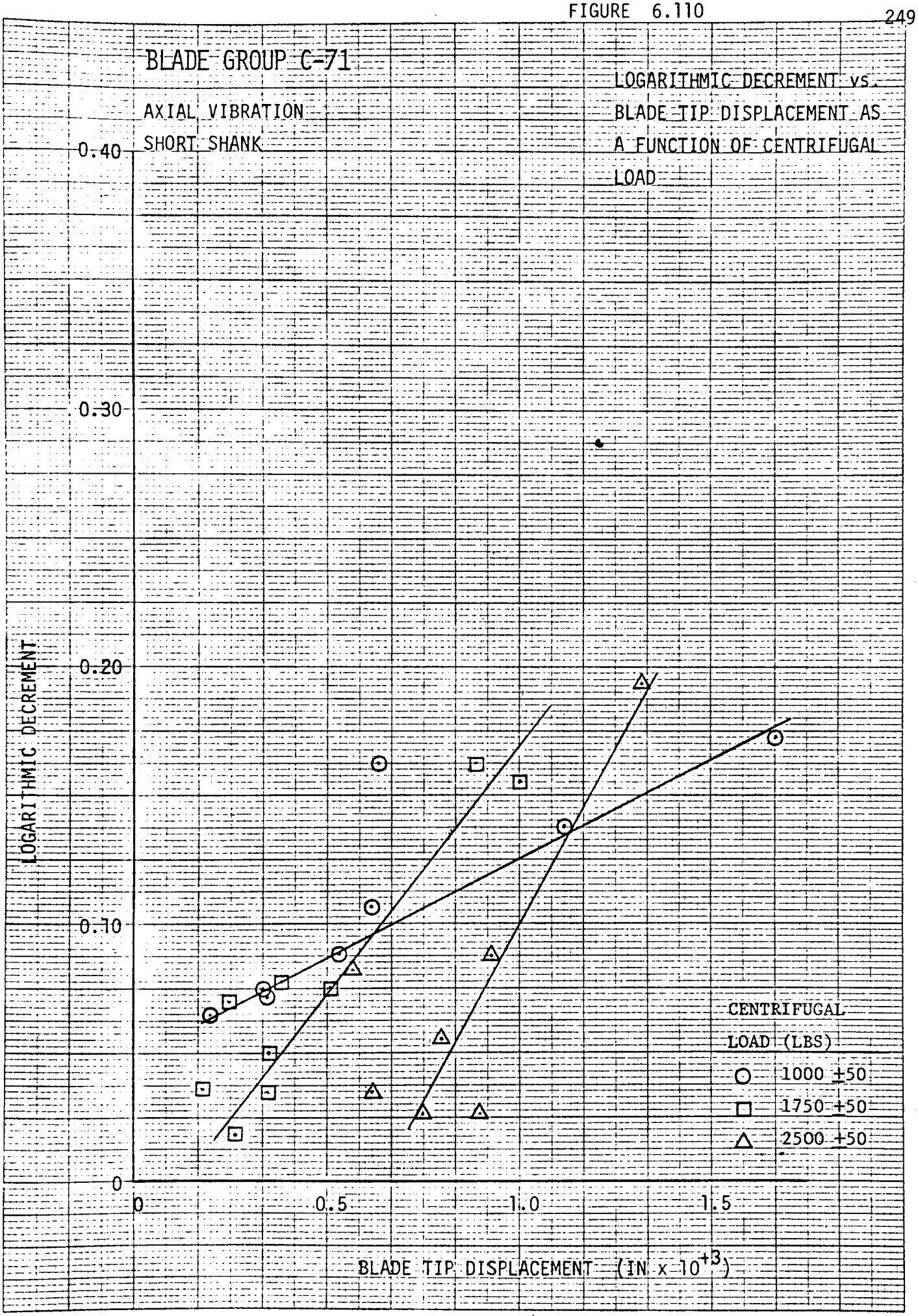
BLADE GROUP C-71
AXIAL VIBRATION
SHORT SHANK
LOGARITHMIC DECREMENT vs. BLADE TIP DISPLACEMENT AS A FUNCTION OF CENTRIFUGAL LOAD
LOGARITHMIC DECREMENT
0.40
0.30
0.20
0.10
0
0
0.5
1.0
1.5
BLADE TIP DISPLACEMENT (IN x 10+3)
CENTRIFUGAL LOAD (LBS)
1000 ±50
1750 ±50
2500 ±50

FIGURE 6.111

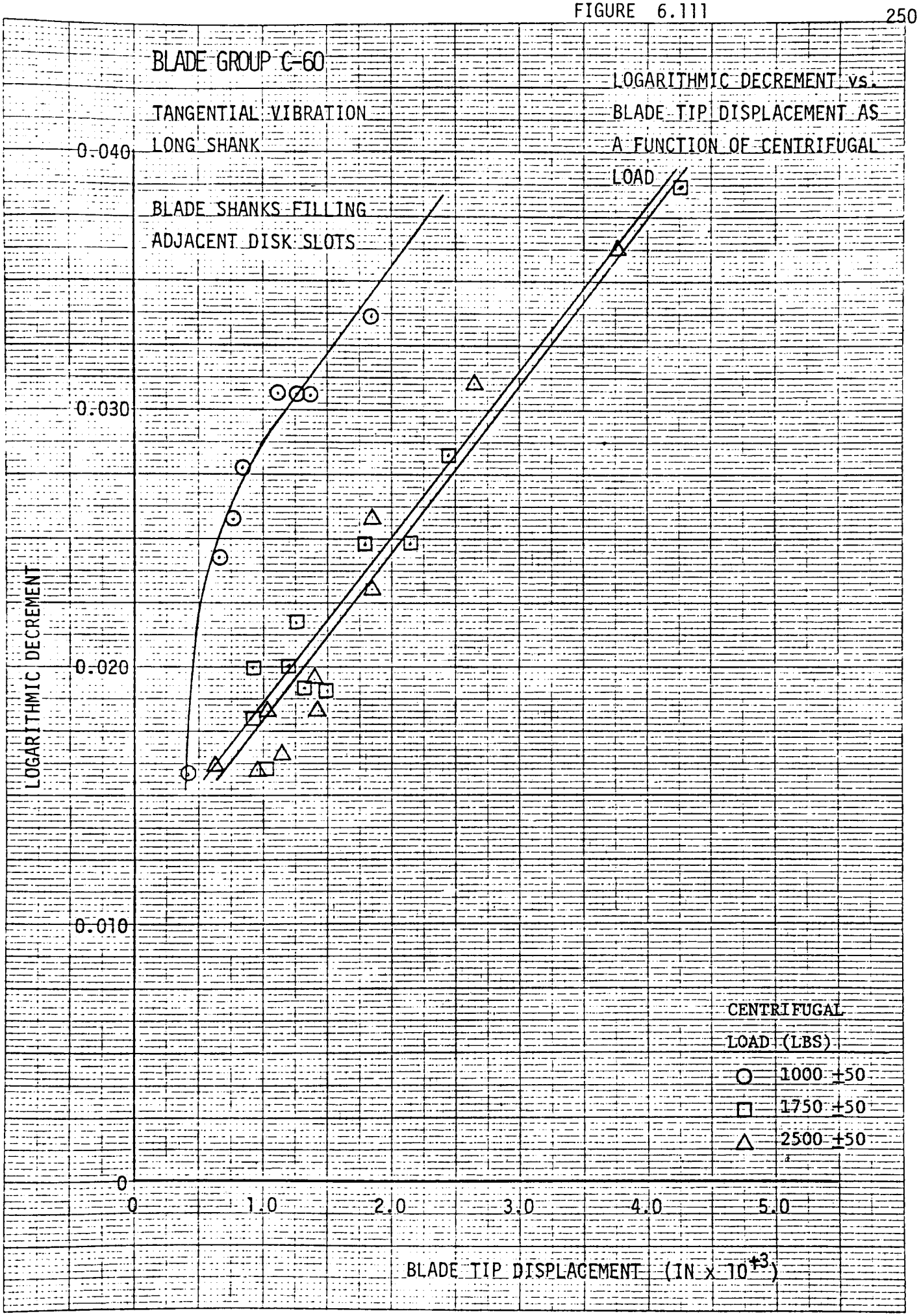
BLADE GROUP C-60
TANGENTIAL VIBRATION
LONG SHANK
BLADE SHANKS FILLING
ADJACENT DISK SLOTS
LOGARITHMIC DECREMENT vs.
BLADE TIP DISPLACEMENT AS
A FUNCTION OF CENTRIFUGAL
LOAD
LOGARITHMIC DECREMENT
0.040
0.030
0.020
0.010
0
CENTRIFUGAL
LOAD (LBS)
1000 ±50
1750 ±50
2500 ±50
0
1.0
2.0
3.0
4.0
5.0
BLADE TIP DISPLACEMENT (IN x 10+3)

7. DISCUSSION OF TEST RESULTS

7.1 Frequency and Amplitude Variation

Not much more can be said about frequency and amplitude variation that was not said in Section 6.1. Evidence is conclusive that two frequency related observations are true. That is, for the blades tested:

a) Once a forcing function is removed from the blades, the frequency will immediately translate to the blades lowest mode in the same direction as the forcing function, and decay from there.

b) Any attempt to excite the blades at any frequency with an electromagnetic exciter physically attached will give erroneous damping data.

There is one characteristic damping curve for a given blade at a given centrifugal load and different vibration amplitudes do not cause different initial characteristic curves.

7.2 Blade Type A

a) Blade damping decreases with increase of axial load. As axial load increases, the blade damping was found to decrease in almost all cases. Exceptions occurred in two cases of axial mode vibrations shown in figures 6.54 and 6.55. The reason for this appears to be that the blade axial load increases, the blade-disc interface locking becomes tighter, allowing less slipping to occur between the contacting surfaces. As axial load increases, the blade damping would increase until lock-up occurred in the root. Blade pair damping would then remain small with any further increase in axial load. These exceptions may be due to specific tolerance conditions in the root junction which are difficult to detect. No other reason was apparent for the different results found in this case.

b) Blade damping increases with an increase of tip displacement. For low axial loads, blade vibrations in the tangential direction gave relatively high logarithmic decrement values, which increased with

an increase of blade tip displacement. It is surmised that for low axial loads, if only one hook pair of the root section was locked in with the second and third hooks free, with an increase of blade tip amplitude more slip would take place and hence more damping would be likely to occur. For tangential vibrations this increase was found to be linear. For axial modes, the observed trend was a second or third degree polynomial curve. This could be due to more of a rocking or slipping action than seen in the tangential direction.

7.3 Blade Type B

a) Blade damping decreases with increase in axial load. The general trend is again for blade damping to decrease with increase in axial load. The reason for this appears to be that higher loads cause higher hook contact forces, higher friction, and eventually reduced (or zero) slippage. The only friction then remaining will be any residual slippage, plus blade internal damping and blade windage.

This root friction lock-up theory depends on the distribution of root tolerances as mentioned above. Where all hooks locked-up simultaneously, a somewhat distinct decrease in root damping might occur. The more usual case would be for the hooks to lock-up over a range of load increase which would smooth out the root damping decrease.

The above trends are evident in figures 6.63 through 6.87. Exceptions are figures 6.64, 6.70 and 6.78. Some suggested reasons for these exceptions are discussed in the preceeding paragraph.

b) Blade damping increases with an increase of tip displacement. For low axial loads, blade vibrations in the tangential direction were once again accompanied by an increase of damping as tip displacement was increased. At small tip displacement and axial loads there is frequently an initial parabolic decrease in damping. As the blade tip displacement is increased from this point, damping increases in a linear manner. The phenomena of initial parabolic response translating into a linear increase is also seen in most of the data for the medium and high axial loads for tangential testing.

With the exceptions of figures 6.73 and 6.79, axial vibration exhibits a continual increase in damping as blade tip displacement is increased. As in the tangential tests, the response is initially parabolic, translating to a linear curve as blade tip displacement increases.

c) Blade damping for high axial loads. Figures 6.77, 6.79, 6.83, 6.86, and 6.87 show test results for 6,000 lbs. centrifugal load. In each case there appears to be a "knee" in the curve, suggesting that some phenomenon possibly a change of damping mechanism, is occurring at a blade displacement around 1.0×10^{-3} inch. The log. dec. increases rapidly beyond this location such that two distinct linear regions exist. At higher tip displacements the blade root may be rocking and sliding in the disk groove, accompanied by slipping and deflection of the disk hooks. Below this level the vibrations may be purely small deflections without relative slippage between hooks.

It should be noted that this is the same characteristic curve that Lazan [9] gives for purely material damping. A copy of this curve is given in figure 7.1. It would have been informative to weld the blade roots into the disk grooves at this load and repeat the tests. Welding would eliminate blade root damping and only material damping and damping due to moving through the air would be left. It the curves were repeated, it would be safe to say that at 6,000 lbs. centrifugal load the roots were locked up and only material damping was present.

Welding was not done due to the high cost of EDM-ing as well as the cost of the steel itself. The disk blocks would have been ruined, and it is desired to save them for blade group testing at a future date.

7.4 Blade Type C

a) Blade damping decreases with increase of axial load for tangential vibration. For tangential tests it is clear that as axial load increases, damping decreases. In the case of axial vibration the curves are almost overlapping. The experimental results show that all axial vibration curves are enclosed by the same scatterband. This means that the ball and shank root type, at the test loads, may have one common damping curve.

b) Blade damping increases with an increase of tip displacement. For both axial and tangential vibration the damping increases with an increase in blade tip displacement.

At low and high axial loads in the tangential test direction there is a predominantly linear increase in damping as blade tip displacement increases. At each of these loads there is a separate region of response. However, at the middle load (1750 lbs.) there is some parabolic response which crosses the low load curve. This phenomena only occurs at the middle load. Apparently the ball and shank is just beginnning to lock up in the root at this test load. Axial test results also have this type of damping-tip displacement relationship.

c) Blade damping for high axial loads. At 2500 lbs. axial load there is no recognizable deviation from the established trends as there was for the Type B blade (at this load).

7.5 Scatter of Results

In general, the test scatter was between 50% and 150%. This is not unacceptable, as typical scatter is between 50% and 200% (see [10]).

Some deviation is due to the width of the loading bands (ie. 3200 ± 250 lbs) used during testing. This was a result of being unable to shim blade groups the same amount in each test. Although three centrifugal loads were obtained for each blade pair tested, it was possible for one load to be too low and/or another to be too high. This explains why some logarithmic decrement plots only have one or two curves on them.

Another cause of scatter is tolerance differences from one blade root to another. If a blade root fits looser than a previous one, it is likely that its damping will be higher at the same centrifugal load.

Experimentally induced scatter can be caused by blade warpage during welding and misalignment when loading the blade group. It is known that a minimal amount of this occurred, but it was unavoidable due to the physical setup.

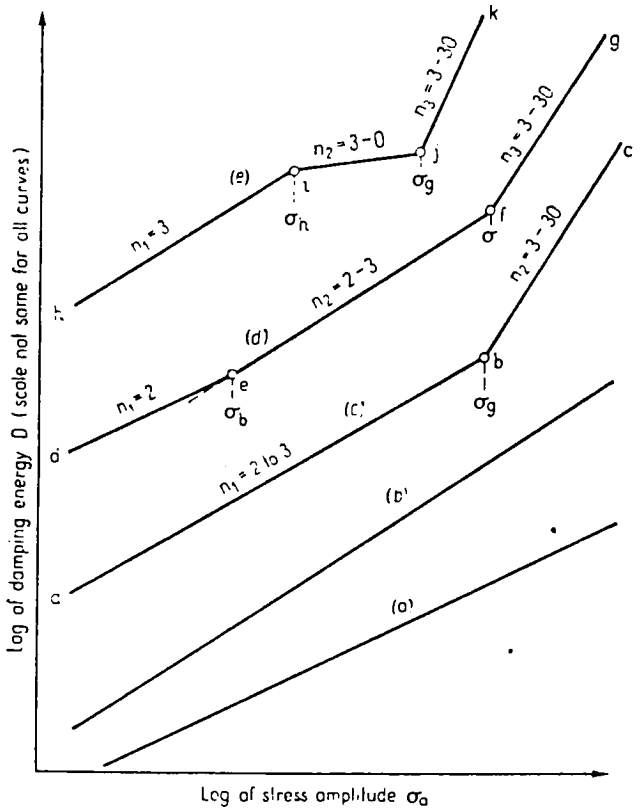

(a) Idealized damping-stress functions (stress history effects not shown).
(a) Linear damping: $D = J\sigma_a^2$. Observed in metals, polymers and elastomers at low stress. Usually rate-dependent ($P'' \sim \dot{X}$).
(b) Power law damping: $D = J\sigma_a^n$. Often observed at intermediate stress. May be rate-dependent or rate-independent.
(c) Idealized anelasto-plastic damping (two-segment curve). Observed in nonferromagnetic materials.
(d) Idealized anelasto-plastic damping (three-segment curve).
(e) Idealized magnetoplastic damping (three-segment curve). Observed in ferromagnetic metals.

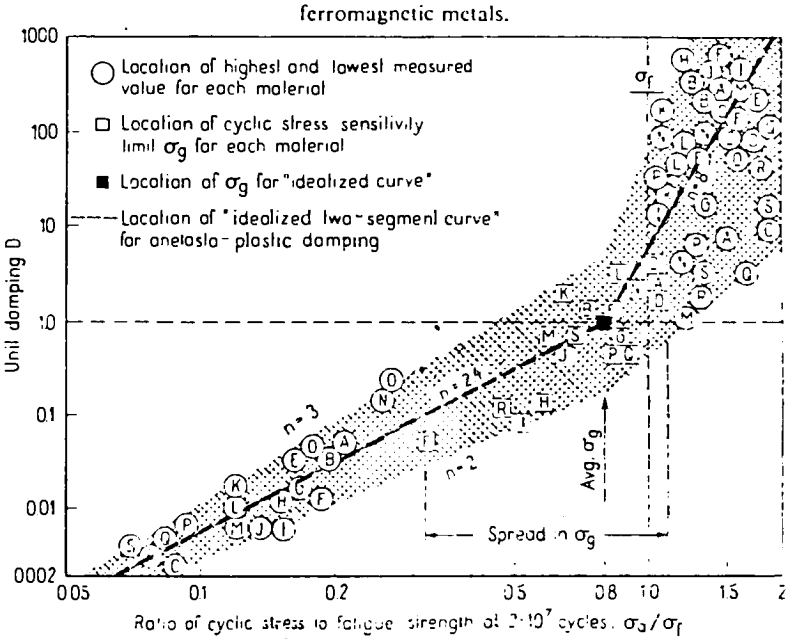

(b) Dependence of unit damping energy of various anelasto-plastic materials upon ratio of cyclic stress to fatigue strength. (A) and (B)—Sandvik steel (Q-T) and (N); (C)—glass laminate; (D) to (I)—titanium alloys at room temperature and 600 F; (J) to (L)—alloy N-155 at room temperature 1350 and 1500°F; (M) to (O)—stellite 31, A.C. at 1200°F, 1350 and 1500°F; (P)—SAE 1020 steel; (Q)—24S-T4 aluminum; (R)—J-1 magnesium alloy; (S)—grey iron.

FIGURE 7.1 Typical Material Damping Curves From Lazan [9]

8. CONCLUSIONS

8.1 Test Rig

1. Functioning of the test rig concept has been demonstrated. The proposed measurement and data reduction techniques have been used successfully to obtain logarithmic decrement values for the blade/root damping for ranges of centrifugal loads and vibration amplitudes.

2. Tests which were repeated under identical centrifugal load conditions showed a very high degree of reproducability of amplitude detail in the vibration decay traces. Even where two traces were initiated with different amplutudes, the decay curves from corresponding vibration amplitudes were usually identical to a high degree of detail. The logarithmic decrement was not shown to be constant with vibration amplitude in any of the tests performed. A decrease of logarithmic decrement with amplitude was constantly observed.

3. The increased scatter of logarithmic decrement results which appears at the lower vibration amplitude levels in some curves is mainly the result of difficulties encountered in reading the decay traces with sufficient accuracy at these smaller amplitudes. Accurate low-amplitude data depends on suitable curve fitting, and on amplitude trace readings within ±0.001 inch.

8.2 Blade Damping

1. Damping studies have been made on three types of axial entry blading. Results for blade tangential vibrations and for blade axial vibrations have been obtained under several conditions.

2. For tangential vibrations of axial-entry blades, an almost-linear relationship exists between logarithmic decrement and vibration amplitude at all but the smallest vibration amplitudes.

3. For axial vibrations of tangential-entry blades, a proportional relation between logarithmic decrement and vibration amplitude exists. This relationship is more complex than for tangential vibrations in keeping with the three-dimensional nature of the structural motions involved in this case.

4. It was generally found that tests conducted at higher centrifugal loads gave lower logarithmic decrement values for corresponding vibration amplitude values. Lower loads may allow a rubbing/shearing action to occur between the hook contact surfaces. Higher loads appear to cause sufficient load, ie. friction, to lock the root surfaces, thus eliminating root damping and so retaining only material damping, mostly in the vane section. The overall blade damping at higher loads was thereby reduced.

5. It seems possible that the damping mechanisms in the tangential direction and in the axial direction are different. Further study is needed to understand the mechanisms involved.

6. The damping logarithmic decrement values obtained include root friction, material hysteresis, and ambient air friction as the primary dissipation mechanisms. The damping values in this report should be most applicable to free-standing, axial-entry blades rotating in dry steam of comparable density to the air enviornment.

7. The following influences were not included in the damping values obtained: Cover, cover-tenon interface, tie wire, above-ambient temperature, steam (moisture, density) environment, varying centrifugal force along vane.

8. The observed increases in damping appear to be associated with vibration amplitude rather than the vibration velocity. This observation was not conclusively shown because the influence of vibration frequency could not be conveniently isolated or tested, and because two damping mechanisms (Coulomb, viscous) may be simultaneously operating.

9. RECOMMENDATIONS

9.1 Shortcomings of Tests

In general the test rig concept worked satisfactorily with the few difficulties mentioned below. The shortcomings of this method relate mainly to convenience of handling the rig. For example, it is difficult for one person to heat, shim, align, and cool a blade group, with alignment being the largest problem. The achievement of higher centrifugal blade loadings than those used for these tests would have meant higher heating of the flexure links, and possibly altering the blade material properties near the tips. The alternate method of gas cooled design may be better for high loads. Some type of positive alignment technique for the disk segments should be devised to avoid bending of the blade pairs. Local high bending stresses may cause increased material damping, and may cause blade failure during tests from high pre-stress.

The heating method requires a long delay period between tests. After heating and installation, it took about one hour for the blade pair to refirm to an ambient temperature for testing. Similar problems could occur with the cooling method.

Shortcomings of the test results relate to the test conditions used (ambient air) and to the accuracy with which the results could be read by eye. For the blade types and attachment designs tested, it is thought that, (a) aerodynamic damping may have contributed little damping (small blade surface area, low viscosity gas), and (b) material damping is less significant than root interface damping, but is more significant than aerodynamic damping. Such conclusions may not apply to long last stage blades, nor to the higher (shell type) modes of any blade. Further studies are needed to develop damping data for the shell modes of actual blade modes at higher frequencies. Also, the load along the length of the test blades is constant, not increasing toward the root, as in the actual case. The relevance of root/material damping data obtained from ambient air tests to ambient steam conditions remains to be demonstrated. For temperatures below 500 degrees F. material properties should not be greatly affected. It is suspected (but not here proven) that the interface properties

will not be much affected. Specific tests are planned to investigate these questions.

The data scatter observed in the chart results at lower amplitudes is mostly attributable to difficulties of reading the decay curves. Reading errors of 0.001 in. are significant at such amplitudes. In all instances a curve of best fit was established by eye, from which the local logarithmic decrement values were obtained. This method was unavoidable because the amplitude decay was frequently influenced by some small residual modal coupling (depending on where the initial blow was struck), and on interactions between the various mechanisms of damping which are acting. For the large volume of data to be reduced in these tests, a microprocessor-based method of data reduction should be developed.

9.2 Technical Developments

1. The damping properties of other types of blade/root combinations should be tested. Tests involving other blade/root types such as finger type dovetail, and straddle-mount should be performed. Both short H.P. blades and L.P. blades, in particular, should be tested for their damping properties.

2. Damping tests should be conducted on blades in steam, at the appropriate operating temperature. Similar axial loads should be applied as were used in the present program.

3. Damping data should be obtained for higher vibration modes. The results should be compared with material and aerodynamic damping data at appropriate stress levels and vibration frequencies.

4. The damping data acquisition and the logarithmic decrement calculation procedures should be automated, ie. by microprocessor, to reduce testing time, and to improve the accuracy of the results obtained.

9.3 Research Developments

1. The influence of the surface finish of the contacting components (hooks) on damping should be investigated in detail. It seems that clean hook surfaces may show different damping characteristics to coated hook surfaces, eg. metal-to-metal slipping (Coulomb) mechanism may give different root damping properties to thin, solid film shear (viscous) damping mechanism.

2. The possibility of different mechanisms occurring in the tangential direction to that in the axial direction for the axial-entry root types should be investigated further.

3. The influence of frequency on vibration of damping coefficient values should be investigated in a specially designed test for both tangential and axial modes, as part of the above damping mechanism study.

4. The possibility of achieving increased blade damping by the application of coatings to the contacting hook surfaces should be investigated.

10. REFERENCES

1. DiTaranto, R.A., "Blade Vibration Damping Device," Journal of Applied Mechanics, Trans. ASME, 80, p. 21-27 (1958).

2. Bears, J.E., "Structural Damping by Slip in Joints," Shock Vib. Digest, 1 (1), pp. 113-119 (1975).

3. Goodman, L.E. and Klumpp, J.H., Analysis of Slip Damping with Reference to Turbine Blade Vibration," Jounral of Applied Mech., Trans. ASME, 23, (3), pp. 421-429, (Sept. 1956).

4. Halvorsen, W.G., Brown, D.L., "Impulse Technique for Structural Frequency Response Testing," S/V, Sound and Vibration, Vol. 11, No. 11, Nov. 1977, pp. 8-21.

5. Jarrett, G.W., Warner, P.C., "The Vibration of Rotating Tapered Twisted Beams," Journal of Appl. Mech., Trans. ASME, Vol. 20, No. 3, Sept. 1953, pp. 381-389.

6. Beards, J.E., "Damping in Structural Joints," Shock Vib. Digest, (8), pp. 35-41 (1979).

7. Lazan , B.J., "Damping Constants and Stress Distribution in Resonant Response, "Journal of Appl. Mech., Trans. ASME, Vol. 20, No. 2, pp. 201-209 (March 1953)

8. Cochardt, A.W., "The Origin of Damping in High Strength Ferromagnetic Alloys," Journal of Appl. Mech., Trans. ASME, Vol. 20, No. 2, pp. 196-200 (March 1953)

9. Lazan, B.J., Damping of Materials and Members in Structural Mechanics, Pergammon Press, Inc., New York, 1968.

10. Rieger, N.F., Nowak, W.J., "Analysis of Fatigue Stresses in Steam Turbine Blade Groups," Paper presented at EPRI Workshop on Steam Turbine Availability, Palo Alto, CA, Jan 18, 1977.

11. Grady, R.F., "Investigation of Material Damping Properties of Propulsion Turbine Blade Material," General Electric Co., Report NOB5-94390, submitted to Bureau of Ships, Department of the Navy, December 1967.

12. Rieger, N.F., Nowak, W.J., "Fatigue Stress Levels in L-5 Turbine Stages for Original Blades and Redesigned Blades," Engineering Consulting Report, February, 1977.

13. Grady, R.F., "Investigation of Dovetail Damping Contribution of Propulsion Steam Turbine Buckets," General Electric Co., Report NOB5-94390, submitted to Bureau of Ships, Department of the Navy, November 1967.

14. Schabtach, C., Fehr, J.O., "Measurement of the Damping of Engineering Materials During Vibration at Elevated Temperatures," Journal of Applied Mech., p. A86-A92, June 1944.

15. Wagner, J.T., "Blade Damping Tests", Westinghouse Engineering Report EC-401, Nobs NOOO24-67-C-5494, May 1969.

16. Jones, D.I.G., "High Temperature Damping of Dynamic Systems," Shock and Vibration Digest, Vol. 8, No. 10, Oct. 1976, Naval Research Laboratory, Washington, DC.

17. Rieger, N.F.,"Damping Properties of Turbine Blades," Shock Vibration Digest, Vol. 11, No. 4, April 1979, pp 3-5.